Publication 1

Chem. Listy *110*, 851−859 (2016) Referát

TERAPEUTIKA AMYLOIDZ

MONIKA HOLUBOVÁ a MARTIN HRUB

stav makromolekulárn chemie, v. v. i., Akademie v ěd České republiky, Heyrovského nám. 6, 162 06 Praha 6
mhruby@centrum.cz

Dolo 31.5.16, p řijato 16.6.16.

Kl čová slova: amyloidza, amyloid, Alzheimerova choroba

Obsah

1. vod

Amyloidzy jsou onemocn ěn spojená s ukládánm normálně rozpustnch protein ů v podobě nerozpustnch amyloidů. Tyto amyloidy se ukládaj v r ůznch orgánech a tkánch a zp ůsobuj jejich dysfunkci, čm p ředstavuj velkou hrozbou pro lidské zdrav [1,2]. Termn amyloid byl poprvé pouit v botanice v roce 1838 Matthiasem Schleidenem pro popis rostlinného krobu, a a poté v roce 1854 Rudolf Virchow tento pojem pouil pro abnormáln makroskopická loiska amyloidz, i kdy u byly známé pod různmi jmény od poloviny sedmnáctého stolet. Virchow pomoc vodného roztoku jodu a kyseliny srové doel k závěru, e látka, která je základem abnormálnch loisek, byla celulosa. Hypotéza celulosového charakteru amyloidu netrvala dlouho. V roce 1859 Friedreich a Kekule prokázali přtomnost proteinu a nep řtomnost sacharid ů v amyloidu, co bylo zaloeno na vysokém obsahu dusku[2,3]. Bennhold zavedl barven kongo červen v roce 1922 pro identifikaci amyloidů ve tkáňovch vzorcch [4]. V roce 1927 Divry a Florkin popsal charakteristick zelen dvojlom, kdy byl amyloid obarven kongo červen pozorován v polarizovaném světle[4]. V roce 1959 Cohen a Calkins detegovali fibriláron povahu amyloidu p ři pozorován pod elektronovm mikroskopem [4]. Povaha amyloidu a proteinů se v průběhu let skládala jako puzzle.

Ne vechny amyloidy jsou vak kodlivé. Existuj tzv. funkčn amyloidy ur čitch protein ů, které se vyuvaj např. u savců pro tvorbu melaninu[5], u bakteri *Escherichia coli* k tvorbě biofilmu[6] apod. Vysoká stabilita, organizovanost a nanometrické rozměry amyloidů z nich dělaj vynikajc kandidáty pro vrobu nanomateriál ů (např. dráty, gely, scaffoldy, tekuté krystaly atd.) za pomoci strategie botom-up [7]. Vyuit amyloidovch fibril jako novch biomateriálů nebo nalezen léku na amyloidzy vyaduje lep pochopen nejen molekulárnch mechanism ů skládán amyloidů, ale i řady dalch faktor ů spojench s tvorbou amyloidů[1].

Kadá depozice proteinu, a ť u fibriláron nebo nefibriláron, se vyzna čuje specifickm proteinem, kter tvo ř hlavn sloku patologického loiska. V p řpad ě amyloidz u člověka je popsáno 27 extracelulárnch protein ů, které mohou tvořit amyloid, v nich je dan protein spojen se specifickm onemocn ěnm [8,9]. Současná nomenklatura amyloidů je zaloena na chemické struktu ře fibrilárnho proteinu, kter za čná psmenem A (amyloid) a k n ěmu je připojena přpona, která je zkrácenou formou prekurzorového proteinu, např. amyloid odvozen od lehkch řetězců imunoglobulinu je označen jako AL a nemoc je AL amyloidza [9,10]. Amyloidy proteinů popsané u lid jsou vypsány v tab. I.

Některé amyloidzy mohou bt systémové (tkajc se několika orgánů či tkán) nebo lokalizované (tkajc se pouze jednoho orgánu nebo tkáně). Systémové formy amyloidz mohou bt primárn, jedná se o formy sporadické nebo zskané (p ř. AL amyloidza). Dále mohou bt systémové formy amyloidz sekundárn, tedy ty, které vznikly na základě dalho onemocn ěn (p ř. AA amyloidza), nebo dědičné (př. ATTR amyloidza). Lokalizované formy amyloidz mohou bt také sporadické nebo zskané (př. AL amyloidza mo čovch cest a Alzheimerova choroba), sekundárn (nap ř. infekčn Creutzfeldt-Jakobova nemoc), nebo dědičné (př. mnoho dystrofi rohovky, d ědičná Alzheimerova choroba)[8].

2. Amyloid

Vechny amyloidy maj spole čnch n ěkolik fyzikálně-chemickch vlastnost: fibriláron morfologie, p řevauje sekundárn struktura β-skládan list (β-sheet), dvojlom po obarven barvivem kongo červeň, nerozpustnost v běnch rozpout ědlech a detergentech a odolnost proti proteasam. Sekvence aminokyselin a struktura proteinů spojench s amyloidzou je vysoce variabiln [11]. Některé amyloidogenn proteiny ve svch rozpustnch stavech vytvá ř

Tabulka I
Lidské amyloidy a jejich proteinové prekurzory[9]

Amyloid	Prekurzorov protein	Systémové (S) nebo lokalizované (L)	Syndrom nebo zúčastněné tkáně
AL	imunoglobulinové lehké řetězce	S,L	primárn spojená s myelomem
AH	imunoglobulinové těké řetězce	S,L	primárn spojená s myelomem
$A\beta_2M$	β_2-mikroglobulin	S	spojená s hemodialzou
		L	klouby
ATTR	transthyretin	S	dědičné seniln systémová
		L	tendosynovitida
AA	sérov amyloid A	S	sekundárn, reaktivn
AApoAI	apolipoprotein AI	S	dědičné
		L	aorta, meniskus
AApoAII	apolipoprotein AII	S	dědičné
AApoAIV	apolipoprotein AIV	S	sporadická, spojené se stárnutm
AGel	gelsolin	S	dědičné (finské)
ALys	lysozym	S	dědičné
AFib	fibrinogen α-řetězce	S	dědičné
ACys	cystatin C	S	dědičné
ABri	ABriPP	S	familiárn demence, britské
ALect2	leukocytárn chemotaktick faktor 2	S	hlavně ledviny
ADan	ADanPP	L	familiárn demence, dánské
Aβ	amyloidov prekurzorov protein (APP)	L	Alzheimerova choroba, stárnut
APrP	prionov protein	L	spongiformn encefalopatie
ACal	pokalcitonin	L	tumory C buněk ttné lázy
AIAPP	amylin (amyloidov polypeptid Langerhansovch ostr ůvků)	L	Langerhansovy ostrůvky inzulinom
AANF	atriáln natriuretick faktor	L	srdce
APro	prolaktin	L	stárnut hypofzy prolaktinom
AIns	insulin	L	iatrogenn pokozen
AMed	laktadherin	L	aorta (hl. média)
AKer	kerato-epitelin	L	rohovka, dědičné
ALac	laktoferin	L	rohovka
AOaap	ODAM (odontogenic ameloblast-associated protein)	L	odogenn nádory
ASemI	semonogelin I	L	semenné váčky

globulárn strukturu (p ř. transthyretin TTR). Ukázalo se, e tyto proteiny mus bt částečně rozvinuty, aby dolo k vytvářen fibril. V t čchto případech v ětina amyloidogennch mutac destabilizuje globulárn strukturu, čm se zv koncentrace v ustáleném stavu částečně sloench globulárnch protein ů a podpoř se tvorba fibril. U proteinů, které nejsou amyloidogenn *in vivo*, se ukázalo, e je lze p řimět k tvorbě fibril, pokud je protein vysta-

ven částečnm denatura čnm podmnkám, které napodob účinek destabilizujc mutace. To nazna čuje tomu, e schopnost vytvářet fibrily je obecnou vlastnost, kterou sdl mnoho protein ů a projev se pouze p ři podmnkách částečné denaturace. Na rozdl od globulárnch protein ů se mnoho amyloidogennch protein ů v jejich nativnm rozpustném stavu vyskytuje ve formě náhodného klubka (např. APP). Tyto proteiny mohou zaujmout metastabiln konformaci, ve které mus bt optimáln obsah α-helixů, aby se upřednostnil přechod od náhodného klubka do struktury β-skládaného listu v průběhu fibrilace[12].

Jak bylo napsáno ve, amyloidy maj fibriláln strukturu. Tyto fibrily s proměnlivou délkou jsou rigidn a nevětvené a jejich průměr je 712 nm (cit. [2,13]). Amyloidn fibrily jsou sloeny nejmén ě ze dvou vláknitch podjetnotek tzv. protofilament, které se stáč podél osy fibrily [13]. Protofilamenty maj pr ůměr 2,53,5 nm a skládaj se z několika antiparalelnch β-skládanch list ů, které se zvolna stáč podél osy protofilamentu a vytvá řej spirálovou strukturu[2,14]. Základn jednotkou β-skládaného listu je tzv. β-řetězec (β-strand), kter je úsekem polypeptidového řetězce a je kolm k ose protofilamentu [14]. Této struktuře se říká cross- β [15].

Tvorba amyloidu obvykle zahrnuje kombinaci několika faktorů, jako jsou zvená a dlouhodobá distribuce proteinu a/nebo náchylnost proteinu tvořit strukturu β-skládaného listu, co m ůe bt zp ůsobeno mutac i denaturujcho prost řed nebo m ůe bt tato vlastnost zskaná během proteolytického t ěpen [10]. Amyloidogenn prot ějky proteinů jsou syntetizovány a sekretovány jako nativn proteiny, ale systém intraceluláro kontroly je za normáln ch okolnost schopen je rozpoznat a odstranit. Vn ě buňky dojde nakonec k rovnovánému stavu mezi zcela sloenmi a částečně sloenmi (amyloidogennmi) formami proteinů. Fluktuace koncentrac obou forem je vysoká. Existuje řada faktorů, které mohou posunout rovnováhu směrem k částečně sloenm stav ům, např. nzké pH, oxidace, zven teploty nebo ionty kov ů[16]. K tvorbě amyloidu docház obecn ě dky oligomeraci jader, které zárove ň tvorbu amyloidu i urychluj. Po nukleaci docház k rychlému růstu fibril. Některé případy tvorby amyloidnch fibril mohou vyadovat proteolzu, p ři které dojde k uvolněn amyloidogennho proteinu. V tomto p řpad ě jde o tzv. fragmenty prekurzorového proteinu (fibrilogenn peptid). Obvykle je citlivost proteolytického prekurzoru k vytvářen fragment ů pro amyloidn fibrily zp ůsobena mutac, tato mutace je nezbytná pro t ěpen proteinu *in vivo*[12].

Pro studium procesu fibrilace se obvykle pro zjednoduen pouvá krátkch peptid ů, jeliko se jedná o velice sloit proces. Ukázalo se, e i relativn ě krátké peptidy, které jsou určitmi fragmenty ur čitého prekurzorového proteinu, maj schopnost vytvá řet typické amyloidn fibrily. Malá velikost peptidů snila sloitost tvorby amyloidu a zároveň umonila zskat fyzikáln ě-chemick pohled na mechanismus tvorby fibril. Typickm spole čnm rysem krátkch peptid ů, které mohou tvořit amyloidn fibrily, je vysok vskyt aromatickch aminokyselinovch zbytk ů[17]. Vznam aromatickch kruh ů při vytvářen amyloidu byla prokázána u mnoha peptidů. Navc jsou tyto interakce důleité v mnoha oblastech strukturáln biologie, v četně vytvářen hydrofbnch jader protein ů dávajc stabilitu terciárn struktu ře, host-guest interakce, porfyrinové agregace v roztoku a stabilizace DNA báz [18]. Navrhovaná role aromatickch interakc p ři tvorbě fibril souvis se zjit ěnm, e struktura amyloidnch fibril se podobá β-helikáln struktu ře, kde je jeden nebo vce β-skládanch listů stočench roubovitm zp ůsobem kolem jádra[19]. Jednou z hlavnch vlastnost β-helixu je vrstven podobnch rezidu na ploch β-skládan list.

Dal vznamné interakce v agregaci a stabilizaci amyloidnch fibril jsou hydrofbn [20]. Substituce aminokyseliny v sekvenci, která hraje kl čovou roli v chován celé sekvence, může snit (nebo zvit) sklon k agregaci p ři snen (nebo zven) hydrofobicity [20,21]. Existuj d ůkazy, e proteinové sekvence se vyvinuly, aby se p ředelo shlukům hydrofobnch zbytk ů (např. skupiny tř nebo vce po sobě následujcch hydrofobnch zbytk ů jsou méně časté v proteinovch sekvencch [21]). Dal vliv na agregaci a stabilizaci maj elektrostatické interakce [20]. V případech, kdy je protein vysoce nabit, je agregace protein ů energeticky nepříznivá. Pokud maj proteiny kladn ě a záporně nabité skupiny na povrchu, může to vést k agregaci [20,22].

Kromě prekurzorového proteinu byl v amyloidech různch amyloidz nalezen sérov amyloidov protein (SAP), glykosaminoglykany (hlavně heparansulfát) a apolipoprotein E (cit.[2,16]). SAP je pentamern globuláro glykoprotein, kter se váe reverzibiln ě do amyloidnch fibril v závislosti na koncentraci Ca^{2+} a je univerzáln slokou amyloidů. SAP tvoř od 12 % do 20 % suiny amyloidu. SAP je normáln protein plazmy, kter je spolu s C-reaktivnm proteinem produkován v játrech. SAP je kl čová komponenta vrozené imunity a zánětu a může také vytvářet amyloidn fibrily, čm zp ůsob sekundárn amyloidzu vzniklou po zán ětu. Nefibriláro forma SAP se velmi ochotně přidruuje k amyloidnm fibrilám. Role SAP v amyloidu nen zcela známa, ale zdá se, e má zabránit degradaci amyloidnch fibril proteolytickmi enzymy.

U glykosaminoglykanů bylo prokázáno, e podporuj agregaci amyloidogennch protein ů. Přesn mechanismus interakce je nejasn, ale podle jedné z teori glykosaminoglykany jako polyanionty hraj d ůleitou roli v katalze agregace proteinu a ve stabilizaci amyloidovch fibril. Tato teorie je podpořena faktem, e jiné polyanionty (nap ř. ATP, heparin) jsou také schopny podporovat agregaci amyloidovch fibril. I kdy p řesná role a vzájemné působen t ěchto sloek nejsou dob ře známé, je pozoruhodné, e *in vitro* může bt amyloid vytvo řen bez pomoci glykoproteinů a glykosaminoglykanů, co p řispvá k nejasné roli v patogenezi amyloidu[2]. Podobná situace je i u apolipoproteinu E, u kterého také nen zcela známá jeho role v patogenezi amyloidu[2].

Amyloidy maj cytotoxické ú činky, ktermi jsou např. indukované selhán autofagie, zven úrovn ě reaktivnch forem kyslku (ROS), mitochondriáln dysfunkce, průchodnost buněčné membrány, dyshomeostase vápnku, nebo ztráta funkce proteinu po agregaci[23,24].

3. Klinicky pouvané terapie

3.1. Systémové amyloidzy

Léčba amyloidzy závis na typu, distribuci a biologickch efektech loisek amyloid ů[25]. Prognza systémové amyloidzy je často infaustn, ale nedávné pokroky zna čně zvily medián p řeit. V současné době je léčba ve větině případ ů zaměřena na snen dodáván prekurzorového proteinu a zároveň na podporu nebo vm ěnu funkce orgánu. Za přznivch okolnost to vede k regresi existujcch amyloidovch depozit, zachován nebo obnov ě funkce postiench orgán ů a delmu p řeit pacient ů[26]. Důleité také je, aby byla amyloidza diagnostikována v čas a léčba byla zahájena co nejdřve, aby brzy dolo ke stabilizaci onemocněn a zabránilo se pokra čujc progresi [4].

3.1.1. AL amyloidza

AL amyloidza je nej častějm typem systémové amyloidzy diagnostikované v rozvinutém sv ětě. Hláen vskyt 512 p řpad ů na milion ročně je velmi pravděpodobně podhodnocen, protoe *post mortem* údaje naznačuj, e je to p ř čina smrti ~1 z 1500 lid ve Velké Británii. Vyhldky pro nelé čenou AL amyloidzou jsou patné s mediánem přeit pouze 615 m ěsc ů a desetiletá mra přeit je mén ě ne 5 %. Onemocn ěn m ůe bt spojeno s jakoukoli poruchou monoklonálnch B-lymfocyt ů. Současná léčba si klade za cl potla čit proliferaci klonů B-lymfocytů a tedy i produkci amyloidogennho proteinu pomoc chemoterapie p ůvodně vyvinuté pro nádorová onemocněn. Existuj vak vedlej faktory ovliv ňujc efektivitu léčby[19]: (1) Chemoterapeutické reimy jsou zaloeny na t ěch, které se pouvaj u mnoho četného myelomu, ale dyskrazie plazmatickch bun ěk u větiny pacientů s AL amyloidzou jsou relativn ě nzkého stupn ě a mohou bt mén ě chemosenzitivn [25,26]. (2) Diagnza je obtná, často zjit ěna pozdě, kdy u mnoho pacient ů má nemoc v pokročilém stadiu, které omezuje pouit chemoterapie, jeliko docház k pokozen imunity kv ůli nzké hladin ě protilátek. (3) Regrese amyloidu je postupn proces, kter nevede k měřitelnému klinickému přnosu po dobu mnoha měsc ů nebo dokonce let, pokud dojde k úspěnému potlačen bun ěčné dyskrazie[26].

Vb ěr léčby je obtn. V polovin ě 90. let se ukázalo, e malé dávky melfalanu a prednisonu podávanch ústn ě vedou k malému zlepen a medián p řeit vzroste ze 78 měsc ů na 1218 m ěsc ů[26]. Vysoké dávky melfalanu podávaného intravenzn ě s transplantac autologncn kmenovch bun ěk je iroce pouváno k lé čbě systémové AL amyloidzy, zejména ve Spojench státech s mediánem přeit 4,6 let. Bohuel, tato forma lé čby je doprovázena vysokou úmrtnost souvisejc s lé čbou 12 a 13 % ve zkuebnch centrech. V multicentrálnch sérich je popsána úmrtnost dokonce 2543 % (cit. [19]). Zjit ěné rizikové faktory pro úmrtnost souvisejc s lé čbou zahrnuj zapojen vce orgán ů, celkov patn stav pacienta a pokročil v ěk[26,27]. Pečlivm vb ěrem pacientů, zaloenm také na základě hodnocen srde čn dysfunkce, vrazn ě snilo úmrtnost v souvislosti s lé čbou[21]. Jiné přstupy v léčbě AL amyloidzy jsou zaloeny na vysokch dávkách na bázi dexamethasonu v kombinaci s melfalanem, cyklofosfamid-thalidomidem a thalidomidem[27]. V současné době neexistuje ádn zp ůsob, jak určit, jak budou konkrétn jednotlivci snáet lé čbu. Prekurzorov protein m ůe bt nyn sledována u vce ne 90 % pacient ů a chemoterapie může bt odpovdajcm zp ůsobem přizpůsobena. Trvalé snen sérové koncentrace volnch monoklonálnch lehkch řetězců sniuje ukládán amyloidu a potla čen o vce ne 50 % a je spojeno se zvenou dobou p řeit [26].

Diskutabiln lé čbou je transplantace orgánu v případ ě AL amyloidzy vzhledem multisystémové povaze této nemoci a riziku recidivy transplantovaného t ěpu. Transplantace orgánů se proto u AL amyloidzy provád z řdka[28].

3.1.2. AA amyloidza

Reaktivn systémová AA amyloidza je monou komplikac jinch onemocn ěn, které vedou ke vzniku trvalé odpovědi akutn fáze. Takové spout ěče jsou např. chronická zánětlivá, infekčn nebo nádorová onemocn ěn, jako jsou revmatoidn artritida, tuberkulza, HIV/AIDS, cystická fibrza, Crohnova nemoc apod. Biopsie *post mortem* naznačuj, e prevalence AA amyloidu u pacientů s chronickm zán ětlivm onemocn ěnm je 3,6 a 5,8 %. AA amyloidn fibrily jsou odvozeny z fragment ů cirkulujcho reaktantu akutn fáze sérového amyloidu A (SAA). Přestoe AA amyloidza se m ůe rozvinout rychle, medián latence mezi přtomnost chronického zán ětlivého onemocněn a klinicky vznamnou amyloidzou je téměř dvacet let. AA amyloidza se obvykle projevuje proteinuri, následovanou progresivn renáln dysfunkc často doprovázenou nefrotickm syndromem. Jatern postien a autonomn neuropatie se obvykle vyskytuje v pokročilej fázi nemoci. Prognza AA amyloidzy závis na m ře poruchy funkce ledvin a jde-li předcházejc zánětlivé onemocněn potla čit[26]. Léčba AA amyloidzy začná kontrolou zán ětlivého stavu, co nen vdy snadné, ale bylo prokázáno, e protizán ětlivé a cytotoxické terapie maj ur čitou účinnost. Pozitivnch vsledk ů bylo dosaeno podáván chlorambucilu u pacient ů s juveniln revmatoidn artritidou. Azathioprin se zase často pouvá ke zpomalen onemocněn u dosp ělch pacient ů s revmatoidn artritidou[29]. Metotrexát[4] a zejména nové biologické léky (př. anakinra[4], tocilizumab[4]) zaclené na cytokinové mediátory zánětu (např. TNF a IL-1), silně potlačuj reakce akutn fáze u mnoha pacient ů např. s revmatoidn artritidou a Crohnovou nemoc. Lé čba kolchicinem je povinná u familiárn st ředomořské horečky, aby se zabránilo AA amyloidze. Excise lymfatické tkán ě produkujc IL-6 u Castlemanovy nemoci, kterou komplikuje AA amyloidza, vede ke zmrn ěn p řznak ů a usnadňuje regresi amyloidu[26]. Pro léčbu onemocněn ledvin u AA amyloidzy se pouvá eprodisát sodn. Jedná se o 1,3-propandisulfonát sodn (viz obr. 1), kter má strukturu podobnou heparansulfátu. Eprodisát se kompetitivně váe na vazebná msta pro glykosaminoglykany na SAA a inhibuje tvorbu

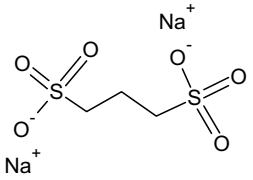

Obr. 1. **Chemická struktura eprodisátu sodného**

fibril a ukládán amyloidu [30].

Sn-li se dodáván SAA po del dobu, loiska AA amyloidů často ustoup a renáln funkce se m ůou zlepit a doba přeit je dlouhodobá. V p řpad ě, e odpov ěď akutn fáze stále pokra čuje, postupné ukládán amyloid ů má často za následek selhánm ledvin. U jedinc ů s pokročilm onemocněnm ledvin nemus bt dostate čné dokonce i kompletn potla čen jejich zán ětlivého onemocněn, aby se zachovala funkce jejich ledvin, a ve vech p řpadech je pokozen ledvin urychleno hypertenz [26].

3.1.3. Dědičné amyloidzy

Dědičné systemické amyloidzy jsou autosomáln ě dominantn onemocn ěn, ve kterch jsou amyloidn fibrily odvozené od genetickch variant nap ř. transthyretinu (TTR), apolipoproteinu AI, AII, lysosymu, gelsolinu nebo fibrinogenu. V případech, kdy je varianta amyloidogenn-ho proteinu pouze nebo převán ě syntetizována v játrech, může bt efektivn lé čbou transplantace jater. Tato forma genové chirurgické terapie, byla úsp ěn ě pouita u mnoha pacientů s dědičnou amyloidn polyneuropati (FAP), která je spojena s genetickou variantou TTR, a také se ukázala účinná u pacientů s AFib a AApoAI amyloidzou[26]. Játra explantované od pacientů s FAP obsahuj pouze mikroskopické amyloidn loiska v cévách a nervech a jinak se onemocněn neú častn [31]. Taková játra nabz monost op ětovného pouit pro tzv. domino transplantaci pro pacienty s chorobami jater v konečném stádiu, pro které zdravá játra nebyla k dispozici[26]. Avak existuj p řpady, kdy dolo po n ěkolika letech k vvoji systematické FAP. I kdy dárci jater s FAP z ůstávaj cennm zdrojem, tato data ukazuj, e je pot řeba přsného dlouhodobého sledován p řjemc ů[31].

3.2. Lokalizované formy amyloidzy

U loisek amyloidu, která se vyskytuj v izolovanch oblastech (např. močov m ěch ř nebo dchac cesty), m ůe zpomalit postup tohoto onemocn ěn radioterapie. Dal monou lé čbou je chirurgické odstraněn loisek. V přpad ě lokálnho zp ůsobu terapie je kontrola nemoci úspěná a je neobvyklé, aby pacient zem řel na amyloidzu[2,10]. Problém nastává, kdy jsou amyloidn loiska soustředěna v centráln nervové soustav ě (CNS), v těchto případech nen efektivn lé čba. Jedna z nejběn ějch forem amyloidz postihujc CNS je Alzheimerova choroba [32].

3.2.1. Alzheimerova choroba

Alzheimerova choroba (AD) je nejčastěj p ř činou demence. Podle Světové zdravotnické organizace 37 milionů lid na celém sv ětě v současné době trp demenc a Alzheimerova choroba postihuje asi 18 milion ů z nich. Vy v ěk je největ rizikov faktor pro AD. Jej prevalence se přiblin ě zdvojnásobuje kadch p ět let po dosaen 60 let (cit. [33]). Současná léčba AD ře symptomy onemocněn [34]. Snahy o snen produkce amyloidu β (Aβ) jsou v experimentálnm stádiu [35]. V současné době existuj dva druhy léků schválench pro lé čbu symptomů: (1) Inhibitory acetylcholinesterasy (IAChE) prodluuj ú činek acetylcholinu v synapsch tm, e brán jeho degradaci. Tato strategie má za následek zlepen kognitivnch funkc, nálady a chován. (2) Antagonista *N*-methyl-D-asparagové kyseliny (NMDA) memantin, u kterého se předpokládá, e pomáhá regulovat hladinu neurotransmiteru glutamátu, kter je nezbytn nap ř. pro paměť[33].

IAChE jsou prvn lini prost ředků pouitch pro lé čbu a nasazen t ěchto inhibitorů je doporučeno okamit ě po určen diagnzy AD. IAChE jsou ur čeny pro lehké a středně těké formy AD [33,34,36,37]. Prvnm IAChE byl tacrin, kter byl schválen v roce 1993, ale jednm z vedlejch účinků tohoto léčiva byla vrazná hepatotoxicita [33]. Pouvanmi IAChE v sou časné době jsou donepezil, galantamin a rivastigmin (viz obr. 2).

Donepezil a galantamin inhibuj selektivn ě acetylcholinesterasu. Galantamin navc jet ě zlepuje cholinergn p řenos tm, e p ůsob jako ligand na nikotinov acetylcholinov receptor, co vede ke zven presynaptického uvolňován acetylcholinu a postsynaptického p řenosu nervovch vzruch ů. Rivastigmin inhibuje kromě acetylcholi-

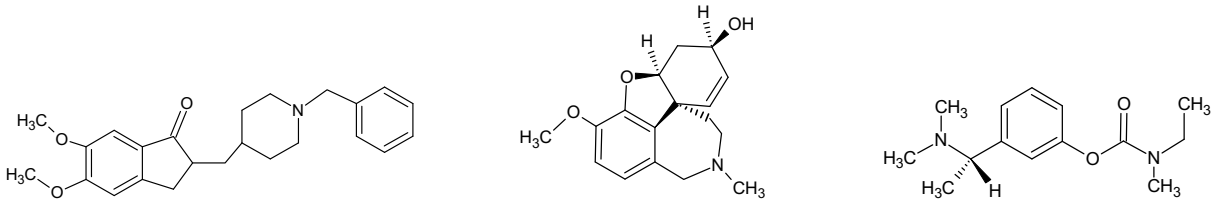

Obr. 2. **Zleva chemická struktura donepezilu, galantaminu a rivastigminu[39]**

nesterasy také butyrylcholinesterasu, která tvoř asi 10 % z celkového mnostv cholinesteras v lidském mozku a je spojena především s gliemi [34]. V průběhu postupu AD se aktivita acetylcholinesterasy sniuje, zatmco aktivita butyrylcholinesterasy se stabilizuje a dokonce zvyuje. Ukazuje se, e butyrylcholinesterasa m ůe p ůsobit jako vyrovnávac mechanismus pro metabolismus acetylcholinu [34,38]. I kdy zmi ňovan donepezil, galantamin a rivastigmin patř do stejné skupiny lé čiv, jejich farmakologie a farmakokinetika se od sebe li. Donepezil je piperidinov derivát, kter nekompetitivn ě a reverzibilně inhibuje acetylcholinesterasu. Jeho poločas eliminace je přiblin ě 70 h, a proto se podává jednou denně. Rivastigmin je pseudoireverzibiln inhibitor acetylcholinesterasy a butyrylcholinesterasy a je hydrolyzován esterasami. Jeho krat poločas eliminace vyaduje dávkován dvakrát denn ě. Galantamin je selektivně reverzibiln inhibitor acetylcholinesterasy a je pozitivnm modulátorem nikotinovch acetylcholinovch receptor ů. Jeho poločas eliminace je přiblin ě 5 h, a proto jsou zapotřeb dv ě dávky denně[34]. Ukazuje se, e IAChE jsou obecně dobře snáeny, ale mohou se vyskytnout neádouc ú činky jako je nevolnost, zvracen, nechutenstv a bradykardie [33,36].

Glutamát je hlavn excita čn neurotransmiter v CNS a má úlohu v neurotransmisi. Glutamátové receptory se děl na *N*-methyl-D-asparagové (NMDA), α-amino-3--hydroxy-5-methyl-4-isoxalonové (AMPA) a kainátové. NMDA receptor má sloitou strukturu s n ěkolika vazebnmi msty pro NMDA a glutamát. Aktivace NMDA receptoru generuje dlouhotrvajc p řliv Ca^{2+} do neuronů, co je podstatou toho, aby dolo k zapojen dlouhodobé potenciace buněčného procesu, kter je základem u čen a pam ěti. U patogeneze, která představuje nárůst extracelulárnho glutamátu, se předpokládá, e vede k nadm ěrné aktivaci NMDA receptorů s následnou intraceluláran akumulac Ca^{2+}. Akumulace vápnku pak iniciuje kaskádu d ějů, které maj za následek smrt neuron ů. Memantin je adamantiov derivát (viz obr. 3)[36] a NMDA antagonista, kter m ůe chránit neurony před glutamátem zprostředkovanou excitotoxicitou, ani by dolo k zabrán ěn fyziologické aktivace NMDA receptoru. Memantin je prvn schválen lék pro léčbu středně těké a t ěké AD [33] a je obecně dobře snáen [34], z neádoucch ú činků se objevuj závrat ě, bolest hlavy a nespavost[36,37]. Lék je často pouván s IAChE [34,36].

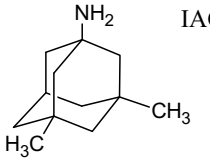

Obr. 3. **Chemická struktura memantinu[40]**

4. Experimentáln terapie

Lep pochopen mechanism ů, které jsou základem vytvářen a perzistence amyloidu, definovalo řadu novch směrů pro léčebné postupy amyloidz [35]. Jednm z velice

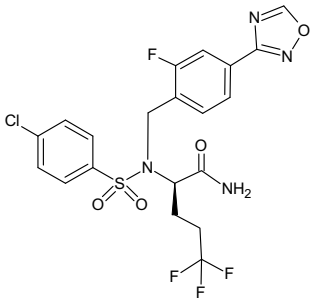

Obr. 4. **Chemická struktura BMS-708163**

rizikovch faktor ů pro rozvoj nemoci je zvená koncentrace amyloidogennho proteinu. Toto plat pro p řirozeně se vyskytujc proteiny, které se mohou abnormáln ě hromadit při patologickch stavech (nap ř. Aβ ve sporadickch formách AD) a také abnormáln formy nativnch protein ů patologicky generovanch bu ď specifickmi enzymy (např. hyperfosforylované tau proteiny při tauopatii), nebo v důsledku mutac kdovanch gen ů[24].

Inhibice enzymů t ěpc prekurzorov protein na fragmenty proteinu představuje jeden z terapeutickch p řstupů prevence patologického hromaděn a agregace amyloidogennch protein ů. Příkladem je A β, kter vzniká z glykoproteinu APP postupnm p ůsobenm dvou enzym ů β-sekretasy (BACE-1) a γ-sekretasy. Naopak od α-sekretasa, která t ěp APP v A β oblasti a zabraňuje tvorbě Aβ. V tomto přpad ě inhibice BACE-1, aktivace α-sekretasy a inhibice γ-sekretasy mohou bt pouity jako potenciáln terapeutické p řstupy k prevenci akumulace A β (cit.[24]). Nicméně jejich úplná inhibice může vést k závanm vedlejm ú činkům, jeliko maj dal substráty, které jsou spojeny s buněčnmi procesy, proto je vhodn ěj vyváená inhibice. P říkladem inhibitoru γ-sekretasy je BMS-708163 (viz obr. 4), kter se dostal do fáze klinickch testů[24].

Dal slibnou strategi pro zablokován agregace je inhibice konformačnho p řechodu, kter zahrnuje: 1) stabilizaci nativn konformace proteinu (nap ř. indukce fyziologickch chaperon ů), 2) zásahy do procesu přechodu (např. inhibitory na bázi peptidů a malch molekul) a 3) inhibice indukujc látky (nap ř. inhibice patologickch chaperonovch molekul) [24]. kolem chaperon ů je zprostředkovat správné sbalen protein ů a usnadnit přenos patn ě sloeného proteinu do proteazomu k degradaci. Z tohoto důvodu molekuláran aktivace chaperonu m ůe zvit p řirozenou schopnost buňky přemoci pokozené nebo patn ě sloené proteiny. Jako příklad lze uvést Hsp70 (heat shock protein 70), kter je schopen interagovat s rozpustnmi α-synukleinovmi monomery zamezenm jejich oligomerizaci. Látka, která aktivuje odezvu na Hsp (pravděpodobně Hsp70), je arimoclomol (viz obr. 5) a vrazn ě oddaluje progresy onemocněn amyotrofické lateraln sklerzy na

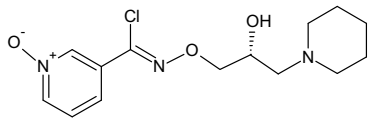

Obr. 5. **Chemická struktura arimoclomolu**[24]

modelu my, a to i v p řpad ě, e byla lé čba zahájena po nástupu přznak ů[24,41].

Stabilizace prekurzorovch protein ů může bt dosaena pomoc protein ů nebo malch molekul, které se vá-ou na prekurzorov protein, inhibuj jeho neádouc konformačn zm ěny a následnou agregaci[41]. Protein blokujc určit clov amyloidogenn protein se skládá z modifikované základn sekvence clového proteinu, která vykazuje vysokou afinitu pro clov protein a nen schopná organizace do β-skládaného listu[24]. Teorie aromatickch interakc jako hnac sly pro tvorbu amyloidu hraje roli ve v-voji malch molekul inhibitor ů[17]. Bylo prokázáno, e n ěkteré polyfenoly doká vznamn ě inhibovat tvorbu fibrilárnch sestav *in vitro* a jejich následnou cytotoxicitu[23,41,42]. Polyfenoly, zejména pak fenolické kyseliny a flavonoidy, rovně p ůsob jako lapa če volnch radikál ů a prokázaly se u nich prospěné ú činky při chronickém a degenerativnm onemocněn. Ukazuje se, e řada polyfenolů inhibuje tvorbu amyloidů *in vitro*[42] (např. apomorfin inhibuje Aβ (cit.[42]), kurkumin inhibuje TTR fibrilaci[43]). Pro inhibici mechanismu tvorby amyloidnch fibril malmi polyfenolickmi molekulami jsou dva p ředpoklady: (1) Specifická strukturáln konformace je nezbytná pro interakci β-skládanch list ů a stabilizaci komplexu s inhibitorem proteinu. (2) Aromatické interakce mezi fenolickmi sloučeninami v molekule inhibitoru a aromatickch zbytk ů (hlavně fenylalaninu) v sekvenci může nasm ěrovat inhibitor na amyloidogenn jádra, čm se usnadn interakce a zabrán se následn ě tvorbě fibril[23]. Jinou látkou, která má siln inhibi čn ú činek konkrétně na agregaci Aβ40 peptidu, je aniontov polyelektrolyt poly(4-styrensulfonát) [44].

Dal strategie v oblasti lé čby je za pomoc inhibice patologickch chaperonovch molekul. Termn patologické chaperony zavedli Wisniewski a Frangione pro popis skupiny proteinů, které aktivně podporuj konforma čn přechody specifickch protein ů pro určité onemocněn a stabilizuj konformace, které jsou náchylné pro agregaci. Příkladem patologického chaperonu pro A β agregaci v AD je E4 isoforma apolipoproteinu E. Navrhované strategie v této oblasti jsou soustředěna na vvoj bu ď chaperonovch mimetik (slou čeniny podobné chaperonovm molekulám, které by se přednostně vázaly na agregujc peptid a bránily by jim reagovat s patologickmi chaperony), nebo rozpustná netoxická peptidová analoga (které napodobuj nteragujc sekvenci, ale nejsou schopné se patn ě sloit). Je dokázáno, e kovy mohou p ůsobit jako patologické chaperony, dky esenciálnm rolm t ěchto kovů v mnoha biologickch procesech je vzkum sm ěřován spe na látky zeslabujc komplex kov-protein ne na chelatačn činidla[24].

Jeliko vechny amyloidy sdl spole čné strukturn motivy, jednou z dalch novch strategi lé čby je monost, e protilátky proti amyloidovm loisk ům mohou zvit jejich degradaci. V minulosti se ukázalo, e vakcinace sebou nese vysoká rizika, ale i přes vysoká rizika zůstává imunoterapie zajmavou strategi a v sou časnosti se zkoumaj jak pasivn, tak aktivn imunologické p řstupy. Příkladem je protilátka MABT5102A, také známá jako anti-Aβ, která byla pouita pro aktivn imunizaci ke zven progresivnho t ěpen A β (cit.[24]).

Selhán proteolytickch systém ů je společnm rysem poruch agregace a ukazuje se, e má kl čovou roli v patogenezi onemocněn. Z tohoto d ůvodu urychlen odklzen agregátu, poslenm hlavnch bun ěčnch cest pro odstraňován mutantnch protein ů nebo podpora specifickch aktivit proteasy, m ůe p ředstavovat dal p řstup pro léčbu onemocněn. Jednou z monost tohoto sm ěru je regulace ubiquitin-proteasomového systému (UPS) a autofagie. Obecně plat, e bu ňky odstraňuj patn ě sloené cytosolické proteiny dvěma hlavnmi cestami: pomoc UPS a autofagie. UPS je zodpovědn za degradaci krátce ijcch patn ě sloench nebo pokozench rozpustnch proteinů a může hrát vraznou roli p ři odstraňován amyloidogennch protein ů. Autofagie je primárnm mechanismem podlejc se na odbouráván stabilnch protein ů s dlouhou ivotnost. Z terapeutického hlediskaje UPS ideálnm clem pro odstran ěn rozpustnch krátkch patn ě sloench protein ů/peptidů, zatmco poslen autofagie dává přednost odstraněn v ětch toxickch oligomernch komplexů.

5. Závěr

Amyloidzy jsou r ůzné nemoci či patologické stavy, při kterch je kone čnm vsledkem p řechodu normálně rozpustnch protein ů v nerozpustn útvar zvan amyloid, kter má fibriláru strukturu. Krom ě proteinu, u kterého převauje v amyloidech sekundárn struktura β-skládan list, osahuje dal komponenty, jako jsou glykosaminoglykany, SAP a apolipoproteiny. Amyloidy se ukládaj v tkánch a naruuj jejich funkci [10].

Léčba se li v závislosti na typu amyloidzy. Vánm typem amyloidz jsou systémové, jeliko problémem současné léčby je, e pouze prodluuje pacient ův ivot, a i kdy se medián p řeit zvil, často je prognza infaustn. U lokalizovanch forem bvá po lé čbě úspěn ě dosaeno kontroly nemoci. Vjimkou u t ěchto forem je např. Alzheimerova choroba, protoe sou časná léčba pouze mrn symptomy nemoci. Novch monost lé čby je celá řada a experimentáln lé čba nen zam ěřena pouze na vvoj látek, které maj specifickm zp ůsobem působit na amyloidogenn protein a zamezit tak jeho fibrilaci, ale je zam ěřena i na okoln komponenty, jako jsou nap ř. enzymy t ěpc prekurzorové proteiny, chaperony, SAP a apolipoproteiny.

Tato práce byla podpořena Ministerstvem kolstv, mládee a t ělovchovy ČR v rámci Národnho programu udritelnosti I (NPU I), projekt POLYMAT LO1507.

Seznam zkratek

AD	Alzheimerova choroba
AMPA	α-amino-3-hydroxy-5-methyl-4-isoxalon
Aβ	amyloid beta
BACE-1	β-sekretasa
CNS	centráln nervová soustava
FAP	dědičná amyloidn polyneuropatie
Hsp70	heat shock protein 70
IAChE	inhibitory acetylcholinesterasy
NMDA	*N*-methyl-D-asparagová kyselina
ROS	reaktivn formy kyslku
SAA	sérov amyloid A
SAP	sérov amyloidov protein
UPS	ubiquitin-proteasov systém

LITERATURA

1. Radford S. E., Weissman J. S.: J. Mol. Biol. *421*, 139 (2012).
2. Sideras K., Gertz M. A.: Adv. Clin. Chem. *47*, 1 (2009)
3. Sipe J. D.: *Amyloid Proteins. The Beta Sheet Conformation and Disease.* Wiley-VCH, Weinheim 2005.
4. Hazenberg B. P. C.: Rheum. Dis. Clin. North. Am. *39*, 323 (2013).
5. Fowler D. M., Koulov A. V., Alory-Jost C., Marks M. S., Balch W. E., Kelly J. W.: PLoS Biol. *4*, 0100 (2006).
6. Dueholm M. S., Nielsen S. B., Hein K. L., Nissen P., Chapman M., Christiansen G., Nielsen P. H., Otzenet D. E.: Biochemistry *50*, 8281 (2011).
7. Cherny I., Gazit E.: Angew. Chem., Int. Ed. *47*, 4062 (2008).
8. Benson M. D., v knize: *Emery and Rimoin's Essential Medical Genetics* (Rimoin D. L., Pyeritz R. D., Korf B. R., ed.), kap. 78. Elsevier Ltd., Amsterdam 2013.
9. Sipe J. D., Benson M. D., Buxbaum J. N., Ikeda S-I., Merlini G., Saraiva M. J. M., Westermark P.: Amyloid *17*, 101 (2010).
10. Picken M. M.: Adv. Anat. Pathol. *20*, 424 (2013).
11. Iannuzzi C., Maritato R., Irace G., Sirangelo I.: Int. J. Mol. Sci. *14*, 14287 (2013).
12. Rochet J-C., Lansbury P. T.: Curr. Opin. Struct. Biol. *10*, 60 (2000).
13. Serpell L. C., Sunde M., Benson M. D., Tennent G. A., Pepys M. B., Fraser P. E.: J. Mol. Biol. *300*, 1033 (2000).
14. Lazo N. D., Downing D. T.: Biochemistry *37*, 1731 (1998).
15. Sipe J. D., Cohen A. S.: J. Struct. Biol. *130*, 88 (2000).
16. Merlini G., Bellotti V.: N. Engl. J. Med. *349*, 583 (2003).
17 Gazit E.: FEBS J. *272*, 5971 (2005).
18. Makin O. S., Atkins E., Sikorski P., Johansson J., Serpell L. C.: Proc. Natl. Acad. Sci. *102*, 315 (2005).
19. Makin O. S., Serpell L. C.: FEBS J. *272*, 5950 (2005).
20. Marshall K. E., Morris K. L., Charlton D., OReilly N.: Biochemistry *50*, 2061 (2011).
21. Chiti F., Dobson C. M.: Annu. Rev. Biochem. *75*, 333 (2006).
22. Chi E. Y., Krishnan S., Randolph T. W., Carpenter J. F.: Pharm. Res. *20*, 1325 (2003).
23. Porat Y., Abramowitz A., Gazit E.: Chem. Biol. Drug. Des. *67*, 27 (2006).
24. Bartolini M., Andrisano V.: ChemBioChem *11*, 1018 (2010).
25. Hawkins P. N.: Ann. Rheum. Dis. *56*, 631(1997).
26. Lachmann H. J., Hawkins P. N.: Curr. Opin. Pharmacol. *6*, 214 (2006).
27. Palladini G., Merlini G.: Haematologica *94*, 1044 (2009).
28. Sattianayagam P. T., Gibbs S. D. J., Pinney J. H., Wechalekar A. D., Lachmann H. J., Whelan C. J., Gilbertson J. A., Hawkinset P. N., Gillmore J. D.: Am. J. Transplant. *10*, 2124 (2010).
29. Benson M. D., v knize: *Encyclopedia of Life Sciences*, kap. 2146, J. Wiley, Chichester 2001.
30. Javaid M. M., Rumjon A., Coats T.: Int. J. Nephrol. Renovasc. Dis. *2012*, 37.
31. Stangou A. J., Heaton N. D., Hawkins P. N.: N. Engl. J. Med. *352*, 2356 (2005).
32. Ghiso J., Frangione B.: Adv. Drug. Deliv. Rev. *54*, 1539 (2002).
33. Mount C., Downton C.: Nat. Med. *12*, 780 (2006).
34. Scarpini E., Scheltens P., Feldman H.: Lancet Neurol. *2*, 539 (2003).
35. Hirschfield G. M., Hawkins P. N.: Int. J. Biochem. Cell Biol. *35*, 1608 (2003).
36. Bednářk J., Ambler Z., R ůi čka E.: *Klinická Neurologie.* Triton, Praha 2010.
37. Winslow B. T., Onysko M. K., Stob C. M., Hazlewood K. A.: Am. Fam. Phys. *83*, 1403 (2011).
38. Nordberg A., Ballard C., Bullock R., Darreh-Shori T., Somogyi M.: Prim. Care Companion CNS Disord. *15*, PCC.12r01412 (2013).
39. Kozurkova M., Hamulakova S., Gazova Z., Paulikova H., Kristian P.: Pharmaceuticals *4*, 382 (2011).
40. Simoni E., Daniele S., Bottegoni G., Pizzirani D., Trincavelli M. L., Goldoni L., Tarozzo G., Reggiani A., Martini C., Piomelli D., Melchiorre C., Rosini M., Cavalli A.: J. Med. Chem. *55*, 9708 (2012).
41. Hrd T., Lendel C.: J. Mol. Biol. *421*, 441 (2012).
42. Doig A. J., Derreumaux P.: Curr. Opin. Struct. Biol. *30*, 50 (2015).
43. Ferreira N., Saraiva M. J., Almeida M. R.: FEBS Lett. *585*, 2424 (2011).
44. Ojha B., Liu H., Dutta S., Rao P. P., Wojcikiewicz E. P., Du D.: J. Phys. Chem. B *117*, 13975 (2013).

M. Holubová and M. Hrub *(Institute of Macromolecular Chemistry, Academy of Sciences of the Czech Republic, Prague):* **Therapeutics Against Amyloidosis**

The first part of this review deals briefly with the concept of amyloid, which is associated with the group of diseases called amyloidoses. The second section brings a brief overview of current clinically used therapeutics for selected types of amyloidoses. In the last section, examples are described of new experimental therapies of amyloidoses, which are currently under investigation.

Publication 2

RSC Advances

PAPER

View Article Online
View Journal | View Issue

Cite this: *RSC Adv.*, 2017, **7**, 53887

Carbon nanospecies affecting amyloid formation†

M. Holubova,[ab] R. Konefał,[a] Z. Moravkova,[a] A. Zhigunov,[a] J. Svoboda,[a] O. Pop-Georgievski,[a] J. Hromadkova,[a] O. Groborz,[a] P. Stepanek[a] and M. Hruby*[a]

Carbon nanospecies (CNPs) are of high interest in current research due to their many unique properties. They may be created by common processes, such as burning. Therefore, they can become potential contaminants and may have a negative impact on human health and the biosphere. Moreover, they may also catalyze protein misfolding and subsequent amyloid formation, which is extremely hard to treat. We investigated the influence of single-walled carbon nanotubes (SWNTs), fullerene (C_{60}), carbon quantum dots (CDs) and nanodiamonds (NDs) on amyloid formation. This research utilized the hen egg-white lysozyme (HEWL) as a model system. Fibrils were detected by fluorescence of thioflavin-T (ThT) or Nile red (NR) and the results were confirmed by transmission electron microscopy (TEM). We have found that NDs promoted amyloid fibril formation at all concentrations. The highest concentration of C_{60} (250 μg ml^{-1}) accelerated the process of fibrillation, while smaller concentrations (16 and 80 μg ml^{-1}) prolonged the lag phase and were comparable to the control. SWNTs prolonged the lag phase of amyloid formation at all concentrations. CDs efficiently terminated the growth of amyloid fibrils. When we compared the amyloidogenicity of all four types of CNPs, the following trend was apparent: NDs > control > C_{60} > CDs > SWNTs.

Received 13th October 2017
Accepted 13th November 2017

DOI: 10.1039/c7ra11296c

rsc.li/rsc-advances

Introduction

Amyloidosis is a group of diseases associated with the deposition of normally soluble proteins in the form of insoluble amyloids. These amyloids deposit in various organs and tissues and cause their dysfunction and thus pose a major threat to human health.[1,2] However, not all amyloids are unhealthy and pathological. There are functional amyloids of specific proteins, which, for example, are used by mammals for the production of melanin[3] and in bacteria such as *Escherichia coli* to form scaffolding for biofilms.[4] The high stability, organized character and nanometric dimensions of amyloids make them excellent candidates for the production of nanomaterials (*e.g.*, wires, gels, scaffolds, liquid crystals, *etc.*) using a "bottom-up" approach.[5]

All amyloids share several physicochemical features such as a fibrillar morphology, secondary structure of the β-sheet, insolubility in common solvents and detergents, birefringence after staining with Congo red and resistance to proteases. The amino acid sequences and proteins structures associated with amyloidosis vary greatly[6] even though they share some structural similarities especially in the phenylalanine-rich sequences responsible for self-assembly.[7]

The formation of amyloid fibrils is a very complex process and short peptides are used for closer study of these processes. Peptides that are certain fragments of the precursor protein also have the ability to generate typical amyloid fibrils. A common feature of short peptides generating amyloid fibrils is the high occurrence of aromatic residues,[8] showing that π–π interactions play an important role in the formation of amyloid fibrils. Hydrophobic interactions are among the significant interactions in the aggregation and stabilization of amyloid fibrils.[9,10] Furthermore, electrostatic interactions have other effects on fibrillation and stabilization.[9,11]

Carbon nanospecies (CNPs), such as fullerenes (C_{60}), carbon quantum dots (CDs), single- (SWNTs) and multiwalled carbon nanotubes (MWNTs), or nanodiamonds (NDs), are of high interest in current research due to their many unique properties. These nanomaterials are produced by high-tech methods; meanwhile they may also be created by common processes (Fig. 1), such as the burning and pyrolysis of organic materials, arc discharge welding and explosions. Therefore, CNPs can occur in nature and become potential contaminants,[12] but their amyloidogenicity is still not sufficiently clear.

C_{60} is a stable compound consisting of 60 carbon atoms (molecular weight 720.66 g mol^{-1}) with a diameter of approximately 0.7 nm, which is roughly the size of many active pharmaceutical ingredients. Thirty carbon–carbon double bonds are present in the structure, to which free radicals can easily be added.[13]

SWNTs have a typical diameter of between 1 nm (approximately 10 atoms around the cylinder) to 5 nm, with a tube

[a]*Institute of Macromolecular Chemistry, Academy of Sciences of the Czech Republic, Heyrovský Sq. 2, 162 06 Prague 6, Czech Republic. E-mail: mhruby@centrum.cz*
[b]*Charles University in Prague, Faculty of Science, Albertov 6, 128 43 Prague 2, Czech Republic*

† Electronic supplementary information (ESI) available. See DOI: 10.1039/c7ra11296c

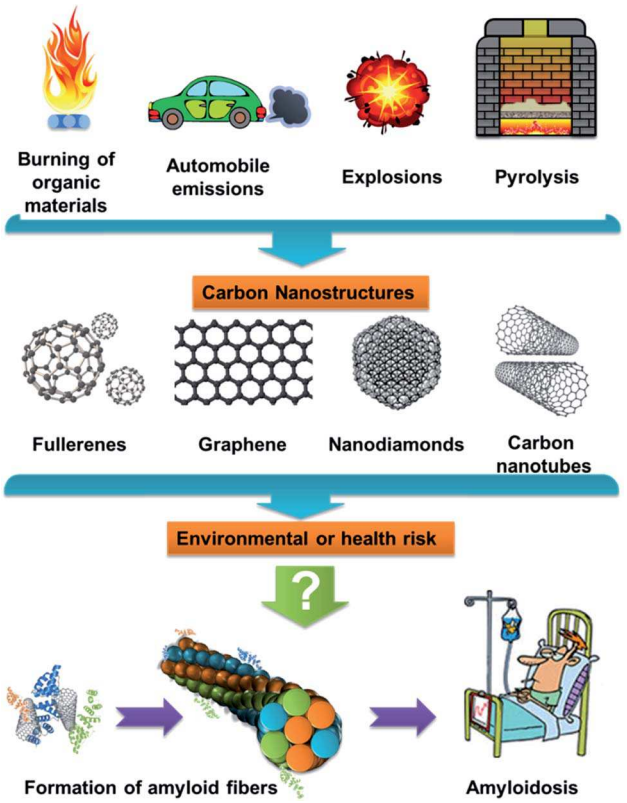

Fig. 1 Scheme of potential paths of CNPs.

length that can range from 1 nm to 1 mm. During their synthesis, Co, Fe, Ni, and Mo are used as catalyzers, which may appear in the final product as residual metal contaminants.[14] C_{60} (ref. 13) and SWNTs[15] contain sp^2-hybridized carbon and therefore may be amyloidogenic, as the aromatic interactions play a key role in amyloid fibrils formation, they may also inhibit amyloid fibrils formation.

NDs consist of sp^3-hybridized carbon and surface groups. They can occur in different size ranges with positive or negative charges depending on their production method.[16] NDs have been synthesized most commonly using a detonation technique,[17,18] but they can also be formed with chemical vapor deposition[18,19] or laser ablation.[19] NDs have interesting properties such as superior hardness and Young's modulus, and optical properties.[19] NDs additives have been used for electrolytic metal plating for many years. More recently, they have been used in other applications such as in magnetic resonance imaging, chromatography, tribology; nanocomposites; drug delivery and other applications.[19,20]

CDs are a type of carbon-based fluorescent nanomaterials with sizes under 10 nm. When comparing CDs with traditional semiconductor quantum dots and organic dyes, CDs are superior in terms of their high solubility in water, facile modification and high resistance to photobleaching. They have excellent biological properties such as low toxicity and good biocompatibility facilitating their application in bioimaging and biomolecule/drug delivery systems. There is a wide range of applications for CDs. Because they have excellent electrical properties as electron donors and acceptors, causing chemiluminescence and electrochemical luminescence, they could be used in optoelectronics or sensors.[21,22] CDs can be prepared by "top-down" or "bottom-up" methods. The "top-down" methods are based on carving bulk carbon materials into nanoparticles using physical or chemical approaches, such as acid oxidation, electrochemical and hydrothermal methods.[23–27] Compared with "top-down" methods, the "bottom-up" methods have obvious advantages in adjusting the composition and physical properties of CDs through the careful selection of different organic precursors and carbonization conditions. "Bottom-up" methods include microwave irradiation, hydrothermal/solvothermal treatment or pyrolysis.[23,28,29] The microwave irradiation of proper carbon sources has many advantages *e.g.*, low cost, speed, efficiency and ease of production.[30,31] Very often, natural sources (glucose,[24,32,33] fructose,[32] citric acid,[24,34,35] urea[24,36] and amino acids[37,38]) are used for the preparation of CDs. Thanks to these known facts, CDs are likely to appear even in common processes that occur during cooking.

The hen egg-white lysozyme (HEWL) is a small protein with four disulfide bonds.[39] This protein has been studied as a model of the human lysozyme,[40] whose mutation (sharing 60% of its sequence identity with HEWL) is associated with hereditary systemic amyloidosis.[41] The release of CNPs into the environment may occur as a results of common processes, such as CNPs production, CNP-containing product manufacturing, and the use and reuse of CNPs products.[42] Therefore, they may have a negative impact on humans and the biosphere. Moreover, they may also catalyze protein misfolding and subsequent amyloid formation, which are extremely hard to treat. Testing for amyloidogenicity has already been carried out with some CNPs,[43] but comparisons of CNPs have never been carried out on one type of protein model system. Based on all the previous information, we decided to study and compare the effects of several selected CNPs (SWNT, C_{60}, NDs and CDs) on HEWL to determine their risks and study their amyloidogenicity. The obtained results may be useful for the production of CNPs and their subsequent use.

Results and discussion

First, we made a detailed characterization of prepared CDs. For other types of particles (NDs, SWNTs, C_{60}), we performed a brief characterization before testing them on HEWL.

Carbon quantum dots

The CDs were obtained a black-brown solution, which was diluted to a light-yellow solution (0.0005 wt%) with blue emission under a UV lamp with a wavelength of 366 nm. The measured ζ-potential of the CDs was −31.2 mV. Elemental analysis (EA) revealed the composition of the CDs to be C 41.94 wt%, H 4.33 wt%, N 19.36 wt% and O (calculated) 34.38 wt%.

For measuring the spectra, we used an aqueous solution with a concentration 0.005 wt% CDs. It has a broad absorption spectrum with maxima at 273 nm, 344 nm and 404.5 nm (Fig. 2A).

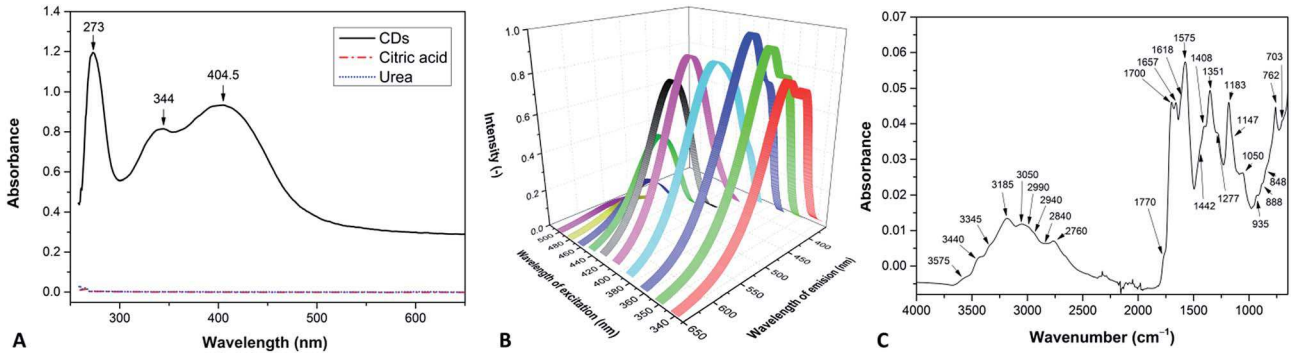

Fig. 2 (A) UV-Vis absorption spectrum, (B) PL spectra at various excitation wavelengths and (C) FTIR spectrum of the CDs.

It exhibits excitation-wavelength-dependent photoluminescence (PL) properties ranging from 455 nm (blue) to 549 nm (green) at excitations from 340 nm to 500 nm. The strongest fluorescence emission band located at 460 nm is observed for 360 nm excitation (Fig. 2B).

The functional groups were detected by Fourier transform infrared (FTIR) spectroscopy (Fig. 2C). The spectra were determined using tables in the literature.[44] The structural band spreading from 3500 to 2600 cm^{-1} belongs to the O–H and N–H stretching vibrations, with a contribution of the C–H stretching vibrations at approximately 2760 cm^{-1}. The bands at 1770 and 1700 cm^{-1} are attributed to C=O stretching vibrations (in oxo- and carboxylic groups, respectively), C=N stretching vibration appears as a band at 1657 cm^{-1}. The N–H deformation vibration absorbs approximately 1575 cm^{-1}. The group of bands approximately 1351 cm^{-1} is due to C–H and O–H deformation vibrations, and contributions from the aromatic C=N stretching are also possible. The band at 1183 cm^{-1} is assigned to the C–N stretching vibration and the band at 1050 cm^{-1} corresponds to the C–O stretching vibration. Absorption in the region below 1000 cm^{-1} is caused by out-of-plane O–H and N–H deformation vibrations and skeletal vibrations of the O- and N-rich carbon materials.

The composition of the CDs was examined by X-ray photoelectron spectroscopy (XPS) and EA (Table 1). The well-corroborated data were further supplemented by determining the covalent structure of the individual functionalities giving rise to characteristic features in the high resolution C 1s, N 1s and O 1s XPS spectra of the CDs (Fig. 3). The C 1s envelope could be resolved with contributions arising from sp^2, sp^3, C–N and C–O, C=O and C(=O)–O moieties centered at 284.3, 285.0, 286.7, 288.1 and 289.9 eV, respectively.[45] The N 1s envelope was characterized by a dominant C–N contribution at 399.7 eV and charged C–NH_3^+ moieties at 401.3 eV, thus verifying the nitrogen doping of the performed CDs arising from urea. Concomitantly, the O 1s spectrum showed the presence of carbonyl O=C moieties at 531.4 eV and O–C moieties of the hydroxyl and ether groups at 533.3 eV. The XPS results indicate that the surface structure of the CDs is heterocyclic with aliphatic defects mainly reflected in sp^3 carbon species.

Small-angle X-ray scattering (SAXS) was used to characterized the CDs in water. Form Fig. 4, one can see the scattering curves, corresponding to the samples with 3 wt%, 5 wt%, 7.5 wt% and 10 wt% CD contents. The intensity was normalized by the concentration. The curves coincide at larger q-values. The intensity slope in this region is approximately 2.5, which indicates rough interface. The influence of the concentration is clearly visible at the lower q-region, where we note difference in the intensity upturn. Such behavior means that the CDs were partially aggregated, and if we assume the same shape, the

Table 1 Composition of the CDs determined by XPS and elemental analysis. For the sake of comparison with XPS, the oxygen content in the CDs from the EA was obtained by subtracting C, H and N from 100 wt%

	Functionality	XPS individual contributions [wt%]	XPS total [wt%]	EA [wt%]
C	C=C	10.1 ± 1.3	50.1 ± 0.8	43.9 ± 0.1
	C–C	14.4 ± 1.2		
	C–N, C–O	6.2 ± 0.1		
	C=O	18.5 ± 0.4		
	C(=O)–O	0.9 ± 0.2		
N	C–N	17.7 ± 0.5	19.9 ± 0.6	20.2 ± 0.1
	C–NH_3^+	2.2 ± 0.3		
O	O=C	27.1 ± 0.5	30.0 ± 0.3	35.9 ± 0.1
	O–C	2.9 ± 0.4		

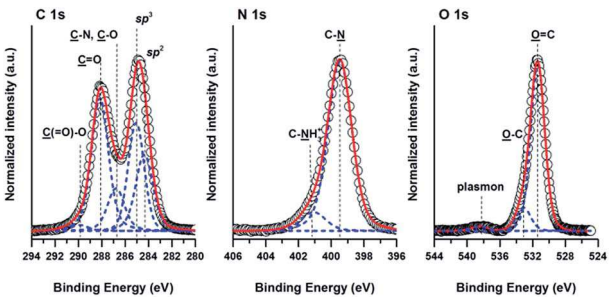

Fig. 3 High-resolution C 1s, N 1s and O 1s XPS spectra of prepared CDs. Measured spectra are presented with black circles, while their corresponding fitted envelopes are presented with red lines. The individual contributions of different functional groups present in the CDs are represented with blue lines.

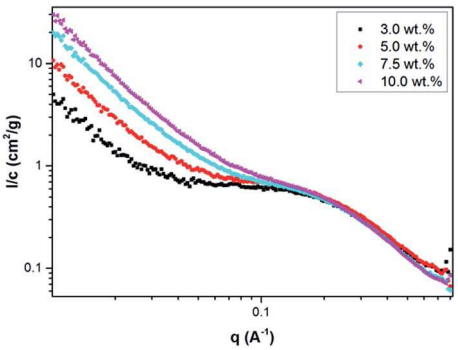

Fig. 4 SAXS curves, normalized by concentration, corresponding to 3.0 wt% (black squares), 5.0 wt% (red rings), 7.5 wt% (light-blue rhombi) and 10 wt% (pink triangles) CDs in water.

aggregates size is smaller for the lower concentration sample. The radius of gyration for the separated particles, which are clearly observed as a shoulder in the middle q-range, is approximately $R_g = 6.8$ Å for all the concentrations. Assuming spherical objects the radius could be calculated as

$$R = \sqrt{\frac{5R_g^2}{3}}$$

That will give us the volume, $V = 2835$ Å^3. As expected, the intensity, extrapolated to $q = 0$, I_0, was roughly the same for all solutions. On the I/c scale, we obtained $I_0 = 0.77$ cm^2 g^{-1}. According to the equation for determining the molecular weight,

$$M_w = \frac{I_0}{c}\frac{N_A}{\Delta b^2}$$

where c is concentration, Δb^2 is scattering contrast and N_A is Avogadro's number. One should know the density of the particles in order to calculate the scattering contrast, but we were not sure about this value. Also due to the presence of aggregates, it was impossible to estimate the scattering contrast of the particles from invariant,[46] but we were observing the higher transmittance for the higher concentrations and that means that the linear absorption coefficient of the CDs is lower than for water. To fulfill this observation particle density should be lower than 1.5 g cm^{-3}. The knowing transmission and the sample thickness (measured by optical microscope), we have estimated the density approximately 1.3 g cm^{-3}. Now we could calculate the scattering contrast and the molecular weight of the particles, which was 1817 g mol^{-1}.

The last characterization method was nuclear magnetic resonance (NMR) spectroscopy. Fig. 5 shows ^{1}H NMR and ^{13}C NMR high-resolution spectra of the CDs in a D_2O solution measured at 295 K. In the ^{1}H NMR spectrum (Fig. 5 up), a strong solvent signal at $\delta = 4.8$ ppm and a group of signals between $\delta = 2$–4 ppm. These signals are related to proton groups with electronegative atoms in nearby, such as nitrogen and oxygen, as well as proton groups next to carbonyl groups (C=O). Additionally, the single peak detected at $\delta = 6$ ppm can be related to the proton from HC= group. Signals related to the

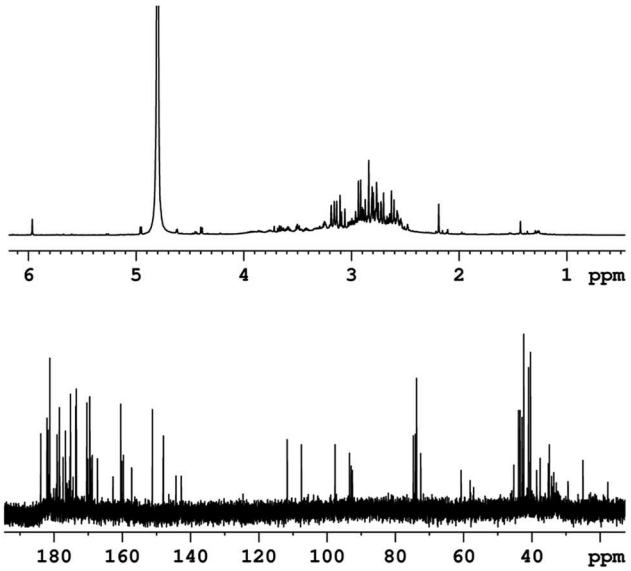

Fig. 5 ^{1}H NMR (up) and ^{13}C NMR spectra (down) of the CDs in a D_2O solution.

OH, (C=O)–OH, NH and NH_2 groups should not appear at the spectrum due to rapid chemical exchanges with the solvent. The ^{13}C NMR spectrum (Fig. 5 bottom) allows us to distinguish carbon atoms with different functionalities. Similar to the proton spectrum, carbons directly neighboring electronegative atoms (N, O), or C=O, (C=O)–O, and C=N groups are detected at $\delta = 20$–80 ppm. In the chemical shift range of $\delta = 80$–120 ppm signals from C=C carbons were observed. The existence of carboxylic acid ((C=O)–OH), carboxylate ester ((C=O)–O), amide ((C=O)–N) and imine (C=N) groups is suggested by the signals detected in the range $\delta = 140$–185 ppm.[47]

Morphology of carbon nanospecies

Nanospecies suspensions with at concentrations of 1 mg ml^{-1} were measured with dynamic light scattering (DLS) showing nanospecies with some clusters, which were also observed by TEM. Nanospecies without surface stabilization tend to create larger clusters, resulting from the high hydrophobicity. In our case, we used SWNTs and C_{60} without surface stabilization to obtain data very close to data for environmental pollutants, as surface stabilization may significantly influence the amyloidogenic activity. The size of the SWNTs clusters was 120 ± 16 nm; however the aspect ratio of carbon nanotubes must be taken into account. Fig. 6A shows very long SWNTs. C_{60} fullerenes are spherical particles, but similar to SWNT, they formed clusters in the suspension. The size measured by DLS of these clusters was 373 ± 86 nm. Fig. 6B shows only clusters of C_{60} that correspond to value measured with DLS. These clusters are similar to clusters shown in the literature.[48,49]

In case of NDs, surface groups stabilize them in solution. The surface groups of the NDs were determined with FTIR, and in addition, Raman spectroscopy measurements were performed. The FTIR spectrum of the NDs (Fig. 7B) displays O–H stretching vibrations in the region above 3000 cm^{-1}, and a weak band of

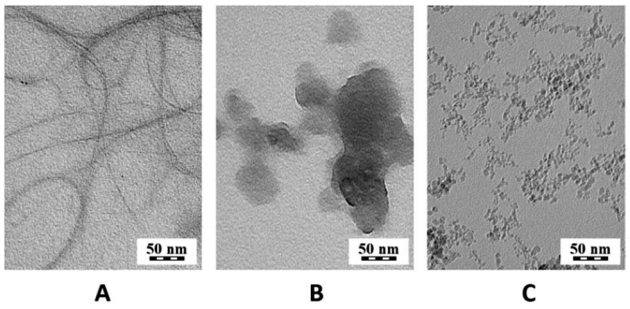

Fig. 6 TEM micrographs of (A) SWNTs, (B) C_{60} and (C) NDs.

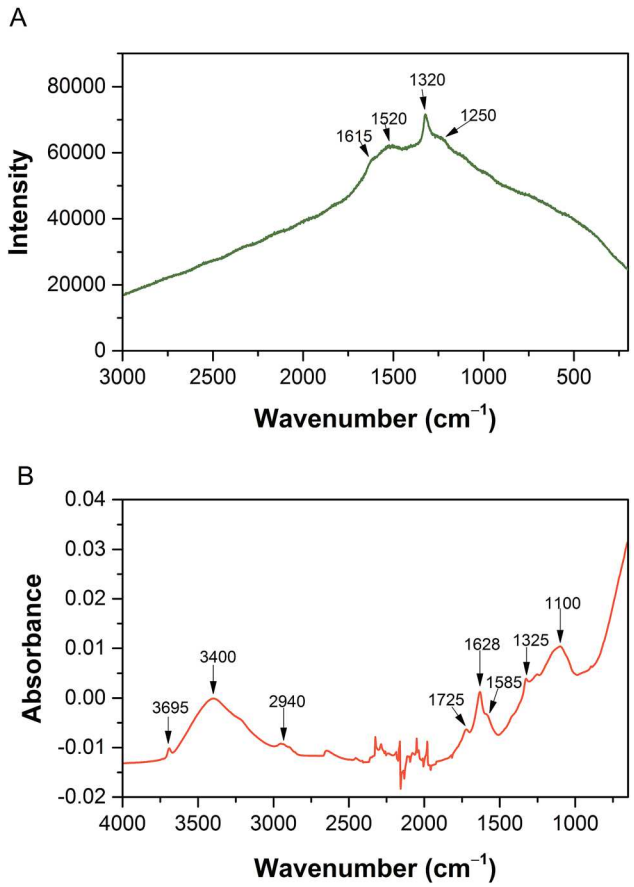

Fig. 7 (A) Raman and (B) FTIR spectra of the NDs.

C–H stretching vibrations is also observed at 2940 cm^{-1}. C=O stretching of the oxo- and carboxylic groups is observed at 1725 and 1628 cm^{-1} with a shoulder at 1585 cm^{-1}. The band at 1325 cm^{-1} is due to C–H and O–H deformation vibrations and the band at 1050 cm^{-1} is a result of the C–O stretching and C–H bending vibrations. Oxygen-based side-groups such as carboxylic, oxo- or alcohol groups strongly dominate in the NDs.

In the Raman spectrum of the NDs (Fig. 7A), a peak of C–C stretching vibrations in sp^3 carbon was detected at 1320 cm^{-1}.[50] This proves the presence of the nanodiamond structure. In addition, broad bands at approximately 1250 (C–O stretching), 1520 (non-specific C–C stretching vibrations) and 1615 cm^{-1} (C=C stretching of aliphatic structures) are visible. The bands typical of sp^2 materials at 1330 and 1570 cm^{-1} are not resolved. Furthermore, the ζ-potential, which is important for the interaction with proteins, was measured for an ND concentration of 1 mg ml^{-1} in water and was +45 ± 3 mV. Using DLS, the NDs were found to produce larger clusters 66 ± 3 nm in size and a further peak for 13 ± 5 nm. The peak for smaller particles corresponds to individual nanodiamonds in Fig. 6C. The CDs are too small and have a low contrast in TEM and the grid, on which the sample is applied, is covered with carbon; therefore CDs could not be observed in TEM.

Characterization and detection of amyloid fibrils

The generation of amyloid fibrils is much faster *in vitro* than *in vivo*,[51] but they share the some structure features. The surface of CNPs was not additionally modified to model environment-related situation as closely as possible.

The most common marker used for the rapid detection of amyloid fibrils is thioflavin T (ThT), which shows a huge fluorescence enhancement upon binding to amyloid aggregates,[52–54] but it does not interact with amyloid oligomers and protofibrils.[50] ThT is a charged molecule, therefore its binding property is different at acidic and neutral pH.[55] A very old method for detecting amyloid in tissues is Congo red staining. The Congo red staining procedure requires the use of polarized light microscopy. The diagnostic "apple green birefringence" may be difficult to visualize and therefore show low sensitivity. Unlike Congo red stain, the experiments with the ThT staining are very easy to perform and the results are much more straightforward to interpret. Another advantage of the ThT is that it detects even very small amounts of amyloid fibrils, where Congo red stain may be doubtful or false negative.[56]

Nile red (NR) can be used to detect amyloid *in vitro*. NR is an uncharged, heterocyclic fluorescence dye.[55] NR does not change fluorescence in the presence of oligomeric states while targeting more mature fibrils.[57] The results obtained from fluorescence must be confirmed by another method and the most appropriate method for a small amount of sample is TEM. TEM micrographs can be used for the qualitative comparison of features, such as the twists in ribbon-like fibrils, curvature fibril and surface smoothness. TEM micrographs can also be used for quantitative analysis, including the length of early aggregates and seeds, the width of fibrils, the number of protofilaments and the periodicity of fibril twists.[58] We used negative staining for all our experiments. This negative staining yields samples with improved contrast and well-preserved morphologies, because the stain not only provides contrast but also protects the sample from radiation damage.[58]

For our experiments, we used the fluorescence of either ThT or NR for quantification. The measured values for the samples were related to the blank that did not contain any fibrils, only the dye. TEM quantification is very complex, so we used TEM micrographs only to determine the morphology of the sample whether it was amyloid fibrils or other formations.

We chose ThT for experiments with the SWNTs, C_{60} and NDs, because ThT is more sensitive at the beginning of the

process of fibrillation. ThT cannot be used for experiments with the CDs because the spectra of ThT and CDs overlap. Based on this information we chose NR for experiments with the CDs. The CDs have a very low fluorescence even in the NR region, but NR by fluorescence exceeds CDs and therefore it can be used.

We decided to use dichloromethane (DCM) for the preparation of the dispersion, which was removed by evaporation to not influence the process of fibrillation. The dispersions were characterized with TEM and DLS (see previous sections). The stock suspensions of SWNTs and C_{60} were prepared at a concentration of 1 mg ml^{-1}. These suspensions were added to individual vials with the HEWL solution. In all samples and in the control, the amount of DCM was same value, so DCM for all the samples was bubbled with nitrogen for the same amount of time. The samples were incubated and characterized at certain times.

Fig. 8 shows a graph of the relative fluorescence of ThT for different concentrations of SWNTs and C_{60} at different times. The graph shows that the highest concentration of C_{60} (250 μg ml^{-1}) accelerated the fibrillation process. On the other hand lower concentrations of C_{60} (16 and 80 μg ml^{-1}) revealed a statistically significant deceleration of the onset of amyloid fibril formation (*i.e.*, prolonging the lag phase of amyloid fibril formation, most plausibly by the depletion of the seeds *via* preferential adsorption on the carbon nanospecies). After a short time, the difference disappears and the samples are comparable to the control. The TEM micrographs of all samples of C_{60} (Fig. 9E–G) show the typically long fibers seen in the control (Fig. 9A). In these pictures there are also some spherical particles, but these are probably artifacts that occurred during the sample preparation. The results for SWNTs differ from C_{60}. The graph (Fig. 8) shows a statistically stronger deceleration of the process of fibrillation for all samples by SWNTs compared to C_{60}, significantly prolonging the lag phase of amyloid formation, most plausibly by depleting the seeds *via* preferential adsorption on the carbon nanospecies as mentioned above for

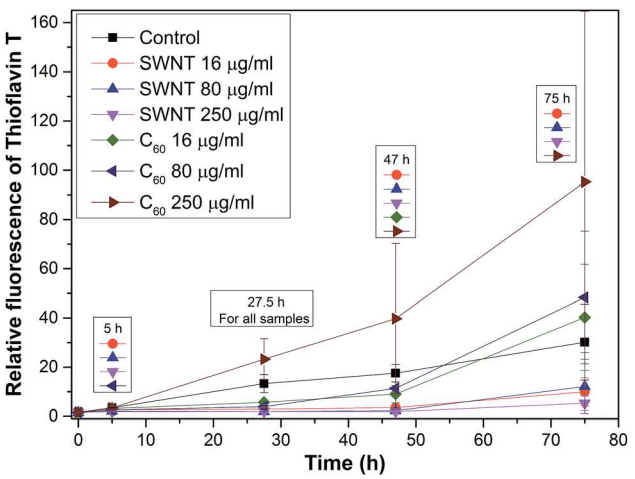

Fig. 8 A Graph of the relative fluorescence of thioflavin T in experiments with SWNTs and C_{60}, where the legend above the results from the same time represents a statistically significant difference ($\alpha < 0.05$) when compared to a control at this certain time.

C_{60}. These results are supported by TEM micrographs of samples with SWNTs (Fig. 9B–D). The TEM micrograph for the 16 μg ml^{-1} concentration SWNTs (Fig. 9B) shows typically long fibers seen in the control (Fig. 9A), but a higher concentration (80 μg ml^{-1} SWNTs) reveals shorter fibrils (Fig. 9C). The highest concentration (250 μg ml^{-1} SWNTs, Fig. 9D) had different morphology than of the control (Fig. 9A). This picture shows a fibrillary morphology, but the fibrils are thick. It seems that the growth of the fibrils is terminated on the surface of the SWNT.

NDs were used in a second experiment. The NDs suspension had 10 mg ml^{-1} concentration in water. This suspension was added to the individual vials with the HEWL solution. In all samples and the control, the amount of HEWL was same value. The samples were incubated and characterized at certain times.

Fig. 10 shows a graph of the relative fluorescence of ThT for different concentrations of NDs at different times. The graph show that all ND concentrations, except for the lowest concentration (16 μg ml^{-1}), significantly accelerated the process of fibrillation by shortening the lag phase, *i.e.*, by being efficient amyloid fibrillation initiators. This is interesting because the surface of the NDs is preferentially sp^3-carbon based, thus not allowing the π–π interactions that govern the amyloid formation. The TEM micrographs of all NDs samples (Fig. 11B–D) show long fibers as similar to in the control (Fig. 11A). In these pictures, some artifacts occurred during the preparation of the sample. Fig. 11E shows a thicker layer of fibrils, correlating to the results of the graph (Fig. 10). Based on these experiments, we can say that NDs initiate fibril growth but do not interfere in the elongation process. This finding is critical for the application of NDs in medicine.

Fig. 12 shows a graph which combines graphs from Fig. 8 and 10. Because the graph combines data from two experiments, the best combination method was the percent fibril formation. The method involves that a control at a certain time was taken as 100% and other data were calculated according to the control at this certain time. The obtained values were plotted. The graph shows a peak for all NDs samples. This peak may be due to the fact that the growth of fibrils in the presence of NDs is immediate while the control is in the lag phase (at the beginning of a fibril growth). After reaching a sufficient number of nuclei for the growth of fibrils in the control occurred the rapid growth of fibrils in the control, but the NDs samples already had a large amount of fibrils and the free protein gradually decreases in the samples to produce additional fibrils. A curve for the highest concentration of C_{60} (250 μg ml^{-1}) gradually rises accelerated the fibrillation process, which means the gradual growth of fibrils and this concentration accelerated the fibrillation process. On the other hand curves for lower concentrations of C_{60} (16 and 80 μg ml^{-1}) show a decline from the beginning, and then begin to rise. This decrease can be explained by prolonging the lag phase of amyloid fibril formation due to protein adsorption on surface. The last three curves are for samples with SWNTs. The curves show a decline that means significantly prolonging the lag phase. The curves show the growth of the fibrils can be terminated on the surface of the SWNT. Based on this comparative graph (Fig. 12), the CNPs (SWNTs, C_{60}, and NDs) and the control

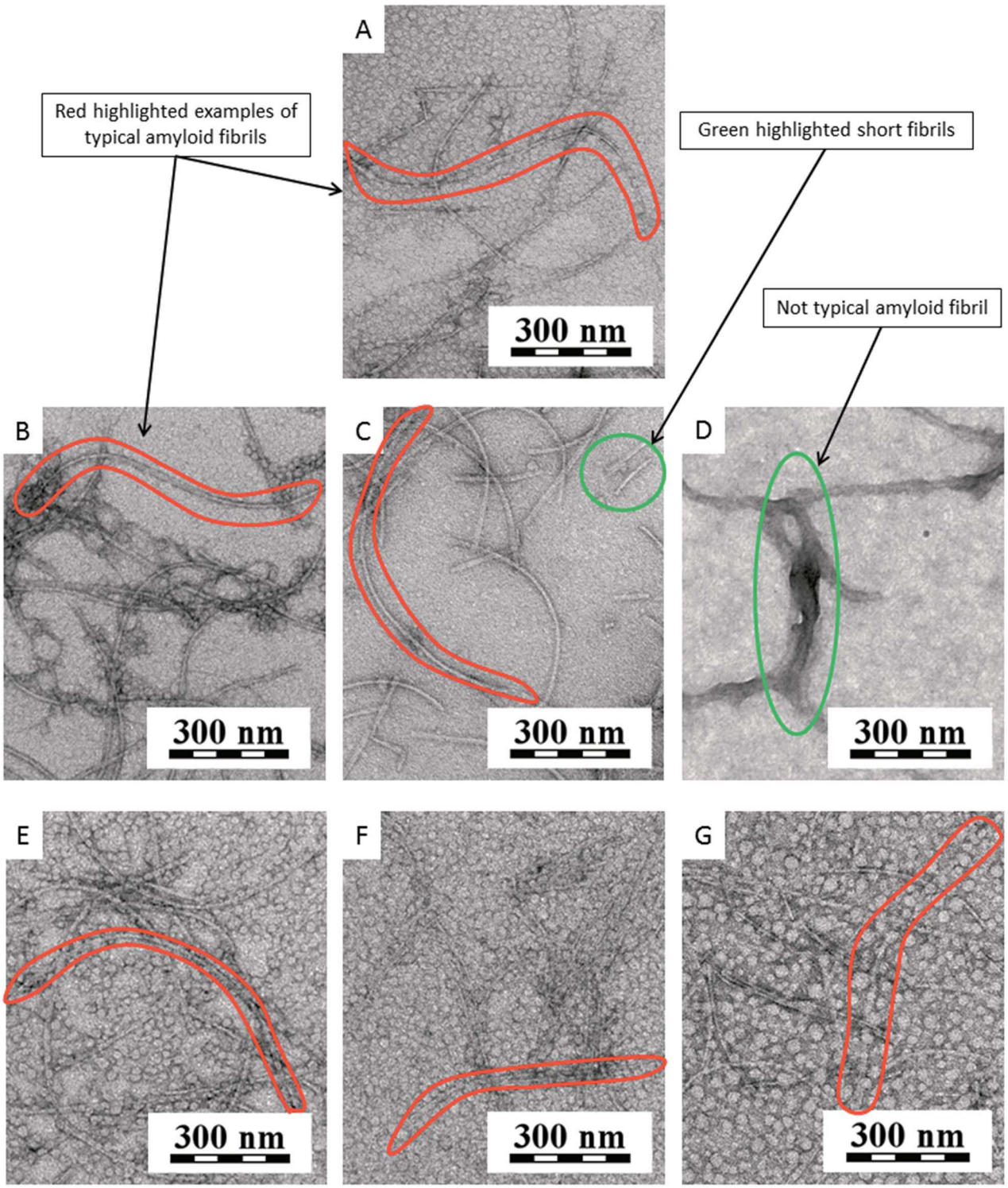

Fig. 9 TEM micrographs of experiments with SWNTs and C_{60}: (A) fibrils of HEWL (control) after 27.5 h of incubation without any nanospecies; (B) fibrils of HEWL after 27.5 h of incubation with 16 μg ml^{-1} SWNTs; (C) fibrils and shorter fibrils of HEWL after 27.5 h of incubation with 80 μg ml^{-1} SWNTs; (D) thick fibrils of HEWL after 27.5 h of incubation with 250 μg ml^{-1} SWNTs; (E) only long typically fibrils of HEWL after 27.5 h of incubation with 16 μg ml^{-1} C_{60}, (F) 80 μg ml^{-1} C_{60} and (G) 250 μg ml^{-1} C_{60}.

can be ranked from the most amyloidogenic to least in the following order: NDs > control > C_{60} > SWNTs.

CDs were used in the final experiment. The CDs were prepared as a lyophilized powder. From this powder, a suspension was prepared in water at a concentration 10 mg ml^{-1}. This suspension was added to individual vials with the HEWL solution. In all samples and the control, the amount of HEWL was same value. The samples were incubated and characterized at certain times.

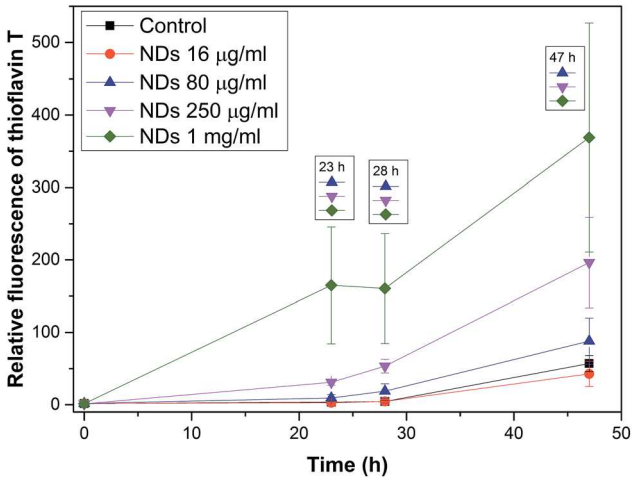

Fig. 10 A graph of the relative fluorescence of thioflavin T in experiments with NDs, where the legend above the results from the same time represents a statistically significant difference ($\alpha < 0.05$) when compared to a control at this certain time.

Fig. 13 shows a graph of the relative fluorescence of NR for different concentrations of CDs at different times. We can see that the CDs significantly affect the process of fibrillation. There is a significant deceleration for almost all concentrations. The smallest concentration of CDs (16 μg ml^{-1}) did not demonstrate any significant influence on the process. The difference from the control was only seen after a long time for the smallest concentration of the CDs. The other three concentrations of CDs (80, 250 and 1000 μg ml^{-1}) significantly decelerated the process of fibrillation. After a long time, the concentration dependence of the process deceleration was demonstrated. These results support the TEM micrographs of the samples (Fig. 14B–E). Fig. 14A shows the TEM micrographs of the control. There are typically long fibrils. The next picture (Fig. 14B) shows typically long fibrils as seen in the control, however, for a higher concentration (80 μg ml^{-1}, Fig. 14C), shorter fibrils occur. As the concentration increases, more short fibrils and clusters appear, as seen in Fig. 14D for a CDs concentration 250 μg ml^{-1}. At the highest concentration (1 mg ml^{-1}), long fibril formation is completely suppressed. The TEM micrograph (Fig. 14E) of this sample shows a completely

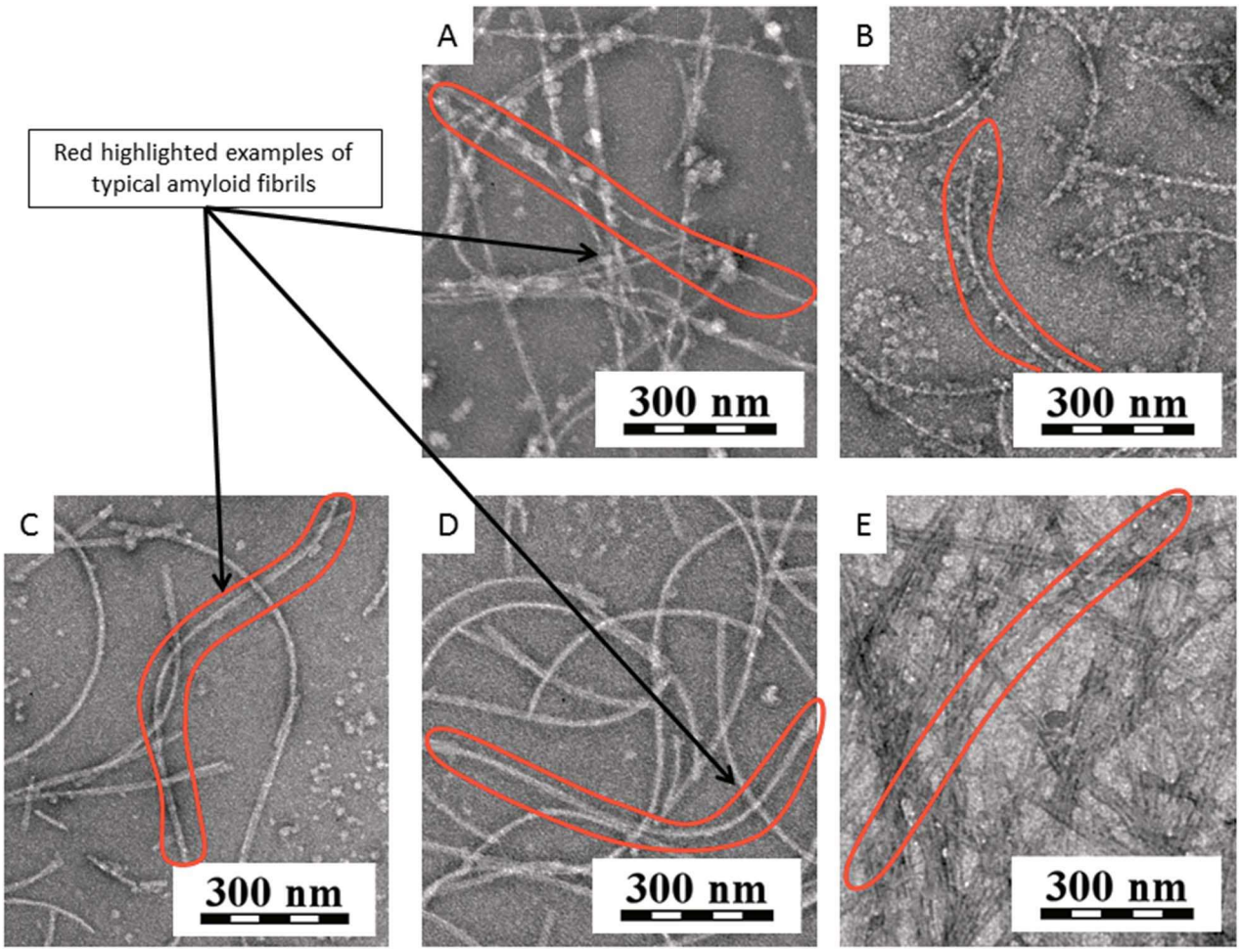

Fig. 11 TEM micrographs of experiments with NDs: (A) fibrils of HEWL (control) after 23 h of incubation without any nanospecies; (B) fibrils of HEWL after 23 h of incubation with 16 μg ml^{-1} NDs; (C) fibrils of HEWL after 23 h of incubation with 80 μg ml^{-1} NDs; (D) fibrils of HEWL after 23 h of incubation with 250 μg ml^{-1} NDs; (E) many fibrils of HEWL after 23 h of incubation with 1 mg ml^{-1} NDs.

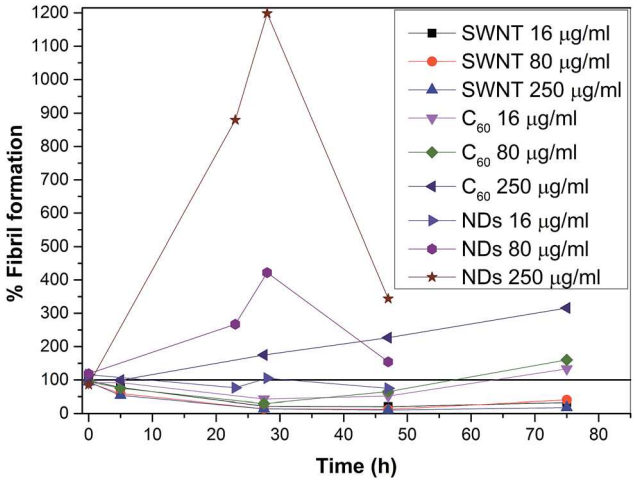

Fig. 12 The effect of different concentrations of CNPs on fibril formation. A graph combines the results from Fig. 8 and 10. The results were always related to a control at a certain time and this control was taken as 100%. The results were displayed without NDs 1 mg ml^{-1} and error bars for a clearer view.

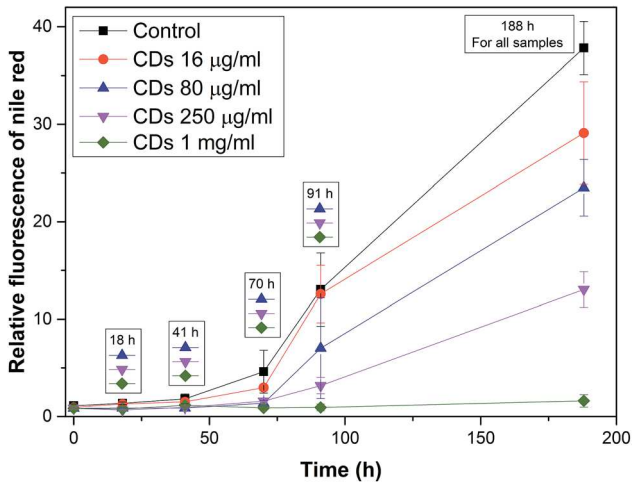

Fig. 13 A graph of the relative fluorescence of NR in experiments with CDs, where the legend above the results from the same time represents a statistically significant difference ($\alpha < 0.05$) when compared to a control at this certain time.

different morphology than of the control. These differences in morphology between the samples containing CDs and the control sample led to a difference in the NR fluorescence. The most plausible mechanism here is that CDs only minimally affect the lag phase, but they efficiently terminate growing fibrils causing their slower growth and shorter lengths (probably similar to the effects of low-molecular-weight aromatic molecules). Interestingly, we found that burnt surfaces are not amyloidogenic, and that the bacterial biofilm created is made of so-called functional amyloids. Therefore "burnt surface" may be a challenge for future applications.

The effect of different concentration of CNPs on the fibril formation is shown in Table 2. It is difficult to compare the results for all nanospecies because, for SWNTs, C_{60} and NDs ThT was used as the fluorescence dye, and NR was used for CDs. Based on the TEM micrographs and all results, CDs can be added to the previous relationship, and the order of all the CNPs is as follows: NDs > control > C_{60} > CDs > SWNTs.

We used a small globular protein (HEWL) for our experiments. In a control sample under the selected conditions (pH 2, 57 °C) occurred unfolding protein, subsequent amyloid fibrils formation. The proposed pathway of the amyloid fibril formation of HEWL according to literature[59] consists of three stages: (1) the formation of dimmers, (2) the formation of protofilaments, and (3) the formation of amyloid fibrils.[59] In order to generate dimmers, there must be large conformational changes in the secondary structure, the increase in the β-sheet structure. These changes were achieved by low pH and high temperature. The structural conversion of the proteins is a key event in the formation of the amyloid fibrils. The created dimmers are the nuclei for the formation of the protofilaments.

What happened when we added CNPs to HEWL. The SWNTs have hydrophobic surface and one side of β-sheet is also hydrophobic, so the hydrophobic interactions between SWNT and β-sheet can create a SWNT-HEWL complex. These interactions can lead to blocking of protein chain for further binding with monomer (in our case HEWL with β-sheet structures) and also it can lead to reduction of population of monomers. Because SWNTs contain sp^2-hybridized carbon atoms, not only hydrophobic interactions but also π–π interactions play a key role in process of inhibition. These interactions can have strong effect on the creation of SWNT-HEWL complex. Their effect can also be in destabilization of β-sheet structures and prolongation the lag phase. Both theories would sit on our obtained results for SWNTs that SWNTs prolonged the lag phase and are able to inhibit the process of fibrillation. In the literature there are described two contrast effects of carbon nanotubes: (1) MWNTs promote amyloid fibril formation from β_2-microglobulin and (2) SWNTs inhibit amyloid fibril formation from Aβ. In contrast to the β_2-microglobulin protein, Aβ peptides had high affinity to carbon nanotubes surface.[60] From the obtained results with SWNTs, we can also say that HEWL has a high affinity for SWNT. In the case of C_{60} the key interactions with HEWL are the same (π–π and hydrophobic interactions) as for SWNTs, but these nanospecies have a different shape and a surface curvature, which may be the main reason for different influence on the process of fibrillation. Based on the results with SWNTs and C_{60}, we can confirm that π–π and hydrophobic interactions play a key role in amyloid formation inhibition, but also a shape of nanospecies and a surface curvature can be important for this inhibition. Only a few studies deal with the influence of NDs on the process of fibrillation while they are a promising material for diagnostics. NDs have also hydrophobic sp^3-hybridized carbon surface and surface groups, which have a positive charge in our case. This means that adsorption of HEWL on a ND surface proceeded *via* electrostatic (isoelectric point of HEWL is 11.3 meaning that this protein is anionic under pH considered in the manuscript) and probably also hydrophobic interactions. The most plausible explanation of influence of NDs on amyloid formation is that NDs have become nuclei for the beginning of

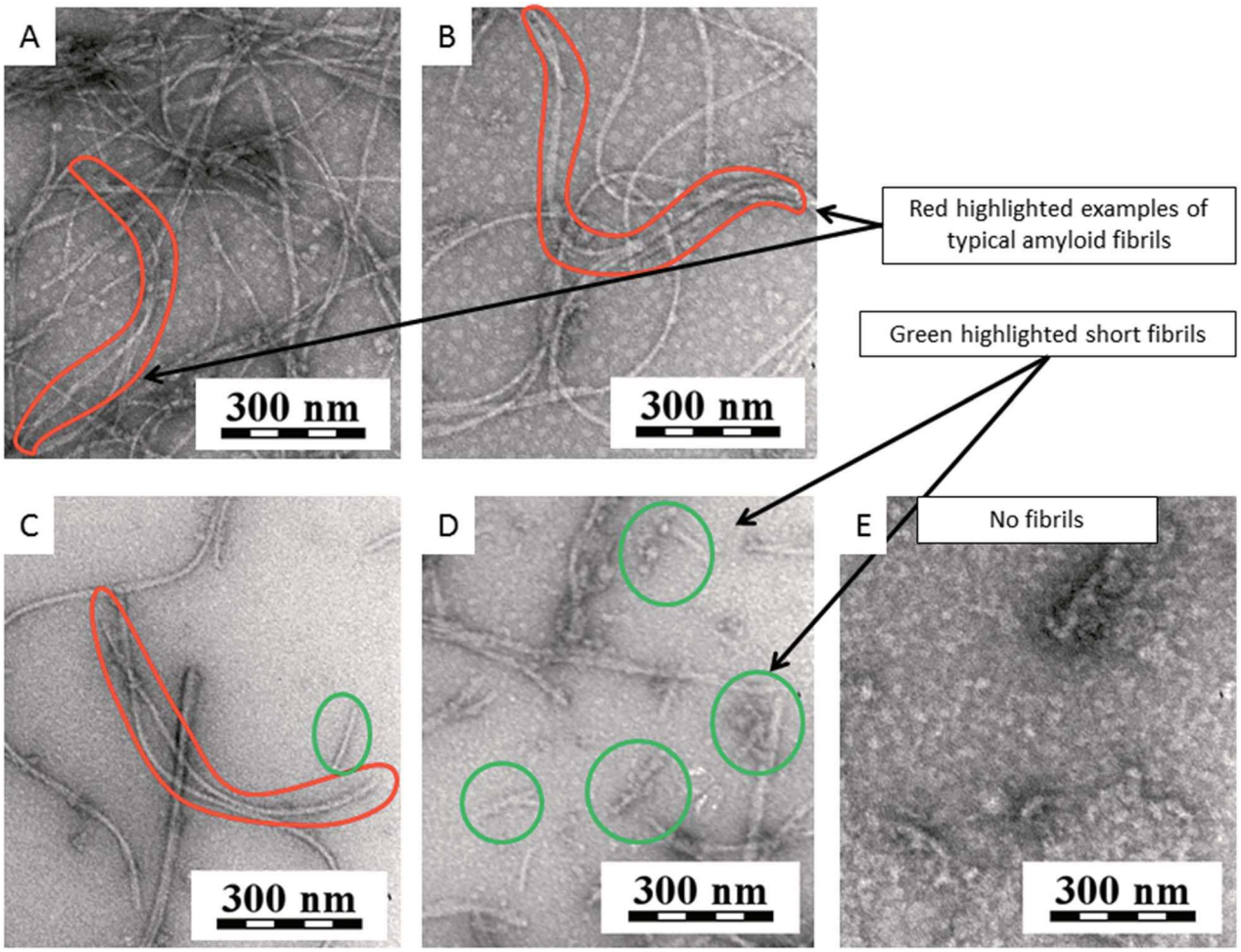

Fig. 14 TEM micrographs of experiments with CDs: (A) fibrils of HEWL (control) after 25 h of incubation without any nanospecies; (B) fibrils of HEWL after 25 h of incubation with 16 μg ml^{-1} CDs; (C) fibrils and shorter fibrils of HEWL after 25 h of incubation with 80 μg ml^{-1} CDs; (D) shorter fibrils of HEWL after 25 h of incubation with 250 μg ml^{-1} CDs. (E) No fibrils of HEWL after 25 h of incubation with 1 mg ml^{-1} CDs.

Table 2 The effect of different concentration of CNPs on the fibril formation. The star (*) represents a statistically significant difference compared to a zero concentration of CNPs (control). Bold data represent statistically significant decreases in the fibrillation process compared to the control

% fibril formation					
Concentration of CNPs (μg ml^{-1})	0	16	80	250	1000
SWNT[a]	100 ± 20	**22 ± 6 (*)**	**13 ± 2 (*)**	**11 ± 1 (*)**	—
C_{60}[a]	100 ± 20	**52 ± 20 (*)**	65 ± 45	227 ± 175 (*)	—
NDs[a]	100 ± 20	75 ± 31	154 ± 56 (*)	344 ± 110 (*)	646 ± 276 (*)
CDs[b]	100 ± 7	**77 ± 14 (*)**	**62 ± 8 (*)**	**34 ± 5 (*)**	**4 ± 2 (*)**

[a] The percent fibril formation was determined from the ThT fluorescence value for 47 h of incubation in Fig. 8 and 10. [b] The percent fibril formation was determined from the NR fluorescence values for 188 h of incubation in Fig. 13.

the fibrillation process significantly shortening the lag phase and an inducing rapid creation of fibrils. CDs significantly decelerated the process of fibrillation. The key interactions between CDs and HEWL are π–π, hydrophobic and probably also electrostatic (however, CDs have negative charged surface groups rather repelling prevailingly negative HEWL molecules).

Based on the results of the influence of four different type of CNPs (NDs, C_{60}, SWNTs, CDs) on formation amyloid fibrils from HEWL, the CNPs can be ranked from the most amyloidogenic to least in the following order NDs > control > C_{60} > CDs > SWNTs.

Experimental

All materials and methods, such as the preparation of CDs and their characterization or the preparation and characterization of the amyloid fibrils from HEWL, are given in the ESI (holubova_ESI.docx†).

Conclusions

From the experiments, we found that NDs promoted amyloid fibril formation. Because the NDs are less toxic than other CNPs (C_{60} or SWNT),[19] this finding may be interesting information for their production by detonation, in which large quantities of NDs may be released, leading to the formation of amyloid fibrils and subsequent disease in humans. Fibril formation *in vivo* and the development of the disease is likely to occur over a longer period of time than for *in vitro* testing. Therefore, it is necessary to take precautions, because the consequences can occur after many years. These experiments showed that the highest concentration of C_{60} accelerated the process of fibrillation, but smaller concentrations prolonged the lag phase. The risks associated with C_{60} cannot be excluded; however under good occupational hygiene conditions, the risk is low.[61] On the basis of the performed experiments, it is important to be take care, especially in applications in medicine, as C_{60} may cause a negative reaction with proteins, which may lead to the formation of amyloid fibrils. A different situation occurred for SWNTs. These nanospecies significantly prolonged the lag phase of amyloid formation. Although a higher toxicity is known for SWNTs than for C_{60},[62] but these results are of interest for drug development. Interestingly, CDs significantly affected the process of fibrillation; as the process was decelerated for almost all concentrations. It seems that CDs efficiently terminate fibril growth. The big advantages of CDs are their excellent biological properties such as low toxicity and good biocompatibility, making their applications in medicine as a drug delivery system possible. The studied CNPs (NDs, C_{60}, SWNTs and CDs) exhibited different behaviors in the presence of HEWL. The amyloidogenicity of studied nanomaterials was not observed in physiological conditions but was in the most suitable condition in which HEWL easily forms fibrils. It should be emphasized that HEWL is only a model system that is very suitable for testing, but the results obtained may not be consistent with proteins and peptides that are the cause of the amyloidosis in humans. Furthermore, *in vitro* testing was studied which may or may not reflect the real effects *in vivo*. Nevertheless, the results show an interesting comparison of four different types of CNPs based on various applications.

Conflicts of interest

There are no conflicts to declare.

Acknowledgements

The authors thank Mariia Rabyk, MSc. for preparation of the graphical abstract and Fig. 1. The authors acknowledge financial support from the Ministry of Education, Youth and Sports of the Czech Republic (grant # LM2015064 ERIC), from the Ministry of Health of the Czech Republic (grant # 16-30544A) and from the Czech Grant Foundation (grant # 16-03156S). OPG and J. S. acknowledge the support from the European Regional Development Fund OPPK (CZ.2.16/3.1.00/21545). J. H. thanks projects TE01020118 (Technology Agency of the CR) and POLYMAT LO1507 (Ministry of Education, Youth and Sports of the CR, program NPU I).

References

1 S. E. Radford and J. S. Weissman, *J. Mol. Biol.*, 2012, **421**, 139–141.
2 K. Sideras and M. A. Gertz, *Adv. Clin. Chem.*, 2009, **47**, 1–44.
3 D. M. Fowler, A. V. Koulov, C. Alory-Jost, M. S. Marks, W. E. Balch and J. W. Kelly, *PLoS Biol.*, 2006, **4**, 0100–0107.
4 B. P. C. Hazenberg, *Rheum. Dis. Clin. North Am.*, 2013, **39**, 323–345.
5 I. Cherny and E. Gazit, *Angew. Chem., Int. Ed.*, 2008, **47**, 4062–4069.
6 C. Iannuzzi, R. Maritato, G. Irace and I. Sirangelo, *Int. J. Mol. Sci.*, 2013, **14**, 14287–14300.
7 J.-C. Rochet and P. T. Lansbury, *Curr. Opin. Struct. Biol.*, 2000, **10**, 60–68.
8 E. Gazit, *FEBS J.*, 2005, **272**, 5971–5978.
9 K. E. Marshall, K. L. Morris, D. Charlton, N. O'Reilly, L. Lewis, H. Walden and L. C. Serpell, *Biochemistry*, 2011, **50**, 2061–2071.
10 F. Chiti and C. M. Dobson, *Annu. Rev. Biochem.*, 2006, **75**, 333–366.
11 E. Y. Chi, S. Krishnan, T. W. Randolph and J. F. Carpenter, *Pharm. Res.*, 2003, **20**, 1325–1336.
12 L. E. Murr and K. F. Soto, *Mater. Charact.*, 2005, **55**, 50–65.
13 G. D. Nielsen, M. Roursgaard, K. A. Jensen, S. S. Poulsen and S. T. Larsen, *Basic Clin. Pharmacol. Toxicol.*, 2008, **103**, 197–208.
14 K. Aschberger, H. J. Johnston, V. Stone, R. J. Aitken, S. M. Hankin, S. A. K. Peters, C. L. Tran and F. M. Christensen, *Crit. Rev. Toxicol.*, 2010, **40**, 759–790.
15 S. Banerjee, T. Hemraj-Benny and S. S. Wong, *Adv. Mater.*, 2005, **17**, 17–29.
16 A. Krueger, *J. Mater. Chem.*, 2008, **18**, 1485.
17 V. N. Mochalin, O. Shenderova, D. Ho and Y. Gogotsi, *Nat. Nanotechnol.*, 2012, **7**, 11–23.
18 A. Krueger, *Adv. Mater.*, 2008, **20**, 2445–2449.
19 V. N. Mochalin, O. Shenderova, D. Ho and Y. Gogotsi, *Nat. Nanotechnol.*, 2012, **7**, 11–23.
20 A. Krueger, *J. Mater. Chem.*, 2008, **18**, 1485.
21 Y. Wang and A. Hu, *J. Mater. Chem. C*, 2014, **2**, 6921.
22 P. G. Luo, S. Sahu, S.-T. Yang, S. K. Sonkar, J. Wang, H. Wang, G. E. LeCroy, L. Cao and Y.-P. Sun, *J. Mater. Chem. B*, 2013, **1**, 2116–2127.
23 R. Jelinek, in *Carbon Quantum Dots: Synthesis, Properties and Applications*, Springer International Publishing, 2017, pp. 5–27.

24 D. Qu, M. Zheng, L. Zhang, H. Zhao, Z. Xie, X. Jing, R. E. Haddad, H. Fan and Z. Sun, *Sci. Rep.*, 2014, **4**, 5294.
25 X. Zhai, P. Zhang, C. Liu, T. Bai, W. Li, L. Dai and W. Liu, *Chem. Commun.*, 2012, **48**, 7955.
26 X. Guo, C.-F. Wang, Z.-Y. Yu, L. Chen and S. Chen, *Chem. Commun.*, 2012, **48**, 2692–2694.
27 J. Shen, Y. Zhu, X. Yang and C. Li, *Chem. Commun.*, 2012, **48**, 3686.
28 W. Liu, C. Li, Y. Ren, X. Sun, W. Pan, Y. Li, J. Wang and W. Wang, *J. Mater. Chem. B*, 2016, **4**, 5772–5788.
29 Y. Wang and A. Hu, *J. Mater. Chem. C*, 2014, **2**, 6921.
30 X. Cao, J. Ma, Y. Lin, B. Yao, F. Li, W. Weng and X. Lin, *Spectrochim. Acta, Part A*, 2015, **151**, 875–880.
31 X. Zhai, P. Zhang, C. Liu, T. Bai, W. Li, L. Dai and W. Liu, *Chem. Commun.*, 2012, **48**, 7955.
32 H. Zhu, X. Wang, Y. Li, Z. Wang, F. Yang and X. Yang, *Chem. Commun.*, 2009, 5118.
33 S. Dey, P. Chithaiah, S. Belawadi, K. Biswas and C. N. R. Rao, *J. Mater. Res.*, 2014, **29**, 383–391.
34 V. Milosavljevic, A. Moulick, P. Kopel, V. Adam and R. Kizek, *J. Metallomics Nanotechnol.*, 2014, **3**, 16–22.
35 M. L. Bhaisare, A. Talib, M. S. Khan, S. Pandey and H. F. Wu, *Microchim. Acta*, 2015, **182**, 2173–2181.
36 S. Dey, P. Chithaiah, S. Belawadi, K. Biswas and C. N. R. Rao, *J. Mater. Res.*, 2014, **29**, 383–391.
37 W. Wei, C. Xu, L. Wu, J. Wang, J. Ren and X. Qu, *Sci. Rep.*, 2014, **4**, 1–7.
38 J. Jiang, Y. He, S. Li and H. Cui, *Chem. Commun.*, 2012, **48**, 9634.
39 A. Cao, D. Hu and L. Lai, *Protein Sci.*, 2004, **13**, 319–324.
40 Y. Tokunaga, M. Matsumoto and Y. Sugimoto, *Int. J. Biol. Macromol.*, 2015, **80**, 208–216.
41 R. Swaminathan, V. K. Ravi, S. Kumar, M. V. S. Kumar and N. Chandra, *Adv. Protein Chem. Struct. Biol.Adv. Protein Chem. Struct. Biol.*, 2011, **84**, 63–111.
42 F. Gottschalk, T. Sonderer, R. W. Scholz and B. Nowack, *Environ. Toxicol. Chem.*, 2010, **29**, 1036–1048.
43 C. Li and R. Mezzenga, *Nanoscale*, 2013, **5**, 6207–6218.
44 G. Socrates, *Infrared and Raman characteristic group frequencies: tables and charts*, John Wiley, New York, 2001.
45 O. Pop-Georgievski, N. Neykova, V. Proks, J. Houdkova, E. Ukraintsev, J. Zemek, A. Kromka and F. Rypaček, *Thin Solid Films*, 2013, **543**, 180–186.
46 J. Pleštil, *Makromol. Chem., Macromol. Symp.*, 1988, **15**, 185–190.
47 J. Lindon, *NMR Biomed.*, 1999, **12**, 168.
48 G. Rambabu and S. D. Bhat, *Electrochim. Acta*, 2015, **176**, 657–669.
49 V. S. Nair, R. D. Mukhopadhyay, A. Saeki, S. Seki and A. Ajayaghosh, *Sci. Adv.*, 2016, **2**, e1600142.
50 J. Robertson, *Adv. Phys.*, 1986, **35**, 317–374.
51 P. C. Ke, M.-A. Sani, F. Ding, A. Kakinen, I. Javed, F. Separovic, T. P. Davis and R. Mezzenga, *Chem. Soc. Rev.*, 2017, **110**, 1221–1232.
52 S. Freire, M. H. De Araujo, W. Al-Soufi and M. Novo, *Dyes Pigm.*, 2014, **110**, 97–105.
53 R. Mishra, D. Sjölander and P. Hammarström, *Mol. BioSyst.*, 2011, **7**, 1232.
54 M. Biancalana and S. Koide, *Biochim. Biophys. Acta, Proteins Proteomics*, 2010, **1804**, 1405–1412.
55 R. Mishra, D. Sjölander and P. Hammarström, *Mol. BioSyst.*, 2011, **7**, 1232.
56 M. M. Picken and G. A. Herrera, *Amyloid and Related Disorders*, Humana Press, Totowa, NJ, 2012.
57 V. N. Uversky and Y. Lyubchenko, *Bio-Nanoimaging: Protein Misfolding & Aggregation*, Elsevier Inc., 2013.
58 A. Fibrils, L. J. Waddington, S. L. Gras, L. J. Waddington and K. N. Goldie, *Protein Folding, Misfolding, and Disease*, Humana Press, Totowa, NJ, 2011, vol. 752.
59 Y. Yonezawa, S. Tanaka, T. Kubota, K. Wakabayashi, K. Yutani and S. Fujiwara, *J. Mol. Biol.*, 2002, **323**, 237–251.
60 C. Li and R. Mezzenga, *Nanoscale*, 2013, **5**, 6207–6218.
61 K. Aschberger, H. J. Johnston, V. Stone, R. J. Aitken, C. L. Tran, S. M. Hankin, S. A. K. Peters and F. M. Christensen, *Regul. Toxicol. Pharmacol.*, 2010, **58**, 455–473.
62 G. Jia, H. Wang, L. Yan, X. Wang, R. Pei, T. Yan, Y. Zhao and X. Guo, *Environ. Sci. Technol.*, 2005, **39**, 1378–1383.

Materials and methods

Chemicals

Hen egg-white lysozyme (~70 000) (HEWL), thioflavin T, phosphate buffered saline, glycine, Nile red, fullerene C_{60} (assay 99.5%), single-walled carbon nanotubes (≥80% carbon as SWNT, diameter 0.71.4 nm) and diamond nanoparticles suspension (~1% w/w) were purchased from Sigma-Aldrich LTD (Prague, Czech Republic). Dichloromethane, anhydrous citric acid, urea, hydrochloric acid (35%), and ethanol (96%) were purchased from Lach-Ner (Neratovice, Czech Republic).

Preparation of carbon quantum dots (CDs)

Citric acid (6.00 g, 15.6 mmol) and urea (6.00 g, 99.6 mmol) were dissolved in 20 ml water. The solution was heated in microwave oven (600 W) for 4 min. During the reaction, the solution changed from colorless over yellow and then black-brown clustered solid was formed. This solid was heated under vacuum at 60C for 2 h to remove volatile residuals. T his solid was dissolved in 70 ml water and the resulting solution of the CDs was purified in a centrifuge at 830g for 30 min to remove agglomerated particles. Finally, the 2 wt. % solution of CDs was purified on the size-exclusion chromatographic column PD-10® (commercial column pre- packed with Sephadex G-25®). The resulting solution was lyophilized and stored in the fridge. The sample was characterized by elemental analysis, ζ- potential, Small-angle X-ray scattering, UVVis absorption, X-ray photoelectron spectroscopy, Infrared spectroscopy (see below). Then the sample was used for experiments with HEWL.

Characterization of carbon nanospecies

Composition: Elemental analyses were done with the Elmer 2400 Series II CHNS/O instrument (Perkin Elmer Inc.).

Absorption and Photoluminescence spectra: UVVis absorption spescopy was performed on a Evolution 220 UVVis Spectrophotometer (ThermoFisher Scientific). Photoluminescence (PL) spectra were measured by FP-6200 Spectrofluorometer (JASCO).

Measuring ζ- potential: The aqueous solution of CDs at concentration 0.5 wt. % was measured with a Zetasizer Nano ZS (Malvern Instruments) to obtain ζ- potential.

X-ray photoelectron spectroscopy (XPS): Measurements were carried out with a K-Alpha$^+$ spectrometer (ThermoFisher Scientific). The samples were analyzed using a micro-focused, monochromated Al Kα X-ray source (400 m spot size) at an angle of incidence of 30 (measured from the surface) and an emission angle normal to the surface. Kinetic energy of the electrons was measured using a 180 hemispherical energy analyzer operated in the constant analyzer energy mode (CAE) at 200 eV and 50 eV pass energy for the survey and high resolution spectra respectively. Data acquisition and processing were performed using Thermo Advantage software. The XPS spectra were fitted with Voigt profiles obtained by convolving Lorentzian and Gaussian functions. The analyzer transmission function, Scofield sensitivity factors, and effective attenuation lengths (EALs) for photoelectrons were applied

for quantification. EALs were calculated using the standard TPP-2M formalism. All spectra were referenced to the C1s peak of hydrocarbons at 285.0 eV. The BE scale was controlled by the well-known position of the photoelectron CC and CH, CO and C(=O)O C1s peaks of polyethylene terephthalate and Cu 2p, Ag 3d, and Au 4f peaks of metallic Cu, Ag and Au, respectively. The BE uncertainty of the reported measurements and analysis is in the range of ± 0.1 eV.

Nuclear magnetic resonance (NMR): ^{1}H NMR and ^{13}C NMR spectra of D_2O solutions were acquired at 295 K with Bruker Avance III 600 spectrometer operating at 600.2 MHz and 150.9 MHz respectively. The width of 90 pulse was 10 μs for ^{1}H NMR, and 8 μs for ^{13}C NMR with relaxation delays 10 s. The acquisition time was 2.18 s with 32 scans and 0.86 s with 31000 scans for ^{1}H NMR, and ^{13}C NMR respectively.

Small-angle X-ray scattering (SAXS): SAXS experiments were performed using a pinhole camera (modified Molecular Metrology System, Rigaku, Japan) attached to a microfocused X-ray beam generator (Rigaku MicroMax 003) operating at 50 kV and 0.6 mA (30 W). The camera was equipped with a vacuum version of Pilatus 300K detector. Two experimental setups were used to cover the q range of 0.0051.1 Å^{-1}. Scattering vector, q, is defined as: $q=(4\pi/\lambda)\sin\theta$, where λ is the wavelength and 2θ is the scattering angle. Typical exposure time was 4 hours. Calibration of primary beam position and sample-to-detector distances was performed using AgBehenate sample. Water was used as absolute intensity calibrant.

Infrared spectroscopy: Fourier transform infrared (FTIR) spectra were recorded in the range of 6504000 cm $^{-1}$ at 256 scans per spectrum at 4 cm^{-1} resolution using a fully computerized Nicolet NEXUS 870 FTIR Spectrometer (ThermoFisher Scientific). Attenuated total reflection (ATR) method was applied using a single reflection Golden GateTM Diamond ATR crystal. The spectra were corrected for the water vapor and carbon dioxide in the optical path.

Raman spectroscopy: Raman spectra excited with an Ar-ion 514 nm laser were collected on a Renishaw inVia Reflex Raman spectroscope. A research-grade Leica DM LM microscope with an objective magnification 50 was used to focus the laser beam. The scattere d light was analyzed by the spectrograph with a holographic grating 2400 lines mm^{-1}. A Peltier-effect cooled CCD detector (576 384 pixels) registered the dispersed light.

Transmission electron microscopy (TEM): Two microliters of nanospecies suspensions was placed on carbon-coated copper grid and dried. The morphology of all carbon nanospecies was observed with Transmission Electron Microscopy Tecnai G2 Spirit (FEI). Voltage was 120 kV.

Dynamic light scattering (DLS): For characterization of size of nanospecies in solution, DLS was performed on a Zetasizer Nano ZS (Malvern Instruments). DLS analyzes the velocity distribution of particle movement by measuring dynamic fluctuations of light scattering intensity caused by the Brownian motion of the particle. This technique yields a hydrodynamic radius, or diameter, to be calculated via the Stokes-Einstein equation from the aforementioned measurements.

Preparation and characterization of hen egg white lysozyme (HEWL) amyloid fibrils

In order to generate amyloid fibrils the stock solution of protein was prepared at concentration 2 mg/ml in 10 mM glycine-HCl buffer, pH 2.0. The solutions were filtered through-out a 0.22 m filter. The stock solution was divided into glass vials to which were added various concentrations of nanospecies. Depending on the experiment the final protein concentration in all vials was even up adding Milli-Q water or filtered dichloromethane. The solutions were incubated at the 57C. Samples (10 l) were taken at different time and were det ected by thioflavin T, Nile red, Transmission electron microscopy (see below).

Thioflavin T (THT) fluorescence assay: Solution of phosphate buffered saline (PBS) was prepared from tables. The solution was used for dissolution ThT at a final concentration 10 μM. HEWL samples (10 μl) taken at different times were added to 240 μl of the ThT solution into one well in 96-well plate. Before measuring fluorescence 96-well plate was briefly mixed on plate reader. ThT fluorescence intensity measurements were performed by exciting samples at 440 nm and recording emission intensities at 485 nm using with Synergy H1 Hybrid plate-reader (Biotek).

Nile red (NR) fluorescence assay: Nile red has the poor solubility in aqueous solution therefore a stock solution of NR at concentration 2.5 mM was prepared in pure ethanol and was kept at 4C. The working solution was prepared by diluting the stock solution into 25 mM HCl (pH 1.6) at a final concentration of NR 10 μM. HEWL samples (10 μl) taken at different times were added to 240 μl of NR working solution into one well in 96-well plate. The mixed samples kept 1 h at room temperature before measuring fluorescence. Samples were excited at 550 nm and emission was recorded at 640 nm using with Synergy H1 Hybrid plate-reader (Biotek).

TEM: Two l of sample was placed on carbon-coated copper grid and dried with paper. The sample was stained with 1 wt. % uranyl acetate for 30 s. Images were obtained with Tecnai G2 Spirit (FEI) at an accelerating voltage of 120 kV.

Statistical analysis: Experimental data were analyzed with Q-test and oneway ANOVA and the significance level was set at $\alpha<0.05$ for all experiments.

Publication 3

Colloid and Polymer Science
https://doi.org/10.1007/s00396-020-04710-8

INVITED ARTICLE

Polymer materials as promoters/inhibitors of amyloid fibril formation

Monika Holubová[1,2] · Petr Štěpánek[1] · Martin Hrubý[1]

Received: 6 May 2020 / Revised: 2 July 2020 / Accepted: 14 July 2020

Abstract

Polymers are omnipresent materials that are widely used in medicine, e.g., as construction materials for medical devices or as polymer nanoparticle drug delivery systems. Therefore, their possible effects on biomolecules, such as lipids, proteins, and other molecules, present in the human body must be examined. This review addresses the effects of polymer materials (such as dendrimers, polysaccharides) on the process of amyloid fibril formation. Amyloidoses are very serious diseases that are characterized by amyloid deposition in various organs and tissues, causing their dysfunction. The treatment of amyloidoses, such as Alzheimer's disease (AD), using polymer materials is a challenge. Studies aiming to elucidate the effects of polymers on the process of amyloid fibril formation are therefore also of key importance for understanding the process of amyloid fibril formation and amyloidoses in general.

Keywords Amyloidosis · Amyloid fibrils · Polymer · Dendrimers · Polysaccharides

Introduction

Amyloid deposits are insoluble forms of peptides/proteins [1]. Amyloids are pathologically deposited in organs and tissues and cause their dysfunction. A group of diseases associated with this pathological deposition of amyloids is called amyloidoses [2, 3]. These diseases include neurological disorders such as Alzheimer's disease (AD) or diseases impairing the function of other internal organs, such as type 2 diabetes [4]. Amyloid fibrils are rigid and non-bunched with variable lengths and a diameter of 7–12 nm [3, 5]. All amyloid fibrils share a core structure with a dense network of hydrogen bonds stabilizing an elongated stack of β-strands that are perpendicular to the fibril axis and separated by 4.8 Å [6]. Laterally connected β-strands compose a generally twisted, pleated sheet known as the β-sheet [1, 7, 8]. The β-sheets run parallel to the fibril axis with typical intersheet distance of 10–12 Å [9]. As shown in the study by Smith et al., amyloid fibrils formed from the protein insulin have a strength of 0.6 ± 0.4 GPa and Young's modulus of 3.3 ± 0.4 GPa [6], which is a considerably higher value than silk [10], with Young's modulus of 6 GPa and a strength of 0.2 GPa, or nylon-6 [11], with Young's modulus of 2–4 GPa and a strength of 0.045–0.09 GPa [10].

In addition to the precursor protein that forms amyloid fibrils, amyloid deposits contain other components, such as serum amyloid P component (SAP) [3], glycosaminoglycans [3] (mainly heparan sulfate) and apolipoprotein E (APOE) [12]. The non-fibrillar form of SAP is very readily associated with amyloid fibrils and appears to prevent degradation of amyloid fibrils by proteolytic enzymes [3]. Glycosaminoglycans as polyanions play an important role in catalyzing an aggregation of a protein and in stabilizing amyloid fibrils [3]. APOE has three major polymorphisms in human: ε2, ε3, and ε4, of which ε4 is associated with an increased risk for developing Alzheimer's disease AD [12].

The process of amyloid fibril formation includes protein misfolding, nucleation, and fibril elongation. Figure 1 shows curves of the process of amyloid fibril formation. The lag phase is the first phase when soluble proteins create nuclei that form oligomeric species with β-sheets. The second phase is the so-called growth phase. During the last phase (saturation phase), the mature fibrils are completely finalized [15]. The formation of amyloid fibrils also includes a number of intermediate states and pathways [1, 13]. The two examples of formation pathways are downhill polymerization (DP) and

✉ Martin Hrubý
mhruby@centrum.cz

[1] Institute of Macromolecular Chemistry, Academy of Sciences of the Czech Republic, Heyrovský Sq. 2, 162 06 Prague 6, Czech Republic

[2] Faculty of Science, Department of Physical and Macromolecular Chemistry, Charles University in Prague, Albertov 6, 128 00 Prague 2, Czech Republic

Published online: 02 August 2020

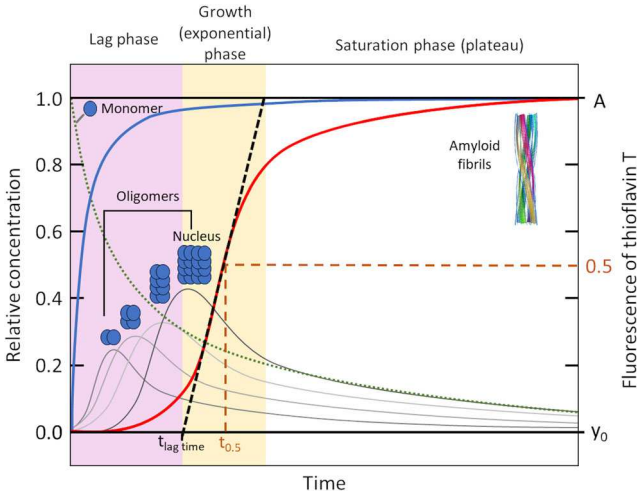

Fig. 1 Illustration of the sigmoidal increase in thioflavin T (ThT) fluorescence/protein concentration in amyloid forms (red line) during the process of amyloid fibril formation. The green dot represents the monomer concentration. The gray lines indicate oligomers of different sizes. The blue line refers to the elimination of the lag phase of fibrillation in reactions seeded with preformed mature fibrils (adapted from ref. [13]). The black dashed line is the slope of the growth phase. The time $t_{0.5}$ is the time at which 50% of the maximal fluorescence is observed. The line y_0 is an initial baseline, and A is the amplitude of fluorescence [14]

nucleated conformational conversion (NCC). In DP, the lag phase is caused by the slow dissociation of stable native monomer [16] into amyloidogenic monomers through misfolding/denaturation [9], rapidly achieving the amyloidogenic conformation [1] (e.g., transthyretin [16] and lysozyme [9]). Amyloid fibrils that are formed by DP do not miss the lag phase of fibrillation in reactions seeded with preformed mature fibrils [1, 9] (the curve of the amyloid fibril formation is similar to the red line in Fig. 1). On the other hand, during NCC, partially or completely disordered soluble monomers initially occur in equilibrium with soluble molten oligomers. These oligomers are rearranged into amyloidogenic oligomers during the lag phase. The lag phase ends when amyloidogenic oligomers create cross-β nuclei. After the creation of cross-β nuclei, the process of amyloid fibril formation rapidly occurs. Amyloid fibrils that are formed by NCC eliminate the lag phase of fibrillation in reactions seeded with preformed mature fibrils [1] (blue line in Fig. 1).

A higher proportion of aromatic residues has been observed in amyloid fibrils, that means that π–π interactions have one of the most important roles in the process of amyloid fibril formation [17]. However, other interactions also play an important role in the formation of amyloid fibrils and their stabilization, including hydrophobic and electrostatic interactions [18, 19].

Although some polymers appeared earlier, since the twentieth century, macromolecular chemistry was established as a separate scientific discipline [20]. Since then, polymers became an inseparable part of our lives. They have found applications in many industries and medical applications. In this review, we focus on the effects of both natural and synthetic polymer materials on the process of amyloid fibril formation. These materials have been extensively investigated as drug delivery systems. Since these materials may interact with many proteins present in the organism, these interactions must be tested. On the one hand, proteins may be bound in a denatured form and polymer materials may catalyze protein misfolding and subsequent amyloid fibril formation, but on the other hand, polymer materials may block amyloid fibril formation and serve as potential drugs.

Dendrimers

Dendrimers represent a significant group of polymer materials. Dendrimers are well-defined, homogenous, and monodisperse nanosized globular macromolecules [21, 22]. Dendrimers possess a distinct molecular architecture that consists of three different domains: (1) a central core with a single atom or a group of atoms having at least two chemical functionalities that provide linkages for the branches; (2) branches that grow from the core and consist of repeating units with at least one junction of branching, where repetition of the junction of branching in a geometric progression produce a series of radially concentric layers termed generations (G); and (3) terminal functional groups. Usually, the presence of highly interactive functionalities on the surface of dendrimers confers them with high reactivity, solubility, and binding properties [21, 22]. Due to the unique properties, such as a nanoscale globular shape, well-defined functional end groups, hydrophobic or hydrophilic cavities, and extremely low polydispersity, dendrimers have been employed in a wide range of potential applications [21–23]. Dendrimers have proven useful as drug delivery systems, anticancer drugs, gene delivery systems, protein mimics, and in biomedical diagnostic applications, such as magnetic resonance imaging (MRI) contrast agents, and dendritic sensors [21–23] (Fig. 2).

Generally, dendrimers are synthesized using a stepwise chemical synthesis approach. Two of the most frequently applied methods for the chemical synthesis of dendrimers are divergent synthesis (Fig. 3a) and convergent synthesis (Fig. 3b). The difference between these methods is that divergent synthesis starts from the multifunctional core, followed by building one monomer layer or generation at a time, while the convergent synthesis starts from the end groups and terminating at the core [21, 22].

Many studies have analyzed the effects of dendrimers on amyloid fibril formation, and thus, we divided this section into three subsections.

Polyamidoamine dendrimers

Polyamidoamine (PAMAM) dendrimers are based on an ethylenediamine core, and the branched units are formed from both methyl acrylate and ethylenediamine. The surface of

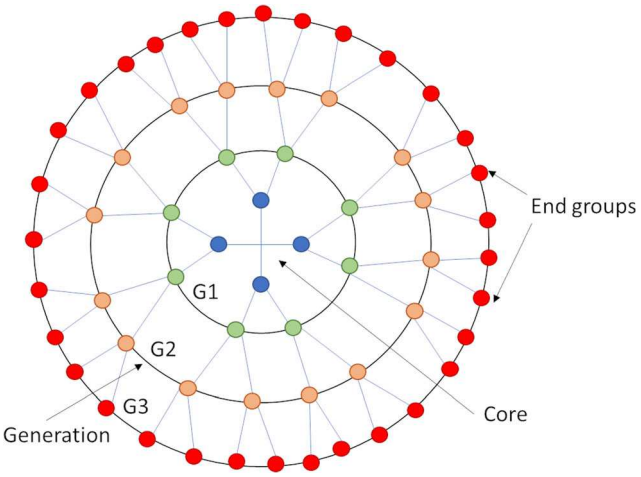

Fig. 2 Structure of dendrimers (adapted from ref. [21])

half-generations of PAMAM dendrimers contains ester groups, while the full-generation surfaces contain amino groups [24].

Klajnert et al. [25, 26] investigated the effects of the third-, fourth-, and fifth-generation PAMAM dendrimers (PAMAM G3, PAMAM G4, and PAMAM G5) on the aggregation of the amyloid beta(1–28) ($A\beta_{1-28}$) peptide and segment 185–208 of the human prion protein ($PrP_{185-208}$). The PAMAM G3, G4, and G5 dendrimers affect aggregation. PAMAM G3 mainly affects the nucleation rate constant of $A\beta_{1-28}$ and the elongation rate constant of $PrP_{185-208}$, depending on the concentration of PAMAM G3. The nucleation rate of the process of amyloid fibril formation is affected in the presence of low concentrations of PAMAM G3, while the elongation rate is altered in the presence of high concentrations of PAMAM G3 [26]. Their finding is interesting because a low concentration of PAMAM G3 decreases the lifetime of low molecular weight intermediates and contributes to decreasing the potential cytotoxic effects of the peptides, because low molecular weight intermediates are more toxic than mature fibrils [27]. On the other hand, high dendrimer concentrations increase the cytotoxicity, because PAMAM G3 increases the lifetime of low molecular weight aggregates. Kinetic inhibitors do not change the final number of fibrils, but the lag time is different. Klajnert et al. observed the kinetic inhibition of $PrP_{185-208}$ aggregation in the presence of 0.1 μmol/l PAMAM G4, and the complete inhibition of amyloid formation of $PrP_{185-208}$ was observed in the presence of 0.1 μmol/l PAMAM G5. On the other hand, thermodynamic inhibitors do not affect the amyloid fibril formation rate, but the final number of fibrils is reduced. It was observed at $A\beta_{1-28}$ aggregation in the presence of PAMAM G4 and PAMAM G5 [25]. Rekas et al. [28] investigated the effects of PAMAM G4, PAMAM G5, and PAMAM G6 on the fibrillation of α-synuclein, whose depositions are associated with Parkinson's disease. Dendrimers inhibited the process of fibrillation and also degraded preexisting fibrils. PAMAM G4 and PAMAM G5 exerted comparable inhibitory effects on α-synuclein fibrillation, but PAMAM G6 was the most efficient dendrimer. Dendrimers inhibited the formation of β-sheet structures and disrupted existing β-sheets or their agglomerates. In both the PAMAM-mediated inhibition and decomposition process, the aggregation of α-synuclein was redirected to the amorphous aggregation pathway [28].

Another study assessed the effects of a second-generation PAMAM G2 on amyloid fibril formation from amyloidogenic transthyretin (ATTR) with the Val30Met mutation [29]. The process of amyloid fibril formation was significantly inhibited by the addition of PAMAM G2 in a concentration-dependent

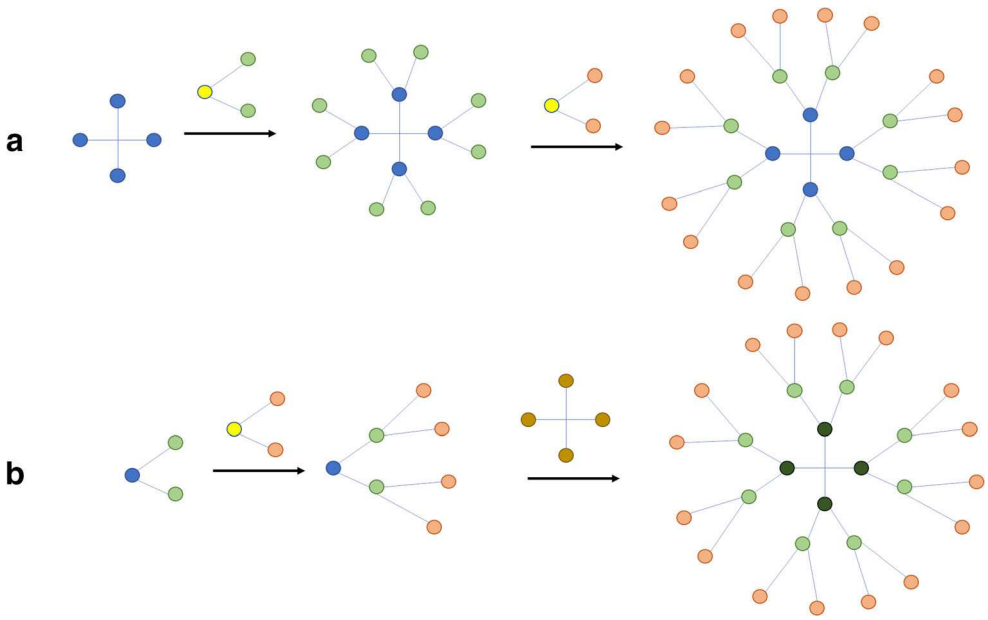

Fig. 3 Syntheses of dendrimers. **a** Divergent synthesis. **b** Convergent synthesis (adapted from ref. [21])

manner. The PAMAM G2 dendrimer probably inhibited ATTR amyloid fibril formation by reducing the conformational change in ATTR. Moreover, PAMAM G2 exerted amyloid-disrupting effects on ATTR amyloid fibrils. Both behaviors are very important to achieve superior therapeutic effects. The interaction between PAMAM G2 and ATTR was investigated with isothermal titration calorimetry (ITC) and revealed the interaction of both compounds. Among other assessments, in vivo experiments with Tg rats encoding a human ATTR Val30Met gene were also performed. This experiment lasted 3 months, during which the Tg rats were intravenously injected with the PAMAM G2 solution. Meanwhile, PAMAM G2 significantly decreased transthyretin deposition in the gastrointestinal tracts. Because PAMAM G2 contains a large number of amino groups and the isoelectric point (pI) of ATTR is approximately 4.7, the electrostatic interaction between PAMAM G2 and ATTR plays a key role in inhibition. Additionally, the hydrogen bonds detected using ITC play an important role in inhibition, and the last interaction involved in inhibition is probably cation-π interactions of PAMAM G2 and aromatic amino acid residues [29]. This study is important because it shows that PAMAM G2 has potential as a novel drug targeting ATTR amyloidosis.

The study by Gurzov et al. [30] investigated the effects of the hydroxyl-terminated PAMAM G3 (PAMAM G3-OH) on the amyloid fibril formation of human islet amyloid polypeptide (hIAPP), whose amyloid deposits are associated with type II diabetes. PAMAM G3-OH inhibited the process of amyloid fibril formation. Molecular dynamics simulations revealed the likely mechanism of inhibition. The PAMAM G3-OH dendrimers bound to the amyloidogenic regions of hIAPP monomers (residues 22–29), and the interaction between PAMAM G3-OH and dimer of hIAPP subsequently disrupted the formation of interpeptide hydrogen bonds and hydrophobic interactions between hIAPP dimers. The study also determined whether the inactivation of hIAPP aggregation by PAMAM G3-OH prevented the toxicity of the peptide toward pancreatic β-cells. The mouse β-cell lines MIN6 and NIT-1 were treated with hIAPP, PAMAM G3-OH, or a combination of the two. All cell lines exhibited significantly reduced cytotoxicity compared with cell lines exposed to hIAPP alone [30].

Poly(propylene imine) dendrimers

Poly(propylene imine) dendrimers are suitable for binding DNA because they contain fully protonatable amine groups [21]. DNA binding and cytotoxicity depend on the generation of PPI dendrimer. Heegaard et al. [31] compared the effects of a second-generation PPI dendrimer (PPI G2) (Fig. 4a) and second-generation PPI dendrimer derivatized with guanidinium surface groups (PPI G2 Gua) (Fig. 4b) on segment 106–126 of the human prion protein ($PrP_{106–126}$). Dendrimers with the highly cationic guanidinium surface groups (PPI G2 Gua) decreased fibril formation, but PPI G2 promoted amyloid fibril formation. The inhibitory effect on amyloid fibril formation was probably attributed to the positive charge on the surface of PPI G2 Gua [31]. The findings were supported by previous experiments showing that the cationic charge of the dendrimer was necessary for the binding to monomers of the prion protein isoform (PrP^{Sc}) and/or oligomers of PrP^{Sc}, allowing dendrimers to segregate proteins from the aggregate and/or prevent this separate PrP^{Sc} protein from reaggregating [32].

Two studies have analyzed poly(propylene imine) dendrimers decorated with maltose. These studies determined the effects of the fourth (G4) and fifth (G5) generations of PPI dendrimers decorated with maltose (m) or maltotrioses (m-III). PPI dendrimers possessing approximately 40% of terminal amino groups modified with sugar molecules are called "open sugar shell dendrimers" (OS), while PPI dendrimers possessing 90–100% of terminal amino groups modified with sugar molecules are described as "dense sugar shell dendrimers" (DS) [33, 34]. The first study compared the effect of G4mDS and G5mDS (Fig. 6) on amyloid fibril formation from $Aβ_{1–40}$, whose deposits are associated with AD. More effective inhibition was observed for G5mDS, because the process of amyloid fibril formation was blocked by all tested concentrations of the dendrimer. In the presence of a low concentration of G4mDS (dendrimer-peptide ratio = 0.1 or 1), clumped fibrils were observed (Fig. 5b), but the process of amyloid fibril formation was blocked at high concentrations (dendrimer-peptide ratio = 10). Additionally, G4mDS and G5mDS were not toxic toward PC12 and SH-SY5Y neuronal cell lines, but dendrimer-peptide aggregates caused some problems. Although G5mDS was more effective at inhibiting the process of amyloid fibril formation, amorphous aggregates (Fig. 5c) resulting from the blockade of the process have been shown to be toxic to PC12 cells [33]. This finding is consistent with the aforementioned finding that low molecular weight intermediates are more toxic than mature fibrils [27]. The second study examined all PPI dendrimers shown in Fig. 6. The study was based on the results reported in a previous study [33]. The second study shows that these dendrimers promote $Aβ_{1–40}$ fibril formation under certain conditions, but all maltose dendrimers (not G4m-IIIOS) reduce the toxicity of $Aβ_{1–42}$. The electroneutral G4mDS and G5mDS dendrimers do not cross the blood-brain barrier (BBB) after an intraperitoneal injection, but G4mDS and G5mDS reach the brain via short-term intranasal administration (approximately 6% of the total single dose), while cationic G4mOS crosses the BBB. Although G4mOS is able to cross BBB and exhibits anti-Aβ properties, it does not prevent memory damage in transgenic mice; moreover, G4mOS is harmful when chronically administered to wild-type non-transgenic mice.

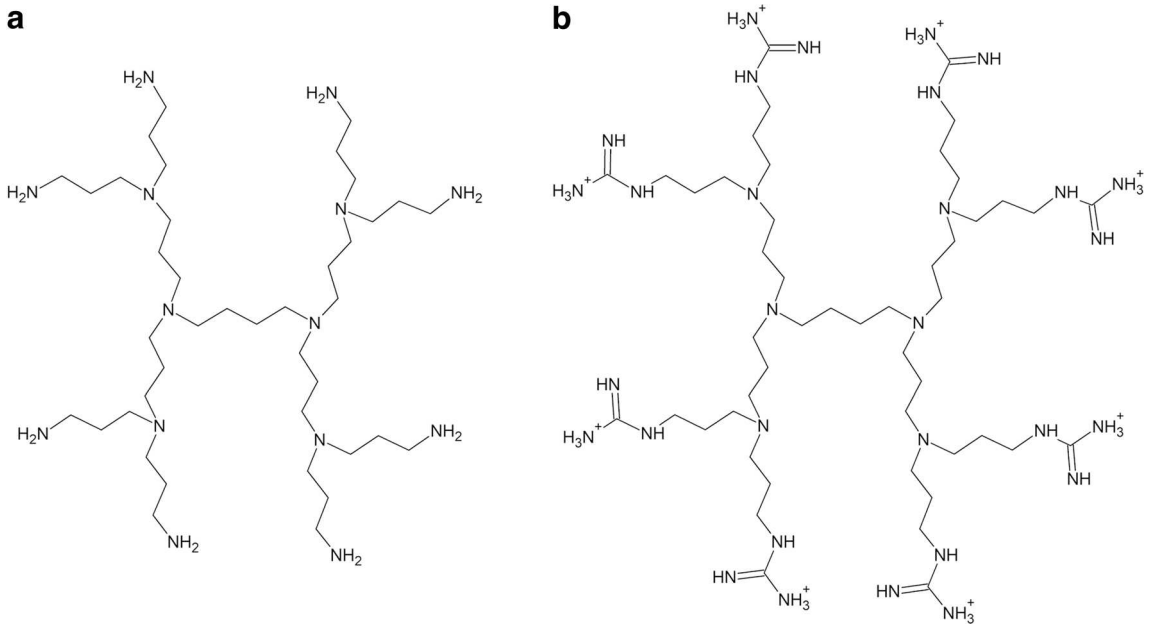

Fig. 4 **a** PPI G. **b** PPI G2. Dendrimers derivatized with guanidinium surface groups (adapted from ref. [31])

A very interesting and new modification of the PPI dendrimer is a dendrimer with PPI core and maltose-histidine shell (G4HisMal) described in one study [35]. The advantage of histidine is that it is selectively transported through the BBB. Dendrimers with the maltose-histidine shell exhibit significantly improved biocompatibility and the ability to cross the BBB compared with G3 and G4 PPI dendrimers with the maltose shell [35]. G4HisMal does not inhibit the fibrillation of $A\beta_{1-40}$ but clumps $A\beta_{1-40}$ and $A\beta_{1-42}$ fibrils together. However, oligomers of $A\beta_{1-40}$ were not detected in the presence of G4HisMal, suggesting that G4HisMal inhibits the cytotoxicity of $A\beta_{1-40}$ toward human neuroblastoma cells. Moreover, the G4HisMal treatment rescued spatial memory deficits in the APP/PS1 mouse model [35].

Other publications have investigated the effects of PPI dendrimers with various surface modifications on amyloid fibril formation. Laumann et al. found out that PPI dendrimers with *N*-methyl-thiourea and urea surface groups dissolved α-synuclein fibrils in human cells into smaller fragments, of which concentrations were not cytotoxic [36]. McCatrthy et al. determined the antiprion activity for PPI dendrimers with different surface groups and charges [37].

Other dendrimers

In addition to the groups of dendrimers mentioned above, other types of dendrimers, e.g., pyridylphenylene dendrimers [38], lysine dendrimers [39], have been developed. The disruption of bovine PrP inclusion bodies (IB), representing amyloid aggregates, by the rigid cationic pyridylphenylene dendrimers of different generations (G2 (Fig. 7), G3, G4) is described in one study [40]. The disruption of amyloid aggregates is one of the potential mechanisms of treatment. Pyridylphenylene dendrimers disrupted amyloid aggregates to create stable and soluble dendrimer-protein complexes. The study suggests possible interactions between the cationic pyridylphenylene dendrimer and ovine PrP IB, where the initial adsorption of the dendrimer on the surface of the amyloid aggregates is mediated by electrostatic and hydrophobic interactions, followed by the release of the soluble dendrimer-protein complex [40]. Another study explored the ability of these cationic pyridylphenylene dendrimers to prevent the amyloid fibril formation of PrP [38]. Dendrimers inhibited amyloid fibril formation and prevented the formation of the most toxic oligomer species [38]. In addition, cationic pyridylphenylene dendrimers were able to prevent to the formation of amyloid fibrils in the presence of fibril seeds. Hydrophobic interactions are very important for inhibition, because they resulted in the formation of the stable PrP-dendrimer complexes [38] and the inhibition of amyloid formation [38], consistent with the previous study showing that dendrimers disrupted amyloid aggregates [40].

Other studied dendrimers include carbosilane dendrimers [41]. The study tested the amyloidogenicity of α-synuclein incubated with two carbosilane dendrimers with different functional groups (Fig. 8). Different concentrations of both dendrimers inhibited the process of amyloid fibril formation. Moreover, the dendrimers did not change the secondary structure of α-synuclein, while α-synuclein alone converted from the disordered α-synuclein structure to the β form [41]. Another interesting finding of the study was that carbosilane dendrimers protect cells from the toxic effect of rotenone, probably due to the reduction in the rotenone concentration caused by encapsulation in the dendrimer and/or attachment to

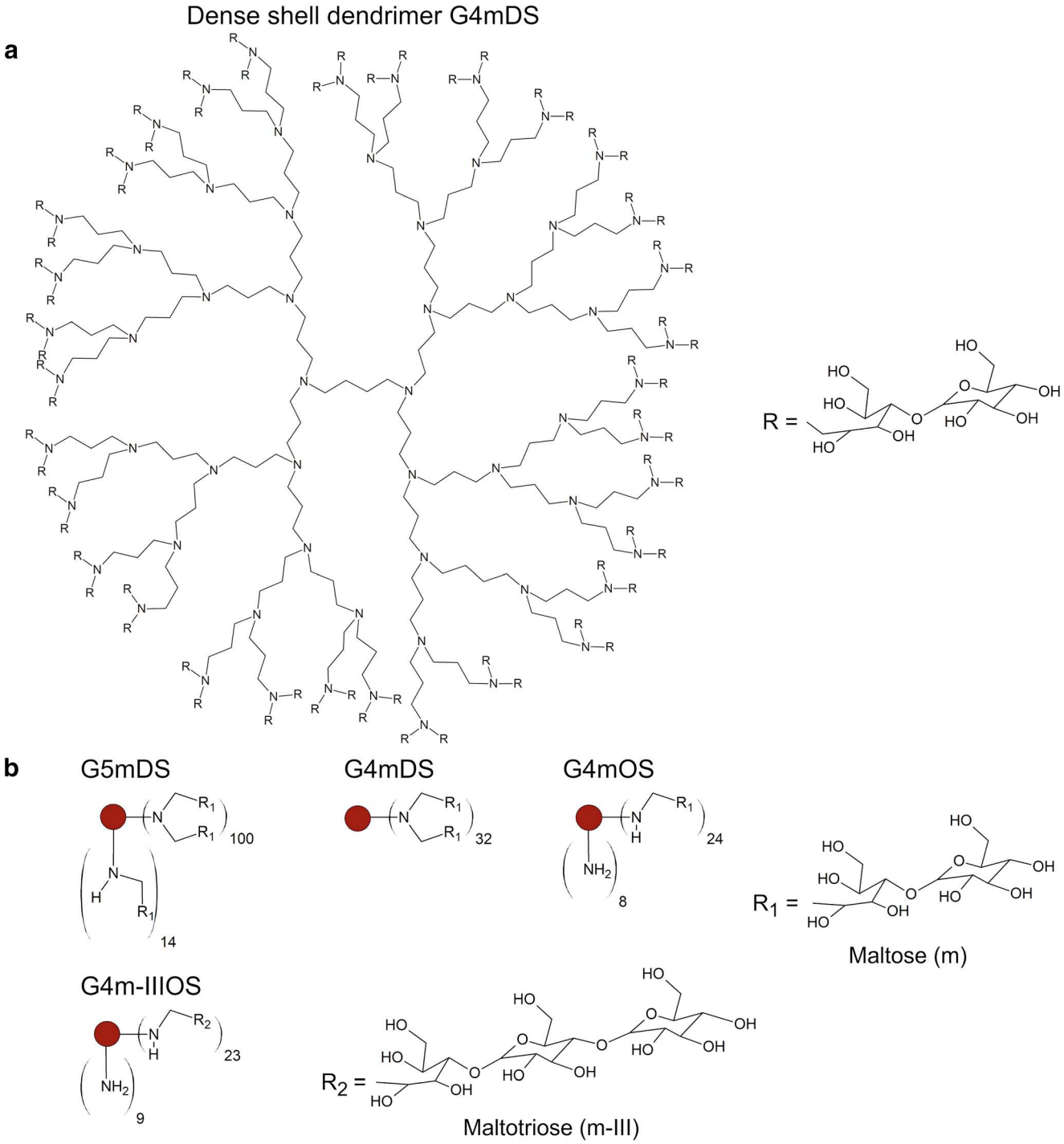

Fig. 6 Structures of G4 and G5 PPI dendrimers possessing maltose (m) or maltotriose (m-III). **a** Structure of PPI G4 with a dense maltose shell, G4mDS. **b** Terminal amino group in maltose shell dendrimers with an open-shell (G4mOS) and dense shell (G4mDS and G5mDS) and maltotriose open-shell dendrimers (adapted from ref. [34])

the surface of dendrimers. Rotenone is used as a pesticide that is unfortunately associated with Parkinson's disease (PD). Rotenone induces the accumulation of α-synuclein in rats [41] and has been used to establish an animal model of Parkinson's disease [42].

Two studies preceded the aforementioned study [41]. The first study examined phosphorus-containing dendrimers and their effects on the process of amyloid fibril formation from α-synuclein [44]. The second study determined the effects of viologen-phosphorus dendrimers on the process of amyloid

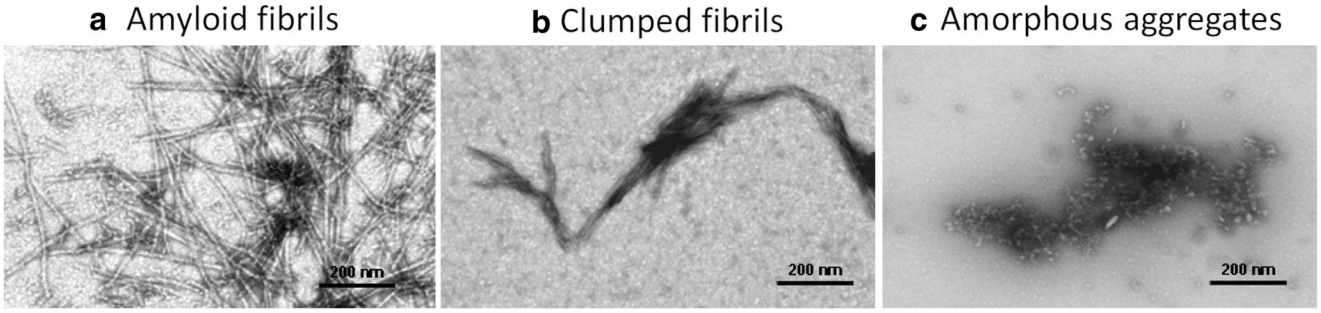

Fig. 5 Transmission electron microscopy (TEM) micrographs. **a** $A\beta_{1-40}$ incubated without dendrimers at pH 7.4 for 12 h. **b** $A\beta_{1-40}$ incubated at pH 7.4 for 12 h in the presence of G4mDS at a dendrimer-peptide ratio of 0.1. **c** $A\beta_{1-40}$ incubated at pH 7.4 for 12 h in the presence of G5mDS at a dendrimer-peptide ratio of 1 (adapted from ref. [33])

fibril formation from α-synuclein [43]. The effects of these three types of dendrimers are summarized in Table 1. As shown in Table 1, the most efficient inhibitors of amyloid formation were carbosilane dendrimers (BDBR7 and BDBR11). Viologen-phosphorus [43] dendrimers also displayed excellent efficiency in inhibiting amyloid formation. The least efficient dendrimers were phosphorus-containing [44] dendrimers, as lower concentrations of these dendrimers were significantly more efficient than higher concentrations and G3 produced better results than G4.

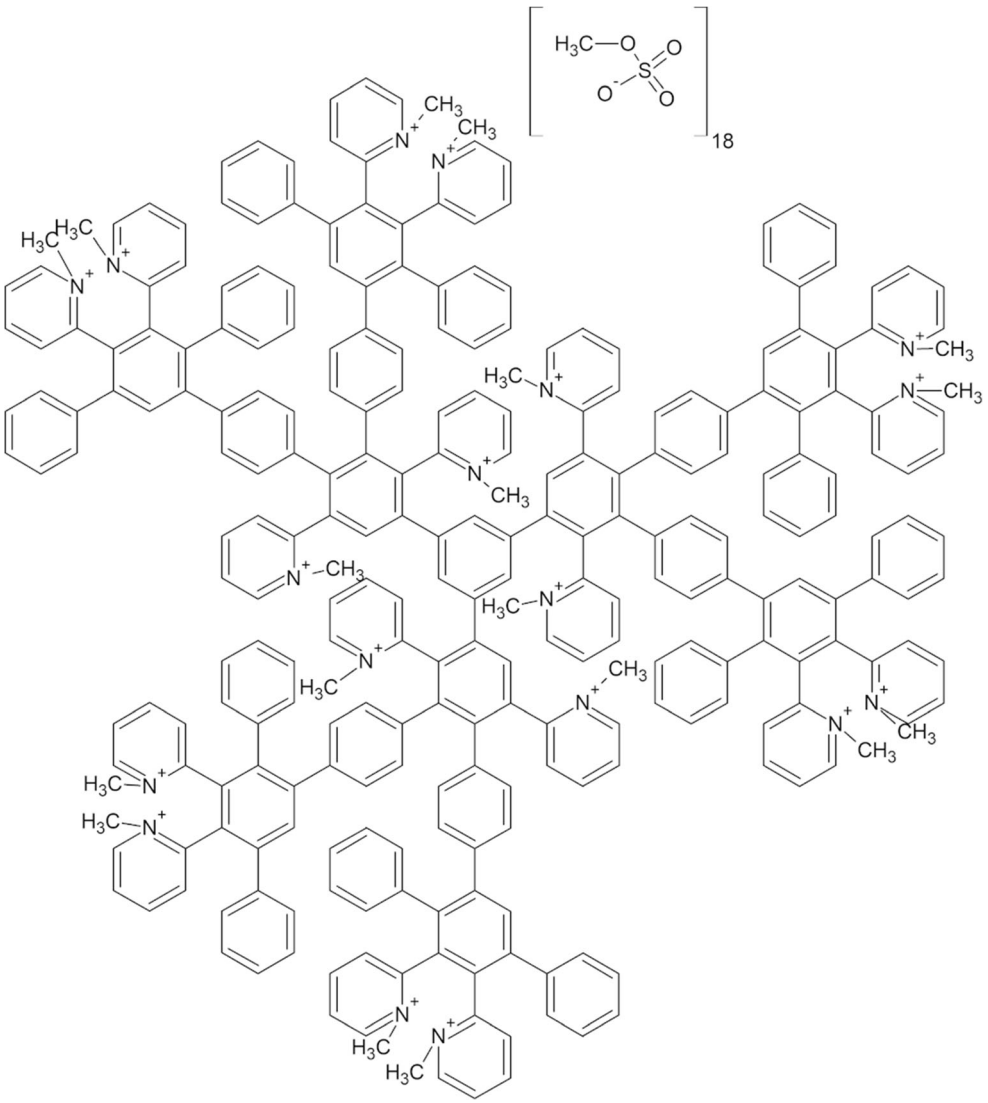

Fig. 7 Second-generation cationic pyridylphenylene dendrimer (adapted from ref. [38])

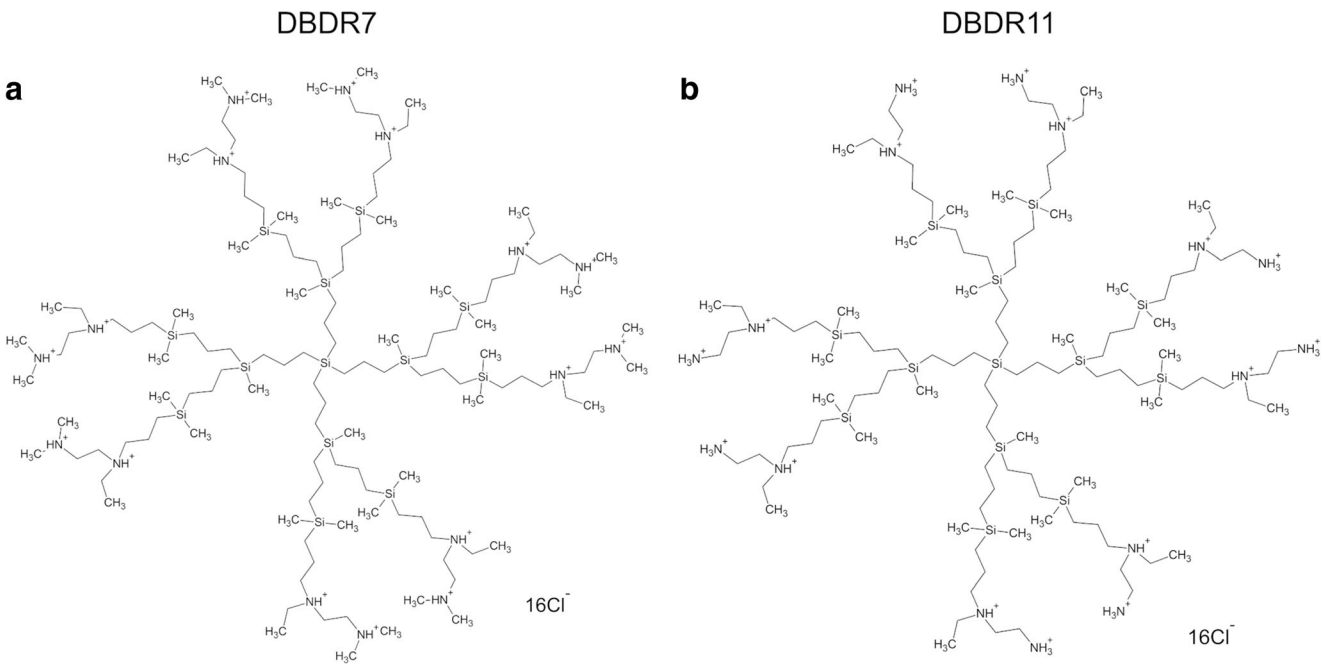

Fig. 8 Structures of carbosilane dendrimers (adapted from ref. [41])

Numerous low-generation (G0 and G1) anionic dendrimers and their effects on amyloid fibril formation from the islet amyloid polypeptide (IAPP) are described in another study [45]. The G0 dendrimer decorated with 4 sulfate groups (Fig. 9) inhibited the formation of amyloid fibrils from IAPP, but an increase in the number of sulfated units from 8 to 16 accelerated amyloid formation [45]. One study reported a computer simulation of lysine dendrimer G2 and showed that lysine dendrimers destroyed the amyloid fibrils [39].

Polymer-coated inorganic nanoparticles

The greatest obstacle to the use of inorganic nanoparticles (INPs) is their potential toxicity (including amyloidogenicity),

Table 1 Efficiency of different types of dendrimers at inhibiting the fibrillation of α-synuclein (adapted from refs. [41, 43, 44])

Dendrimer	Generation	End groups	Charge	Molar α-synuclein/dendrimer ratio	% inhibition
Phosphorus [44]	G3	$-N^+HEt_2$	+ 48	1:0.1	63.9 ± 3
				1:0.5	59.7 ± 2.5
				1:1	7.8 ± 3.4
				1:2	6.0 ± 3.0
	G4	$-N^+HEt_2$	+ 96	1:0.1	48.5 ± 3.3
				1:0.5	36.3 ± 2.7
				1:1	3.2 ± 2.7
				1:2	1.2 ± 0.7
Viologen-phosphorus [43]	G0	$-P(O)(OEt)_2$	+ 12	1:0.1	90.7 ± 3.4
				1:0.5	86.7 ± 1.9
				1:1	71.8 ± 1.3
				1:2	73.7 ± 1.2
	G0	PEG (Mw = 2000 g/mol)	+ 12	1:1	74.0 ± 2.5
				1:2	71.2 ± 1.9
BDBR7 [41]	G2	$-^+NH(Me)_2$	+ 16	1:1	91.8 ± 0.5
				1:2	95.2 ± 1.3
BDBR11 [41]	G2	$-^+NH_3$	+ 16	1:1	96.9 ± 1.9
				1:2	93.6 ± 2.5

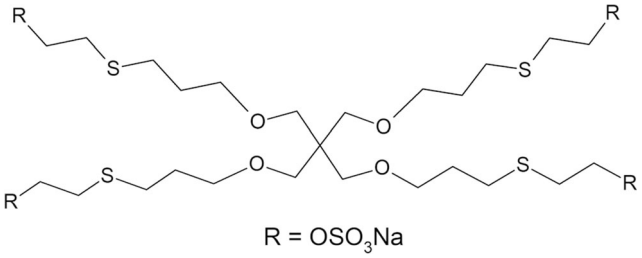

Fig. 9 The structure of anionic dendrimer G0 (adapted from ref. [45])

reducing their possible applications in medicine. In this case, the NP surface is often one of the most important factors determining toxicity. A very elegant method to circumvent the inappropriate surface properties of NPs is to coat them with natural or synthetic polymers. The use of an appropriate polymer coating can reduce the toxicity [46] of the whole system, and these coated NPs can then be used as a drug delivery system or for MRI monitoring [47].

The effects of iron oxide nanoparticles (IONPs) grafted with brushed poly(ethylene glycol) (bPEG-IONPs) (Fig. 10b) or brushed phosphorylcholine (PC-IONPs) (Fig. 10c) and of silver nanoparticles coated with branched polyethyleneimine (bPEI-AgNP) (Fig. 10a) on human islet amyloid polypeptide (IAPP) fibrillation have been described [48]. In this study, bPEG-IONPs did not exert any effect on amyloid fibrils. bPC-IONPs produced a very weak effect because they only compromised the stiffness of the IAPP fibrils. The most important finding was the significant decrease in the toxicity of IAPP fibrils induced by both types of IONPs [48]. Moreover, bPEI-AgNPs inhibited the process of IAPP fibrillation (Fig. 11). The inhibitory effect of bPEI-AgNPs was probably mediated by the strong electrostatic repulsion between bPEI and IAPP and by the interaction between the hydrophobic interior of bPEI and hydrophobic amyloidogenic region of IAPP (residues 20–29) [48].

Other studied NPs with polymer coatings include polymer-coated gold nanoparticles (AuNPs) [49]. The study used (a) a histidine-based polymer coating; (b) a polyacrylate coating with PEG and amine groups; (c) a polyacrylate coating with PEG, amine, and carboxylate groups; (d) a polyacrylate coating with PEG, amine, and phthalic groups; and (e) a polyacrylate coating with PEG, amine, and oleyl groups (Fig. 12). All polymer-coated AuNPs inhibited the amyloid fibrillation process of the $A\beta_{1-42}$ peptide. Experiments with various functional groups showed that both cationic and anionic surface charges, along with weakly hydrophobic functional groups, are necessary for efficient inhibition of amyloid fibril formation [49].

INPs include carbon nanoparticles that are functionalized by polymers. Fullerenes (C_{60}) are one example of INPs. C_{60} is often functionalized, such as the complex of C_{60} with polyvinylpyrrolidone (PVP) that was tested to establish its effect on the process of amyloid fibril formation in two studies [50, 51].

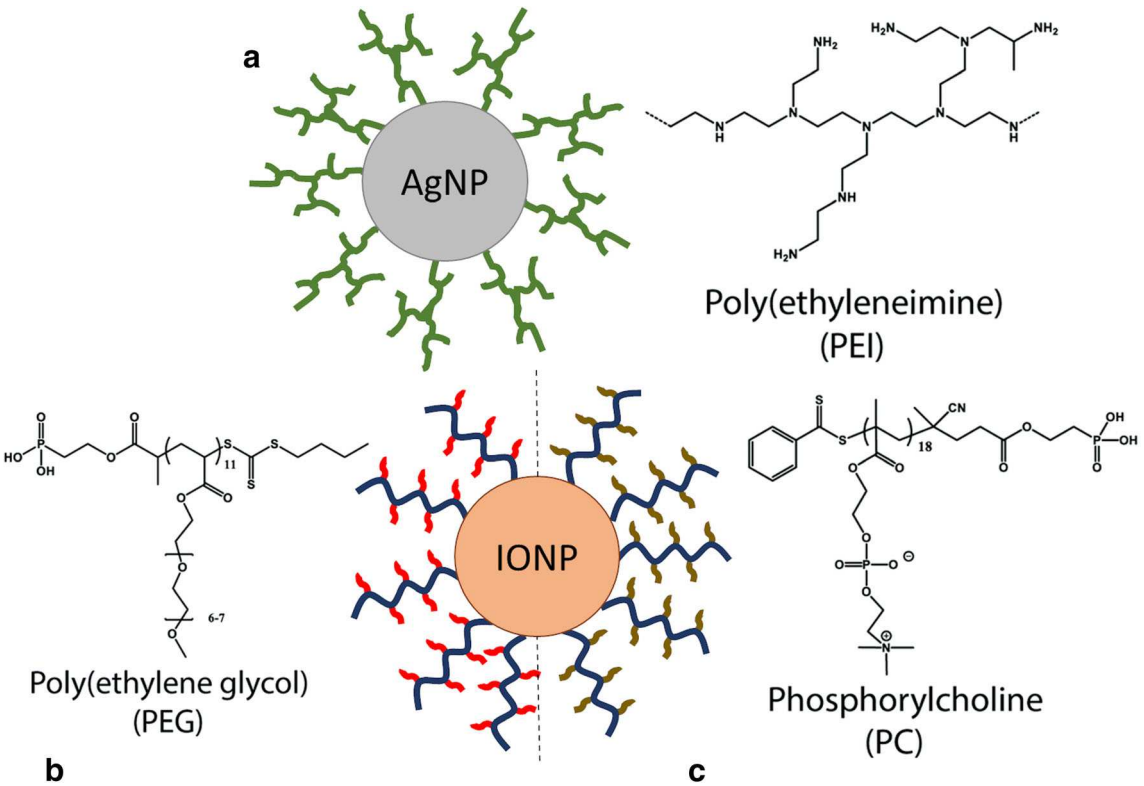

Fig. 10 Scheme of polymer-coated AgNP and IONP. **a** AgNPs with branched poly(ethyleneimine). **b** IONP grafted with brushed poly(ethylene glycol). **c** IONP grafted with brushed phosphorylcholine (adapted from ref. [48])

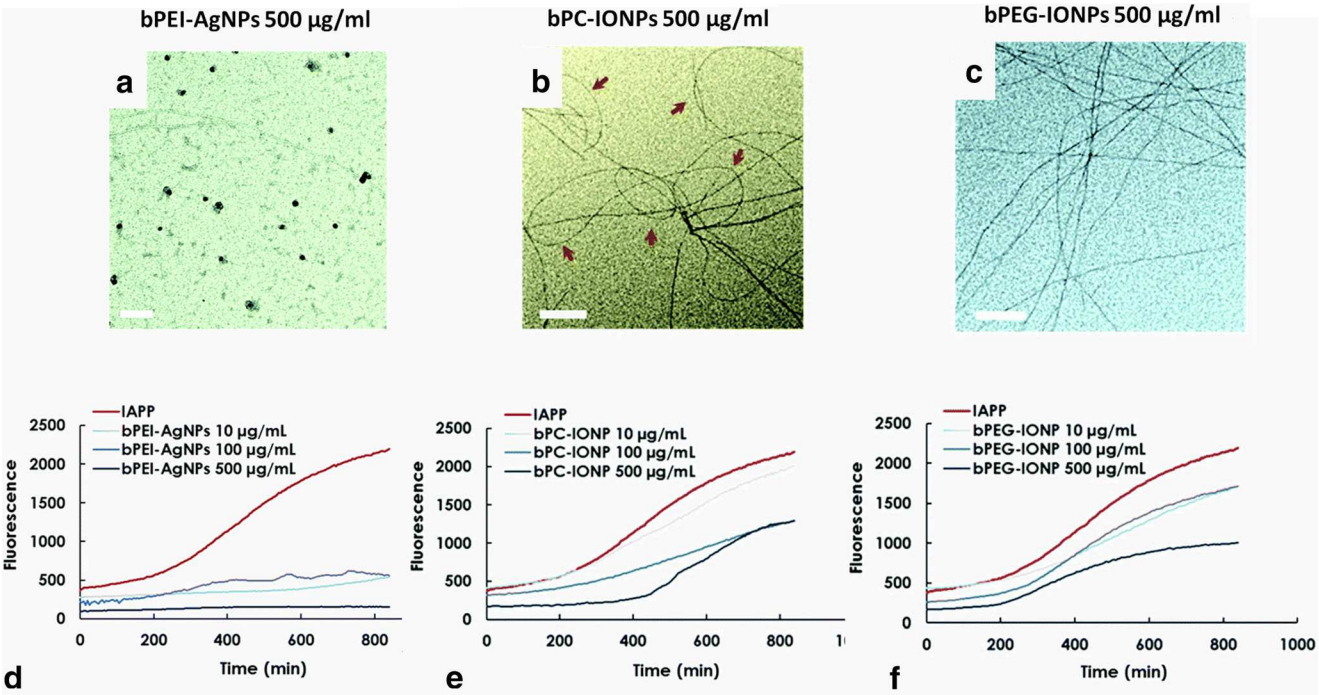

Fig. 11 **a**–**c** TEM micrographs of the effects of bPEI-AgNPs, bPC-IONPs, and bPEG-IONPs on IAPP fibrillation (scale bars: 200 nm). **d**–**f** Graphs of the ThT fluorescence (adapted from ref. [48])

C_{60}/PVP destroys the amyloid fibrils of $A\beta_{1-42}$ and muscle X-protein and even prevents fibril formation [50, 51]. Notably, the X-protein belongs to the muscle cytoskeletal proteins of the titin family (titin, C-, X-, and H-proteins). They also have the ability to form amyloids. Titin family proteins have 90% of the β-structure necessary for the formation of amyloid fibrils; in particular, X-protein forms helically twisted ribbon fibrils resembling Aβ peptides that play an important part in the development of AD. The X-protein is the only model system similar to Aβ [52].

Other INPs with polymer coatings are chitosan-coated silver (Ag-CHT) nanoparticles. Chitosan functions as a reducing and stabilizing agent during synthesis [53]. Ag-CHT nanoparticles were examined for their effects on human serum

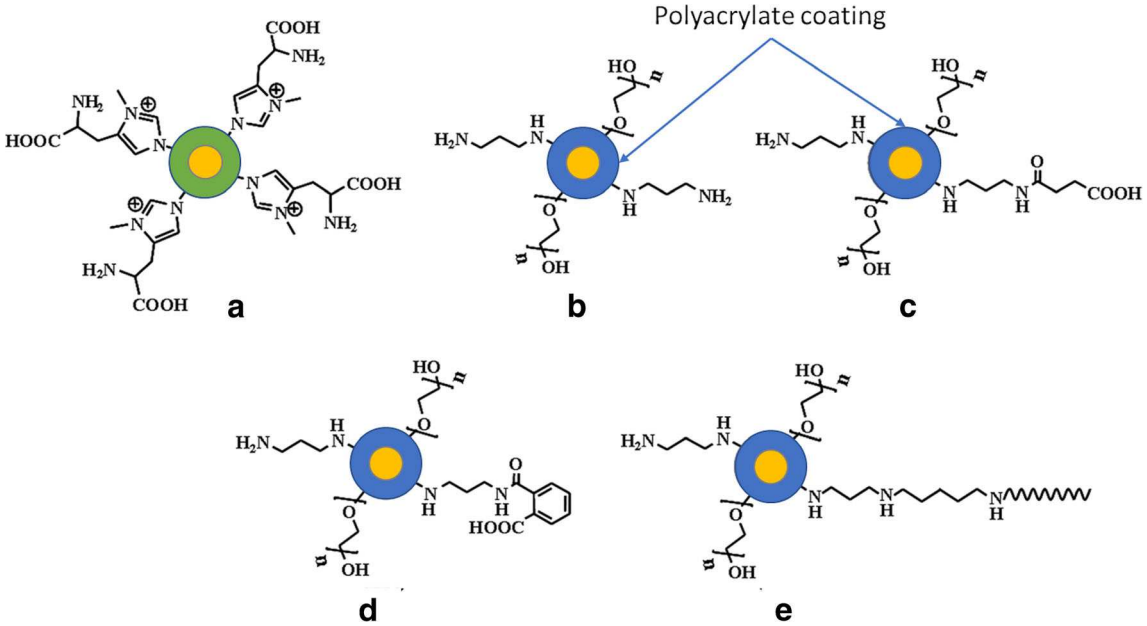

Fig. 12 Structures of polymer-coated AuNPs with different functional groups on their surface. a Histidine-based polymer coating. **b** Polyacrylate coating with PEG and amine groups. **c** Polyacrylate coating with PEG, amine, and carboxylate groups. **d** Polyacrylate coating with PEG, amine, and phthalic groups. **e** Polyacrylate coating with PEG, amine, and oleyl groups (adapted from ref. [49])

albumin (HAS) fibrillation. The Ag-CHT nanoparticles inhibited the process of amyloid fibril formation from HSA. Moreover, in the presence of Ag-CHT nanoparticles, HSA forms amorphous and globular aggregates, but not amyloid fibrils. The advantages of these Ag-CHT nanoparticles are their very good cytocompatibility and hemocompatibility within the application limit (150 μM) for HAS fibrillation [54].

Polysaccharides

Glycosaminoglycans (GAGs) play an important role in the formation of amyloid fibrils [55–58]. GAGs are unbranched linear polymers consisting of disaccharide units. Hyaluronic acid is a non-sulfated GAG, but most other types of GAGs are sulfated (e.g., heparan sulfate is largely composed of iduronic acid and *N*-acetylglucosamine-(4/6/2)-sulfate) [58]. Heparin is the hypersulfated form of heparan sulfate [58]. Another group similar to GAGs is proteoglycans (PGs). PGs have also been reported to be significant components of amyloid deposits. PGs are proteins that contain at least one (covalently bound, except for hyaluronan) GAG chain [59]. The GAGs/PGs are included in the extracellular matrix (ECM) [59]. The strength of the effect of GAGs on amyloid fibril formation depends on the particular peptide/protein and a specific GAG. For example, heparin and dextran sulfate exert the strongest effects on α-synuclein amyloid formation, while polyglutamic acid, polylysine, chondroitin-4-sulfate, and dermatan sulfate exerted weaker effects on α-synuclein amyloid formation [56]. Figure 13 shows differences in the strength of the effects of GAGs on α-synuclein fibrillation [56].

Valle-Delgado et al. describe the mechanism in which, on the one hand, GAGs promoted the amyloid fibril formation from Aβ, but on the other hand, they reduced the toxicity of the peptide in neuronal cell, because GAGs trapped more toxic oligomer forms of Aβ [60]. Radko et al. performed more complex experiment with heparin and Zn^{2+}-induced $A\beta_{1–42}$ aggregation. It was shown that heparin sterically hinders inclusion of the formed Zn^{2+}/ $A\beta_{1–42}$ oligomeric complex which then does not form amyloid fibrils [61]. Since protease-resistant form of the protein PrP is containing sulfated GAGs, Caughey et al. deal with sulfated polyanion as potential inhibitor of amyloid fibril formation [62]. Rosú et al. brings an understanding of the effect of GAGs on the amyloid fibril formation [63].

In addition to GAGs, another polysaccharide, chitin, is also an important component of the insoluble Aβ fibrils associated with AD [64, 65]. Chitin likely serves as a scaffold for the growth of fibrils and thus supports growth of amyloid fibrils [64–66]. Another polysaccharide that promotes fibril formation is dextran sulfate, which is mentioned in the next section with other polyanions [67].

Chitosan (CHT) is a structurally similar polysaccharide to chitin, but its effect on the process of amyloid fibrils is different. CHT (Fig. 14a) is a polysaccharide obtained from the deacetylation of chitin, which explains why the structure of CHT also contains residual 2-acetamido-2-deoxy-D-glucopyranose units from chitin. CHT is a linear cationic base biopolymer with a pK_a of ~ 6.5 that carries positive charges in an acidic environment. The properties of CHT are altered by modifying the side chain groups, e.g., introducing permanently charged moieties in *N*-trimethyl chitosan (TMC, Fig. 14b). The effects of CHT and TMC on $A\beta_{1–40}$ fibrillation have been described [68], and both CHT and TMC inhibited the process of amyloid fibril formation. The electrostatic interactions between negatively charged residues in $A\beta_{1–40}$ and the positively charged CHT/TMC play an important role in inhibition, and TMC exerted a stronger inhibitory effect than CHT. This finding was supported by an experiment performed at pH 4. At pH 4, $A\beta_{1–40}$ become positively charged, and the inhibitory effects of CHT and TMC were completely lost. It was also supported by molecular docking studies [68].

Nucleic acids

Nucleic acids (NAs) are polyanions that carry the genetic information and play a key role in protein biosynthesis. NA binding was determined for PrP, α-synuclein, Aβ, and huntingtin, which are associated with transmissible spongiform encephalopathies, and Parkinson, Alzheimer, and Huntington diseases [69]. There are many research groups that deal with interactions of proteins/peptides and NAs that showed that NAs have a significant effect on the process of amyloid fibril formation, and that they accelerate the amyloid fibril formation [69]. It is confirmed also by Calamai et al. that single-stranded and double-stranded DNAs accelerated the amyloid fibril formation form human lysozyme that was positively charged in the experiment. It was shown that the binding affinity for the amyloid protein was through electrostatic interactions [70]. Another group deals with a detailed investigation of the interaction between the prion and the NAs [71].

Synthetic polymers

The amyloidogenicity of synthetic polymers is mainly tested due to their applications in medicine and pharmacy. Dendrimers are reviewed above; here, we will mention other polymers that have been investigated for their effects on amyloid growth.

Mambule et al. [72] intravenously injected mice with an aqueous solution containing 10,000 g/mol polyethylene glycol (PEG). Simultaneously, all mice received a subcutaneous injection of silver nitrate ($AgNO_3$), because $AgNO_3$ has been used to experimentally induce secondary systemic amyloidosis (AA-amyloidosis). Amyloid deposits were observed in all

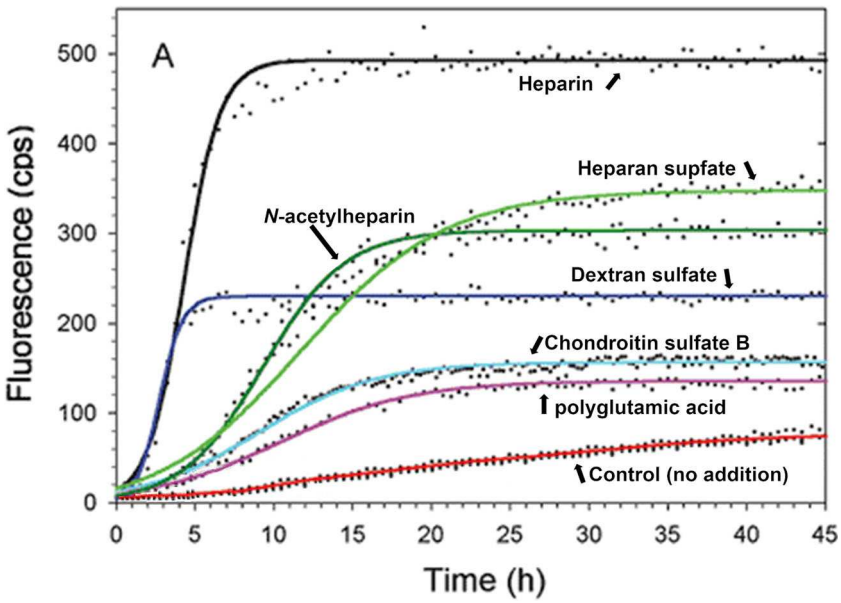

Fig. 13 The different effects of GAGs on α-synuclein fibrillation (detected as ThT fluorescence intensity) (adapted from ref. [56])

investigated organs of mice that received PEG, suggesting that PEG with a molecular weight of 10,000 g/mol might promote amyloidogenesis [72]. On the other hand, another study determined the effects of PEG with a molecular weight 2000 g/mol on the formation of amyloid-like fibrils from trypsin [73]. Trypsin is a serine protease that forms the β-sheet structure typical of amyloid fibrils. The same methods (e.g., fluorescence of ThT, TEM, circular dichroism) are used to detect amyloid-like fibrils formed from trypsin and typical amyloidogenic proteins/peptides (e.g., Aβ, IAPP) [73]. In the study, 2000 g/mol PEG inhibited the formation of amyloid-like trypsin fibrils and stabilized the protein structure [73]. These two studies produced different results, but each of them used PEG with different molecular weights and completely different experiments.

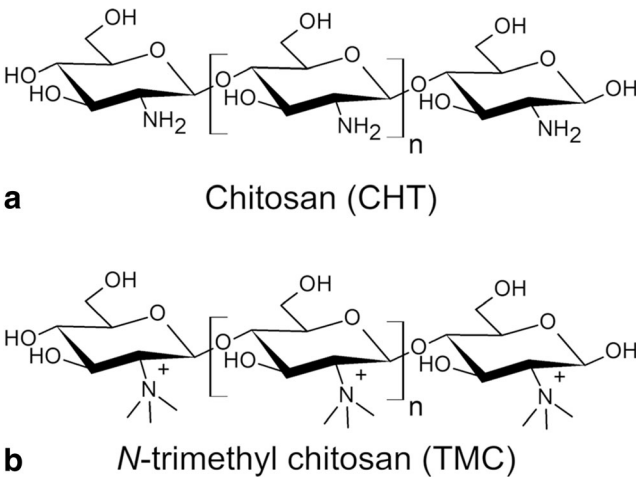

Fig. 14 Structures of chitosan (**a**) and *N*-trimethyl chitosan (**b**) (adapted from ref. [68])

The fibrillation of amyloid $A\beta_{1-40}$ in the presence of thermoresponsive polymers is displayed in Fig. 16, and structures and properties of polymers are shown in Fig. 15 and Table 2 [74]. The study investigated the effect of three polymers (3a–3c) at temperatures below the lower critical solution temperature (LCST) and one polymer (6c) at temperatures above the LCST, because measurements were performed at 37 °C. The fluorescence of ThT was used to monitor amyloid formation and is shown in Fig. 16 [74]. The time-dependent increase in ThT fluorescence follows a sigmoidal curve (Fig. 1) that is typical for the process of amyloid fibril formation. The fluorescence intensity was fitted using the following equation [75, 76]:

$$I(t) = y_0 + \frac{A}{1-e^{-[(t-t_{0.5})/\tau]}}$$

where $I(t)$ is intensity of fluorescence ThT, y_0 is the initial baseline, A is the amplitude of fluorescence, $t_{0.5}$ is the characteristic time when the fluorescence intensity reaches half of its maximum value, and the lag time is given by $t_{0.5}$-2τ with τ as the inverse of the rate constant [75, 76].

As shown in Fig. 16b, polymer 6c shortened the lag phase of $A\beta_{1-40}$. Most plausibly, the chains of polymer 6c acted as seeds, because the polymer was incubated at a temperature above its LCST. As shown in Fig. 16a, all three polymers (3a–3c) initially appeared to shorten the lag phase; however, when fitting the curve, polymer 3a slightly prolonged the lag phase from 18.3 to 19.3 h. The slopes of all three curves were steeper than the control curve of $A\beta_{1-40}$, indicating that polymers accelerated the fibrillation and increased the secondary nucleation and elongation rates [74].

α-Synuclein, whose amyloid deposits are associated with Parkinson's disease, was the amyloidogenic protein examined

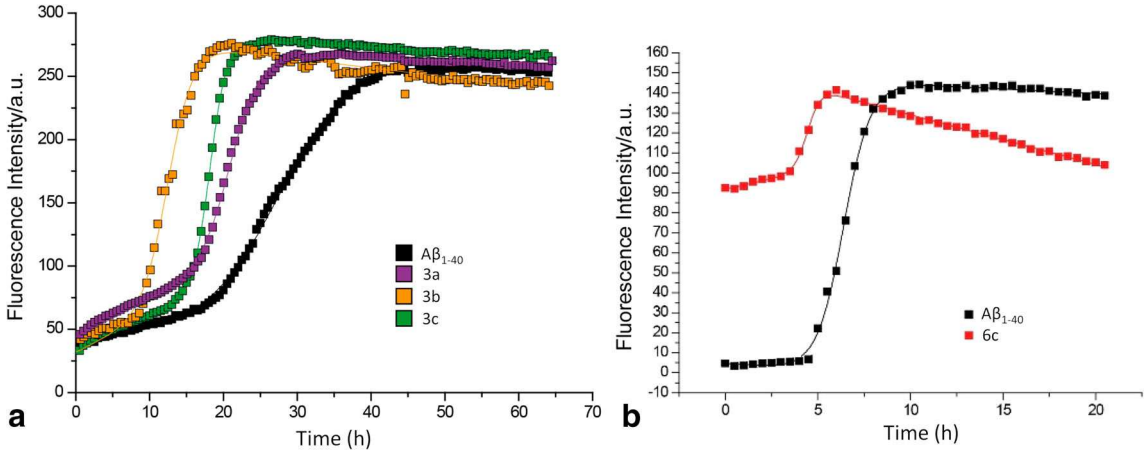

Fig. 16 Graphs of the fluorescence of ThT in the presence of polymers. **a** 3a–3c. **b** 6c (adapted from ref. [74])

in the study of the effect of polyanions and polycations (Fig. 17) on the process of amyloid fibril formation [67]. PSS and PAS polyanions inhibited α-synuclein amyloid formation. On the other hand, DS accelerated the process of amyloid fibril formation [67], consistent with the finding that glycosaminoglycans such as heparan sulfate promote the aggregation of amyloidogenic proteins [3, 56]. Additionally, PVS enhanced the process to a greater extent than DS. The α-synuclein protein immediately formed amyloid fibrils in the presence of PMA. After mixing PMA and α-synuclein, the solution immediately became turbid and then large flakes formed and the ThT fluorescence increased significantly. A similar phenomenon was observed in the presence of PEVP. The solution of PEVP and α-synuclein became turbid almost immediately after mixing, indicating the formation of large aggregates, but ThT fluorescence did not increase, supporting the hypothesis that these aggregates were not α-synuclein amyloid fibrils. Notably, PEPV-50% also inhibited the process, but to a lesser extent than PEVP [67].

There is a study dealing with proteolysis of glyceraldehyde-3-phosphate dehydrogenase (GAPDH) in the complexes with polyelectrolytes by proteinase K and thermolysin. It was shown that sodium PSS induced proteolysis of prion fibrils by proteinase K [77]. Another study investigated the influence of polyamino acids and polyelectrolytes on the amyloid fibril formation from $A\beta_{1–42}$. The experiment was performed at pH 8, that means that $A\beta_{1–42}$ was negatively charged. It was shown that positively charged polymers (polylysine, polyethylenimine, and poly(diallyldimethylammonium chloride) accelerated the amyloid fibril formation from $A\beta_{1–42}$, while positively charged or neutral polymers (polyacrylic acid, polyglutamic acid, and polythreonine) did not have any effect on the amyloid fibril formation [78].

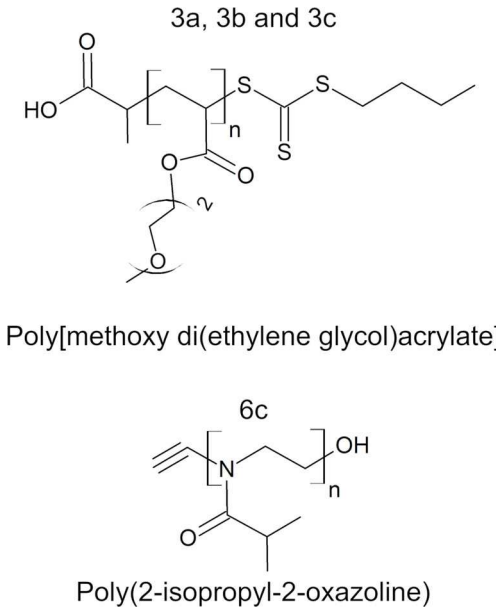

Fig. 15 Structures of thermoresponsive polymers (adapted from ref. [74])

Polymeric nanoparticles

A study investigating *N*-isopropylacrylamide and *N-tert*-butylacrylamide (NiPAM:BAM) copolymer nanoparticles and their effects on fibrillation of recombinant.

$A\beta_{M1–40}$ with an *N*-terminal methionine utilized four NiPAM:BAM nanoparticles with different ratios of NiPAM:BAM (50:50, 65:35, 85:15, and 100:0). Pure NiPAM nanoparticles exerted the greatest inhibitory effect on fibrillation, as they prolonged the lag phase to the greatest extent. As the amount of BAM increased, the prolongation of the lag phase decreased. Moreover, $A\beta_{M1–40}$ interacted directly with NiPAM:BAM nanoparticles. The greater inhibitory effect of pure NiPAM particles was explained by the formation of a large number of hydrogen bonds on the surface of NiPAM particles that potentially hinders the formation of nuclei and elongation of the fibrils [79].

The effects of self-assembled chitosan-hyaluronic acid nanoparticles on $A\beta_{1–40}$ fibrillation have been investigated

Table 2 Properties of thermoresponsive polymers [74]

Polymer	Molecular weight (M_N) (g/mol)	Cloud point temperature in sodium borate buffer (pH = 9.2) T (°C)
3a	3600	No LCST detectable
3b	8500	52.7
3c	14,600	49.5
6c	11,000	36.2

[80]. CHT is a polycation and hyaluronic acid (HA) is a polyanion, together forming interpolyelectrolyte complex nanoparticles via electrostatic interactions. Seven types of CHT-HA nanoparticles were tested with different ratios of positively to negatively charged groups. The CHT-HA nanoparticles also possessed different hydrodynamic radii (R_h). The effect of CHT-HA nanoparticles on $A\beta_{1–40}$ fibrillation was tested at different pH values (4.0, 7.4, and 8.5) to understand the effect of nanoparticles on the process of amyloid fibril formation. At pH 7.4, most of the CHT-HA nanoparticles with a positive or negative ζ-potential inhibited $A\beta_{1–40}$ fibrillation, but nanoparticles with a positive ζ-potential were more effective. Pure CHT and HA did not exert inhibitory effects. Thus, both positively and negatively charged components were important for inhibiting amyloid formation, but they had different mechanisms of action. At pH 4.0, the effect was changed; nanoparticles with a negative ζ-potential maintained the inhibitory effect, while nanoparticles with a positive ζ-potential lost their inhibitory effect, because $A\beta_{1–40}$ is also positively charged at pH 4.0. At pH 8.5, only $A\beta_{1–40}$ and nanoparticles with a negative ζ-potential showed lower fluorescence of ThT, indicating that no fibril formation occurred. On the other hand, nanoparticles with a positive ζ-potential promoted $A\beta_{1–40}$ fibrillation, which was probably caused by the partial neutralization of the highly negatively charged $A\beta_{1–40}$ by nanoparticles with a positive ζ-potential that promoted the aggregation and formation of amyloid fibrils from $A\beta_{1–40}$ [80]. The results of this study are consistent with a study examining chitosan and *N*-trimethyl chitosan described above [68].

Two studies have analyzed poly(lactic-co-glycolic acid)-poly(ethylene glycol) (PLGA-b-PEG) nanoparticles loaded with different molecules [81, 82]. The first is loaded with selegiline [81] and the second is loaded with donepezil [82]. Selegiline is a selective monoamine oxidase-B (MAO-B) inhibitor that increases the levels of dopamine in the brain. It is used as a drug to treat Parkinson's disease [83]. The first study showed that selegiline-loaded PLGA-b-PEG destabilized Aβ ($A\beta_{1–40}$ and $A\beta_{1–42}$) formation [81]. On the one hand, selegiline has been suggested as a treatment for AD, but evidence of a clinically meaningful benefit of this treatment is not available [83]. On the other hand, this study showed the potential challenge and direct targeting to the brain during the treatment of AD. The second study is based on the findings from the first study, but analyzes donepezil-loaded PLGA-b-PEG nanoparticles [82]. The results of the second study are consistent with the results of the first study. Donepezil is a selective acetylcholinesterase (AChE) inhibitor used to treat AD. AChE inhibitors prolong the effect of acetylcholine at synapses by preventing its degradation. This strategy results in improved cognitive function, mood, and behavior [8]. Additionally, donepezil-loaded PLGA-b-PEG nanoparticles destabilize Aβ ($A\beta_{1–40}$ and $A\beta_{1–42}$) formation. Moreover,

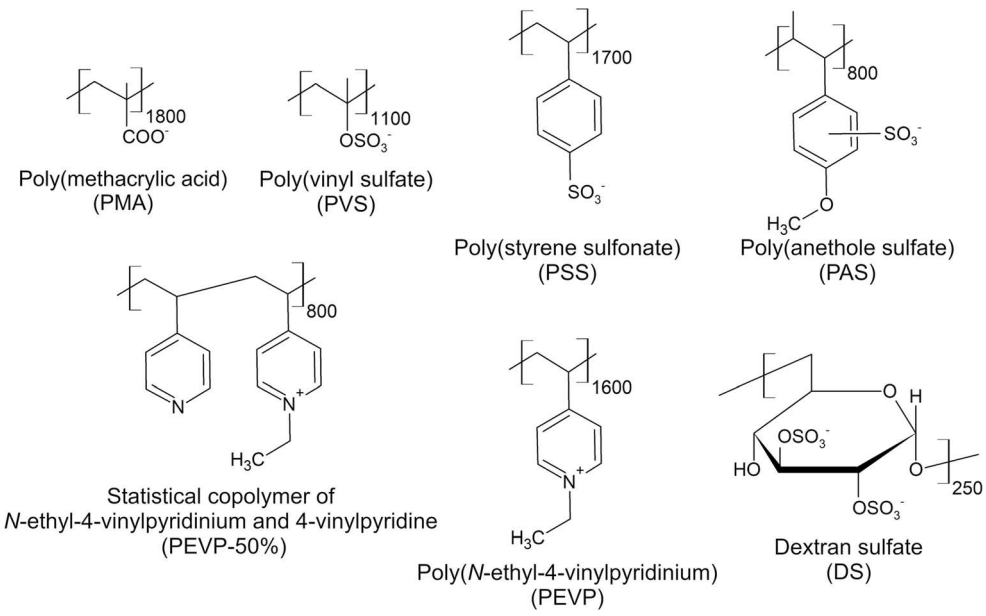

Fig. 17 Structures of polyanions and polycations (adapted from ref. [67])

donepezil-loaded PLGA-b-PEG nanoparticles pass through the BBB in an in vitro model [82].

Advantages of polymers/nanoparticles over small molecules

There is a number of studies dealing with inhibition of amyloid fibril formation by small molecules. Giorgetti et al. wrote an excellent review considering low molecular weight molecules that act as inhibitors of amyloid fibril formation. The review deals with therapeutic efficacy of drugs and nutraceuticals currently in use or under investigation [84]. Beside small molecules, polymers [67] and polymer/polymer-coated nanoparticles [25, 26, 48, 82] are promising candidates for the inhibition of the process of amyloid fibril formation. However, to design molecules efficiently inhibiting the process of amyloid fibril formation is very difficult and brings a number of problems that must be avoided such as poor blood-brain barrier (BBB) permeability, complex synthesis route, low in vivo stability, and cytotoxicity. Polymers [67] and nanoparticles [82] (especially polymer nanoparticles or polymer-coated inorganic nanoparticles) bring considerable advantages over small molecule amyloid fibril formation inhibitors such as possibility of multiple amyloidogenic protein-inhibitor interaction, good in vivo stability, non-toxicity, biocompatibility, possibility to tailor structure for a certain amyloid protein/peptide, or high variability in architecture. Polymers/nanoparticles can also simultaneously serve as drug delivery systems or as theranostics [21–23, 47]. Summarizing the advantages of polymers/nanoparticles over small molecules as inhibitors of amyloid formation, polymers/nanoparticles offer us a much wider range of properties mentioned above that can be used to influence the process of amyloid fibril formation.

Properties of polymers affecting of promotion/inhibition of amyloid fibril formation

Various polymer properties such as molecular weight, hydrophobicity, molecular structure, or charge are very important for their inhibitory/promoting activity toward amyloid fibril formation. The same polymer of different molecular weight may behave differently. An example is the mentioned experiments with PEG, where 10,000 g/mol PEG probably acted as a promoter [72], but 2000 g/mol PEG was an inhibitor [73]. Not only the difference in the performed experiments but also the molecular weight could lead to different results. Furthermore, the similarity of the molecular weight of the tested polymer with $A\beta_{1-40}$ in ref. [74] (mentioned in the part synthetic polymers) led to the elongation of the lag phase. This similarity may be one of the parameters that, with a suitable polymer structure, could significantly improve efficiency of the inhibition.

One of the most important roles in the process of amyloid fibril formation plays is the π–π interactions [17, 85]. In the past, it has been shown that short sequences of Aβ with aromatic residues can be used for inhibition of amyloid fibril formation from Aβ [86–88]. Based on these observations, the introduction of an aromatic ring into the polymer structure can significantly affect the interaction with the peptide/proteins and vastly alter the amyloid fibril formation or completely block it. The theory is supported by the fact that many polyphenols are good inhibitors of the amyloid fibril formation [89].

However, also hydrophobic and electrostatic interactions play important roles in the amyloid fibril formation. This is why many research groups combine in the polymer inhibitors' structure multiple functional groups, such as aromatic rings plus charged groups [38, 67], hydrophobic groups plus charged groups [31, 41], and hydrophobic plus electroneutral hydrophilic groups [74]. In the case of charged groups in the polymer structure, it is necessary to be very careful when testing the amyloidogenicity of these polymers, because proteins/peptides contain both acidic and basic functional groups. At a pH below their pI, proteins/peptides are positively charged, and above their pI, the proteins/peptides are negatively charged, and therefore, the obtained results are strongly dependent on the pH of the testing condition that was shown in ref. [68, 80] mentioned above in parts about polysaccharides and polymeric nanoparticles. Several approximate pIs for model proteins/peptides are given in Table 3. Model systems of HEWL, ATTR, and hIAPP have testing conditions set under their pI as in ref. [29, 30, 94]. On the other hand, model systems of $A\beta_{1-40}$ and $A\beta_{1-42}$ are very often negatively charged in experiments as in ref. [33, 50].

Of course, not only the mentioned properties above are important for influencing the process of amyloid fibril formation. Different behaviors can be expected for linear polymer and nanosized globular macromolecules (such as dendrimers), which means that 3D structure also can play some role in amyloid fibril formation promotion/inhibition. In conclusion, it is necessary to take into account all properties of both the inhibitor and of the amyloidogenic protein to design an efficient inhibitory polymer architecture.

Table 3 Approximate pI of several proteins/peptides

Protein/peptide	pI	References
HEWL	10.7	[90]
$A\beta_{1-42}$	5.5	[91]
$A\beta_{1-40}$	5.3	[92]
ATTR	4.7	[29]
hIAPP	8.8	[93]

Conclusions

Polymers have extensive uses. Their properties are easily modified, which facilitate their wide range of applications. Hence, the molecular mechanisms underlying the interactions between polymers and biological systems must be understood. In a biological medium, polymers may interact with biomolecules, such as proteins, nucleic acids, and lipids. One of the most important interactions is the adsorption of proteins, which may induce a conformational change in the native structure of the adsorbed protein molecule, causing it to unfold. This conformational change may lead to protein misfolding and subsequent amyloid fibril formation to create amyloid deposits that are associated with serious diseases known as amyloidoses. Amyloidoses are various diseases or pathological conditions in which the final result is the transformation of normally soluble proteins into insoluble amyloids with a fibrillar structure. Amyloids are deposited in the tissues and disrupt their function.

Methods for assessing the effects of polymer materials on the process of amyloid fibril formation are very complex. Most studies start with a solution of only one purified protein at high concentration in a closed system to test the effects of polymers, which is far from the actual biological environment that simultaneously contains thousands of different proteins at different concentrations and different stoichiometries to the polymers. These proteins may dynamically compete with each other, particularly in the adhesion to the polymer nanoparticles such as dendrimers (e.g., so-called Vroman effect [95]), the essential step in any interaction with amyloid formation.

One of the main goals is the inhibition of amyloid fibril formation, which has also been achieved with polymers. One of the most commonly used modifications is the introduction of charged groups or the use of charged polymer materials (e.g., CHT-HA nanoparticles [80], TMC [68], and dendrimers [41, 43, 44]). In this case, testing must be conducted carefully, as the inhibitory effect may be lost when the pH changes, as the protein/peptide also has some acquired groups that may change with pH [68, 80]. Not only electrostatic interaction but also π–π and hydrophobic interactions play important roles in the process of amyloid fibril formation, providing other options for the modification of polymer materials.

Some studies extend testing by examining targeting, for example, to determine the ability to cross through the BBB, which is one of the challenges in the treatment of AD, an amyloidosis. For example, the G4HisMal dendrimers described in a previous study [35] did not inhibit the fibrillation of $A\beta_{1-40}$, but crossed the BBB and improved spatial memory deficits in a mouse model. Another example is the donepezil-loaded PLGA-b-PEG nanoparticles described in a published report [82]. The authors of this study are very close to a treatment for AD, because donepezil-loaded PLGA-b-PEG nanoparticles crossed though BBB, destabilized Aβ amyloid fibrils, and carried a drug, donepezil, used to treat AD.

On the other hand, studies have analyzed common polymers in our body, such as GAGs, their roles in amyloidosis, why they are present in amyloids, and their functions in forming amyloid fibrils. An understanding of the roles of these polymers may provide important insights into the process of amyloid fibril formation in the human body, but may also be important for the treatment of amyloidoses.

Funding information Monika Holubová received financial support from Charles University, project GA UK No. 386218. PS and MH also received financial support from the Czech Science Foundation (grants nos. 19-01438S and 18-07983S).

Compliance with ethical standards

Conflict of interest The authors declare that they have no conflicts of interest.

References

1. Chuang E, Hori AM, Hesketh CD, Shorter J (2018) Amyloid assembly and disassembly. J Cell Sci 131:jcs189928. https://doi.org/10.1242/jcs.189928
2. Radford SE, Weissman JS (2012) Special issue: the molecular and cellular mechanisms of amyloidosis. J Mol Biol 421:139–141. https://doi.org/10.1016/j.jmb.2012.05.042
3. Sideras K, Gertz MA (2009) Chapter 1 amyloidosis. In: Advances in clinical chemistry. pp 1–44
4. Sipe JD, Benson MD, Buxbaum JN, Ikeda SI, Merlini G, Saraiva MJM, Westermark P (2010) Amyloid fibril protein nomenclature: 2010 recommendations from the nomenclature committee of the International Society of Amyloidosis. Amyloid 17:101–104. https://doi.org/10.3109/13506129.2010.526812
5. Serpell LC, Sunde M, Benson MD, Tennent GA, Pepys MB, Fraser PE (2000) The protofilament substructure of amyloid fibrils. J Mol Biol 300:1033–1039. https://doi.org/10.1006/jmbi.2000.3908
6. Ionescu-Zanetti C, Khurana R, Gillespie JR, Petrick JS, Trabachino LC, Minert LJ, Carter SA, Fink AL (1999) Monitoring the assembly of Ig light-chain amyloid fibrils by atomic force microscopy. Proc Natl Acad Sci 96:13175–13179. https://doi.org/10.1073/pnas.96.23.13175
7. Taglialegna A, Lasa I, Valle J (2016) Amyloid structures as biofilm matrix scaffolds. J Bacteriol 198:2579–2588. https://doi.org/10.1128/JB.00122-16
8. Holubová M, Hrubý M (2016) Terapeutika amyloidóz. Chem List 110:851–859
9. Wei G, Su Z, Reynolds NP, Arosio P, Hamley IW, Gazit E, Mezzenga R (2017) Self-assembling peptide and protein amyloids: from structure to tailored function in nanotechnology. Chem Soc Rev 46:4661–4708. https://doi.org/10.1039/C6CS00542J
10. Cheung H-Y, Lau K-T, Ho M-P, Mosallam A (2009) Study on the mechanical properties of different silkworm silk fibers. J Compos Mater 43:2521–2531. https://doi.org/10.1177/0021998309345347
11. Engineering ToolBox (2003) Young's modulus - tensile and yield strength for common materials. https://www.engineeringtoolbox.com/young-modulus-d_417.html. Accessed 27 Feb 2020

12. Hori Y, Hashimoto T, Nomoto H, Hyman BT, Iwatsubo T (2015) Role of apolipoprotein E in β-amyloidogenesis: isoform-specific effects on protofibril to fibril conversion of Aβ in vitro and brain Aβ deposition in vivo. J Biol Chem 290:15163–15174. https://doi.org/10.1074/jbc.M114.622209
13. Bemporad F, Chiti F (2013) Pathways of amyloid formation. Amyloid fibrils and prefibrillar aggregates. Wiley-VCH Verlag GmbH & Co. KGaA, Weinheim, pp 151–166
14. Arosio P, Knowles TPJ, Linse S (2015) On the lag phase in amyloid fibril formation. Phys Chem Chem Phys 17:7606–7618. https://doi.org/10.1039/c4cp05563b
15. Iannuzzi C, Maritato R, Irace G, Sirangelo I (2013) Misfolding and amyloid aggregation of apomyoglobin. Int J Mol Sci 14:14287–14300. https://doi.org/10.3390/ijms140714287
16. Hurshman AR, White JT, Powers ET, Kelly JW (2004) Transthyretin aggregation under partially denaturing conditions is a downhill polymerization. Biochemistry 43:7365–7381. https://doi.org/10.1021/bi049621l
17. Gazit E (2005) Mechanisms of amyloid fibril self-assembly and inhibition. FEBS J 272:5971–5978. https://doi.org/10.1111/j.1742-4658.2005.05022.x
18. Marshall KE, Morris KL, Charlton D, O'Reilly N, Lewis L, Walden H, Serpell LC (2011) Hydrophobic, aromatic, and electrostatic interactions play a central role in amyloid fibril formation and stability. Biochemistry 50:2061–2071. https://doi.org/10.1021/bi101936c
19. Chiti F, Dobson CM (2006) Protein misfolding, functional amyloid, and human disease. Annu Rev Biochem 75:333–366. https://doi.org/10.1146/annurev.biochem.75.101304.123901
20. Mülhaupt R (2004) Hermann Staudinger and the origin of macromolecular chemistry. Angew Chem Int Ed 43:1054–1063. https://doi.org/10.1002/anie.200330070
21. Nimesh S (2013) Dendrimers. In: Gene therapy. Elsevier, pp 259–285
22. Abbasi E, Aval SF, Akbarzadeh A et al (2014) Dendrimers: synthesis, applications, and properties. Nanoscale Res Lett 9:1–10
23. Noriega-Luna B, Godínez LA, Rodríguez FJ, Rodríguez A, Zaldívar-Lelo de Larrea G, Sosa-Ferreyra CF, Mercado-Curiel RF, Manríquez J, Bustos E (2014) Applications of dendrimers in drug delivery agents, diagnosis, therapy, and detection. J Nanomater 2014:1–19. https://doi.org/10.1155/2014/507273
24. Klajnert B, Stanisławska L, Bryszewska M, Pałecz B (2003) Interactions between PAMAM dendrimers and bovine serum albumin. Biochim Biophys Acta, Proteins Proteomics 1648:115–126. https://doi.org/10.1016/S1570-9639(03)00117-1
25. Klajnert B, Cortijo-Arellano M, Cladera J, Bryszewska M (2006) Influence of dendrimer's structure on its activity against amyloid fibril formation. Biochem Biophys Res Commun 345:21–28. https://doi.org/10.1016/j.bbrc.2006.04.041
26. Klajnert B, Cortijo-Arellano M, Bryszewska M, Cladera J (2006) Influence of heparin and dendrimers on the aggregation of two amyloid peptides related to Alzheimer's and prion diseases. Biochem Biophys Res Commun 339:577–582. https://doi.org/10.1016/j.bbrc.2005.11.053
27. Sengupta U, Nilson AN, Kayed R (2016) The role of amyloid-β oligomers in toxicity, propagation, and immunotherapy. EBioMedicine 6:42–49. https://doi.org/10.1016/j.ebiom.2016.03.035
28. Rekas A, Lo V, Gadd GE, Cappai R, Yun SI (2009) PAMAM dendrimers as potential agents against fibrillation of α-synuclein, a Parkinson's disease-related protein. Macromol Biosci 9:230–238. https://doi.org/10.1002/mabi.200800242
29. Inoue M, Ueda M, Higashi T, Anno T, Fujisawa K, Motoyama K, Mizuguchi M, Ando Y, Jono H, Arima H (2019) Therapeutic potential of polyamidoamine dendrimer for amyloidogenic transthyretin amyloidosis. ACS Chem Neurosci 10:2584–2590. https://doi.org/10.1021/acschemneuro.9b00059
30. Gurzov EN, Wang B, Pilkington EH, Chen P, Kakinen A, Stanley WJ, Litwak SA, Hanssen EG, Davis TP, Ding F, Ke PC (2016) Inhibition of hIAPP amyloid aggregation and pancreatic β-cell toxicity by OH-terminated PAMAM dendrimer. Small 12:1615–1626. https://doi.org/10.1002/smll.201502317
31. Heegaard PMH, Pedersen HG, Flink J, Boas U (2004) Amyloid aggregates of the prion peptide PrP106-126 are destabilised by oxidation and by the action of dendrimers. FEBS Lett 577:127–133. https://doi.org/10.1016/j.febslet.2004.09.073
32. Supattapone S, Wille H, Uyechi L, Safar J, Tremblay P, Szoka FC, Cohen FE, Prusiner SB, Scott MR (2001) Branched polyamines cure prion-infected neuroblastoma cells. J Virol 75:3453–3461. https://doi.org/10.1128/jvi.75.7.3453-3461.2001
33. Klementieva O, Benseny-Cases N, Gella A, Appelhans D, Voit B, Cladera J (2011) Dense shell glycodendrimers as potential nontoxic anti-amyloidogenic agents in Alzheimer's disease. Amyloid–dendrimer aggregates morphology and cell toxicity. Biomacromolecules 12:3903–3909. https://doi.org/10.1021/bm2008636
34. Klementieva O, Aso E, Filippini D, Benseny-Cases N, Carmona M, Juvés S, Appelhans D, Cladera J, Ferrer I (2013) Effect of poly(propylene imine) glycodendrimers on β-amyloid aggregation in vitro and in APP/PS1 transgenic mice, as a model of brain amyloid deposition and Alzheimer's disease. Biomacromolecules 14:3570–3580. https://doi.org/10.1021/bm400948z
35. Aso E, Martinsson I, Appelhans D, Effenberg C, Benseny-Cases N, Cladera J, Gouras G, Ferrer I, Klementieva O (2019) Poly(propylene imine) dendrimers with histidine-maltose shell as novel type of nanoparticles for synapse and memory protection. Nanomed Nanotechnol Biol Med 17:198–209. https://doi.org/10.1016/j.nano.2019.01.010
36. Laumann K, Boas U, Larsen HM, Heegaard PMH, Bergström AL (2015) Urea and thiourea modified polypropyleneimine dendrimers clear intracellular α-synuclein aggregates in a human cell line. Biomacromolecules 16:116–124. https://doi.org/10.1021/bm501244m
37. McCarthy JM, Rasines Moreno B, Filippini D et al (2013) Influence of surface groups on poly(propylene imine) dendrimers antiprion activity. Biomacromolecules 14:27–37. https://doi.org/10.1021/bm301165u
38. Sorokina SA, Stroylova YY, Tishina SA, Shifrina ZB, Muronetz VI (2019) Promising anti-amyloid behavior of cationic pyridylphenylene dendrimers: role of structural features and mechanism of action. Eur Polym J 116:20–29. https://doi.org/10.1016/j.eurpolymj.2019.03.053
39. Popova E, Khamidova D, Neelov I, Komilov F (2018) Lysine dendrimers and their complexes with therapeutic and amyloid peptides: computer simulation. In: Dendrimers - fundamentals and applications. InTech
40. Sorokina SA, Stroylova YY, Shifrina ZB, Muronetz VI (2016) Disruption of amyloid prion protein aggregates by cationic pyridylphenylene dendrimers. Macromol Biosci 16:266–275. https://doi.org/10.1002/mabi.201500268
41. Milowska K, Szwed A, Mutrynowska M, Gomez-Ramirez R, de la Mata FJ, Gabryelak T, Bryszewska M (2015) Carbosilane dendrimers inhibit α-synuclein fibrillation and prevent cells from rotenone-induced damage. Int J Pharm 484:268–275. https://doi.org/10.1016/j.ijpharm.2015.02.066
42. Cannon JR, Tapias V, Na HM, Honick AS, Drolet RE, Greenamyre JT (2009) A highly reproducible rotenone model of Parkinson's disease. Neurobiol Dis 34:279–290. https://doi.org/10.1016/j.nbd.2009.01.016
43. Milowska K, Grochowina J, Katir N, el Kadib A, Majoral JP, Bryszewska M, Gabryelak T (2013) Viologen-phosphorus

dendrimers inhibit α-synuclein fibrillation. Mol Pharm 10:1131–1137. https://doi.org/10.1021/mp300636h
44. Milowska K, Gabryelak T, Bryszewska M, Caminade AM, Majoral JP (2012) Phosphorus-containing dendrimers against α-synuclein fibril formation. Int J Biol Macromol 50:1138–1143. https://doi.org/10.1016/j.ijbiomac.2012.02.003
45. Nguyen PT, Sharma R, Rej R, de Carufel CA, Roy R, Bourgault S (2016) Low generation anionic dendrimers modulate islet amyloid polypeptide self-assembly and inhibit pancreatic β-cell toxicity. RSC Adv 6:76360–76369. https://doi.org/10.1039/c6ra15373a
46. Baldrighi M, Trusel M, Tonini R, Giordani S (2016) Carbon nanomaterials interfacing with neurons: an in vivo perspective. Front Neurosci 10:250
47. Chertok B, Moffat BA, David AE, Yu F, Bergemann C, Ross BD, Yang VC (2008) Iron oxide nanoparticles as a drug delivery vehicle for MRI monitored magnetic targeting of brain tumors. Biomaterials 29:487–496. https://doi.org/10.1016/j.biomaterials.2007.08.050
48. Wang M, Kakinen A, Pilkington EH, Davis TP, Ke PC (2017) Differential effects of silver and iron oxide nanoparticles on IAPP amyloid aggregation. Biomater Sci 5:485–493. https://doi.org/10.1039/C6BM00764C
49. Palmal S, Jana NR, Jana NR (2014) Inhibition of amyloid fibril growth by nanoparticle coated with histidine-based polymer. J Phys Chem C 118:21630–21638. https://doi.org/10.1021/jp505613g
50. Bobylev AG, Shpagina MD, Bobyleva LG, Okuneva AD, Piotrovsky LB, Podlubnaya ZA (2012) Antiamyloid properties of fullerene C60 derivatives. Biophysics (Oxf) 57:300–304. https://doi.org/10.1134/S0006350912030050
51. Bobylev AG, Marsagishvili LG, Podlubnaya ZA (2010) Fluorescence analysis of the action of soluble derivatives of fullerene C60 on amyloid fibrils of the brain peptide Aβ(1–42). Biophysics (Oxf) 55:699–702. https://doi.org/10.1134/S0006350910050027
52. Marsagishvili LG, Bobylev AG, Shpagina MD, Troshin PA, Podlubnaya ZA (2009) Effect of fullerenes C60 on X-protein amyloids. Biophysics (Oxf) 54:135–138. https://doi.org/10.1134/S000635090902002X
53. Wei D, Qian W (2008) Facile synthesis of Ag and Au nanoparticles utilizing chitosan as a mediator agent. Colloids Surf B: Biointerfaces 62:136–142. https://doi.org/10.1016/j.colsurfb.2007.09.030
54. Sen S, Konar S, Das B, Pathak A, Dhara S, Dasgupta S, DasGupta S (2016) Inhibition of fibrillation of human serum albumin through interaction with chitosan-based biocompatible silver nanoparticles. RSC Adv 6:43104–43115. https://doi.org/10.1039/c6ra05129d
55. McLaurin J, Franklin T, Zhang X, Deng J, Fraser PE (1999) Interactions of Alzheimer amyloid-β peptides with glycosaminoglycans. Eur J Biochem 266:1101–1110. https://doi.org/10.1046/j.1432-1327.1999.00957.x
56. Cohlberg JA, Li J, Uversky VN, Fink AL (2002) Heparin and other glycosaminoglycans stimulate the formation of amyloid fibrils from α-synuclein in vitro. Biochemistry 41:1502–1511. https://doi.org/10.1021/bi011711s
57. Stewart KL, Radford SE (2017) Amyloid plaques beyond Aβ: a survey of the diverse modulators of amyloid aggregation. Biophys Rev 9:405–419. https://doi.org/10.1007/s12551-017-0271-9
58. Díaz-Nido J, Wandosell F, Avila J (2002) Glycosaminoglycans and β-amyloid, prion and tau peptides in neurodegenerative diseases. Peptides 23:1323–1332. https://doi.org/10.1016/S0196-9781(02)00068-2
59. Magnus JH, Stenstad T (1997) Proteoglycans and the extracellular matrix in amyloidosis. Amyloid 4:121–134. https://doi.org/10.3109/13506129708995282
60. Valle-Delgado JJ, Alfonso-Prieto M, Groot NS, Ventura S, Samitier J, Rovira C, Fernàndez-Busquets X (2010) Modulation of Aβ 42 fibrillogenesis by glycosaminoglycan structure. FASEB J 24:4250–4261. https://doi.org/10.1096/fj.09-153551
61. Radko SP, Khmeleva SA, Mantsyzov AB, Kiseleva YY, Mitkevich VA, Kozin SA, Makarov AA (2018) Heparin modulates the kinetics of zinc-induced aggregation of amyloid-β peptides. J Alzheimers Dis 63:539–550. https://doi.org/10.3233/JAD-171120
62. Caughey B, Raymond GJ (1993) Sulfated polyanion inhibition of scrapie-associated PrP accumulation in cultured cells. J Virol 67:643–650. https://doi.org/10.1128/JVI.67.2.643-650.1993
63. Rosú SA, Toledo L, Urbano BF, Sanchez SA, Calabrese GC, Tricerri MA (2017) Learning from synthetic models of extracellular matrix; differential binding of wild type and amyloidogenic human apolipoprotein A-I to hydrogels formed from molecules having charges similar to those found in natural GAGs. Protein J 36:374–383. https://doi.org/10.1007/s10930-017-9728-8
64. Castellani R, Siedlak S, Fortino A, Perry G, Ghetti B, Smith M (2005) Chitin-like polysaccharides in Alzheimers disease brains. Curr Alzheimer Res 2:419–423. https://doi.org/10.2174/156720505774330555
65. Castellani RJ, Perry G, Smith MA (2007) The role of novel chitin-like polysaccharides in Alzheimer disease. Neurotox Res 12:269–274. https://doi.org/10.1007/BF03033910
66. Sotgiu S, Musumeci S, Marconi S, Gini B, Bonetti B (2008) Different content of chitin-like polysaccharides in multiple sclerosis and Alzheimer's disease brains. J Neuroimmunol 197:70–73. https://doi.org/10.1016/j.jneuroim.2008.03.021
67. Semenyuk P, Kurochkina L, Barinova K, Muronetz V (2020) Alpha-synuclein amyloid aggregation is inhibited by sulfated aromatic polymers and pyridinium polycation. Polymers (Basel) 12:517. https://doi.org/10.3390/polym12030517
68. Liu H, Ojha B, Morris C, Jiang M, Wojcikiewicz EP, Rao PPN, du D (2015) Positively charged chitosan and N-trimethyl chitosan inhibit Aβ40 fibrillogenesis. Biomacromolecules 16:2363–2373. https://doi.org/10.1021/acs.biomac.5b00603
69. Liu C, Zhang Y (2011) Nucleic acid-mediated protein aggregation and assembly. In: Advances in protein chemistry and structural biology. Academic Press Inc., pp 1–40
70. Calamai M, Kumita JR, Mifsud J, Parrini C, Ramazzotti M, Ramponi G, Taddei N, Chiti F, Dobson CM (2006) Nature and significance of the interactions between amyloid fibrils and biological polyelectrolytes. Biochemistry 45:12806–12815. https://doi.org/10.1021/bi0610653
71. Silva JL, Cordeiro Y (2016) The "Jekyll and Hyde" actions of nucleic acids on the prion-like aggregation of proteins. J Biol Chem 291:15482–15490
72. Mambule C, Ando Y, Anan I, Holmgren G, Sandgren O, Stigbrandt T, Tashima K, Suhr OB (2000) Enhancement of AA-amyloid formation in mice by transthyretin amyloid fragments and

polyethylene glycol. Biochim Biophys Acta, Gen Subj 1474:331–336. https://doi.org/10.1016/S0304-4165(00)00032-5
73. Kotormán M, Simon L, Borics A, Szabó M, Szabó K, Szögi T, Fülöp L (2015) Amyloid-like fibril formation by trypsin in aqueous ethanol. Inhibition of fibrillation by PEG. Protein Pept Lett 22:1104–1110. https://doi.org/10.2174/0929866522666151002154324
74. Funtan S, Evgrafova Z, Adler J, Huster D, Binder W (2016) Amyloid beta aggregation in the presence of temperature-sensitive polymers. Polymers (Basel) 8:178. https://doi.org/10.3390/polym8050178
75. Nielsen L, Khurana R, Coats A, Frokjaer S, Brange J, Vyas S, Uversky VN, Fink AL (2001) Effect of environmental factors on the kinetics of insulin fibril formation: elucidation of the molecular mechanism. Biochemistry 40:6036–6046. https://doi.org/10.1021/bi002555c
76. Wallin C, Friedemann M, Sholts SB, Noormägi A, Svantesson T, Jarvet J, Roos PM, Palumaa P, Gräslund A, Wärmländer SKTS (2020) Mercury and Alzheimer's disease: Hg(II) ions display specific binding to the amyloid-β peptide and hinder its fibrillization. Biomolecules 10:44. https://doi.org/10.3390/biom10010044
77. Evstafyeva DB, Izumrudov VA, Muronetz VI, Semenyuk PI (2018) Tightly bound polyelectrolytes enhance enzyme proteolysis and destroy amyloid aggregates. Soft Matter 14:3768–3773. https://doi.org/10.1039/c8sm00101d
78. Assarsson A, Linse S, Cabaleiro-Lago C (2014) Effects of polyamino acids and polyelectrolytes on amyloid β fibril formation. Langmuir 30:8812–8818. https://doi.org/10.1021/la501414j
79. Cabaleiro-Lago C, Quinlan-Pluck F, Lynch I, Lindman S, Minogue AM, Thulin E, Walsh DM, Dawson KA, Linse S (2008) Inhibition of amyloid β protein fibrillation by polymeric nanoparticles. J Am Chem Soc 130:15437–15443. https://doi.org/10.1021/ja8041806
80. Jiang Z, Dong X, Sun Y (2018) Charge effects of self-assembled chitosan-hyaluronic acid nanoparticles on inhibiting amyloid β-protein aggregation. Carbohydr Res 461:11–18. https://doi.org/10.1016/j.carres.2018.03.001
81. Baysal I, Yabanoglu-Ciftci S, Tunc-Sarisozen Y, Ulubayram K, Ucar G (2013) Interaction of selegiline-loaded PLGA-b-PEG nanoparticles with beta-amyloid fibrils. J Neural Transm 120:903–910. https://doi.org/10.1007/s00702-013-0992-2
82. Baysal I, Ucar G, Gultekinoglu M, Ulubayram K, Yabanoglu-Ciftci S (2017) Donepezil loaded PLGA-b-PEG nanoparticles: their ability to induce destabilization of amyloid fibrils and to cross blood brain barrier in vitro. J Neural Transm 124:33–45. https://doi.org/10.1007/s00702-016-1527-4
83. Birks J, Flicker L (2003) Selegiline for Alzheimer's disease. Cochrane Database Syst Rev. https://doi.org/10.1002/14651858.cd000442
84. Giorgetti S, Greco C, Tortora P, Aprile FA (2018) Targeting amyloid aggregation: an overview of strategies and mechanisms. Int J Mol Sci 19
85. Gazit E (2002) A possible role for π-stacking in the self-assembly of amyloid fibrils. FASEB J 16:77–83. https://doi.org/10.1096/fj.01-0442hyp
86. Findeis MA, Musso GM, Arico-Muendel CC, Benjamin HW, Hundal AM, Lee JJ, Chin J, Kelley M, Wakefield J, Hayward NJ, Molineaux SM (1999) Modified-peptide inhibitors of amyloid β-peptide polymerization. Biochemistry 38:6791–6800. https://doi.org/10.1021/bi982824n
87. Soto C, Sigurdsson EM, Morelli L, Asok Kumar R, Castaño EM, Frangione B (1998) β-Sheet breaker peptides inhibit fibrillogenesis in a rat brain model of amyloidosis: implications for Alzheimer's therapy. Nat Med 4:822–826. https://doi.org/10.1038/nm0798-822
88. Tjernberg LO, Näslundt J, Lindqvist F et al (1996) Arrest of β-amyloid fibril formation by a pentapeptide ligand. J Biol Chem 271:8545–8548. https://doi.org/10.1074/jbc.271.15.8545
89. Porat Y, Abramowitz A, Gazit E (2006) Inhibition of amyloid fibril formation by polyphenols: structural similarity and aromatic interactions as a common inhibition mechanism. Chem Biol Drug Des 67:27–37. https://doi.org/10.1111/j.1747-0285.2005.00318.x
90. Vilcacundo R, Méndez P, Reyes W, Romero H, Pinto A, Carrillo W (2018) Antibacterial activity of hen egg white lysozyme denatured by thermal and chemical treatments. Sci Pharm 86:48. https://doi.org/10.3390/scipharm86040048
91. Jiang D, Rauda I, Han S, Chen S, Zhou F (2012) Aggregation pathways of the amyloid β(1 42) peptide depend on its colloidal stability and ordered β-sheet stacking. Langmuir 28:12711–12721. https://doi.org/10.1021/la3021436
92. Hortschansky P, Schroeckh V, Christopeit T, Zandomeneghi G, Fändrich M (2005) The aggregation kinetics of Alzheimer's β-amyloid peptide is controlled by stochastic nucleation. Protein Sci 14:1753–1759. https://doi.org/10.1110/ps.041266605
93. Liu P, Zhang S, Chen MS, Liu Q, Wang C, Wang C, Li YM, Besenbacher F, Dong M (2012) Co-assembly of human islet amyloid polypeptide (hIAPP)/insulin. Chem Commun 48:191–193. https://doi.org/10.1039/c1cc14285b
94. Holubova M, Konefał R, Moravkova Z, Zhigunov A, Svoboda J, Pop-Georgievski O, Hromadkova J, Groborz O, Stepanek P, Hruby M (2017) Carbon nanospecies affecting amyloid formation. RSC Adv 7:53887–53898. https://doi.org/10.1039/C7RA11296C
95. Hirsh SL, McKenzie DR, Nosworthy NJ et al (2013) The Vroman effect: competitive protein exchange with dynamic multilayer protein aggregates. Colloids Surf B: Biointerfaces 103:395–404. https://doi.org/10.1016/j.colsurfb.2012.10.039

Monika Holubova is a PhD student on Charles University in Prague, Faculty of Science. She is working as a researcher in the Institute of Macromolecular Chemistry of the Czech Academy of Sciences in Prague, Czech Republic. She obtained the school grant of Charles University. Her research is focused on the process of amyloid fibril formation and materials that may have an effect on the process.

Petr Štěpánek is the Deputy Director of the Institute of Macromolecular Chemistry of the Czech Academy of Sciences in Prague, Czech Republic. His research interests are focused on self-organization phenomena in macromolecular systems, design, and characterization of functional polymeric materials for biomedical applications, in particular for diagnostic and therapeutic applications, biodegradable polymers for drug delivery, and block and gradient copolymers forming complex supramolecular assemblies.

Martin Hruby was born in Prague, Czech Republic, in 1978. He is working as a senior researcher at the Institute of Macromolecular Chemistry, Czech Academy of Sciences, Prague. His research is focused on the field of self-assembled stimuli-responsive biocompatible polymer nanostructures as drug and radionuclide carriers.

Publication 4

Soft Matter

Does polysaccharide glycogen behave as a promoter of amyloid fibril formation at physiologically relevant concentrations?

Journal:	*Soft Matter*
Manuscript ID	Draft
Article Type:	Paper
Date Submitted by the Author:	n/a
Complete List of Authors:	Holubová, Monika; stav makromolekuláru chemie Akademie věd České republiky Lobaz, Volodymyr; Institute of Macromolecular Chemistry, Supramolecular Systems and Selfassociation Processes Loukotová, Lenka; Institute of Macromolecular Chemistry, Academy of Sciences of the Czech Republic, Biomacromolecular and Bioanalogous Systems Rabyk, Mariia; Institute of Macromolecular Chemistry, Academy of Sciences of the Czech Republic, Biomacromolecular and Bioanalogous Systems Prague 6, Czech Republic, 210 Hromadkova, Jirina; Institute of Macromolecular Chemistry, Academy of Sciences of the Czech Republic, Trhlikova, Olga; Institute of Macromolecular Chemistry AS CR Pechrová, Zdislava; stav makromolekuláru chemie Akademie věd České republiky Groborz, Ondřej; Institute of Macromolecular Chemistry Czech Academy of Sciences Stepanek, Petr; Akademie ved Ceske republiky Ustav makromolekularni Chemie, Hruby, Martin; Institute of Macromolecular Chemistry, Academy of Sciences of the Czech Republic, Biomacromolecular and Bioanalogous Systems

ARTICLE

Does polysaccharide glycogen behave as a promoter of amyloid fibril formation at physiologically relevant concentrations?

Received 00th January 20xx,
Accepted 00th January 20xx

DOI: 10.1039/x0xx00000x

Monika Holubová[a,b], Volodymyr Lobaz[a], Lenka Loukotová[a], Mariia Rabyk[a], Jiina Hromádková[a], Olga Trhlková [a], Zdislava Pechrová[a], Ondej Groborz[a,b], Petr těpánek [a], Martin Hrub* [a]

We investigated the influence of glycogen (GG), phytoglycogen (PG), mannan (MAN) and cinnamoyl-modified GG (GG-CIN) on amyloid fibril formation. We used hen egg-white lysozyme (HEWL) as a model system and amyloid beta peptide (1-42) ($A\beta_{1-42}$) as an Alzheimers disease-relevant system. For brief detection of fibrils was used thioflavin T (ThT) fluorescence assay and the results were confirmed by transmission electron microscopy (TEM). We also deal with the interaction of polysaccharides and HEWL with isothermal titration calorimetry (ITC) and dynamic light scattering (DLS). We found that all polysaccharides accelerated the formation of amyloid fibrils from both HEWL and $A\beta_{1-42}$. At high but physiologically relevant concentrations of GG, amyloid fibril formation was extremely accelerated for HEWL. Therefore, on the basis of the herein presented in vitro data, we hypothesize, that dietary D-glucose intake may influence amyloid fibril formation not only by influencing regulatory pathways, but also by direct glycogen-amyloid precursor protein molecular interaction, as glycogen levels in tissues are highly dependent on D-glucose intake.

Introduction,

The appropriate self-assembly and aggregation of peptides and proteins is essential for many functions of the human body[1]. Amyloid fibrils rank among the most stable supramolecular assemblies of proteins and peptides. The pathophysiological formation of amyloid fibrils is traditionally associated with several incurable degenerative human diseases, e.g., Alzheimers disease. These amyloid fibrils are the result of aberrant misfolding of soluble and functional proteins followed by self-assembly of these misfolded proteins[24] .

All amyloid fibrils are formed from proteins or peptides and eventually contain other components such as serum amyloid P component (SAP), glycosaminoglycans (mainly heparan sulfate) and apolipoprotein E[5]. Amyloid fibril formation is a very complex process, and understanding it can enable the development of drugs to preserve the native protein state and prevent amyloidogenesis[5]. The kinetics of fibril formation can be described as sigmoidal curves[6,7] that consist of three phases (Fig. 1). The first phase is the lag phase, where there is no change in thioflavin T (ThT) fluorescence, which is used for the rapid detection of fibrils. An amyloidogenic protein or protein misfolding (e.g., under denaturation conditions) creates nuclei that form oligomeric species with β-sheets. The second phase is the growth phase, where the elongation and growth of fibrils occur; the fluorescence of ThT increases rapidly during this phase. The third (last) phase is the saturation phase, where the mature fibrils are completely finalized[8]. The formation of amyloid fibrils is dependent on π π interactions, which play a crucially important role. It was shown that in amyloid fibrils, there is a high occurrence of aromatic residues[9]. Finally, hydrophobic and electrostatic interactions also play a significant role in the aggregation and stabilization of amyloid fibrils[10,11].

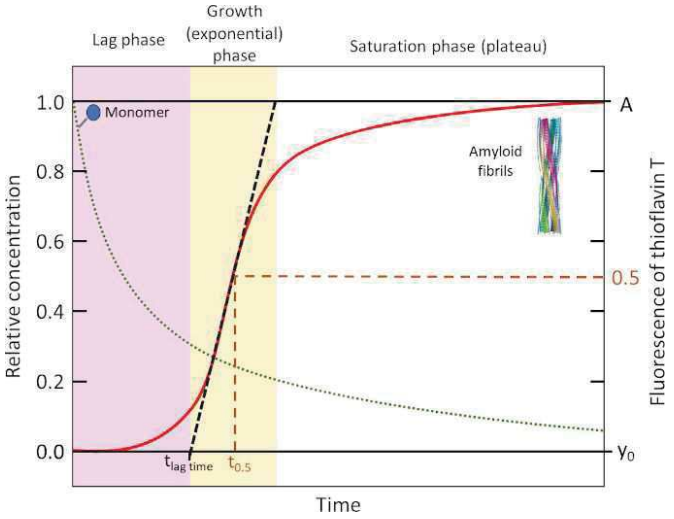

Fig. 1. Schematic illustration of the sigmoidal increase in thioflavin T fluorescence/concentration of proteins in amyloid forms (red line) upon fibril formation. The dotted green line represents the monomer concentration. The red line represents the concentration of proteins in amyloid forms[12]. The dashed black line represents the slope of the growth phase. The time $t_{0.5}$ is that at 50% maximal fluorescence. The line y_0 is an initial baseline, and A is the fluorescence amplitude [13].

[a] Institute of Macromolecular Chemistry, Academy of Sciences of the Czech Republic, Heyrovsk Sq. 2, 162 06 Prague 6, Czech Republic, e-mail address: mhruby@centrum.cz
[b] Charles University in Prague, Faculty of Science, Albertov 6, 128 43 Prague 2, Czech Republic

Electronic Supplementary Information (ESI) available: [supplementary information.pdf]. See DOI: 10.1039/x0xx00000x

Polysaccharides are naturally abundant biopolymers that play important roles in different biological mechanisms[14]. There are few studies that describe the influence of natural polysaccharides on amyloid fibril formation. In the past, the effect of plant glucan (from *Lonicera japonica* Thunb.) on $A\beta_{1-42}$ fibril formation was tested. This study showed that this plant glucan could inhibit the formation of amyloid fibrils from $A\beta_{1-42}$ and thus inhibit neurotoxicity[15]. Furthermore, poly(propylenimine) glycodendrimers with bound maltose were also tested as antiamyloidogenic substances. These glycodendrimers inhibited the formation of amyloid fibrils from $A\beta_{1-40}$ [16,17]. On the other hand, amyloids formed in the body during pathogenesis very often contain, in addition to proteins/peptides, glycosaminoglycans (mainly heparan sulfate). Glycosaminoglycans have been shown to promote the aggregation of amyloidogenic proteins. Glycosaminoglycans, as polyanions, play an important role in catalyzing protein aggregation and stabilizing amyloid fibrils[18].

D-glucose metabolism and amyloidoses such as Alzheimer's disease or type II diabetes are closely connected. Both Alzheimer's disease and type II diabetes are typical consequences of insulin dysregulation leading to aberrant D-glucose metabolism. The role of glycogen synthase kinase-3β, primarily regulating glycogen synthesis, in the pathogenesis of Alzheimer's disease is notoriously known. However, all known interactions are on the signaling pathway level[1922] .

We decided to study and compare the effects of several selected polysaccharides (mannan (the structure is shown in supplementary information Fig. S1), glycogen (the structure is shown in supplementary information Fig. S2), and phytoglycogen) on the formation of amyloid fibrils of hen egg-white lysozyme (HEWL) and amyloid beta peptide (1-42) $A\beta_{1-42}$. Glycogen (GG) was also tested at physiologically relevant concentrations in animal organisms. GG is a major storage form of D-glucose in humans and animals, and its typical concentrations in tissues are rather high (liver, approximately 6-8% by weight[23,24]; muscles, approximately 1-2% by weight [23,24]; brain, approximately 0.1% by weight[25]; and pancreas, approximately 4 % of that of the liver (in normal rats)[26]). Therefore, we hypothesize in this study on the basis of the herein presented *in vitro* data that GG may contribute to the pathogenesis of amyloidosis not only indirectly through signaling pathways by influencing, e.g., tau protein phosphorylation by glycogen synthase kinase-3β, but also by the direct interaction of GG macromolecules with amyloid protein precursors that induce amyloid fibril formation. As the content of GG in tissues is extremely dependent on nutritional status, this may also be one of the ways that lifestyle influences the induction of amyloidosis. The advantage of GG is that it can be chemically modified by various groups that could change the behavior of GG. We selected cinnamoylated GG (GG-CIN) to determine the effect of possible additional π-π interactions and to gain better insight into GG-protein interactions. This modification could help us understand the influence of the functionalization of GG on its interaction with protein/peptide amyloid precursors and to compare unmodified and modified GG in the HEWL model and $A\beta_{1-42}$. We also tested PG, a plant analog of GG with a significantly larger molecule size than that of GG, which is currently gaining attention in the cosmetic industry and is present in high amounts in, e.g., maize[27] specifically in sweet corn [28]. The comparison of GG and PG was intended to mainly evaluate the effect of molecule size (and of surface curvature geometry, which was previously shown to play an important role in amyloidogenicity., e.g., that of carbon-based nanoparticles[29]) on protein-polysaccharide interactions. The hydrodynamic diameter of model protein HEWL (approximately 4 nm) as well as hydrodynamic diameters of most other amyloidogenic proteins and diameters of their fibrils (approximately 7 12 nm [18,30]) are considerably smaller than hydrodynamic diameter of both oyster GG and PG, therefore the fibrillation can see only the local microstructure (which is the same as big GG α particles are composed of smaller β particles (Sullivan et al., 2015). However, PG is a big ball not composed of smaller particles[27] and therefore different surface curvature. The last selected polysaccharide was mannan (MAN), a major soluble polysaccharide constituent of fungal and yeast cell walls, which is relevant to the possible induction of amyloidoses by mycosis[14,3234] . None of the abovementioned polysaccharides have been previously tested for amyloid formation induction/inhibition.

Experimental

Materials

HEWL (molecular weight of 14 300 g/mol), ThT, phosphate buffered saline (PBS), glycine, glycogen from oysters type II (≥75% dry basis), mannan from Saccharomyces *cerevisiae* prepared by alkaline extraction, 1,1,1,3,3,3-hexafluoro-2-propanol (HFIP), sodium azide (NaN_3) and cinnamoyl chloride were purchased from Sigma-Aldrich Ltd. (Prague, Czech Republic). $A\beta_{1-42}$ was purchased from Kaneka Eurogentec S.A. (Seraing, Belgium), and phytoSpherix® (phytoglycogen) was purchased from Mirexus Inc. (Guelph, Canada). Diethyl ether and dimethyl sulfoxide (DMSO) were purchased from Lachner Ltd. (Neratovice, Czech Republic). All chemicals were used without further purification unless stated otherwise.

Methods

Proton nuclear magnetic resonance (^{1}H NMR). ^{1}H NMR spectra were obtained on a Bruker Avance III HD 400 MHz spectrometer system (Bruker Co., Germany).

Synthesis of cinnamoyl-modified glycogen. Glycogen from oysters (0.50 g, $M_w = 5.710^6$ g/mol) was dissolved in anhydrous DMSO (25 mL), and sodium hydride was added (1.50 g as a 60% dispersion in mineral oil). The reaction mixture was stirred at 60 C for 3 h (until hydrogen bubbles were evolving). Thereafter, cinnamoyl chloride (154 mg, 0.93 mmol, a solution in 0.50 mL DMSO) was added, and the reaction mixture was stirred overnight at 60 C. Water (25 mL) was poured into the reaction mixture, which was then washed twice with diethyl ether to remove the mineral oil. The aqueous layer was dialyzed (MWCO 3.5 kDa) against water for 72 h and freeze-dried to yield the product GG-CIN (461 mg).

The ^{1}H-NMR (400 MHz, DMSO) δ (ppm) data were as follows: 3.11-5.30 (m, glucose: H2-H6), 5.27-6.12 (m, glucose: H1), and 6.98-7.60 (m, cinnamoyl, 6H).

Preparation of HEWL amyloid fibrils. A stock solution of HEWL protein was prepared at a concentration of 2.2 mg/mL in 10 mM glycine-HCl buffer at pH 2.0 and containing 0.2% w/v NaN_3. The stock solution was filtered through a 0.22 µm PVDF filter and divided into glass vials to which the required amounts of polysaccharide solutions in pH 2.0 10 mM glycine-HCl buffer containing 0.2% w/v NaN_3 were added. A final protein concentration of 2 mg/mL was achieved in all vials by adding pH 2.0 10 mM glycine-HCl buffer. The solutions were incubated at 57 C. Samples (10 µL) were taken at different times and were detected by ThT and transmission electron microscopy (TEM) (see below).

Thioflavin T fluorescence assay of HEWL. A staining solution of ThT was prepared at a concentration of 10 µM in PBS at pH 7.4. This ThT solution was used for staining HEWL samples at different times, and measurements were conducted in a 96-well plate. In one well, a 10 µL aliquot of a HEWL sample and 240 µL ThT solution were mixed. Before fluorescence measurement, the 96-well plate was briefly mixed on the plate reader.

Pretreatment of A $_{1-42}$. A total of 1 mg $A\beta_{1-42}$ was dissolved in 450 L HFIP on ice at a final peptide concentration of 0.5 mM. The solution was sonicated for 5 min and then incubated for 30 min at room temperature in a shaker at 300 rpm, and then a 25 µL aliquot of the solution, containing 12 nmol $A\beta_{1-42}$, was transferred to a chilled Eppendorf tube. HFIP was evaporated using a vacuum pump connected to a desiccator. Tubes were stored at -20 C.

Preparation of A $_{1-42}$ amyloid fibrils and the thioflavin T assay. A total of 500 L 50 mM phosphate buffer (pH=7.4) was added to the 12 nmol of $A\beta_{1-42}$. Then, $A\beta_{1-42}$ was dissolved for 1 min in an ultrasonication bath. The required amounts of polysaccharide solutions in 50 mM phosphate buffer were added to certain tubes. A staining solution of ThT was prepared at a concentration of 250 µM in 50 mM phosphate buffer solution. The staining solution was added to each sample so that the final concentration in the sample was 20 M ThT. The samples were incubated at 37 C and 600 rpm in an incubator shaker.

Determination of the influence of polysaccharides on amyloid fibril formation. The stock solutions of polysaccharides were prepared at a concentration of 5 mg/mL in 10 mM glycine-HCl buffer for the HEWL model and a concentration of 6 mg/mL in 50 mM phosphate buffer for the $A\beta_{1-42}$ model. These stock solutions were distributed into individual vials or Eppendorf tubes, and the samples were incubated and characterized at certain reaction times.

Measuring the fluorescence of thioflavin T. ThT fluorescence intensity measurements were performed by exciting samples at 440 nm and recording emission intensities at 485 nm using a Synergy H1 hybrid plate reader (BioTek, Czech Republic).

Transmission electron microscopy (TEM). Two microliters of sample were placed on a carbon-coated copper grid and dried with paper, and then the sample was stained with 1 wt. % uranyl acetate for 30 s. The final images were obtained with a Tecnai G2 Spirit (FEI) at an accelerating voltage of 120 kV.

Statistics. Experimental data were analyzed with the Q-test or Grubbs test and one-way ANOVA, and the significance level was set at $\alpha<0.05$ for all experiments.

Fluorescence data fitting. ThT fluorescence measurements were plotted as a function of time and fitted by a sigmoidal curve (Fig. 1) described by the following equation (1) [6,7,13]:

$$\boldsymbol{Y(t) = y_0 + \frac{A}{1 + \exp\,(-k(t - t_{0.5}))}} \qquad (\mathbf{1})$$

where *Y(t)* is the fluorescence intensity, *t* is the time, y_0 is an initial baseline, *A* is the amplitude of fluorescence, $t_{0.5}$ is the time at 50% maximal fluorescence, and *k* is an apparent growth rate. According to the equation, the lag time ($t_{lag\ \ time}$) was defined as $t_{lag\ \ time}=t_{0.5}\ \ 2/k$. This definition of lag time is equivalent to the extrapolation from the maximal growth rate to the intercept with the baseline (Fig. **1**).

Dynamic light scattering (DLS). DLS was performed to determine the effect of temperature on the polysaccharide hydrodynamic radius (R_h) with and without HEWL in solution. Experiments were performed on a Zetasizer Nano ZS instrument (Malvern Instruments, UK). The measured intensity correlation function was analyzed using the REPES algorithm [35] to obtain the distribution of hydrodynamic radii. The system of HEWL and PG, GG or GG-CIN was very complex for data processing, but we solved this problem by performing the two-step inverse Laplace transformation[36,37]. The polymer contribution (in our case, PG, GG or GG-CIN) obtained in the first step was subtracted from the correlation function, which was then analyzed again in a second step to make HEWL visible[36,37]. We also performed the DLS measurements for GG and PG samples at different angles (from 30 to 150) on the ALV to to ascertain whether an observed relaxation component has a diffusive character, i.e. $\boldsymbol{\Gamma = Dq^2}$ and then a size can be calculated from the Stokes-Einstein equation $\boldsymbol{R_h = \frac{kT}{6\pi\eta D}}$. Local internal modes have relaxation times (or relaxation rates $\Gamma = 1/$) independent of the angle and the previous relations do not apply[3840] . We observed linear dependence of Γ on q^2, that means that the Stokes-Einstein equation really applies (supplementary information Fig. S3).

Refractive index increment (d*n*/dc). The refractive index increment (d*n*/dc) of polysaccharides was measured with a PSS DnDc2010/620 differential refractometer operating at a wavelength of 620 nm (Polymer Standard Service, Mainz, Germany).

Asymmetric flow field-flow fractionation (AFFFF)

The weight-average molar mass (M_W) of the polysaccharides were measured by AFFFF. The solvent and sample delivery part of the system consisted of an Agilent G1310A pump, a G1322A degasser and a G1329A autosampler. A long field-flow fractionation channel was assembled with a 350 µm spacer and a regenerated cellulose membrane with a cutoff of 10 000 g/mol. Three detectors were used in series: a Spectromonitor 3200 UV/VIS unit (Thermo Separation Products, Fremont USA), a Wyatt Optilab-rEX RI detector and a Wyatt Dawn 8+ multiangle light scattering unit. Wyatt Astra V (version 5.3.4.15) software controlled all system components through a Wyatt ECLIPSE 3+ unit. Water with NaN_3 was used as the mobile phase. Molar mass measurements were conducted with a

constant detector flow rate of 1 mL/min. The focusing time was 5 min at a cross-flow of 3.5 mL/min. The injection flow was 0.2 mL/min, and 100 L sample was injected in all cases. After the focusing step, the cross-flow was linearly decreased from 2.0 mL/min to 0.1 mL/min in 20 min and was then kept constant at 0.1 mL/min for the next 20 min, followed by 20 min without cross-flow. The Berry method was used to determine M_W, that is linear over a broad molar mass range[41].

Density and relative excluded volume. The density of a polysaccharide was calculated according to the following equation (2):

$$\rho = \frac{M_W}{\frac{4}{3}\pi R_h^3} \qquad (2)$$

where ρ is the density, M_W is the weight-average molar mass, and R_h is the hydrodynamic radius. The relative excluded volume of a polysaccharide was determined according to the following equation (3):

$$V_{ex} = \frac{4\pi R_h^3 m N_A}{3 V M_W} \qquad (3)$$

where V_{ex} is the relative excluded volume, m is the mass of the polysaccharide in solution, N_A is the Avogadro constant (6.02210 ^{23} mol^{-1}), and V is the solution volume.

Isothermal titration calorimetry (ITC). ITC was performed on a MicroCal ITC200 (Malvern Panalytical Ltd, UK) in a series of 3 to 5 subsequent titrations of the HEWL solution batch (14.3 mg/mL, 1 mM) in solutions with GG (50 mg/mL, 8.83 M), GG-CIN (44 mg/mL, 7.26 M), PG (75 mg/mL, 2.76 M) and MAN (75 mg/mL, 1.35 mM) in 10 mM glycine-HCl buffer with 0.2% w/v NaN_3 (pH 2.0). The titrations were performed at 25 and 57 C. The titrations with GG, PG and MAN were performed with a 0.4-L injection, followed by 9 4-L injections; for GG-CIN, the first injection was 0.3 L, followed by 14 3-L injections. Additionally, the polysaccharide solutions were titrated into pure buffer and the HEWL titration data were corrected to the corresponding heats of dilution. The series of raw titration data were combined using ConCat32 software.

ITC data fitting. Combined titration data were fitted with models of one binding site or two binding sites (when applicable). The affinity constant (K_a), binding free energy (ΔG), binding enthalpy (H) and binding entropy (S) were calculated with HEWL as a ligand. For MAN, PG and GG, calorimetric data with low sigmoidicity, which is typical for weak binding, were obtained. The suggested stoichiometry of HEWL to polysaccharide (n) was calculated for each system from geometrical considerations (the sizes of interacting macromolecules); then, the exact (n) value was accepted from the best fit and kept fixed for fitting the binding curves with one binding site model. The shape of the GG-CIN calorimetric titration curves suggested strong binding followed by weak binding. The curves were fitted with the two binding sites model (GG-CIN1, high C, and GG-CIN2, low C), applying the same limitations on n for the weak binding, as described above.

Results and discussion,

First, we synthesized of the modified GG-CIN and performed a brief characterization of all polysaccharides before testing them on HEWL and $A\beta_{1-42}$.

Synthesis of GG-CIN

Although the mechanism of amyloidogenesis and its inhibition are not yet completely understood[42], it is known that the presence of an aromatic ring in the structure of the investigated compounds influences amyloid formation due to π-π interactions with amyloidogenic peptides[43,44]. Therefore, a first approach to the chemical modification of the natural polysaccharide glycogen was to modify its structure with cinnamoyl groups to elucidate how surface modification with groups capable of forming π-π interactions will influence the effect of polysaccharides on amyloid formation. GG was alkylated via a reaction of its alkoxide groups with cinnamoyl chloride to produce GG-CIN (Fig. 2). The degree of functionalization f_{cin} (number of cinnamoyl groups per D-glucose unit) was calculated from the ^{1}H-NMR spectrum (supplementary information, Fig. S4) using the following equation (4):

$$f_{cin} = \frac{I_{\delta = 7.24\ ppm}}{6 \cdot I_{\delta = 5.48\ ppm}} \qquad (4)$$

where $I_{=7.24\ ppm}$ is the integral intensity of all hydrogens in the cinnamoyl group except the double bond hydrogen closer to oxygen (see Fig. S4 in supplementary information) and $I_{=5.48\ ppm}$ is the integral intensity of the H1 hydrogen from the D-glucose unit. The obtained degree of functionalization f_{cin} for GG-CIN was 1.3 mol.% (molar percent, based on glucose unit).

Characterization of polysaccharides and GG-CIN

We measured the dn/dc in water for all polysaccharides and the modified GG-CIN. These measured values of dn/dc were subsequently used to determine M_W by AFFFF with light scattering detection. The individual dn/dc and M_W values are given in Tab. S1 in supplementary information. Tab. S1 in supplementary information also shows intensity-weighted R_h values obtained from DLS. Fig. S5 in supplementary information shows the size distribution represented by the intensity obtained from DLS for all polymers.

MAN is a linear polysaccharide, the shape of which is a random coil, R_h of MAN was the smallest and had the narrow distribution. While GG, PG and GG-CIN are hyperbranched spherical polymers. PG had the largest spherical particles, GG-CIN had smaller particles, but with a wide distribution, and GG had the smallest particles.

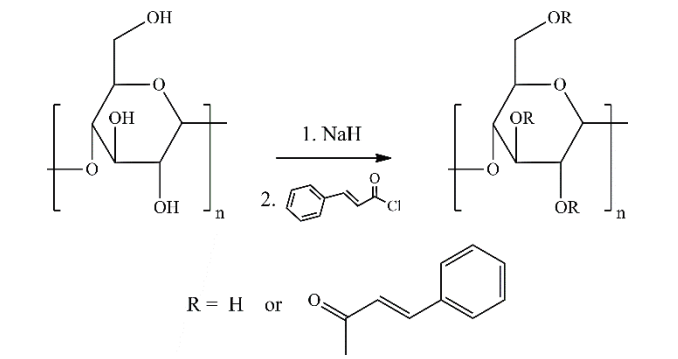

Fig. 2. Synthesis of cinnamoyl-modified glycogen (GG-CIN).

Characterization and detection of amyloid fibril formation

One of the most significant differences between the growth of fibrils *in vitro* and *in vivo* is the duration of amyloid fibril formation. In the case of *in vitro* growth, fibril formation requires minutes or days depending on the type of amyloidogenic protein/peptide. *In vivo* growth takes much longer, sometimes decades[45]. The fastest and easiest way to detect amyloid fibrils is by ThT fluorescence. ThT shows a large fluorescence enhancement upon binding to amyloid aggregates[46,47], but at an acidic pH, the intensity of fluorescence is decreased nearly 10-fold[47]. For our experiments, we used the fluorescence of ThT. Micrographs from TEM were very important for determining sample morphology[48] and confirmed that the ThT fluorescence results accurately corresponded to amyloid fibrils.

HEWL model results. HEWL is a small protein with four disulfide bonds and excellent solubility in aqueous media[49,50]. HEWL easily forms amyloid fibrils under low pH and a relatively high temperature [29]. The tertiary structure, protein folding, and function of HEWL are almost the same as those of human lysozyme (HL), which is a key protective antibacterial enzyme due to its ability to digest bacterial cell walls.

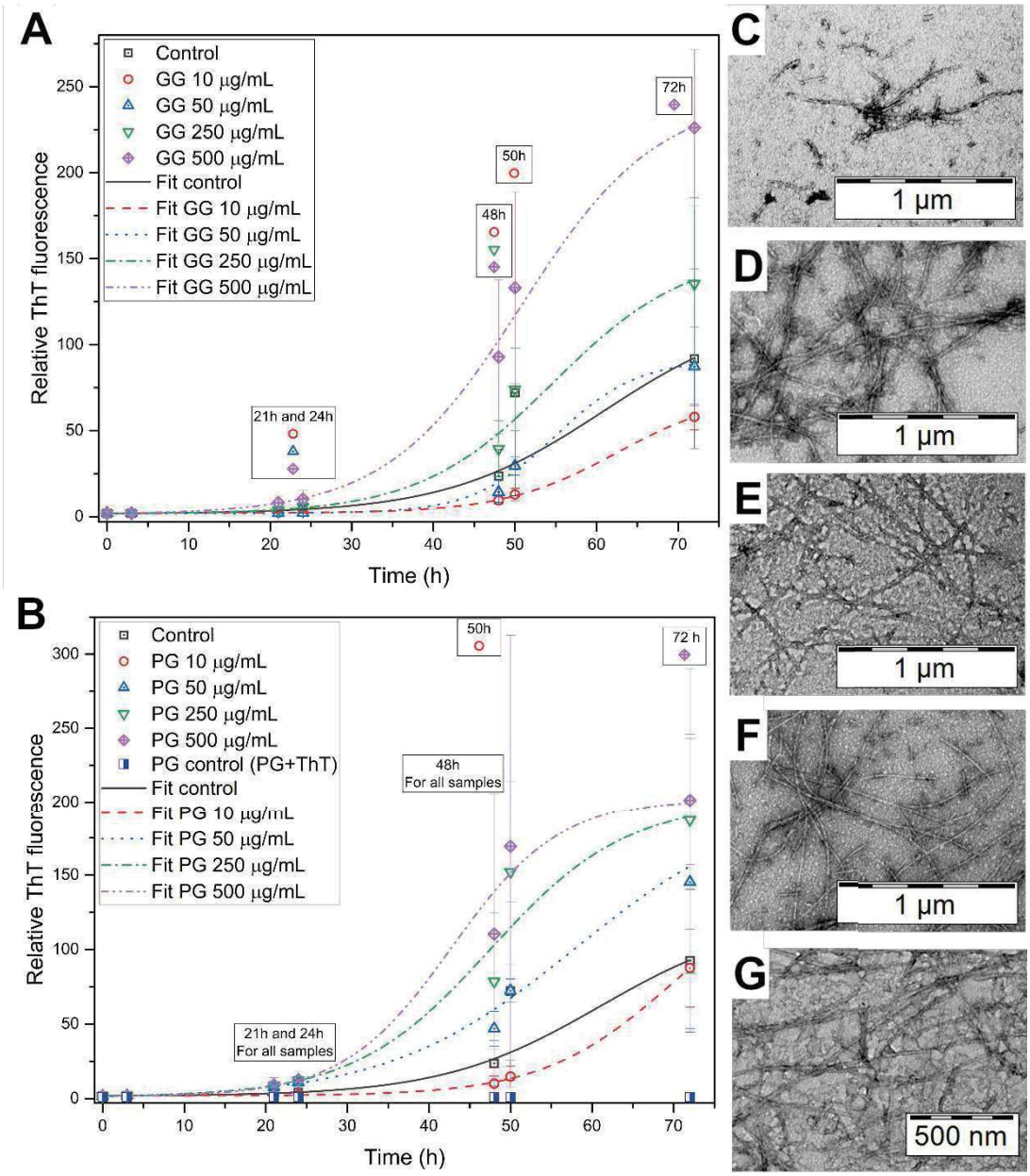

Fig. 3. Results of polysaccharides amyloid fibril formation experiments. Graphs of relative ThT fluorescence with the fit of data. The legend above the results from the same time point represents a statistically significant difference (α<0.05) when compared to the control at this time. (A) Control (only HEWL) and different concentrations of GG, (B) HEWL and different concentrations of PG. TEM micrographs after 48 h of incubation: (C) shorter fibrils of HEWL; long, mature fibrils for samples containing (D) 250 g/mL and (E) 500 g/mL GG and (F) 250 g/mL and (G) 500 g/mL PG. The TEM micrographs were used just to illustrate and check morphology.

ARTICLE

Mutated forms of HL are connected to hereditary systemic amyloidosis[51]; therefore, HEWL can serve as a model system to understand protein aggregation[49,50]. Based on the experience gained, we always chose 2 points close to each other, at a time when there was expected a significant change to catch it. In our experiments, mature fibrils of HEWL were formed after 72 h in control experiments, so the experiments were conducted for 72 h. We added a control for polysaccharide and GG-CIN to the fluorescence graphs, which were the highest concentration of polysaccharide or GG-CIN mixed with ThT solution. In all cases, neither polysaccharides nor GG-CIN were shown to contribute to fluorescence.

We investigated the influence of three polysaccharides (MAN, GG and PG) on amyloid fibril formation. Fig. S7I shows the graph of the relative fluorescence of ThT for the control (only HEWL) and for HEWL combined with four concentrations of MAN after different incubation times. Fig. 3A and B show graphs of the relative fluorescence of ThT for the control (only HEWL) and for HEWL combined with four concentrations of GG or PG after different incubation times. All graphs show a fit for individual measured data corresponding to equation (1), from which $t_{0.5}$ and $t_{lag\ time}$ were obtained. These times for all polysaccharides are shown in Fig. 4. When comparing TEM micrographs, we compared morphology with respect to the presence and type of fibers. Furthermore, we compared the length of the fibers since mature amyloid fibrils are a few micrometers in length; therefore, fibrils can appear to be endless because of the small scale of TEM micrographs.

MAN showed interesting behavior during the incubation experiments. The values of $t_{lag\ time}$ had not any concentration dependence and the statistics show no difference compared to the control. But MAN exhibited a significant shortening $t_{0.5}$ for 250 µg/mL and 500 µg/mL. This would mean that its effect was pronounced mainly in the growth phase. Although the fluorescence graph and values of $t_{0.5}$ showed several significant differences between MAN samples and the control, these differences were not detectable in the morphology of TEM micrographs after incubation for 24 h, 48 h, and 72 h in supplementary information (Fig. S6A-E, Fig. S7A-D and Fig. S8A and B, respectively). Generally, MAN had only a very small effect on HEWL amyloid fibril formation and therefore is probably not very relevant for the induction of amyloidoses in connection with mycosis.

GG and PG are structurally very close, and their behavior in amyloid fibril formation with HEWL was little bit similar, and their effect was dependent on their concentration. The lowest concentration of PG (10 µg/mL) prolonged the lag time and also $t_{0.5}$. The other lower concertation of GG and PG (10 µg/mL GG, 50 µg/mL GG and 50 µg/mL PG) do not show a significant elongation of the lag phase. There can appeared to be a slight decrease in fibril formation at low concentrations but not inhibition. The reduced fibril formation was not confirmed by the TEM micrographs because the TEM micrograph of the control after 72 h of incubation showed long, mature fibers, as did the samples containing 10 µg/mL GG, 50 µg/mL GG and 10 µg/mL PG (supplementary information Fig. S8).

ARTICLE

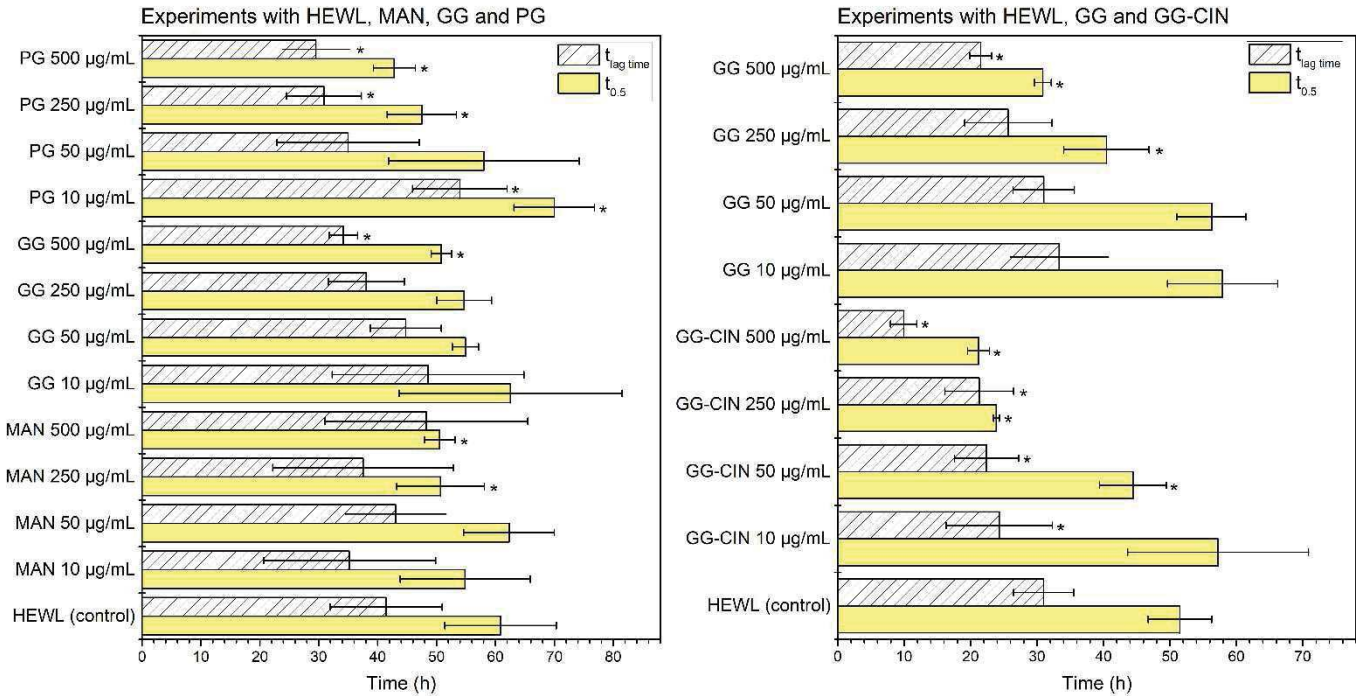

Fig. 4. Graphs of lag times ($t_{lag\ time}$) and times ($t_{0.5}$) at 50% maximal fluorescence for experiments with HEWL, MAN, GG and PG and for experiments with HEWL, GG and GG-CIN, according to the data fitted by equation (1). The star (*) means a statistically significant difference ($\alpha<0.05$) when compared to the control.

On the other hand, other concentrations of PG and GG (500 µg/mL GG, 250 µg/mL PG and 500 µg/mL PG) shortened the lag phase. These results of formation acceleration (500 µg/mL GG, 250 µg/mL PG and 500 µg/mL PG) were supported by TEM micrographs after 48 h of incubation (Fig. 3E-G). All TEM micrographs of samples containing 500 µg/mL GG, 250 µg/mL PG and 500 µg/mL PG indicated mature amyloid fibrils, while the TEM micrograph of the control showed only relatively short fibrils (Fig. 3C). In case of the concentration of 250 µg/mL GG, there is not statistical difference for the lag time compared to control, but the TEM micrograph shows long fibrils (Fig. 3D). The same situation is for 50 µg/mL PG, long, fibrils appeared in the TEM micrographs, as well as relatively short fibers (Fig. S7H in supplementary information).

The results indicated that the chemical composition of the hyperbranched polysaccharide molecule surface was what promoted amyloid fibril formation. GG and PG were compared to evaluate the effect of molecular size (and therefore surface curvature geometry, which was previously shown to play an important role in amyloidogenicity., e.g., that of carbon-based nanoparticles[29]) on the protein-polysaccharide interactions because PG is much larger in size than GG. Additionally, it has been shown that a larger dimension speeded up the process of amyloid fibrils formation.

The effect of the surface chemistry of the polysaccharide on amyloid formation was further examined for GG-CIN (cinnamoyl-modified GG), which possesses strong π-π interactions with aromatic substances such as phenylalanine, tyrosine and tryptophan amino acid residues in the structure of proteins. As no significant aggregation was observed at relevant concentrations by DLS in GG-CIN solutions that would be a sign of intermolecular cinnamoyl-cinnamoyl interactions and the level of substitution is low to see such interaction intramolecularly, these interactions are mostly kept at the GG-CIN protein level in our system. To compare the effects of GG-CIN and GG, an experiment with GG was concurrently conducted. The experimental data surely differ when repeating experiments due to unavoidable experimental errors. However precise statistical evaluation is provided showing statistical significance of the presented trends.

The results for GG-CIN and HEWL are shown in Fig. 5A-C. Moreover, Fig. 4 also shows values of $t_{0.5}$ and $t_{lag\ time}$ for GG in these experiments. Graphs comparing the same concentrations of GG and GG-CIN are in supplementary information Fig. S9 part A and B. The results for GG

are in agreement with the previous results. The highest concentration of GG (500 μg/mL) shortened the lag phase and accelerated amyloid fibril formation. There was a different effect in GG-CIN, where the lag phase was shortened for all concentrations of GG-CIN. Fibril formation was significantly accelerated, and the lag phase was shortened for 500 μg/mL GG-CIN. For this concentration, long fibrils appeared on the TEM micrographs after 24 h of incubation (Fig. 5C), while the control contained only short fibers (Fig. 5B). It should be reiterated that the data fitting was in agreement with the ANOVA results. Interestingly, in the case of GG-CIN, we observed both long, mature fibrils and short fibrils in the TEM micrographs of GG-CIN after 72 h of incubation, but this was not observed in the control (supplementary information Fig. S12).

As it can be seen on Fig. 3, the data points 21 h and 24 h cover the (most important) initial fibrillation phase (in the matter of the fact, these two time points were selected to be so close to each other exactly just to show this point) while the time point 48 h shows the middle growth phase and 72 h point shows the point where the formation of fibrils is mostly finished. Similar time point selection was used onFig. 5.

Based on the results, we could tell that fibril growth in the presence of GG-CIN was different than that in the presence of GG. When we compared the effect of unsubstituted GG and cinnamoyl-substituted GG, unsubstituted GG promoted the natural growth of HEWL amyloid fibrils and only accelerated amyloid fibril formation, while substituted GG (GG-CIN) disrupted the natural growth of fibrils but did not promote inhibition. GG-CIN accelerated amyloid fibril formation, but it also promotes the formation of short fibrils, which are more toxic to cells than long, mature fibrils[52].

GG is a storage polysaccharide serving as a major storage unit of D-glucose in humans and animals; this polysaccharide is mainly found in the liver and in muscles [23,24]. A small amount of GG is accumulated in kidneys and lesser amounts in glial cells in the brain [24]. The amount of GG in the body is also dependent on the diet of the individual, among other factors. Based on the possible predicted GG concentration in the body, we decided to test even higher concentrations of GG and to determine the effect of these higher GG concentrations on amyloid fibril formation.

Fig. 5D-N and Fig S13 (in supplementary information) show the results for high biologically relevant concentrations of GG at different times. The high-concentration experiment was set up slightly differently than the previously described experiments. The stock solution of HEWL had a concentration of 4 mg/mL, and the stock solution of GG had a concentration of 31.25 mg/mL. Both stock solutions were filtered through 0.22 μm PVDF filters. These stock solutions were divided into vials to achieve a final HEWL concentration of 2 mg/mL and the required concentration of GG in each vial. For lower GG concentrations, the amount of solution was adjusted with 10 mM glycine-HCl buffer (0.2% w/v NaN_3, pH 2.0). Due to this slight change, amyloid fibril formation was faster at these concentrations; however, the results were in good agreement with the results of the low-concentration GG samples mentioned above.

Amyloid fibril formation was accelerated for all concentrations of GG. Even though the highest concentration of GG (25 mg/mL) showed extremely accelerated formation. This strong acceleration was also confirmed by a TEM micrograph after 4 h of incubation, which showed fibrils (Fig. 5E), while that of the control did not contain any fibrils (Fig. 5D). We could also observe a large acceleration in ThT fluorescence for 10 mg/mL GG and 5 mg/mL GG, for which we could see long amyloid fibrils in the TEM micrographs after 24 h of incubation (Fig. 5I and J), and TEM micrographs after 24 h of incubation for the control showed only shorter fibrils (Fig. 5F). The smallest concentration of GG (1 mg/mL and 0.5 mg/mL) probably also accelerated the process, because the mature amyloid fibrils appeared in TEM micrographs after 48 h of incubation (Fig. 5L and M), but the control had both short and long fibrils (Fig. 5K).

Generally, we have proven that GG has a strong promoting effect on amyloid formation, even though GG at physiological concentrations is a strong amyloid formation inducer. Because glycogen is a major storage form of D-glucose in humans and animals, and its typical concentrations in tissues are rather high, we hypothesize that glycogen may significantly contribute to the pathogenesis of amyloidoses not only indirectly by influencing tau protein phosphorylation by glycogen synthase kinase-3β but also by direct via the interaction of GG macromolecules with amyloid protein precursors to induce amyloid fibril formation. As the content of GG in tissues is extremely dependent on nutritional status, this may also be one of the ways lifestyle may influence the induction of amyloidoses. However, the effect of lifestyle on amyloidosis induction may be relatively complicated due to the tissue localization of amyloids and GG (GG is generally localized in the cytoplasm close to the cytoplasmic membrane). However, GG accumulation may also occur extracellularly if the tissue is damaged. Amyloid localization is dependent on the particular case but is mostly extracellularly; however, amyloids are also known to be present intracellularly[53]). In fact, there is some evidence that intracellular amyloids, e.g., β-amyloid, may be even more Alzheimer's disease-relevant than extracellular amyloids[54].

ARTICLE

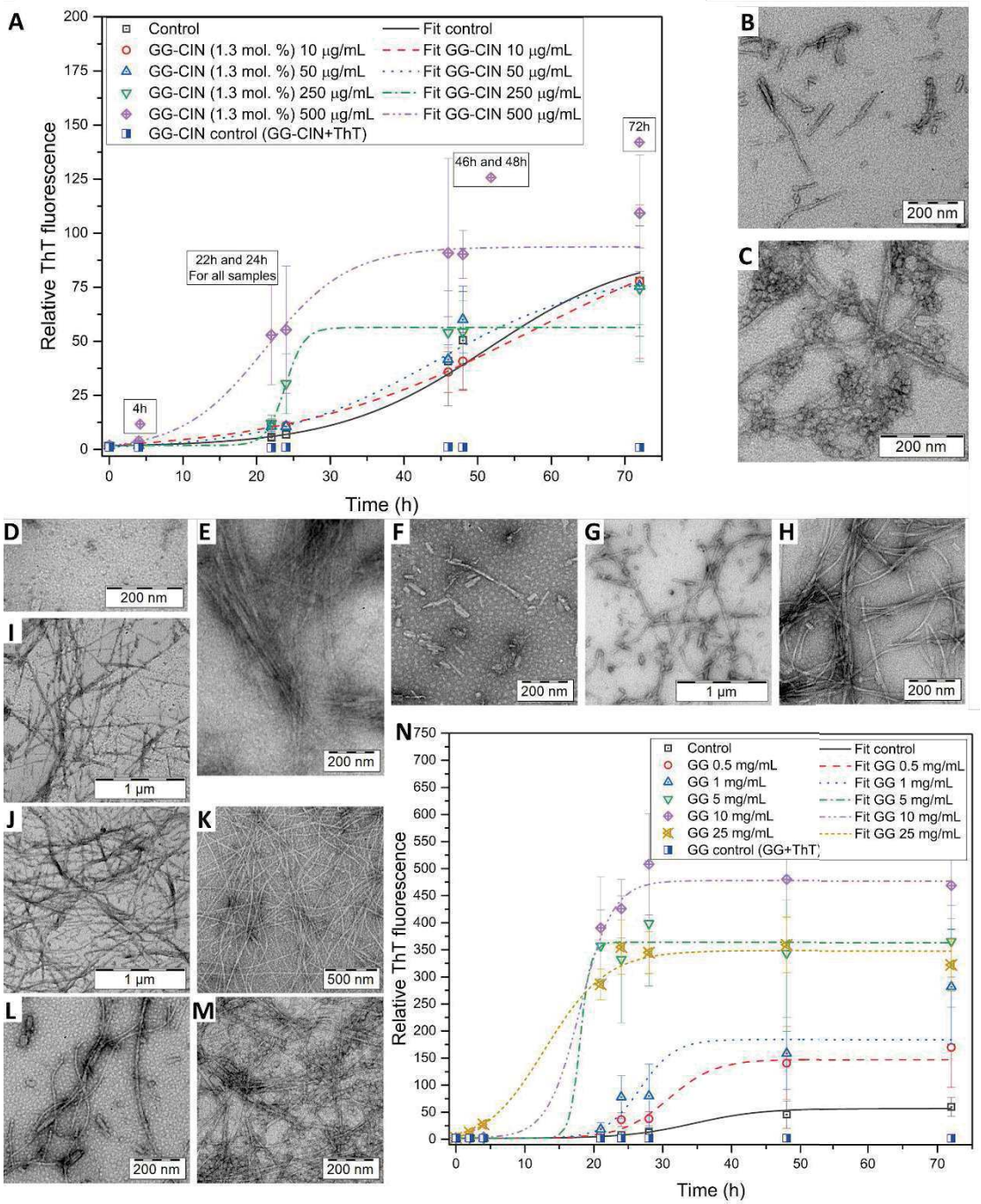

Fig. 5. (A) A graph of relative ThT fluorescence with fitted data. The legend above the results from the same time point represents a statistically significant difference ($\alpha<0.05$) when compared to the control at this time. TEM micrographs after 24 h of incubation: (B) control (only HEWL); (C) 500 g/mL GG-CIN. (D-N) Results of the experiments with high concentrations of GG. TEM micrographs after 4 h: (D) any fibrils in the control (only HEWL); (E) fibrils formed with 25 mg/mL GG. TEM micrographs after 24 h: (F) control; (G) 0.5 mg/mL GG; (H) 1 mg/mL GG; (I) 5 mg/mL GG and (J) and 10 mg/mL GGy. TEM micrographs after 48 h: (K) control, (L) 0.5 mg/mL GG and (M) 1 mg/mL GG. A worse contrast was observed for uranyl acetate staining of amyloid fibrils and polysaccharides at high concentrations. (N) A graph of relative ThT fluorescence with fitted data for HEWL samples without (control) and with high concentrations of GG. The TEM micrographs were used just to illustrate and check the morphology.

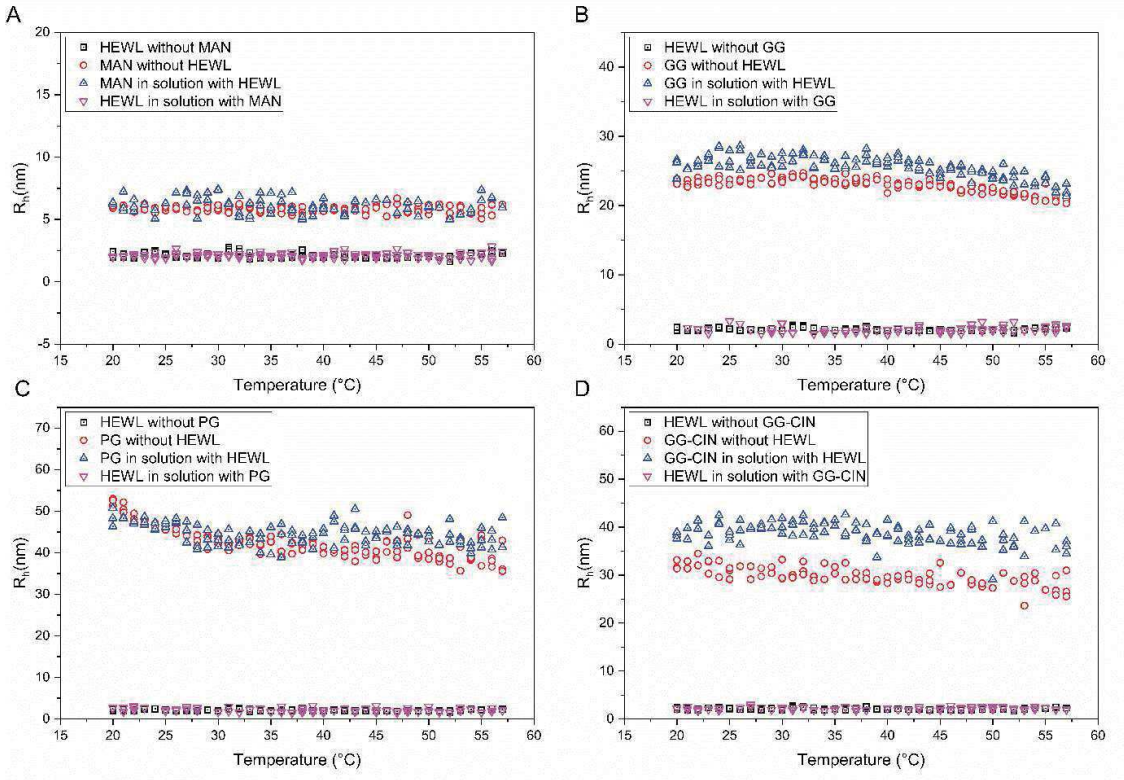

Fig. 6. Dependence of hydrodynamic radius R_h on temperature for the solutions of HEWL with (A) MAN, (B) GG, (C) PG, and (D) GG-CIN.

Understanding amyloid fibril formation in the presence of polysaccharides. DLS experiments were performed at different temperatures to determine the effect of temperature on polysaccharides without HEWL and in the presence of HEWL (20 C 57 C with increments of 1 C). Fig. 6 shows the temperature dependence of the hydrodynamic radii (R_h) of various objects identified in the size distributions. We found that the R_h of GG and GG-CIN decreased slightly with increasing temperature; however, the change was generally low. The R_h of PG changed more with temperature than that of GG and GG-CIN. The R_h of MAN was almost unchanged with increasing temperature. We also performed a DLS experiment on HEWL. For HEWL, we found that the R_h was approximately 2 nm, which was consistent with the literature[55] (black points in Fig. 6). We then determined the temperature dependence of the HEWL-polysaccharide interaction with DLS. For the DLS measurements, we used a polysaccharide concentration of 500 µg/mL and a HEWL concentration of 2 mg/mL.

For MAN, the R_h values of HEWL (approximately 2 nm) and MAN (approximately 6 nm) were similar, regardless of whether they were separate or mixed (see Fig. 6A). As MAN is a linear polymer in a random coil conformation, its R_h may have been less sensitive to adsorption of HEWL than the more compact GG, PG and GG-CIN. Based on the results of fibril formation with HEWL where MAN had only a small effect, it was confirmed that mannan does not significantly interact with HEWL. For the system with GG, the R_h increased immediately after mixing it with HEWL (blue points in Fig. 6B) compared to the value that we obtained without HEWL (red points in Fig. 6B). This increase in R_h in the presence of a protein may indicate that HEWL interacted with GG, which would suggest the molecular mechanism behind the acceleration of amyloid fibril formation. Although GG and PG have similar structures, their behaviors were different. At relatively low temperatures, the DLS data for PG in the presence of HEWL and without HEWL overlapped. However, there was a certain increase in the R_h of PG at temperatures above 35 C (Fig. 6C). This increase in R_h may have indicated the interaction between PG and HEWL, which may have affected HEWL and thereby accelerated amyloid fibril formation.

There was a large increase in the R_h of GG-CIN in the presence of HEWL (Fig. 6D) that was approximately equivalent to the thickness of a unimolecular layer of HEWL on the polysaccharide surface, indicating the significance of aromatic cinnamyl structures on the polysaccharide surface to protein adsorption. GG-CIN was a stronger amyloid formation inducer of amyloid fibril formation than GG, indicating that how HEWL adsorbs onto the polysaccharide surface may be different for GG and GG-CIN.

The ITC titrations of HEWL with the solutions of three native polysaccharides (GG, PG and MAN) and the synthetically modified GG-CIN were carried out at 25 and 57C. The titration curves and thermodynamic parameters of the interaction are shown in the supplementary information, Fig. S16-S19. Table 1 shows the affinity constant (K_a), Gibbs energy (G), enthalpy (H) and entropy (S) for the binding of HEWL to polysaccharides at 25C and 57C.

The addition of polysaccharides to the solution of HEWL at 25 C was always exothermic, with non-sigmoidal curves for GG, PG and MAN

and complex, two-step curve for GG-CIN (Fig. S19A). The ITC titration of HEWL with MAN showed measurable interactions (K_a ~10^3 M^{-1}) with negative enthalpy and positive entropy changes (Table 1 and Fig S16A in supplementary information), but without detectable changes in R_h of macromolecules. Therefore, we suggest no binding of HEWL to MAN, but desolvation of macromolecules due to conformational changes. Similar thermodynamic parameters were found for the titration of HEWL with PG and GG (Table 1, Fig. S17 and S18 in ESI). But in case of GG the titration yielded a DLS-detectable complex. Further modification of GG with cinnamoyl residues increased the interactions, which were happening in two steps: strong exothermic binding (Ka~10^6 M^{-1}) followed by weak exothermic binding (K_a ~10^3 M^{-1}). The latter was similar to the binding of HEWL to native GG. Again. binding of HEWL to GG-CIN at 25 C was clearly detectable with DLS (Fig. 6).

At 57 C the affinity constant (K_a) decreased slightly for the interaction of HEWL with MAN and PG, more significantly for GG-CIN strong binding site and was reduced down to 16 M^{-1} (no binding) for native GG and GG-CIN weak binding site. Similar trend is observed for derived from K_a Gibbs energy of binding (G). When compared to G at 25C, the values were almost unchanged for MAN and PG and decreased near twice for GG-CIN string binding site. The magnitude of measured enthalpy (H) increased one order in comparison with 25C for MAN, PG and native GG. Together with the results from DLS (minor changes in R_h) the results of ITC titrations indicate an enthalpy-entropy compensation, where measured exo- or endothermic effects during mixing of HEWL with PG, MAN and GG originate from rearrangement of the solvation shell around macromolecules without direct binding of protein to polysaccharide. On the other hand, for GG-CIN strong binding site the decrease of binding enthalpy (H) at 57C is observed, pointing on different binding mechanism in comparison with that of native polysaccharides.

The interaction of native polysaccharides with HEWL, is complex. Only for GG at lower temperatures was observed direct binding. The modification of GG with an aromatic motif increased its affinity to HEWL at all temperatures. The interactions of PG, MAN and GG at 57C with HEWL were accompanied by rearrangement of the solvation shell, which was mainly responsible for the measurable calorimetric effects. However, as it was demonstrated by TEM and ThT assay both direct binding of HEWL to polysaccharide and indirect changes in HEWL solvation shell, triggered by the addition of non-interacting co-solute alter the kinetic of the nucleation of HEWL fibrils and accelerate of their growth.

At the end of the ITC part, we have to note that since HEWL is a relatively stable protein. At 25C it will most likely be a folded or partially-unfolded protein, ITC was measured immediately after dissolution. And at 57 C, which is the temperature of the experiment, we assume an at least partly unfolded protein. Nevertheless, it can always be considered as interacting with HEWL. The interaction may differ at 25 C and 57 C.As the ITC measurement was performed for temperatures of 25 C and 57 C, we decided to calculate the corresponding relative excluded volume (equation (3) in the methods) and density (equation (2) in the methods) of polymer particles (Tab. S2) to determine the effect of temperature and whether there was a significant increase in the concentration of HEWL after adding a polysaccharide. In the case of MAN, there were negligible changes in the density and the relative excluded volume. In the case of other polymers, the R_h decreased with increasing temperature, which corresponded to an increase in density and a decrease in volume. We also found that the relative excluded volume was negligible for all polymers at a concentration of less than 0.5 mg/mL. However, the relative excluded volumes for high concentrations of GG were important. High relative excluded volumes were observed for 10 mg/mL GG and 25 mg/mL GG at 25 C, but amyloidogenicity testing on the HEWL model system was performed at 57 C. For a temperature of 57 C, only 25 mg/mL GG had a relative excluded volume exceeding 5%. A relative excluded volume above 5% could mean that acceleration of amyloid fibril formation was due to the crowding effect [56], but due to the results of DLS and ITC, the crowding effect was determined to not be the driving mechanism for acceleration, as the interaction between GG and HEWL seemed to be more important.

Table 1 . Thermodynamic parameters of the interaction of MAN, PG, GG and GG-CIN with HEWL.

Sample	*T, C*	*Conc., mg/mL*	*Conc., M*	*n**	*K_a, M^{-1}*	*ΔG, kJ/mol*	*ΔH, kJ/mol*	*ΔS, J/K·mol*
MAN	25	75	1.3510 ^{3}	0.5	5.010 ^{3}	-21,1	-13.4	26.0
	57				2.710 ^{3}	-21,7	-167.4	-443.5
PG	25	75	2.76	815	1.410 ^{4}	-23,7	-1.4	74.5
	57			89	2.410 ^{3}	-21,3	376.6	1200.8
GG	25	50	8.83	515	0.710 ^{3}	-16,2	-9.3	23.0
	57				67**	-11,5	exoth	-
GG-CIN	25	44	7.26	31	9.610 ^{5}	-34,1	-20.2	46.0
				1400	2.610 ^{4}	-27,9	-0.3	83.7
	57			31	2.110 ^{3}	-19,0	-1.9	66.9
				1400	16**	-7,6	exoth.	-

*Stoichiometry of the interaction: number of HEWL molecules bound to one polysaccharide molecule
** At K_a<100 M^{-1} no interaction is

ARTICLE

Influence of polysaccharides on amyloid formation with the A $_{1-42}$ peptide. The Aβ peptide is formed when amyloid precursor protein (APP) is cleaved by the so-called amyloidogenic pathway. Aβ occurs in sizes of 38-43 amino acids depending on the cleavage site. The most common isoforms are $Aβ_{1-40}$ (90%) and $Aβ_{1-42}$ (10%), the latter of which is the most fibrillogenic form[57]. The physiological concentration of Aβ is important for normal memory function and synaptic plasticity[58]. On the other hand, a high concentration of Aβ and its aggregation in senile plaques cause neurotoxicity and cell death. This senile plaque where Aβ occurs in the form of amyloid fibrils is associated with Alzheimers disease [5759] .

We used a polysaccharide concentration of 500 g/mL to study polysaccharide interactions with $Aβ_{1-42}$. In the case of GG, we also evaluated two higher but physiologically relevant concentrations (5 mg/mL and 25 mg/mL). Fig. 7 **Error! Reference source not found.**and supplementary information (Fig. S14 and Fig. S15) contain the results for experiments of $Aβ_{1-42}$ fibril formation without (control) and with polysaccharides and GG-CIN with appropriate fitting of the data. As in experiments with HEWL, there was also added a control for polysaccharides and GG-CIN to the fluorescence graphs. Also, in $Aβ_{1-42}$ experiments we did not observe contribution of ThT fluorescence.

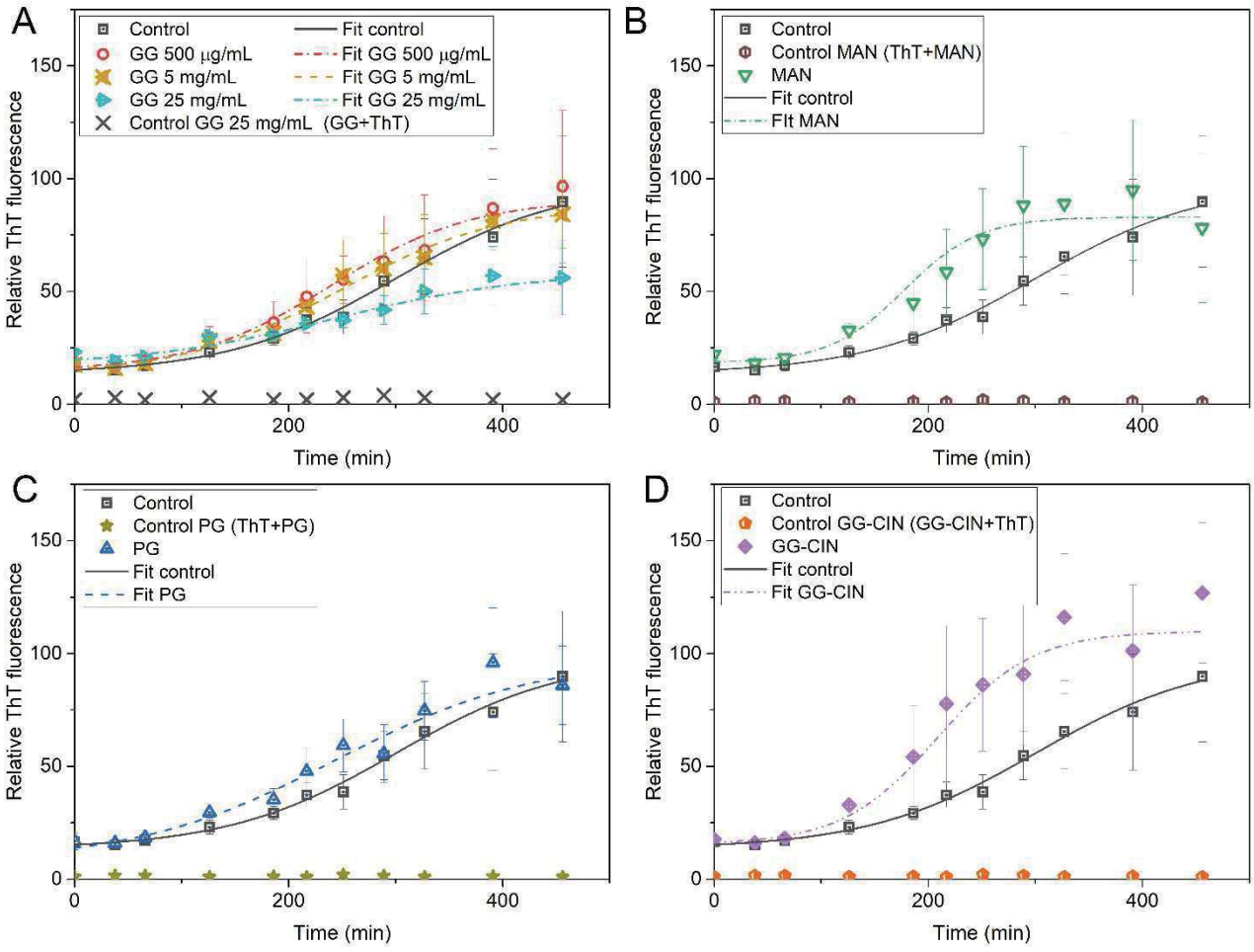

Fig. 7. Graphs of relative fluorescence of ThT, where black symbols are control data ($Aβ_{1-42}$ without polysaccharides): A) experiments for 500 g/mL GG, 5 mg/mL GG and 25 mg/mL GG ;(B) experiments for 500 g/mL MAN; (C) experiments for 500 g/mL PG; (D) experiments for 500 g/mL GG-CIN.

ARTICLE

All polysaccharides (except MAN) and GG-CIN shortened the lag phase of A_{1-42}. In the case of MAN, the lag phase was not significantly shortened, but the main role of MAN was in the growth phase that was significantly shortened. Neither GG nor PG had as great an effect on the growth phase as MAN and GG-CIN..

For GG, we tested three concentrations (500 g/mL, 5 mg/mL, and 25 mg/mL). With increasing GG concentration, the lag phase duration decreased. However, the sample with 25 mg/mL GG behaved more complexly. On the one hand, shortening of the lag phase was observed, but on the other hand, the growth phase was prolonged. We concluded that there was an interaction between A_{1-42} and GG and the seed nuclei and verified the observation of GG and A_{1-42} interactions using DLS. We performed 100 measurements of 500 g/mL GG and 100 measurements of GG 500 g/mL with A_{1-42} and found that the mean R_h of GG without A_{1-42} was 23.72 nm and the mean R_h of GG in the presence of A_{1-42} was 24.67 nm. Although the values did not seem vastly different, the population means were significantly different (with $\alpha<0.05$). As GG has a large surface area and A_{1-42} is relatively small (R_h below 1 nm), we assumed that more A_{1-42} was bound to a polysaccharide than in the case of HEWL, which indicated that some A_{1-42} would be bound that would have otherwise moved freely in solution. As part of the peptide was blocked, the concentration of A_{1-42} decreased, which would explain why 25 mg/mL GG shortened the lag phase, but the growth phase was delayed because the free peptide concentration was low. After approximately 26 h, we also collected TEM micrographs (in supplementary information Fig. S15) to evaluate the morphology. A_{1-42} had a worse contrast than HEWL, but the fibrillar structure was evident in all samples.

Conclusions

We have advanced our overall understanding of the influence of GG and other polysaccharides on amyloid fibril formation and found that they may significantly contribute to the pathogenesis of amyloidosis. We determined the following with the HEWL model:

- With increasing concentrations of PG and GG, HEWL fibril formation was promoted, while MAN had a very weak influence on amyloid fibril formation.
- Slight changes in the polysaccharide surface led to different behaviors (GG vs GG-CIN).
- Physiologically relevant concentrations of GG tremendously accelerated HEWL fibril formation, but it was found by DLS and ITC that this effect was most plausible not due to the crowding effect but caused by direct HEWL and GG interaction.

We determined the following from the A_{1-42} model:

- The results obtained for HEWL and A_{1-42} were in great agreement.
- GG-CIN shortened the lag phase of A_{1-42} and accelerated the growth phase of $A_{1-42.}$
- MAN did not have a drastic effect on HEWL, but A_{1-42} readily formed fibrils in the presence of MAN. This is relevant for the eventual promoting effect of fungal/yeast parasites on amyloid formation.
- PG and GG shortened the lag phase of A_{1-42} but only slightly accelerated the growth phase of A_{1-42}.
- The highest concentration of GG shortened the lag phase of A_{1-42} but prolonged the growth phase because of the direct interaction of GG and A_{1-42}.

On the basis of the herein presented *in vitro* data, we hypothesize thathe sharp fluctuations of D-glucose intake may cause GG cumulation and GG pathology in storage that may lead amyloid fibril formation and the development of related pathologies probably by direct molecular interaction mechanism, as glycogen levels in tissues are highly dependent on D-glucose intake. In addition, the pathology of insulin is associated with amyloidosis (AD and diabetes type II)[19]. All these findings are important for further investigation into amyloid-associated diseases, such as lysozyme-associated hereditary amyloidosis or Alzheimers disease.

Conflicts of interest

The authors have no conflicts of interest to declare.

Acknowledgements

This study was supported by Charles University, project GA UK No. 386218. We would like to thank the Ministry of Education, Youth and Sports of the Czech Republic (grant # LM2015064 ERIC) and the Czech Science Foundation (M.H.: grant # 19-01602S and P.S.: grant # 18-07983S) for financial support. We also would like to acknowledge Corinne Nardin from University in Pau, who introduced us to amyloid beta.

Notes and references

1 A. Aguzzi and T. OConnor, *Nat. Rev. Drug Discov.*, 2010, **9**, 237248.

2 A. Taglialegna, I. Lasa and J. Valle, *J. Bacteriol.*, 2016, **198**, 25792588.

3 M. Holubová and M. Hrub, *Chem. List.*, 2016, **110**, 851 859.

4 G. Wei, Z. Su, N. P. Reynolds, P. Arosio, I. W. Hamley, E.

Gazit and R. Mezzenga, *Chem. Soc. Rev.*, 2017, **46**, 4661 4708.

5 E. Chuang, A. M. Hori, C. D. Hesketh and J. Shorter, *J. Cell Sci.*, 2018, **131**, jcs189928.

6 L. Nielsen, R. Khurana, A. Coats, S. Frokjaer, J. Brange, S. Vyas, V. N. Uversky and A. L. Fink, *Biochemistry*, 2001, **40**, 60366046.

7 C. Wallin, M. Friedemann, S. B. Sholts, A. Noormgi, T. Svantesson, J. Jarvet, P. M. Roos, P. Palumaa, A. Grslund and S. K. T. S. Wrmlnder, *Biomolecules*, 2020, **10**, 44.

8 C. Iannuzzi, R. Maritato, G. Irace and I. Sirangelo, *Int. J. Mol. Sci.*, 2013, **14**, 1428714300.

9 E. Gazit, *FEBS J.*, 2005, **272**, 59715978.

10 K. E. Marshall, K. L. Morris, D. Charlton, N. OReilly, L. Lewis, H. Walden and L. C. Serpell, *Biochemistry*, 2011, **50**, 20612071.

11 F. Chiti and C. M. Dobson, *Annu. Rev. Biochem.*, 2006, **75**, 333366.

12 F. Bemporad and F. Chiti, in *Amyloid Fibrils and Prefibrillar Aggregates*, Wiley-VCH Verlag GmbH & Co. KGaA, Weinheim, Germany, 2013, pp. 151166.

13 P. Arosio, T. P. J. Knowles and S. Linse, *Phys. Chem. Chem. Phys.*, 2015, **17**, 76067618.

14 S. Yasar Yildiz and E. Toksoy Oner, in *Application of Nanotechnology in Drug Delivery*, InTech, 2014, vol. i, p. 13.

15 P. Wang, W. Liao, J. Fang, Q. Liu, J. Yao, M. Hu and K. Ding, *Carbohydr. Polym.*, 2014, **110**, 142147.

16 O. Klementieva, N. Benseny-Cases, A. Gella, D. Appelhans, B. Voit and J. Cladera, *Biomacromolecules*, 2011, **12**, 3903 3909.

17 M. Holubová, P. těpánek and M. Hrub, *Colloid Polym. Sci.*, , DOI:10.1007/s00396-020-04710-8.

18 K. Sideras and M. A. Gertz, in *Advances in clinical chemistry*, 2009, vol. 47, pp. 144.

19 S. Chatterjee and A. Mudher, *Front. Neurosci.*, 2018, 12.

20 J. Avila, G. Len-Espinosa, E. Garca, V. Garca-Escudero, F. Hernández and J. Defelipe, *Int. J. Alzheimers. Dis.*, 2012, 2012, 17.

21 S. Chatterjee, T. K. Sang, G. M. Lawless and G. R. Jackson, *Hum. Mol. Genet.*, 2009, **18**, 164177.

22 F. Hernandez, J. J. Lucas and J. Avila, *J. Alzheimers Dis.* , 2012, **33**, S141S144.

23 L. R. Engelking, in *Textbook of Veterinary Physiological Chemistry*, Elsevier, 2015, pp. 147152.

24 L. Cole and P. R. Kramer, in *Human Physiology, Biochemistry and Basic Medicine*, Elsevier, 2016, pp. 1730.

25 A. Brown, S. Baltan and B. R. Ransom, in *Encyclopedia of Neuroscience*, Elsevier, 2009, pp. 929934.

26 W. J. Malaisse, L. Ladrière, J. Cancelas, A. Acitores, M. L. Villanueva-Peñacarrillo and I. Valverde, *Mol. Cell. Biochem.*, 2001, **219**, 4549.

27 L. Huang and Y. Yao, *Carbohydr. Polym.*, 2011, **83**, 1665 1671.

28 M. Grossutti, C. Miki and J. R. Dutcher, *Househ. Pers. Care Today*, 2017, **12**, 4751.

29 M. Holubova, R. Konefał, Z. Moravkova, A. Zhigunov, J. Svoboda, O. Pop-Georgievski, J. Hromadkova, O. Groborz, P. Stepanek and M. Hruby, *RSC Adv.*, 2017, **7**, 53887 53898.

30 L. C. Serpell, M. Sunde, M. D. Benson, G. A. Tennent, M. B. Pepys and P. E. Fraser, *J. Mol. Biol.*, 2000, **300**, 10331039.

31 M. Sullivan, B. Harcourt, P. Xu, J. Forbes and R. Gilbert, *Curr. Drug Targets*, 2015, **16**, 10881093.

32 L. R. S. Moreira and E. X. F. Filho, *Appl. Microbiol. Biotechnol.*, 2008, **79**, 165178.

33 K. B. Gilchrist, M. C. Garcia, R. Sobonya, P. N. Lipke and S. A. Klotz, *J. Infect. Dis.*, 2012, **206**, 14731478.

34 N. N. Pearsall and D. Lagunoff, *Infect. Immun.*, 1974, **10**, 13971400.

35 J. Jake, *Collect. Czechoslov. Chem. Commun.*, 1995, **60**, 17811797.

36 P. těpánek and R. M. Johnsen, *Collect. Czechoslov. Chem. Commun.*, 1995, **60**, 19411949.

37 P. Stepanek and T. P. Lodge, *Macromolecules*, 1996, **29**, 12441251.

38 S. P. Cadogan, C. J. Hahn, M. H. Rausch and A. P. Frba, *J. Colloid Interface Sci.*, 2017, **499**, 202208.

39 M. W. Ishaq, N. Hao, M. Zhu and L. Li, *Macromolecules*, 2020, **53**, 558568.

40 G. Galinsky and W. Burchard, *Macromolecules*, 1997, **30**, 69666973.

41 S. Podzimek, *Light Scattering, Size Exclusion Chromatography and Asymmetric Flow Field Flow Fractionation: Powerful Tools for the Characterization of Polymers, Proteins and Nanoparticles*, John Wiley & Sons, Inc., Hoboken, NJ, USA, 2011.

42 T. V. Andreeva, W. J. Lukiw and E. I. Rogaev, *Biochem.*, 2017, **82**, 122139.

43 L.-H. Tu and D. P. Raleigh, *Biochemistry*, 2013, **52**, 333342.

44 D. D. Soto-Ortega, B. P. Murphy, F. J. Gonzalez-Velasquez, K. A. Wilson, F. Xie, Q. Wang and M. A. Moss, *Bioorg. Med. Chem.*, 2011, **19**, 25962602.

45 P. C. Ke, M.-A. Sani, F. Ding, A. Kakinen, I. Javed, F. Separovic, T. P. Davis and R. Mezzenga, *Chem. Soc. Rev.*, 2017, **46**, 64926531.

46 S. Freire, M. H. De Araujo, W. Al-Soufi and M. Novo, *Dye. Pigment.*, 2014, **110**, 97105.

47 R. Mishra, D. Sjlander and P. Hammarstrm, *Mol. Biosyst.*, 2011, **7**, 1232.

48 S. L. Gras, L. J. Waddington and K. N. Goldie, eds. A. F. Hill, K. J. Barnham, S. P. Bottomley and R. Cappai, Humana Press, Totowa, NJ, 2011, vol. 752, pp. 197214.

49 A. Cao, D. Hu and L. Lai, *Protein Sci.*, 2004, **13**, 31924.

50 R. Swaminathan, V. K. Ravi, S. Kumar, M. V. S. Kumar and N. Chandra, *Adv. Protein Chem. Struct. Biol.*, 2011, **84**, 63 111.

51 V. K. Ravi, T. Swain, N. Chandra and R. Swaminathan, *PLoS One*, 2014, **9**, e87256.

52 U. Sengupta, A. N. Nilson and R. Kayed, *EBioMedicine*, 2016, **6**, 4249.

53 F. M. LaFerla, K. N. Green and S. Oddo, *Nat. Rev. Neurosci.*, 2007, **8**, 499509.

54 E. Cruz, S. Kumar, L. Yuan, J. Arikkath and S. K. Batra, *PLoS One*, 2018, **13**, e0191696.

55 L. R. Nemzer, B. N. Flanders, J. D. Schmit, A. Chakrabarti and C. M. Sorensen, *Soft Matter*, 2013, **9**, 21872196.
56 Y. Hata, T. Sawada and T. Serizawa, *J. Mater. Chem. B*, 2018, 6, 63446359.
57 M. del C. Crdenas-Aguayo, M. del C. Silva-Lucero, M. Cortes-Ortiz, B. Jimnez-Ramos, L. Gmez-Virgilio, G. Ramrez-Rodrguez, E. Vera- Arroyo, R. Fiorentino-Prez, U. Garca, J. Luna-Muoz and M. A. Meraz Ros, in *Neurochemistry*, InTech, 2014.
58 Z. U. Khan, E. Martn-Montañez, I. Navarro-Lobato and E. C. Muly, in *Progress in Molecular Biology and Translational Science*, Academic Press, 2014, vol. 122, pp. 129.
59 G. Chen, T. Xu, Y. Yan, Y. Zhou, Y. Jiang, K. Melcher and H. E. Xu, *Acta Pharmacol. Sin.*, 2017, **38**, 12051235.

Does polysaccharide glycogen behave as a promoter of amyloid fibril formation at physiologically relevant concentrations?

Monika Holubová[a,b], Volodymyr Lobaz[a], Lenka Loukotová[a], Mariia Rabyk[a], Jiřina Hromádková[a], Olga Trhlková [a], Zdislava Pechrová[a], Ondřej Groborz[a,b], Petr těpánek [a], Martin Hrub [a,*]

[a]*Institute of Macromolecular Chemistry, Academy of Sciences of the Czech Republic, Heyrovsk Sq. 2, 162 06 Prague 6, Czech Republic, e-mail address: mhruby@centrum.cz*

[b]*Charles University in Prague, Faculty of Science, Albertov 6, 128 43 Prague 2, Czech Republic*

Supplementary information:

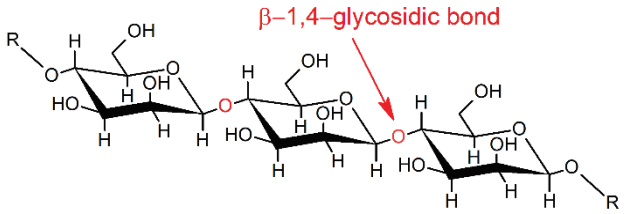

Fig. S1. Structure of mannan (MAN).

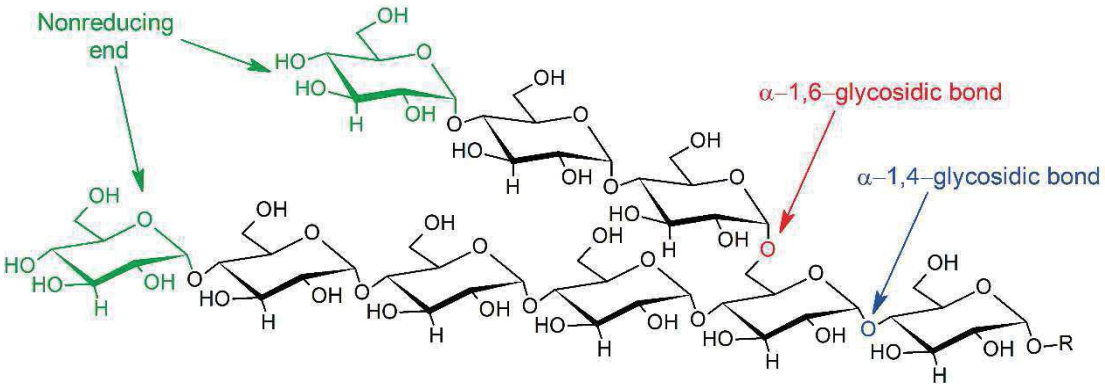

Fig. S2. Structure of glycogen (GG).

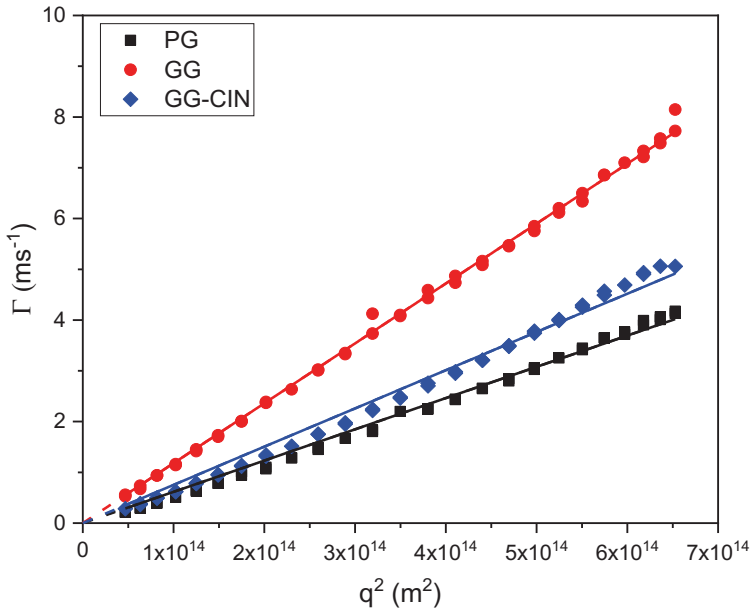

Fig. S3 The graph of dependence on q^2

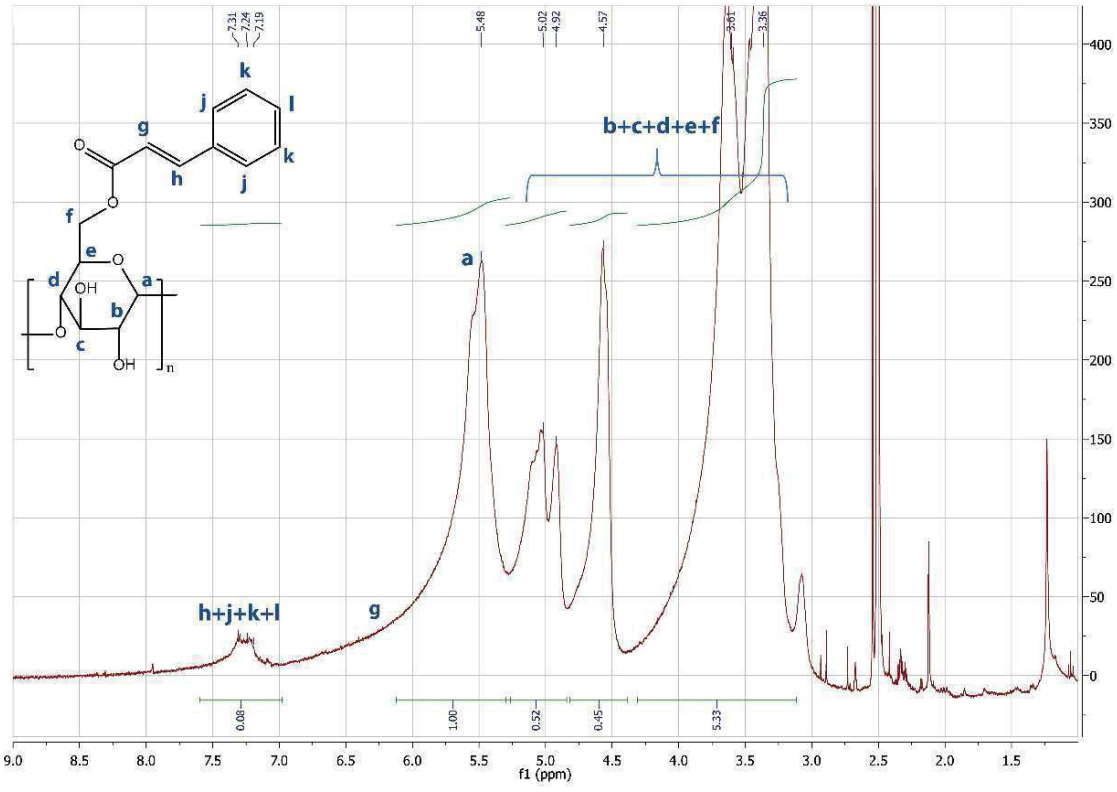

Fig. S4. ^{1}H-NMR of cinnamoylated glycogen (GG-CIN).

Tab. S1. The refractive index increment (d*n*/d*c*), molecular weight (M_W) and intensity-weighted R_h values obtained from DLS of all polysaccharides and GG-CIN.

	MAN	*GG*	*PG*	*GG-CIN*
dn/dc (mL/g)	0.1355±0.0039	0.1483±0.0017	0.1471±0.0002	0.1505±0.0019
M_W *(g/mol)*	5.510^{4}	5.710^{6}	27.110^{6}	6.110^{6}
Intensity-weighted R_h *(nm)*	5.9±1.5	23.5±8.1	45.1±19.9	30.4±19.0

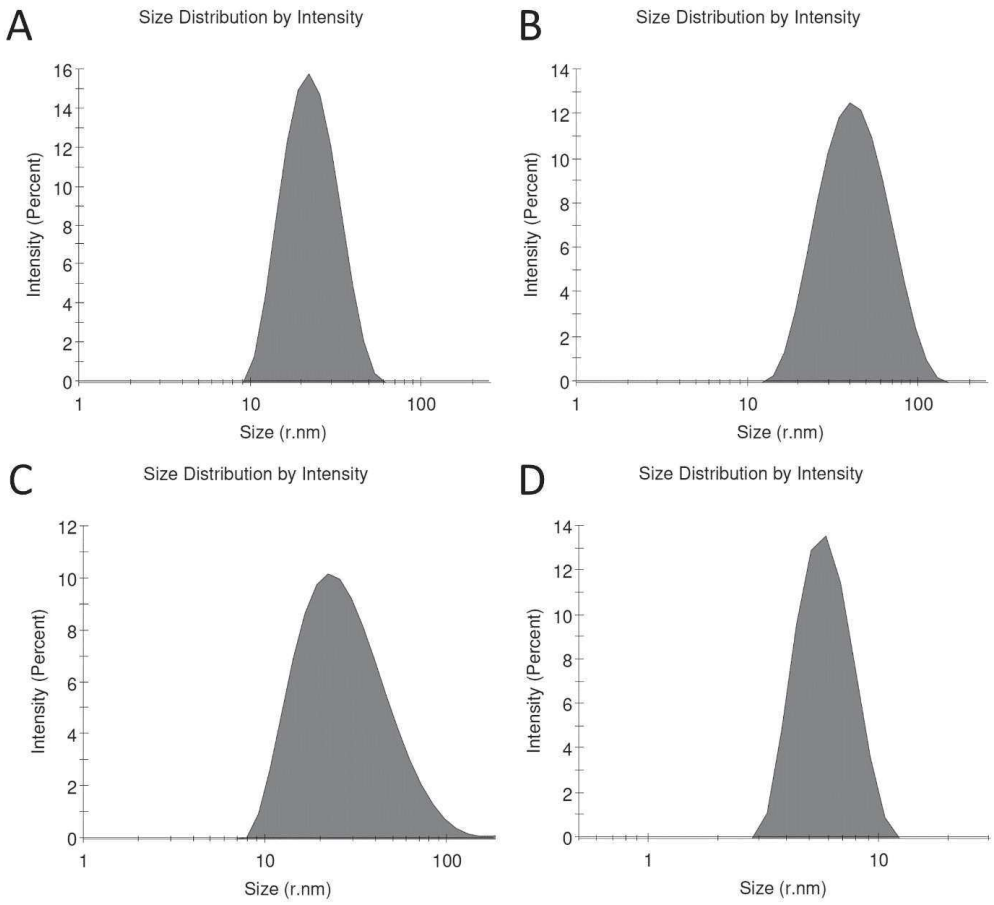

Fig. S5. Size distribution by intensity for (A) GG, (B) PG, (C) GG-CIN and (D) MAN.

Experiments with HEWL, MAN, GG and PG

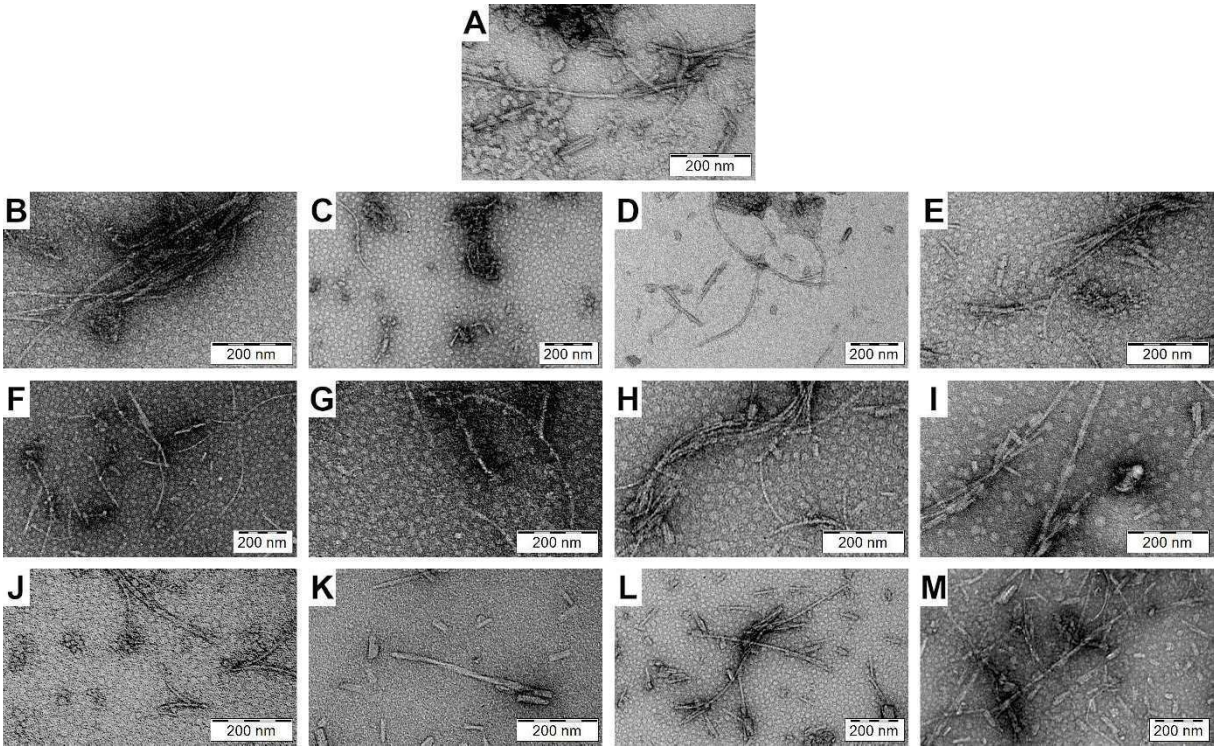

Fig. S6. Experiments with HEWL, MAN, GG and PG: TEM micrographs after 24h: (A) shorter and longer fibrils of HEWL (control) without any polysaccharides; shorter and longer fibrils for samples containing (B) 10 g/m L, (C) 50 g/m L, (D) 250 g/m L and (E) 500 g/ mL MAN; shorter and longer fibrils for samples containing (F) 10 g/ mL, (G) 50 g/ mL, (H) 250 g/ mL and (I) 500 g/m L GG; shorter and longer fibrils for samples containing (J) 10 g/ mL, (K) 50 g/ mL, (L) 250 PG g/ mL and (M) 500 g/m L PG. The TEM micrographs were used just to illustrate and check the morphology.

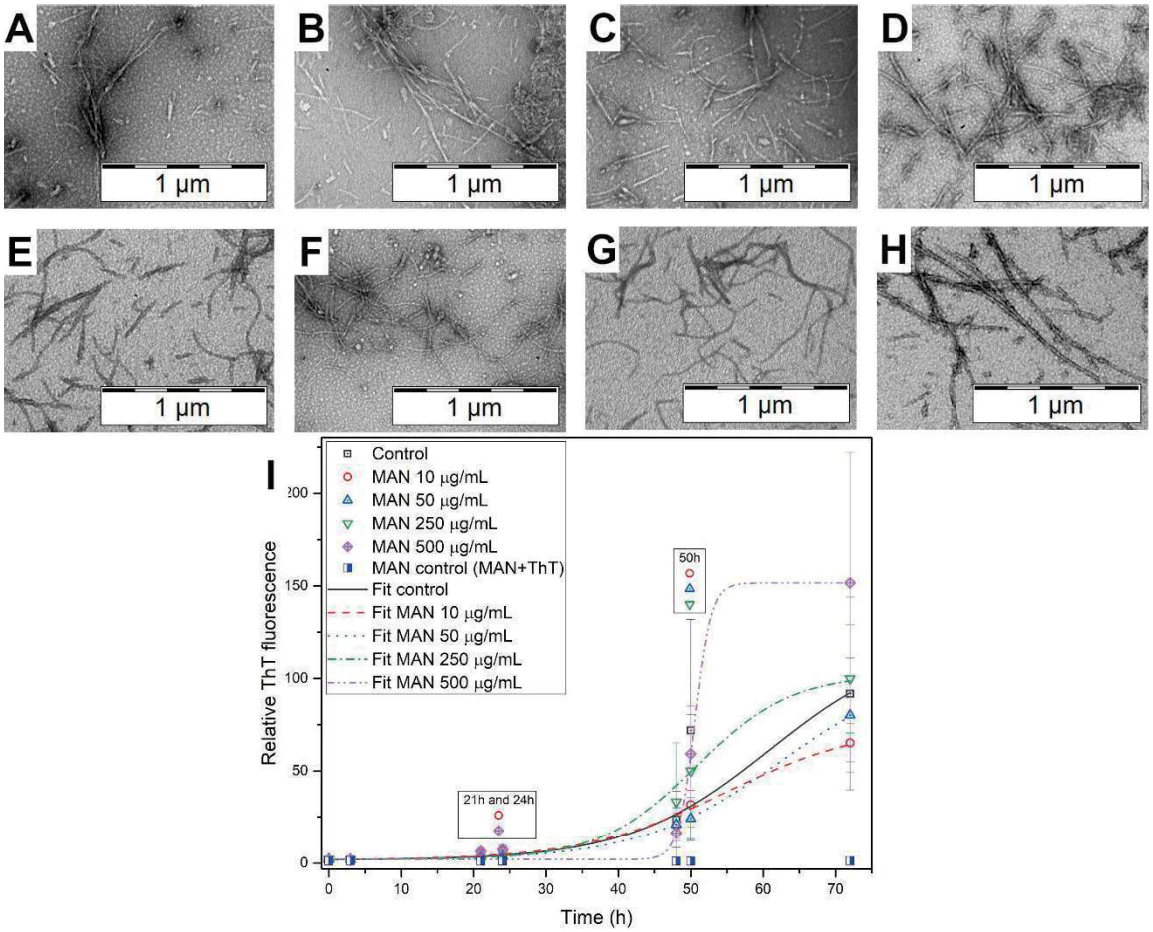

Fig. S7 Experiments with HEWL, MAN, GG and PG: TEM micrographs after 48h: (A-D) shorter and longer fibrils for samples containing (A) 10 g/mL,(B) 50 g/mL, (C) 250 g/mL and (D) 500 g/mL MAN ; (E) and (F) shorter and longer fibrils for samples containing 10 g/mL and 50 g/mL GG; (G) shorter and longer fibrils for the sample containing 10 g/mL PG; (H) shorter and long fibers for the sample containing 50 g/mL PG. (I) Graphs of relative ThT fluorescence with the fit of data. The legend above the results from the same time represents a statistically significant difference (<0.05) when compared to control at this time. The TEM micrographs were used just to illustrate and check the morphology.

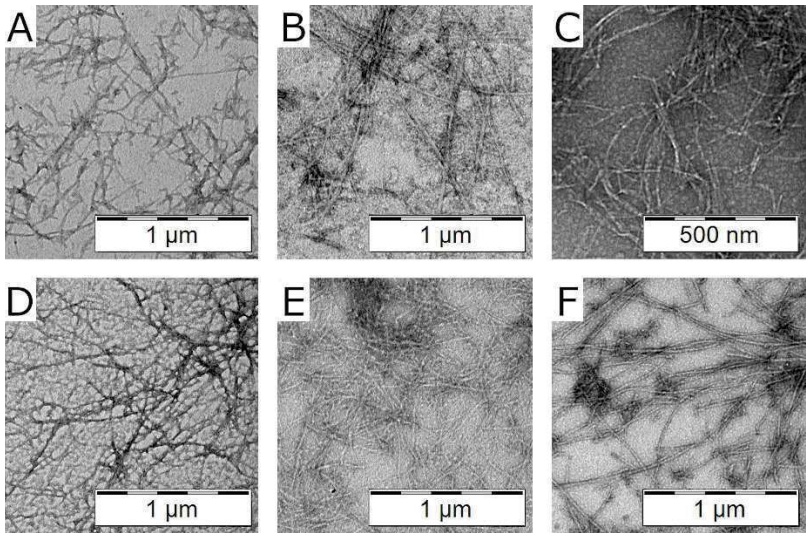

Fig. S8. Experiments with HEWL, MAN, GG and PG: TEM micrographs after 72 h: (A) mature amyloid fibrils of HEWL (control) without any polysaccharides; (B) mature amyloid fibrils of 250 g/ mL MAN; (C) and (D) mature amyloid fibrils for samples containing 10 g/ mL and 50 g/ mL GG; (E) and (F) mature amyloid fibrils for samples containing 10 g/m L and 50 g/ mL GG. The TEM micrographs were used just to illustrate and check the morphology.

Experiment with HEWL, GG and GG-CIN

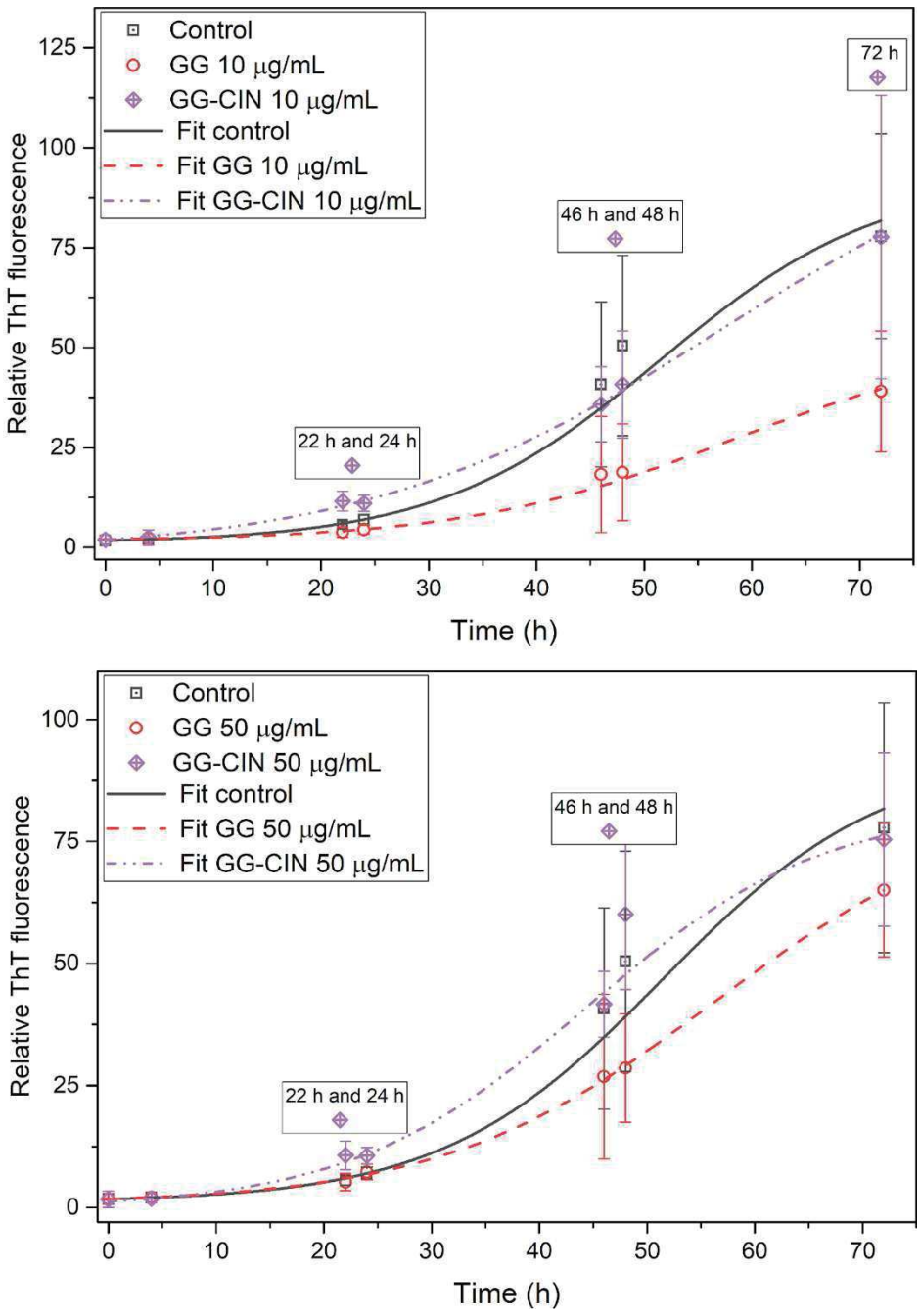

Fig. S9 part A. Experiments with HEWL, GG and GG-CIN: The graphs of comparison same amount unmodified GG and GG-CIN. The legend above the results at the same time represents a statistically significant difference (<0.05) when GG -CIN was compared to GG at this time.

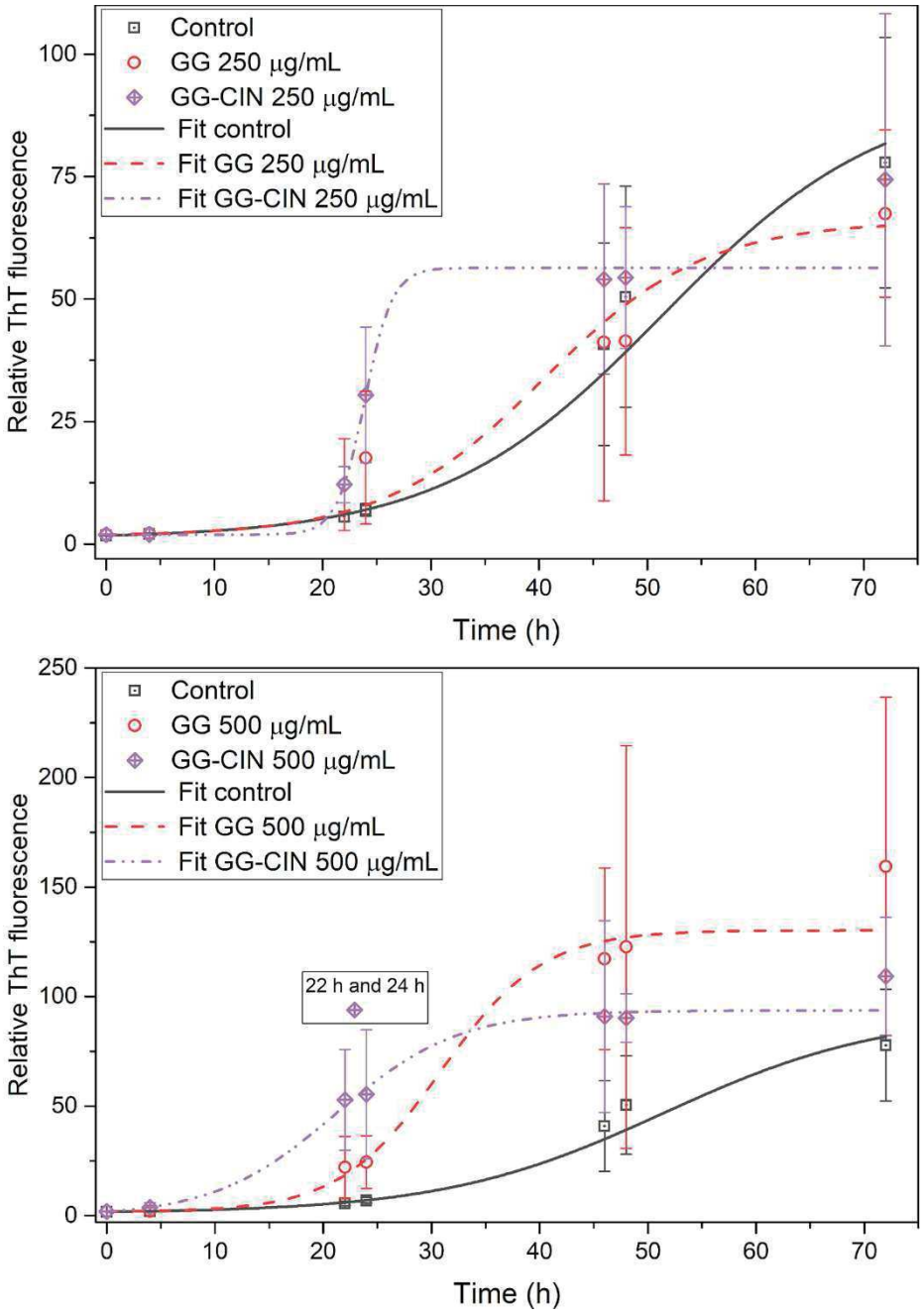

Fig. S9 part B. Experiments with HEWL, GG and GG-CIN: The graphs of comparison same amount unmodified GG and GG-CIN. The legend above the results at the same time represents a statistically significant difference (<0.05) wh en GG-CIN was compared to GG at this time.

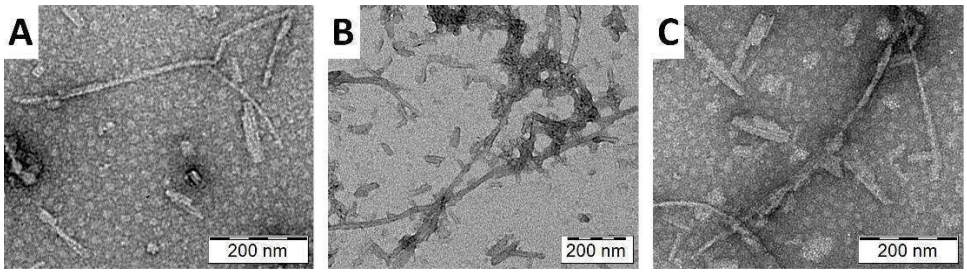

Fig. S10. Experiments with HEWL, GG and GG-CIN: TEM micrographs after 24h incubation: shorter and longer fibrils for samples containing (A) 10 g/m L, (B) 50 g/ mL and (C) 250 g/ mL GG-CIN. The TEM micrographs were used just to illustrate and check the morphology.

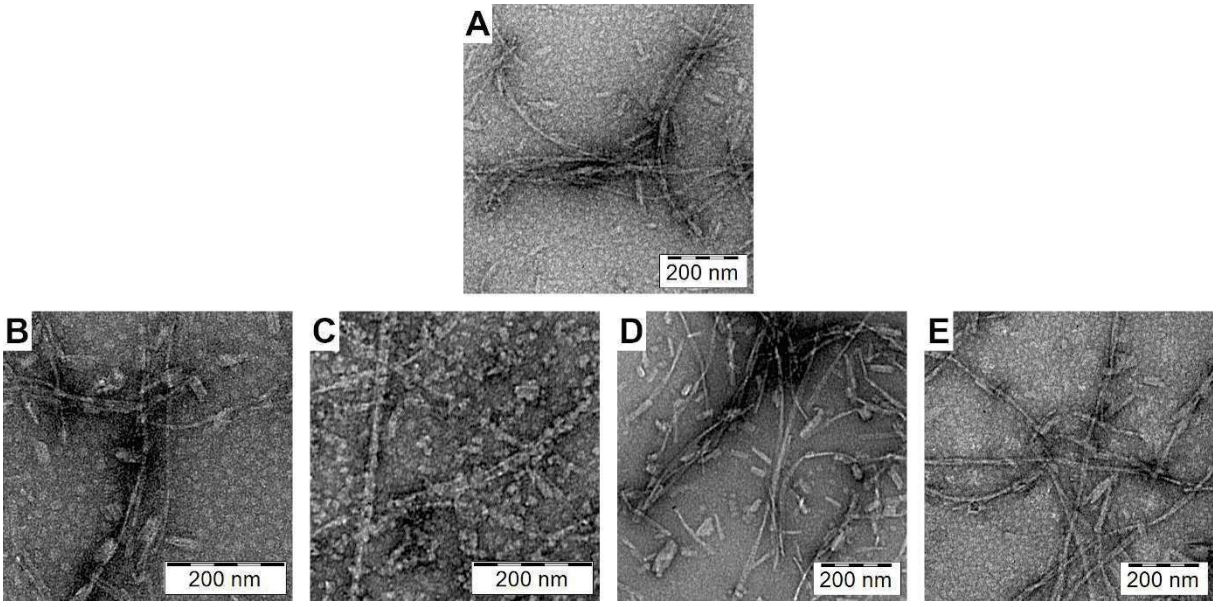

Fig. S11. Experiments with HEWL, GG and GG-CIN: TEM micrographs after 48h incubation: (A) shorter and longer fibrils of HEWL (control); (B) shorter and longer fibrils for the sample containing 10 g/ mL GG-CIN, (C) longer fibrils for the sample containing 50 g/m L GG-CIN, (D) many shorter fibrils and some longer fibrils for the sample containing 250 g/ mL GG-CIN, (E) long mature fibrils for the sample containing 500 g/ mL GG-CIN. The TEM micrographs were used just to illustrate and check the morphology.

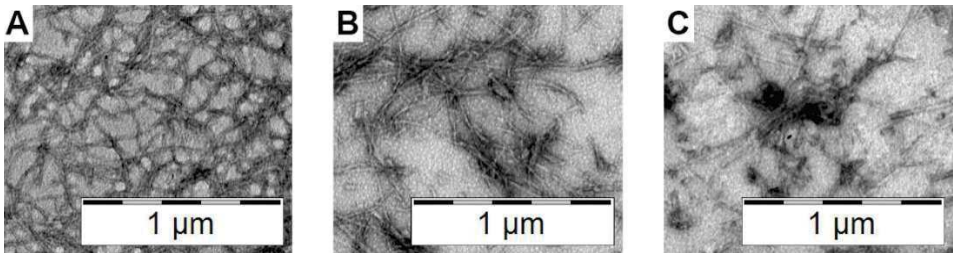

Fig. S12. Experiments with HEWL, GG and GG-CIN: TEM micrographs after 72 h incubation: (A) long mature fibrils of HEWL (control); (B) long mature fibrils and some shorter fibrils of samples containing 10 g/m L GG-CIN, (C) long mature fibrils and some shorter fibrils of samples containing 250 g/ mL GG-CIN. The TEM micrographs were used just to illustrate and check the morphology.

Experiment with biologically relevant concentrations of GG

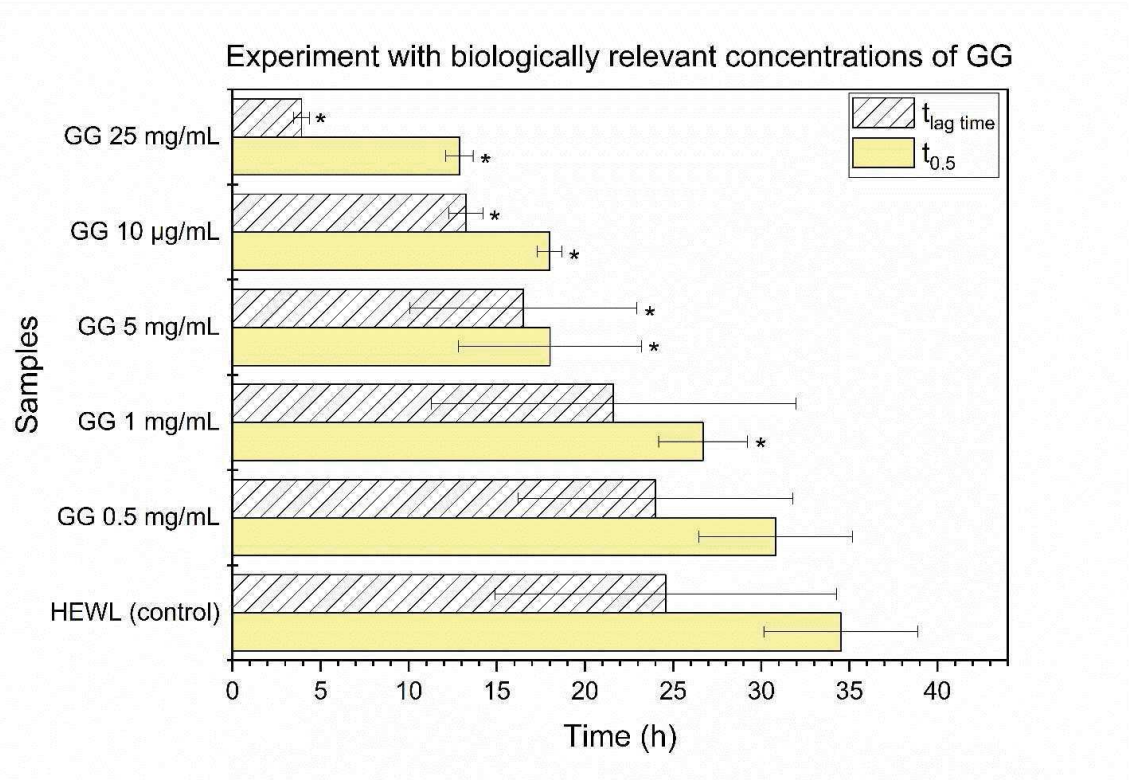

Fig. S13 The graph of the lag times ($t_{lag\ time}$) and times ($t_{0.5}$) at 50% maximal fluorescence for experiments with high concentrations of GG. The star (*) means a statistically significant difference (<0.05) when compared to the control.

Experiment for A $_{1-42}$, MAN, PG, GG-CIN and GG.

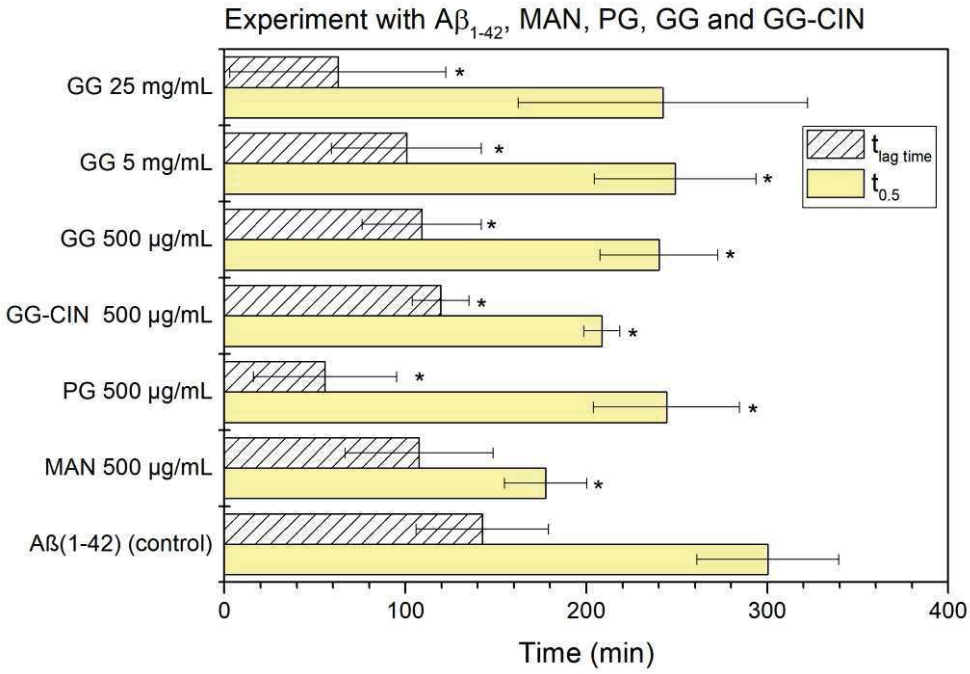

Fig. S14 A graph of the lag times ($t_{lag\ time}$) and times ($t_{0.5}$) at 50% maximal fluorescence for experiments of A $_{1-42}$ fibril formation without and with polysaccharides. The star (*) means a statistically significant difference ($\alpha<0.05$) when compared to the control.

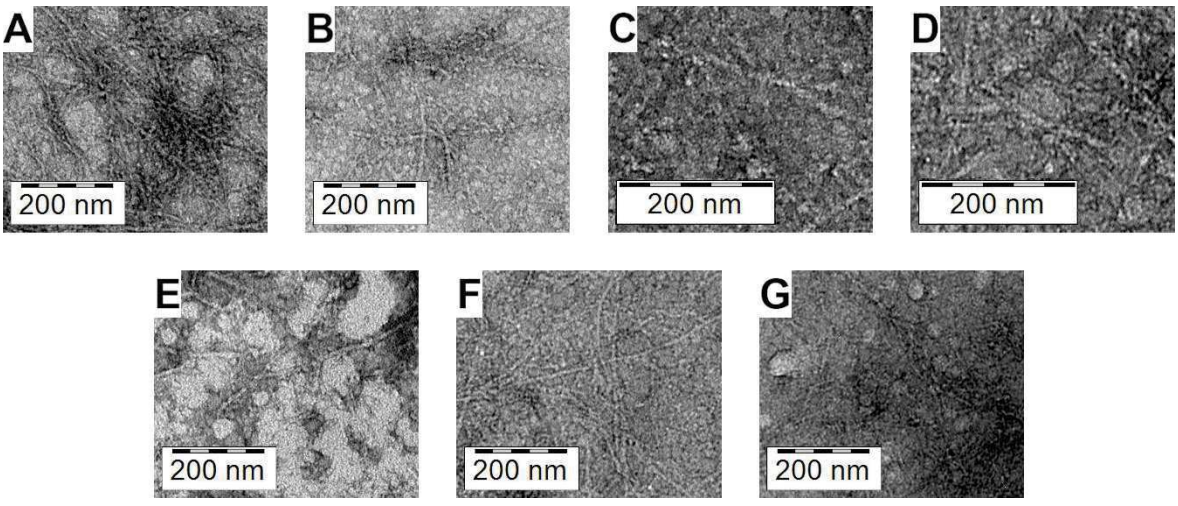

Fig. S15. TEM micrographs after 26 h incubation: (A) fibrils of A $_{1-42}$ (control); (B) hint of fibrils of the sample containing 500 g/m L PG, (C) hint of fibrils of the sample containing 500 g/ mL MAN, (D) hint of fibrils of the sample containing 500 g/ mL GG-CIN; a hint of fibrils the sample containing (E) 500 g/ mL, (F) 5 mg/mL and (G) 25 mg/mL GG. The TEM micrographs were used just to illustrate and check morphology.

Isothermal titration calorimetry (ITC) the upper graph heat flow per injection corrected to the heat of dilution, lower graph integrated heat vs molar ratio (the line is a fit to the experimental data)

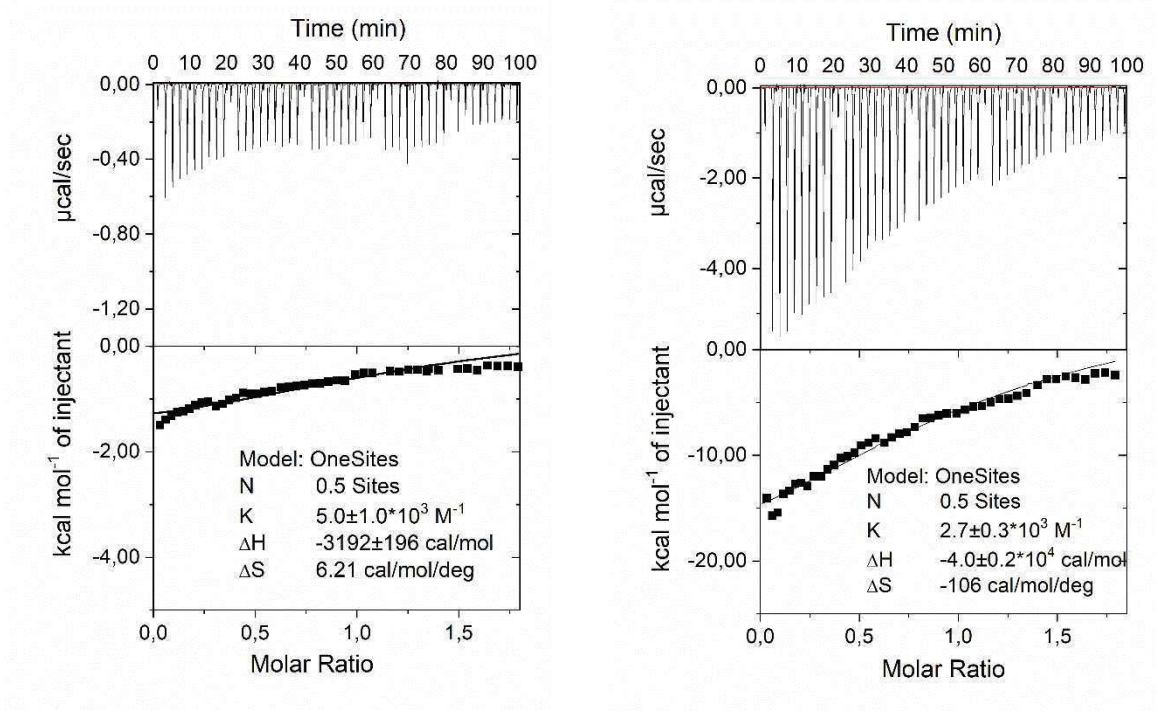

A B

Fig.S16 Titration of 1mM HEWL with 1.35mM MAN at 25C (A) and 57C (B).

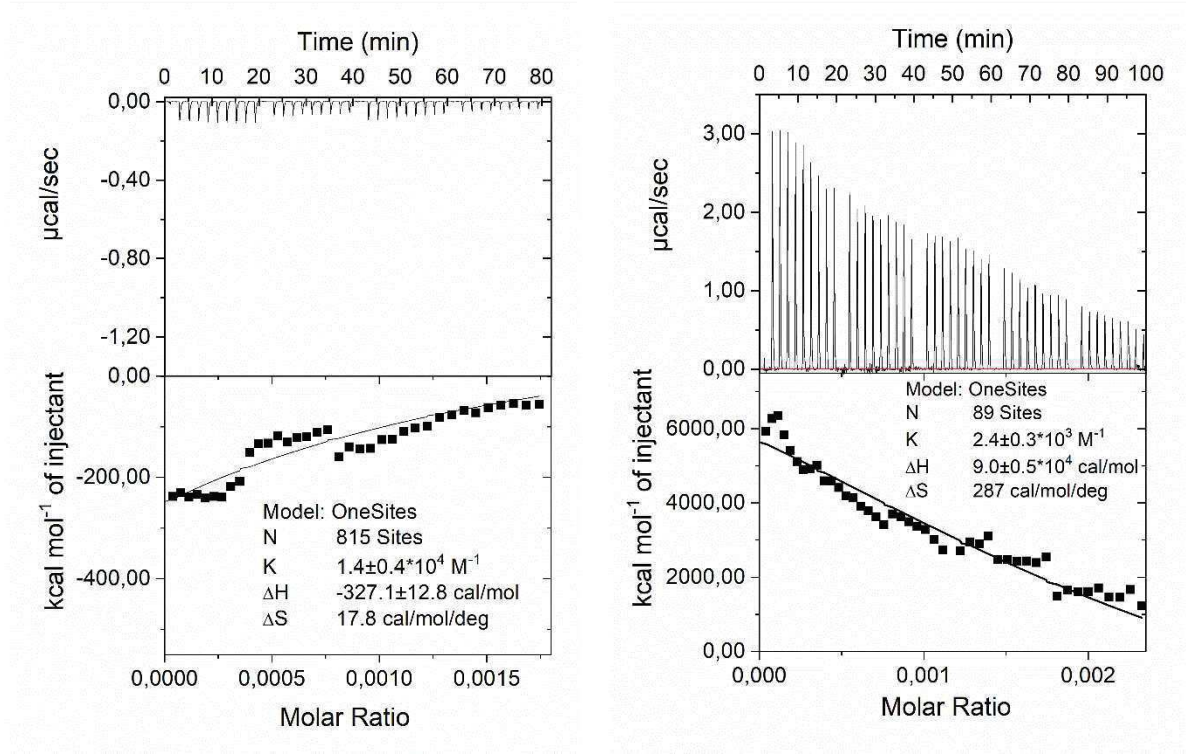

A B

Fig.S17 Titration of 1mM HEWL with 2.76 M PG at 25C (A) and 57C (B).

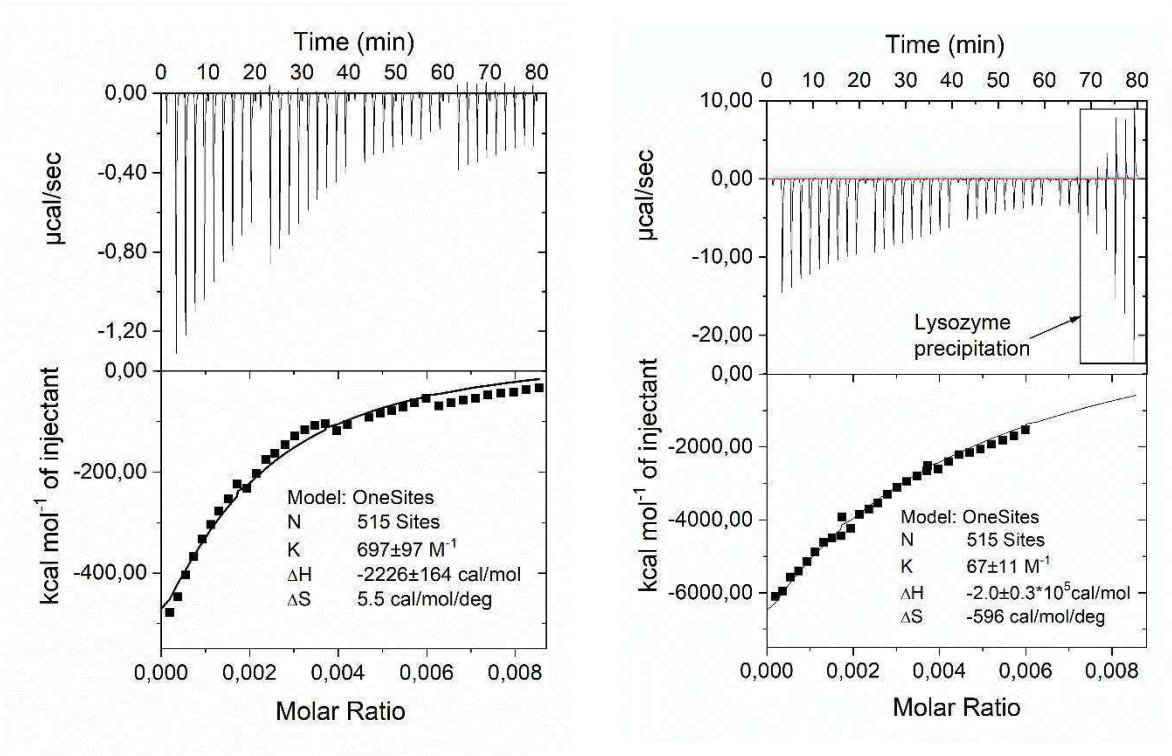

A B

Fig.S18 Titration of 1mM HEWL with 8.83 M GG at 25C (A) and 57C (B).

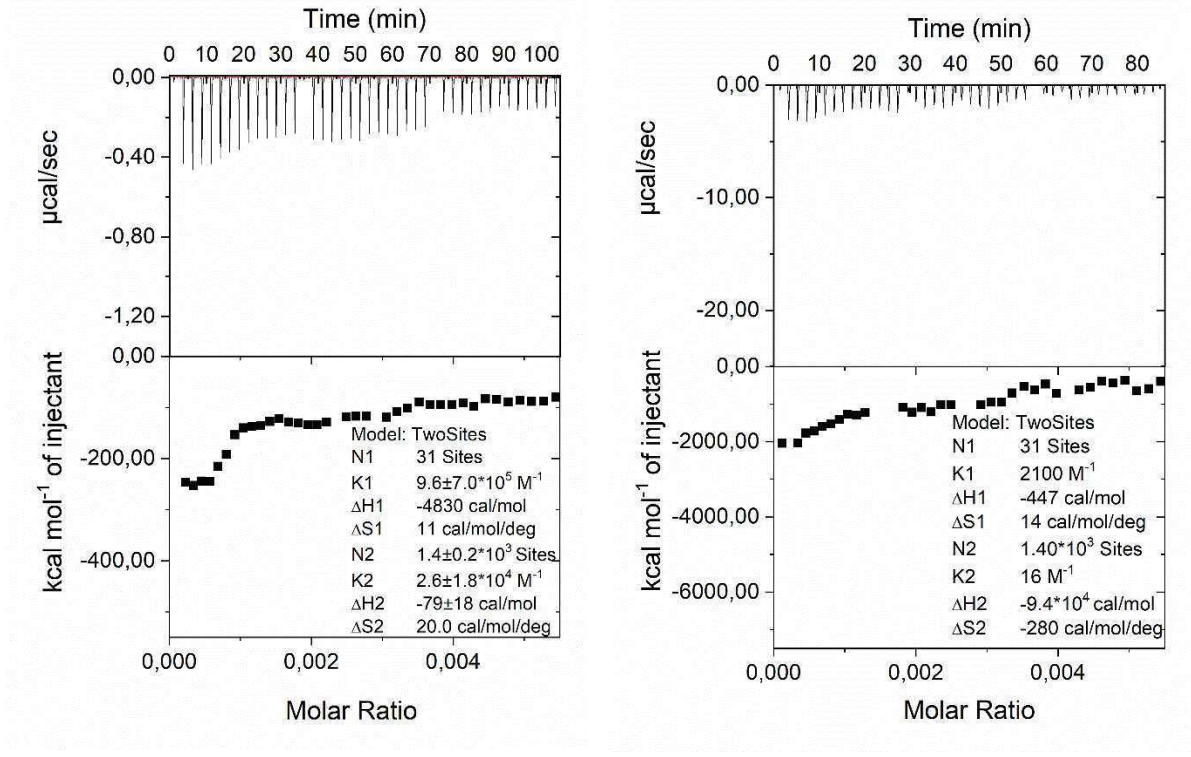

A B

Fig.S19 Titration of 1mM HEWL with 7.26 M GG -CIN at 25C (A) and 57C (B).

Tab. S2 Intensity R_h of polymers at temperatures of 25 C and 57 C and their corresponding relative excluded volume and density.

		25 C			57 C		
	concentration (mg/mL)	*R_h (nm)*	*Density (g/mL)*	*Relative excluded volume (%)*	*R_h (nm)*	*Density (g/mL)*	*Relative excluded volume (%)*
GG	0.5	23.5	0.174	0.29	20.6	0.259	0.19
	1			0.58			0.39
	5			2.87			1.93
	10			5.74			3.87
	25			14.36			9.67
MAN	0.5	5.9	0.106	0.47	6.2	0.091	0.55
PG	0.5	45.1	0.118	0.43	38.2	0.193	0.26
GG-CIN	0.5	30.4	0.086	0.58	27.7	0.113	0.44

Publication 5

Soft Matter

Chemically modified glycogens: How they influence formation of amyloid fibrils?

Journal:	*Soft Matter*
Manuscript ID	Draft
Article Type:	Paper
Date Submitted by the Author:	n/a
Complete List of Authors:	Holubová, Monika; stav makromolekuláry chemie Akademie věd České republiky Lobaz, Volodymyr; Institute of Macromolecular Chemistry, Supramolecular Systems and Selfassociation Processes Loukotová, Lenka; Institute of Macromolecular Chemistry, Academy of Sciences of the Czech Republic, Biomacromolecular and Bioanalogous Systems Rabyk, Mariia; Institute of Macromolecular Chemistry, Academy of Sciences of the Czech Republic, Biomacromolecular and Bioanalogous Systems Prague 6, Czech Republic, 210 Hromadkova, Jirina; Institute of Macromolecular Chemistry, Academy of Sciences of the Czech Republic, Trhlikova, Olga; Institute of Macromolecular Chemistry AS CR Pechrová, Zdislava; stav makromolekuláry chemie Akademie věd České republiky Groborz, Ondřej; Institute of Macromolecular Chemistry, Academy of Sciences of the Czech Republic, Stepanek, Petr; Akademie ved Ceske republiky Ustav makromolekularni Chemie, Hruby, Martin; Institute of Macromolecular Chemistry, Academy of Sciences of the Czech Republic, Biomacromolecular and Bioanalogous Systems

ARTICLE

Chemically modified glycogens: How they influence formation of amyloid fibrils?

Received 00th January 20xx,
Accepted 00th January 20xx

DOI: 10.1039/x0xx00000x

Monika Holubov [a,b], Volodymyr Lobaz[a], Lenka Loukotov [a], Mariia Rabyk[a], Jiřina Hromdkov [a], Olga Trhlíkov [a], Zdislava Pechrov [a], Ondřej Groborz[a,b], Petr Štěpnek [a], Martin Hrubý*[a]

The formation of amyloid fibrils from certain proteins stays behind a number of pathologies, so-called amyloidoses. Glycosaminoglycans are polysaccharides and are known natural constituents of amyloids in vivo. However, little is known about the effect of other naturally abundant polysaccharides, and even less is known about the effect of chemically modified polysaccharides on the formation of amyloid fibrils. In the case of low-molecular weight compounds, aromatic substances are known to often influence amyloid formation significantly. We investigated the influence of glycogen (GG) and several modifications of GG with cinnamoyl groups, benzoyl groups and phenylacetyl groups. As model systems, hen egg-white lysozyme (HEWL) and amyloid beta peptide (1-42) ($A\beta_{1-42}$), which is an Alzheimer disease-relevant system, were used. The fluorescence of thioflavin-T (ThT) was used for the rapid detection of fibrils, and the fluorescence results were confirmed by transmission electron microscopy (TEM). Other techniques, such as isothermal titration calorimetry (ITC) and dynamic light scattering (DLS), were employed to determine the interactions between HEWL and the modifications. We achieved similar results with both model systems (HEWL and $A\beta_{1-42}$). We showed that π-π interactions played an important role in the process of amyloid fibril formation because fundamental changes were observed in this process even with a very small number of groups containing an aromatic ring. It was found that almost all GG modifications accelerated the formation of amyloid fibrils in both model systems, HEWL and $A\beta_{1-42}$, except for GG-Ph1 (1.6 mol. % phenylacetyl groups), which had a retarding effect compared to all other modifications.

Introduction

The term "amyloid" was first used by Rudolf Virchow in 1854 for abnormal macroscopic deposits of amyloidoses. Later, in 1859, Friedreich and Kekule demonstrated the presence of protein in amyloids[1,2]. The nature of amyloids and proteins has been a puzzle over the years. Each amyloid deposition is characterized by a specific protein that forms amyloid fibrils and is a major component of the pathological deposit. In the case of amyloidoses in humans, twenty-seven extracellular proteins have been described to form amyloids, in which the protein is associated with a specific disease, such as Alzheimer's disease, Creutzfeldt-Jakob disease or type 2 diabetes[3,4]. All amyloids share several physicochemical properties, e.g., fibrillar morphology, β-sheet secondary protein structure, and insolubility in common solvents and detergents [5]. Amyloid fibril formation consists of three phases: the lag phase, the growth phase and the saturation phase. The formation of amyloid fibrils can be monitored by the fluorescence of thioflavin T (ThT)[6], which follows via a sigmoidal curve over time and can be used for rapid detection of amyloid fibrils. An example of a curve is shown in Fig. 1[7,8]. Based on this curve, we can estimate which phase is affected by the added substance.

Glycosaminoglycans, as natural polysaccharides, have been shown to promote amyloid fibril formation[1]. Glycogen (GG) is also a nature polysaccharide, that serves as a storage of D-glucose [9,10]. Hydrophobic and electrostatic interactions play important roles in the process of amyloid fibril formation[11,12], but the key role is played by ππ interactions [13]. Therefore, we decided to examine the influence of GG modifications on the process of amyloid fibril formation. Due to the importance of π π interactions, we decided to introduce cinnamoyl, benzoyl or phenylacetyl groups into the GG structure. This study compared the effect of GG modifications on the amyloid fibril formation and their interactions with HEWL and provides a further understanding of the effect of modified and unmodified GG. In this study, we showed that modification of natural polysaccharides with a relatively small amount of aromatic structures dramatically influenced the effect of these polymers on amyloid formation. According to the importance of the π-π interactions on amyloid formation and the strong effect of the electronic properties of the aromatic ring on the π-π interactions (the aromatic counterparts on the protein side are electron-rich aromatic compounds on the Phe, Tyt and Trp amino acid residues[13,14]), we selected the following aromatic acyls: A) Benzoyl as the simplest aromatic acyl with carboxyl directly conjugated to the aromatic ring. Due to the electron-

[a] Institute of Macromolecular Chemistry, Academy of Sciences of the Czech Republic, Heyrovsk Sq. 2, 162 06 Prague 6, Czech Repu blic e-mail address: mhruby@centrum.cz
[b] Charles University in Prague, Faculty of Science, Albertov 6, 128 43 Prague 2, Czech Republic

Electronic Supplementary Information (ESI) available: [ESI.pdf]. See DOI: 10.1039/x0xx00000x

withdrawing properties of the ester group, the ring is relatively electron-deficient; B) Phenylacetyl, basically similar to benzoyl, but the electron-withdrawing ester is separated from the aromatic ring by a methylene group, so the ring is relatively electron-rich; and C) Cinnamoyl, where the aromatic ring is extended by an additional ring-conjugated double-bond spacer between the ring and ester.

The study also points out how relatively small changes in structure may strongly influence the amyloidogenicity of biopolymer materials, which is important to consider in the design of drug delivery systems (due to possible amyloidogenic side effects) and polymer amyloid formation inhibitors in general to ensure their efficient biosafety.

Experimental

Materials

Amyloid beta peptide (1-42) ($A\beta_{1-42}$) was purchased from Kaneka Eurogentec S.A. (Seraing, Belgium). Diethyl ether and dimethyl sulfoxide (DMSO) were purchased from Lachner Ltd. (Neratovice, Czech Republic). Spectra/Por dialysis membranes (molecular weight cut-off, MWCO, 3.5 kDa) were purchased from P-LAB (Prague, Czech Republic). The 6D-DMSO was purchased from Eurisotope (Saint-Aubin, France). The remaining chemicals were purchased from Sigma-Aldrich s.r.o (Prague, Czech Republic). All chemicals were used without further purification unless stated otherwise.

Methods

Proton nuclear magnetic resonance (^{1}H NMR). ^{1}H NMR spectra were acquired with Bruker Avance III HD 400 MHz spectrometer (Bruker, Billerica, USA). All spectra were acquired long relaxation delays (D_1 = 20.0 s).

Synthesis of glycogen modified with benzoyl groups. Glycogen from oysters (0.50 g) was dissolved in anhydrous DMSO (25 mL), and sodium hydride was added (1.50 g of a 60% dispersion in mineral oil). The reaction mixture was stirred at 60 C for 3 h (until hydrogen bubbles evolved). Thereafter, benzoyl chloride (130 mg, 0.93 mmol for **GG-B2** or 327 mg, 2.32 mmol for **GG-B1**, both as a solution in 0.50 mL DMSO) was added, and the reaction mixture was stirred overnight at 60 C. The reaction mixture was diluted with water (25 mL), and the solution was washed twice with diethyl ether to remove the mineral oil. The aqueous layer was dialyzed against water (with dialysis tubing with a molecular weight cutoff of 3.5 kDa) for 72 h and freeze-dried to obtain the product.

GG-B1: Yield 322 mg: ^{1}H NMR (400 MHz, DMSO), δ (ppm): 2.88-5.23 (m, glucose: H2-H6), 5.26-6.15 (m, glucose: H1), 7.05-7.48 (m, benzoyl, 5H).

GG-B2: Yield: 375 mg. ^{1}H NMR (400 MHz, DMSO), δ (ppm): 2.87-5.22 (m, glucose: H2-H6), 5.29-6.03 (m, glucose: H1), 6.98-7.42 (m, benzoyl, 5H).

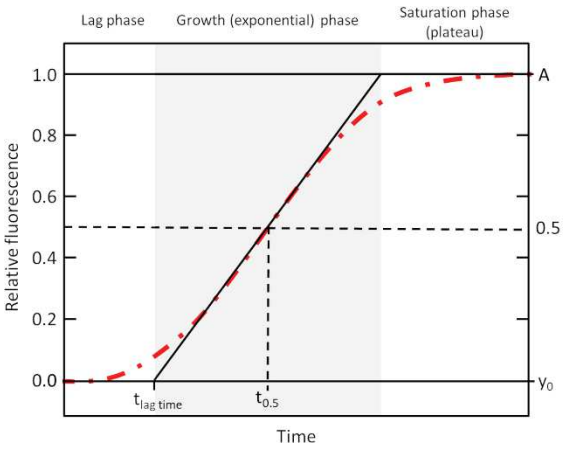

Fig. 1. The sigmoidal curve of ThT fluorescence (red dotted dashed line) in amyloid fibril formation. The black line refers to the slope of the growth phase. The time $t_{0.5}$ is the time at which the fluorescence is 50%. The initial baseline is the line y_0, and the amplitude of fluorescence is the line A[15].

Synthesis of glycogen modified with phenylacetyl groups. The same procedure as described above for benzoylation was employed using phenylacetyl chloride (72 mg, 0.46 mmol for **GG-Ph1** or 143 mg, 0.93 mmol for **GG-Ph2**, both as a solution in 0.50 mL DMSO) instead of benzoyl chloride.

GG-Ph1: Yield 297 mg. ^{1}H NMR (400 MHz, DMSO), δ (ppm): 2.91-5.20 (m, glucose: H2-H6, phenylacetyl, 1H), 5.21-6.19 (m, glucose: H1), 7.09-7.46 (m, phenylacetyl, 5H).

GG-Ph2: Yield 340 mg. ^{1}H NMR (400 MHz, DMSO), δ (ppm): 2.861-5.22 (m, glucose: H2-H6, phenylacetyl, 1H), 5.26-6.15 (m, glucose: H1), 7.10-7.44 (m, phenylacetyl, 5H).

Synthesis of glycogen modified with cinnamoyl groups. The same procedure as described above for benzoylation was employed using cinnamoyl chloride (77 mg, 0.47 mmol for **GG-CIN1**, 154 mg, 0.93 mmol for **GG-CIN2** or 307 mg, 1.85 mmol for **GG-CIN3**, as a solution in 0.50 mL DMSO) instead of benzoyl chloride.

GG-CIN1: Yield 405 mg. ^{1}H NMR (400 MHz, DMSO), δ (ppm): 2.99-5.21 (m, glucose: H2-H6), 5.26-6.19 (m, glucose: H1), 7.04-7.45 (m, cinnamoyl, 6H).

GG-CIN2: Yield 461 mg. ^{1}H NMR (400 MHz, DMSO), δ (ppm): 3.11-5.30 (m, glucose: H2-H6), 5.27-6.12 (m, glucose: H1), 6.98-7.60 (m, cinnamoyl, 6H).

GG-CIN3: Yield 415 mg. ^{1}H NMR (400 MHz, DMSO), δ (ppm): 2.95-5.19 (m, glucose: H2-H6), 5.23-6.04 (m, glucose: H1), 6.82-7.61 (m, cinnamoyl, 6H).

The degree of functionalization f_{benz} /f_{phenac}/f_{cin} (number of benzoyl, phenylacetyl or cinnamoyl groups per D-glucose unit). It was calculated from the ^{1}H NMR spectrum using the following equations (1), (2) and (3):

$$f_{benz} = \frac{I_{\delta=7.21\ ppm}}{(5 \cdot I_{\delta=5.48\ ppm})} \quad (1)$$

$$f_{phenac} = \frac{I_{\delta=7.28\ ppm}}{(5 \cdot I_{\delta=5.48\ ppm})} \quad (2)$$

$$f_{cin} = \frac{I_{\delta=7.24\ ppm}}{(6 \cdot I_{\delta=5.48\ ppm})} \quad (3)$$

where $I_{=7.2x\ ppm}$ is the integral intensity of hydrogens in the benzoyl/phenylacetyl or cinnamoyl groups and $I_{=5.48}$ ppm is the integral intensity of the acetal hydrogen H^1 from the D-glucose unit.

HEWL amyloid fibril formation. A stock solution of HEWL was prepared at a concentration of 2.2 mg/mL protein in 10 mM glycine-HCl buffer at pH 2.0 containing 0.2% w/v NaN_3. In glass vials, a mixed stock solution of HEWL (0.5 mL) and the required amounts of the solutions of GG/modified GG (concentration 5 mg/mL) was prepared in the same buffer as HEWL and the required amounts of glycine-HCl buffer; the final HEWL concentration was 2 mg/mL. All samples were incubated at 57 C. At different times, the samples were evaluated by ThT fluorescence measurements and transmission electron microscopy (TEM). ThT was dissolved in 10 M PBS (pH 7.4) to a final concentration of 10 M. This ThT solution was used for the detec tion of HEWL amyloids at different times in a 96-well plate. One well contained a 10 L aliquot of the HEWL sample and 240 L ThT solution. Prior to the fluorescence measurement, the 96-well plate was briefly mixed on a plate reader. A Synergy H1 hybrid plate reader (BioTek, Czech Republic) was used to measure the ThT fluorescence intensity. Measurements were performed by exciting the samples at 440 nm and recording their emission intensities at 485 nm.

A $_{1\text{-}42}$ amyloid fibril formation. $A\beta_{1\text{-}42}$ was pretreated before use. In 450 L HFIP, 1 mg $A\beta_{1\text{-}42}$ was dissolved. The $A\beta_{1\text{-}42}$ solution, containing 12 nmol $A\beta_{1\text{-}42}$, was divided into 18 chilled Eppendorf tubes. HFIP was evaporated, and the tubes were stored at -20 C. Twelve nanomoles of $A\beta_{1\text{-}42}$ were dissolved in 500 L of 50 mM phosphate buffer (pH=7.4). The required amounts of GG/modified GG solutions (6 mg/mL in 50 mM phosphate buffer) were added to certain Eppendorf tubes. ThT was dissolved to a final concentration of 250 M in 50 mM phosphate at pH 7.4. The ThT solution (50 L) was added to each sample, and the final concentration of ThT was 20 M in each sample. The samples were incubated at 37 C and 200 rpm in an incubator. The fluorescence was read as described above for HEWL.

Transmission electron microscopy (TEM). The TEM images were acquired with a Tecnai G2 Spirit (FEI Co., OR, U.S.A.) microscope at an accelerating voltage of 120 kV. For better contrast, 1 wt. % uranyl acetate was used to stain the samples.

Statistics. The Q-test or Grubbs test and one-way ANOVA were used for data analysis, and the significance level was $\alpha<0.05$ for all experiments. The data analysis was performed with the graphing software Origin (OriginLab Co., MA, U.S.A.).

Fluorescence data fitting. The graphs of ThT fluorescence were fitted by a sigmoidal curve (Fig. 1) described by the following equation (4)[7,8,15]:

$$Y(t) = y_0 + \frac{A}{1+\exp(-k(t-t_{0.5}))} \quad (4)$$

where t is the time, $Y(t)$ is the fluorescence intensity, y_0 is an initial baseline fluorescence intensity (see Fig. 1), A is the amplitude of fluorescence, $t_{0.5}$ is the time at 50% maximal fluorescence, and k is an apparent growth rate of the intensity. The lag time ($t_{lag\ time}$) was defined as:

$$t_{lag\ time} = t_{0.5} - \frac{2}{k} \quad (5)$$

This definition of lag time corresponds to the extrapolation from the maximal growth rate to the intercept with the baseline (Fig. 1).

Dynamic light scattering (DLS). The effect of the hydrodynamic radii (R_h) of GG and its modifications on the temperature with and without HEWL in solution was measured with a Zetasizer Nano ZS instrument (Malvern Instruments, UK). The REPES algorithm[16] was used for data analyses. A two-step inverse Laplace transformation[17,18] was used to visualize HEWL in the presence of GG or the modifications. DLS was also performed at different angles (from 30 to 150) with an ALV instrument equipped with a 22 mW He Ne laser and goniometer to determine whether an observed relaxation component had a diffusive character, i.e.

$$\Gamma = Dq^2 \quad (6)$$

where is the relaxation rate, D is the diffusion coefficient and q is the scattering vector. Then, the size (hydrodynamic radius) can be calculated from the Stokes-Einstein equation:

$$R_h = \frac{kT}{6\pi\eta D} \quad (7)$$

where k is Boltzmann's constant, T is the absolute temperature and is the viscosity of the fluids. In the case of local internal modes, the relaxation times τ (or relaxation rates $\Gamma = 1/\tau$) are independent of the angle, which means that the previous relations do not apply[19 21]. In our cases, a linear dependence of Γ on q^2 was observed, and the Stokes-Einstein equation applied (ESI Figure S1).

Refractive index increment (dn/dc). The refractive index increment (dn/dc) of GG and its modifications were obtained with a PSS DnDc2010/620 differential refractometer (Polymer Standard Service, Mainz, Germany). The measurements were performed at a wavelength of 620 nm.

Asymmetric flow field-flow fractionation (AFFFF). The weight-average molar masses (M_W) of GG and its modifications were obtained by AFFFF. The solvent and sample delivery part of the system consisted of an Agilent G1310A pump, a G1322A degasser and a G1329A autosampler. Three detectors were used in series: a Spectromonitor 3200 UV/VIS unit (Thermo Separation Products, Fremont USA), a Wyatt Optilab-rEX RI detector and a Wyatt Dawn 8+ multiangle light scattering unit. Wyatt Astra V (version 5.3.4.15) software controlled all system components through a Wyatt ECLIPSE 3+ unit. The field-flow fractionation long channel was assembled with a 350 m spacer and a regenerated cellulose membrane with a cutoff of 10 000 g/mol. Water with NaN_3 was used as a solvent. A constant detector flow rate of 1 mL/min, focusing time 5 min at a cross-flow of 3.5 mL/min, injection flow 0.2 mL/min was used. 100 L of the sample was injected, after that the cross -flow was linearly decreased from 2.0 mL/min to 0.1 mL/min in 20 min and then was kept constant at 0.1 mL/min for 20 min. The Berry fit method was used to determine M_W[22].

Isothermal titration calorimetry (ITC). ITC measurements were performed with a MicroCal ITC200 (Malvern Panalytical Ltd, UK) in a series of 2 to 4 subsequent titrations of the HEWL solution batch (14.3 mg/mL, 1 mM) with GG (50 mg/mL, 8.83 M) and the selected modifications GG-B2 (33 mg/mL, 13.8 M), GG -Ph1 (40 mg/mL, 16.0 M)) and GG -CIN2 (44 mg/mL, 7.2 M) in 10 mM glycine -HCl buffer

with 0.2% w/v NaN_3 (pH 2.0). The titrations with GG were performed with a 0.4-L injection, followed by 9 4 -L injections; for all modifications, the first injection was 0.3 L, followed by 13 3 -L injections. Additionally, the polysaccharide solutions were titrated into pure buffer, and the HEWL titration data were corrected to the corresponding heats of dilution. The series of the raw titration data were combined using ConCat32 software. The combined titration data with low sigmoidicity (weak binding) were fitted according to a single binding site model and with a fixed value of the stoichiometric ratio (n). The data with high sigmoidicity were fitted according to a two binding site model, where strong binding is followed by weak binding, and the same fitting limitations as described above were applied to the latter. The affinity constant (K_a), binding free energy (ΔG), binding enthalpy (ΔH) and binding entropy (ΔS) were calculated for each binding site with HEWL as the ligand.

Results and discussion

We synthesized a series of GG modifications to evaluate the effect of aromatic acyl groups on HEWL and $A\beta_{1-42}$ fibril formation in detail.

Synthesis of modified GG

GG was alkylated via a reaction of its alkoxide with cinnamoyl, benzoyl or phenylacetyl chloride to produce the desired modified glycogen (Fig. 2). We tested three different aromatic acyls (benzoyl, phenylacetyl, cinnamoyl) with different degrees of modification. The highest degree of modification was selected based on its highest retained water solubility, as the acyls are relatively hydrophobic. The obtained degrees of functionalization f_{benz} /f_{phenac} /f_{cin} are summarized in Tab. 1. The modification was performed statistically, and no preferred position of modification was observed.

Characterization of GG modifications

First, we measured *dn/dc* in water and found that the *dn/dc* values of the modifications were similar to the *dn/dc* values of GG. This is because the modifications contained a very small percentage of new functional groups. The values of *dn/dc* were used for M_W determination by AFFFF via light scattering detection. Tab. 1 shows the individual values of *dn/dc* and M_W. Interestingly, for modifications with benzoyl and phenylacetyl groups, a reduction in the apparent M_W was observed, but all

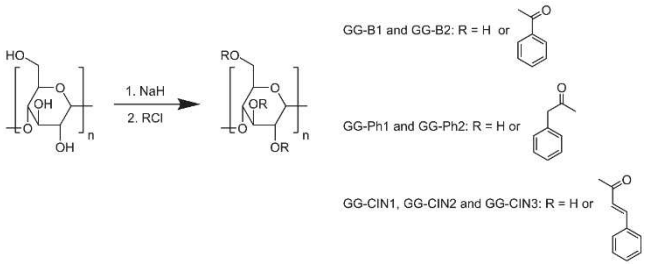

Fig. 2 Synthesis of the modified glycogen with benzoyl, phenylacetyl or cinnamoyl groups.

were within the same order. Although GG is relatively stable, this reduction in the M_W may occur during preparation.

Figure S2 in the ESI shows the size distribution by intensity of all modifications and GG. All modifications showed a comparably wide distribution of R_h compared to that of the original GG. We chose to show the intensity distribution, as it is a direct output of the instrument. The large particle peak observed for GG-CIN3 contributed with a very small proportion to the total molecular weight (approximately 2.8 vol. %).

HEWL fibrillation in the presence of the modifications and GG

HEWL is a useful protein and suitable as a first choice for testing the amyloidogenicity of particles. It contains four disulfide bonds and shows very good solubility in aqueous media[23,24]. HEWL is similar to human lysozyme (HL), whose mutations are connected with hereditary systemic amyloidosis[25]. Due to the similarities of HEWL and HL, HEWL can be used as a useful model system to test the influence of materials on the process of amyloid fibril formation and to understand the process[23,24]. The HEWL has an isoelectric point value (pI) of approximately 10.7; the most suitable conditions for forming HEWL amyloid fibrils are low pH and high temperature, which means that HEWL is positively charged under the conditions of testing[26]. It should be noted that testing the same substance on a protein/peptide under different conditions may lead to different results[27]. When using HEWL, the mature amyloid fibrils of HEWL were fully formed after approximately 76 h, so after 76 h, the saturation phase was reached (Fig. 1). We investigated the influence of GG and three types of GG modifications to understand the reasons for the small surface change in the process of amyloid fibril formation. The results are shown in Fig. 3, Fig. 4, Fig. 5, and Fig. 6.

Tab. 1 Refractive index increment (dn/dc), molecular weights (M_w) and hydrodynamic radii (R_h) of the modifications and GG.

Groups	Amount of mol. %[a]	Name	dn/dc	M_W (g/mol)	R_h (nm)
		GG	0.1483±0.0017	5.70×10^6	23.5±8.1
Benzoyl	0.5	GG-B1	0.1380±0.0004	3.80×10^6	20.9±8.3
	1.5	GG-B2	0.1593±0.0007	2.40×10^6	21.7±10.6
Phenylacetyl	1.6	GG-Ph1	0.1613±0.0009	2.50×10^6	19.5±7.9
	2.4	GG-Ph2	0.1490±0.0003	4.00×10^6	20.7±9.7
Cinnamoyl	0.6	GG-CIN1	0.1536±0.0003	4.80×10^6	22.9±10.0
	1.3	GG-CIN2	0.1505±0.0019	6.10×10^6	30.4±10.0
	2.6	GG-CIN3	0.1426±0.0001	7.5×10^6	
				M_{W1} (4.5×10^6)	R_{h1} 20.0±7.1 (97.2 vol %)
				M_{W2} (1.1×10^8)	R_{h2} 143.8.0±63.1 (2.8 vol. %)

[a]determined by ^{1}H NMR

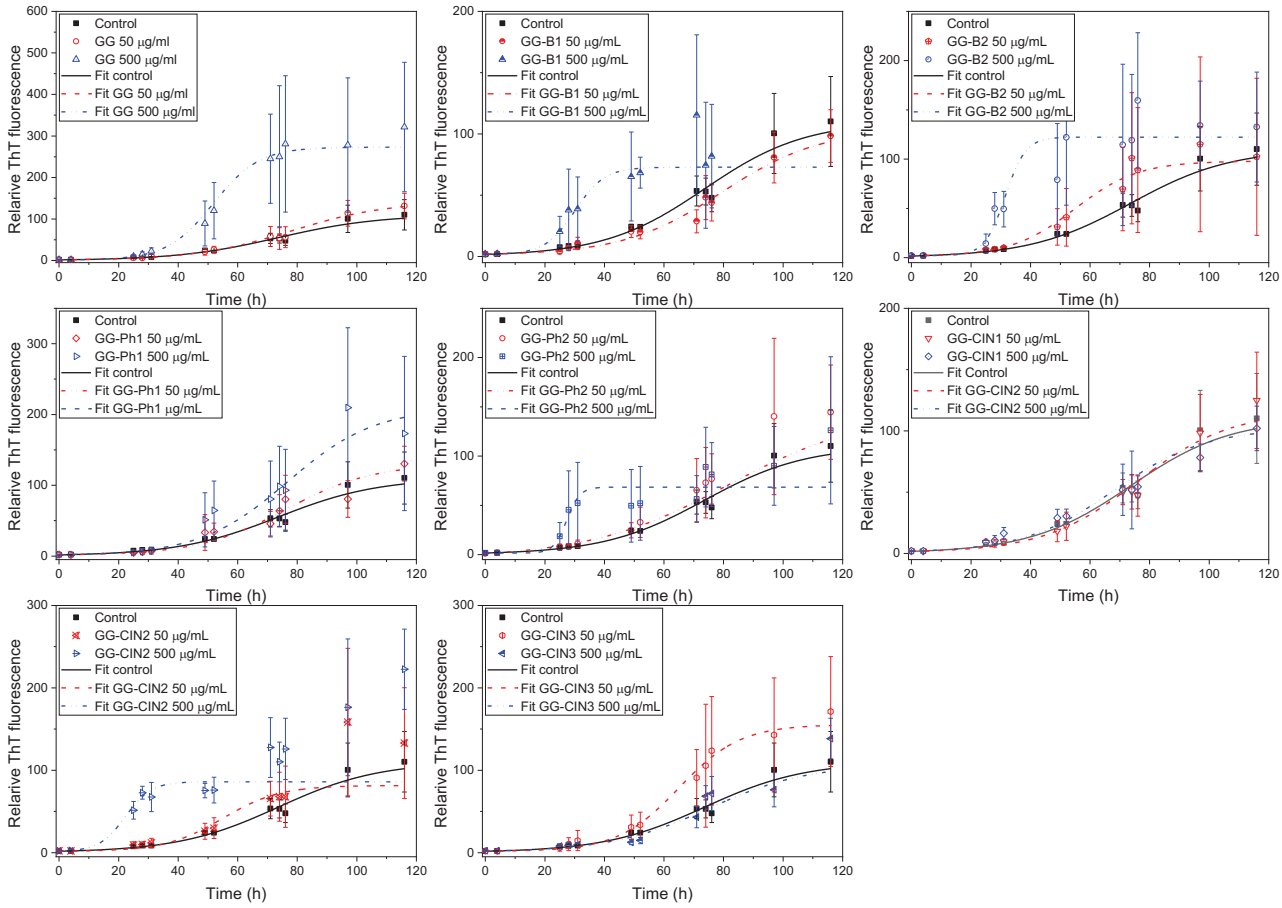

Fig. 3 Graphs of ThT fluorescence for GG and all GG modifications with data fits

In the case of GG, there appears to be a small acceleration in the formation of amyloid fibrils. But TEM micrographs of both concentrations after 28 h and 76 h showed similar morphology compared to the control (Fig. 4B and C, Fig. 5B and C). The results would indicate that the chemical composition of the hyperbranched polysaccharide molecule surface was what could promote amyloid fibril formation. The first type of GG modification was benzoylated GG. We tested two modifications of GG-B1 (0.5 mol. % benzoyl groups per D-glucose unit) and GG-B2 for as many comparable degrees of modification with other acyls as possible. In the case of GG-B1, we observed a shortening of the lag phase at a concentration of 500 g/mL, but the TEM micrograph after 28 h did not show a large difference in the morphology compared to the control (Fig. 4E). There was probably a higher concentration of shorter fibrils than in the control, and therefore, the ThT fluorescence increased. On the other hand, both concentrations of GG-B2 shortened the lag phase and $t_{0.5}$. The TEM micrograph of 50 g/mL GG -B2 after 28 h incubation (Fig. 4F) showed a morphology similar to that of the control, but 500 g/mL GG -B2 (Fig. 4G) showed clumped short fibrils, as the interaction of this modified polysaccharide with the growing fibrils may retard its growth. This morphology was not observed in the other modifications after 28 h incubation.

The second modification tested was phenylacetylated GG. In this case, we tested the two modifications GG-Ph1 (1.6 mol. % of phenylacetyl groups per D-glucose unit) and GG-Ph1 (2.4 mol. % of phenylacetyl groups per D-glucose unit). The phenylacetylated modifications behaved very interestingly. In the case of GG-Ph1, the lag phase was prolonged for both concentrations, but $t_{0.5}$ was not prolonged, implying that there was an effect on the fibril nucleation. On the one hand, the TEM micrographs after 28 h incubation (Fig. 4H and I) showed a morphology similar to that of the control (shorter fibrils and some nuclei). On the other hand, the TEM micrographs after 76 h incubation (Fig. 5H and I) showed different morphologies than the control. At a concentration of 50 g/mL, some clumped short fibrils could be observed (Fig. 5H). At a concentration of 500 g/mL, we observed clumped sh ort fibrils only (Fig. 5I), indicating that there was a similar effect on the fibril elongation as in some previous cases, probably due to direct interaction of the modified polysaccharide with the growing fibril ends, while the control showed various folded long mature fibrils (Fig. 5A). The fact that GG-Ph2 shortened the lag phase for both concentrations was confirmed by the TEM micrographs after 28 h incubation. With 50 g/mL GG -Ph2, Fig. 4J showed some long fibrils. In the case of 500 g/mL GG -Ph2, Fig. 4K showed long mature fibrils.

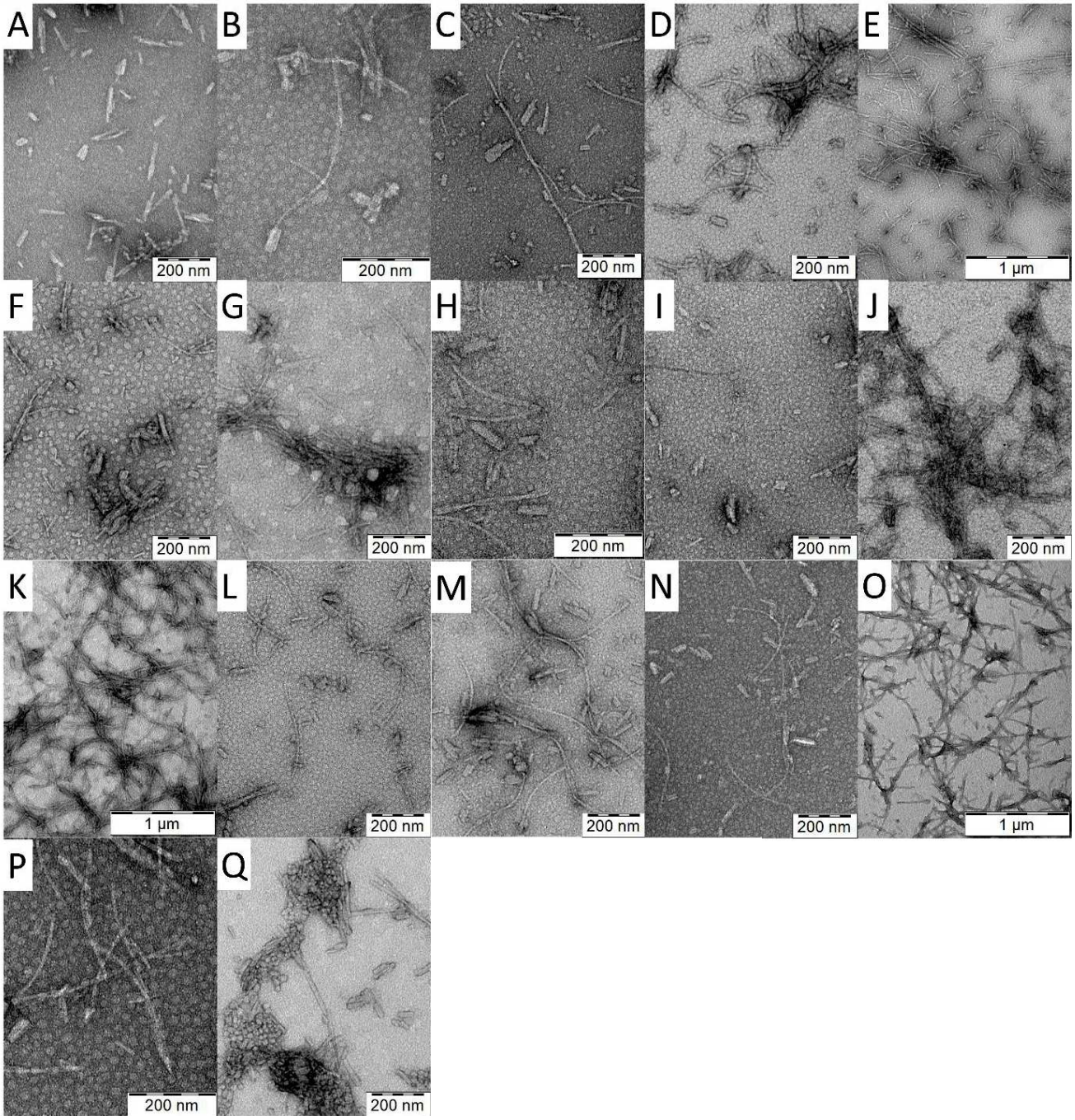

Fig. 4 TEM micrographs after 28 h incubation: (A) control (only HEWL); (B) 50 g/mL GG; (C) 500 g/mL GG; (D) 50 g/mL GG -B1; (E) 500 g/mL GG -B1; (F) 50 g/mL GG -B2; (G) 500 g/mL GG -B2; (H) 50 g/mL GG -Ph1; (I) 500 g/mL GG -Ph1; (J) 50 g/mL GG -Ph2; (K) 500 g/mL GG -Ph2; (L) 50 g/mL GG -CIN1; (M) 500 g/mL GG -CIN1; (N) 50 g/mL GG -CIN2; (O) 500 g/mL GG -CIN2; (P) 50 g/mL GG -CIN3; and (Q) 500 g/mL GG -CIN3

When we compared the three cinnamoyl-modified GGs, GG-CIN1 (0.6 mol. % cinnamoyl groups per D-glucose unit), the system behaved very similar to the control (only HEWL). The lag phase did not shorten for either concentration, and $t_{0.5}$ was shortened only for a concentration of 500 g/mL GG -CIN1. GG showed the same results as GG-CIN1, and higher absolute fluorescence intensities were observed for GG, but the important parameters in the course of fibril growth (course of ThT fluorescence) were similar. In the case of GG-CIN2 (1.3 mol. % cinnamoyl groups per D-glucose unit), $t_{0.5}$ was shortened for both tested concentrations, and the lag phase was distinctly shortened for a concentration of 500 g/mL, and long mature amyloid fibers were formed after one day of incubation (Fig. 4O). The most densely cinnamoylated GG-CIN3 (2.6 mol. % cinnamoyl groups per D-glucose unit) behaved differently than the two previous groups (GG-CIN1 and GG-CIN2). GG-CIN3 did

not appear to have an effect on the lag phase but on the growth phase. For a concentration of 50 g/mL, $t_{0.5}$ was shortened, which we attributed to the fact that at a lower concentration, the modification dissolve more easily; however, at a higher concentration of 500 g/mL, $t_{0.5}$ was prolonged, as the interaction of this modified polysaccharide with the growing fibrils may retard its growth (see Fig. 5Q).

Next, we compared GG-B2 (1.5% benzoyl groups per D-glucose unit), GG-Ph2 (1.6% phenylacetyl groups per D-glucose unit) and GG-CIN2 (1.3% cinnamoyl groups per D-glucose unit), which contained similar amounts of different functional groups. The lag phase was shortened the most for GG-CIN2. On the other hand, GG-Ph1 prolonged the lag phase. Although GG-B2 shortened the lag phase, the effect was not as significant as for GG-CIN2. We also compared GG-CIN1 (0.6% cinnamoyl groups per D-glucose unit) and GG-B1 (0.5% benzoyl groups per D-glucose unit). In the case of GG-B1, the effect on amyloid fibril formation was more pronounced than in the case of GG-CIN1, which showed a similar behavior as GG. The last two modifications to be compared had similar degrees of functionality, which were GG-CIN3 (2.6 mol. % cinnamoyl groups per D-glucose unit) and GG-Ph2 (2.4 mol. % phenylacetyl groups per D-glucose unit). Interestingly, more cinnamoyl groups (GG-CIN3) did not result in a stronger effect on the process of amyloid fibril formation, whereas the phenylacetyl groups affected the process of amyloid fibril formation significantly.

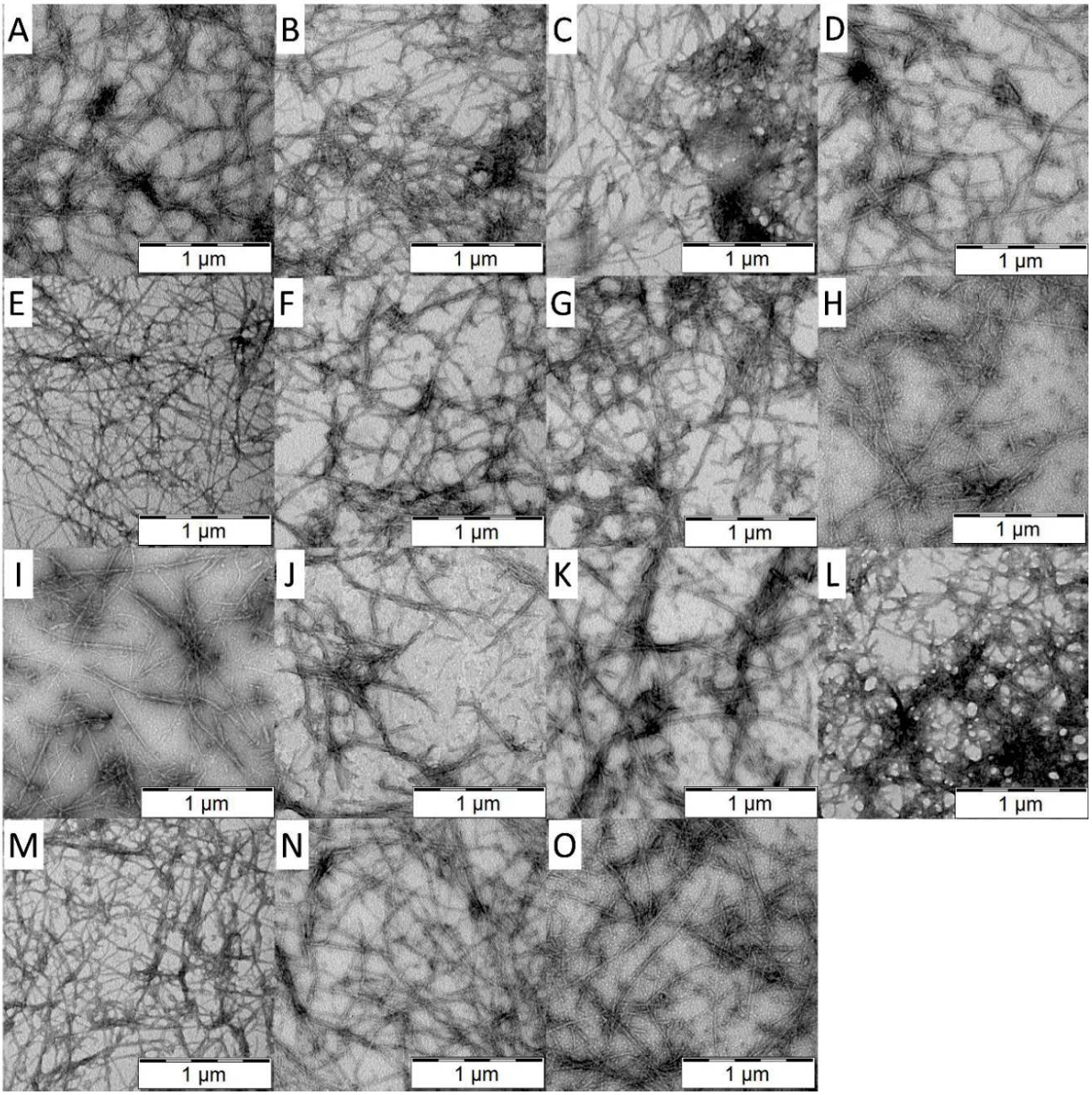

Fig. 5 TEM micrographs after 76 h incubation: (A) control (only HEWL); (B) 50 g/mL GG; (C) 500 g/mL GG; (D) 50 g/mL GG -B1; (E) 500 g/mL GG -B1; (F) 50 g/mL GG -B2; (G) 500 g/mL GG -B2; (H) 50 g/mL GG -Ph1; (I) 500 g/mL GG -Ph1; (J) 50 g/mL GG -Ph2; (K) 50 g/ mL GG-CIN1; (L) 500 g/mL GG -CIN1; (M) 50 g/mL GG -CIN2; (N) 50 g/mL GG -CIN3; and (O) 500 g/mL GG -CIN3

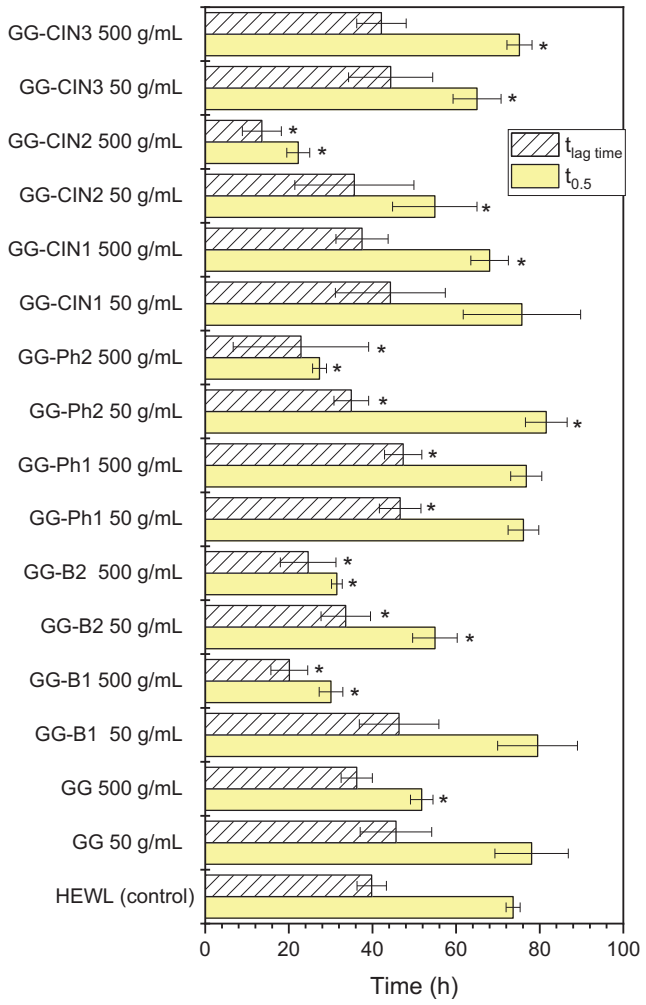

Fig. 6 A graph of $t_{lag\ time}$ and $t_{0.5}$ obtained from the experiments with HEWL, GG and GG modifications according to the data fitted by equation (1). The star (*) represents a statistically significant difference (<0.05) when compared to the control (onl y HEWL).

Based on these experiments, even a small change in the functional groups can have a major impact on the process of amyloid fibril formation. Therefore, it cannot be predicted that increasing the amount of functional groups will also increase the observed effect. By introducing an arene ring into the structure of GG, there was a fundamental change in the amyloid formation process compared to GG. This supports the significance of the π-π and hydrophobic interactions in the formation of amyloid fibrils. The effect of modification on the amyloid formation was most pronounced when phenylacetyl groups were used, which are most similar to phenylalanine residues, confirming that Phe-Phe π-π interactions are crucial for amyloid formation[14].

Effect of GG om their modification with amyloidogenic proteins

DLS and ITC studies. To determine the effect of temperature on the modification, we performed DLS experiments with the modification solutions without HEWL and in the presence of HEWL (20 C57 C with increments of 1 C). Fig. 7 shows the temperature dependence of the hydrodynamic radii (R_h) of the various samples.

For the system with GG, the R_h slightly increased immediately after mixing it with HEWL (blue points in Fig. 7A) compared to the value that we obtained without HEWL (red points in Fig. 7A). This increase in R_h in the presence of a protein may indicate that HEWL interacted with GG, which would suggest the molecular mechanism behind the acceleration of amyloid fibril formation. An overlay of the data without HEWL and in the presence of HEWL was observed in the case of GG-B1 (0.5 mol. % benzoyl groups per D-glucose unit). Therefore, we assumed that there were no strong interactions but rather very weak or no interactions between HEWL and GG-B1. In the case of GG-B2 (1.5% benzoyl groups per D-glucose unit), only one peak was observed without HEWL (red dots, in Fig. 7C). In the presence of HEWL, two peaks were observed for GG-B2. In the case of the smaller peak (green triangles, in Fig. 7C), R_h decreased in the presence of HEWL when we compared GG-B2 without HEWL and in the presence of HEWL. In the presence of HEWL, GG-B2 formed another larger peak (blue triangles, Fig. 7C). There are two possibilities of second peak formation. First, particles of GG-B2 (above ~ 20 nm) could interact with HEWL and form large particles with sizes above 100 nm. Second, the formation of larger particles may be caused by the presence of HEWL because of the change in the solubility of GG-B2 in the presence of another substance (in this case HEWL), which may cause predominant interactions between GG-B2 and subsequent aggregation. The HEWL fibrillation experiments confirmed that GG-B1 had a weaker effect than GG-B2.

For the other two modifications GG-Ph1 (1.6 mol.% phenylacetyl groups per D-glucose unit) and GG-Ph2 (2.4 mol.% phenylacetyl groups per D-glucose unit), the R_h values were slightly increased in the presence of HEWL. In the case of GG-Ph1, the increase in the R_h was more pronounced than in the case of GG-Ph2. For GG-Ph2, the R_h increase was very small, so there was only a weak or no interaction between GG-Ph2 and HEWL. Additionally, their effects on HEWL fibrillation were different, and therefore, their influence on the protein was different. This is consistent with the fluorescence data, which revealed that phenylacetylation probably more influenced the fibril elongation (interaction with the growing fibrils) rather than the nucleation (interaction with amyloidogenic protein not yet embedded into the fibrils, which is relevant to the DLS experiment, at which point no fibrils have been formed).

We also found that the R_h of cinnamoylated GG-CIN1 (0.5 mol. % cinnamoyl groups per D-glucose unit) in the presence of HEWL also increased, but this increase was not as pronounced as in the case of GG-CIN2 (1.3 mol. % cinnamoyl groups per D-glucose unit), consistent with the lower degree of modification with cinnamoyl groups in GG-CIN1. The effect of GG-CIN1 on the amyloid fibril formation was similar to that of GG. GG-CIN1 had a similar effect as GG. There was a large increase in the R_h of GG-CIN2 in the presence of HEWL (Fig. 7G) that was approximately equivalent to the thickness of a unimolecular layer of HEWL on the polymer surface, indicating the significance of aromatic cinnamoyl structures on the polysaccharide surface to protein adsorption. GG-CIN2 was a stronger amyloid formation inducer of amyloid fibril formation

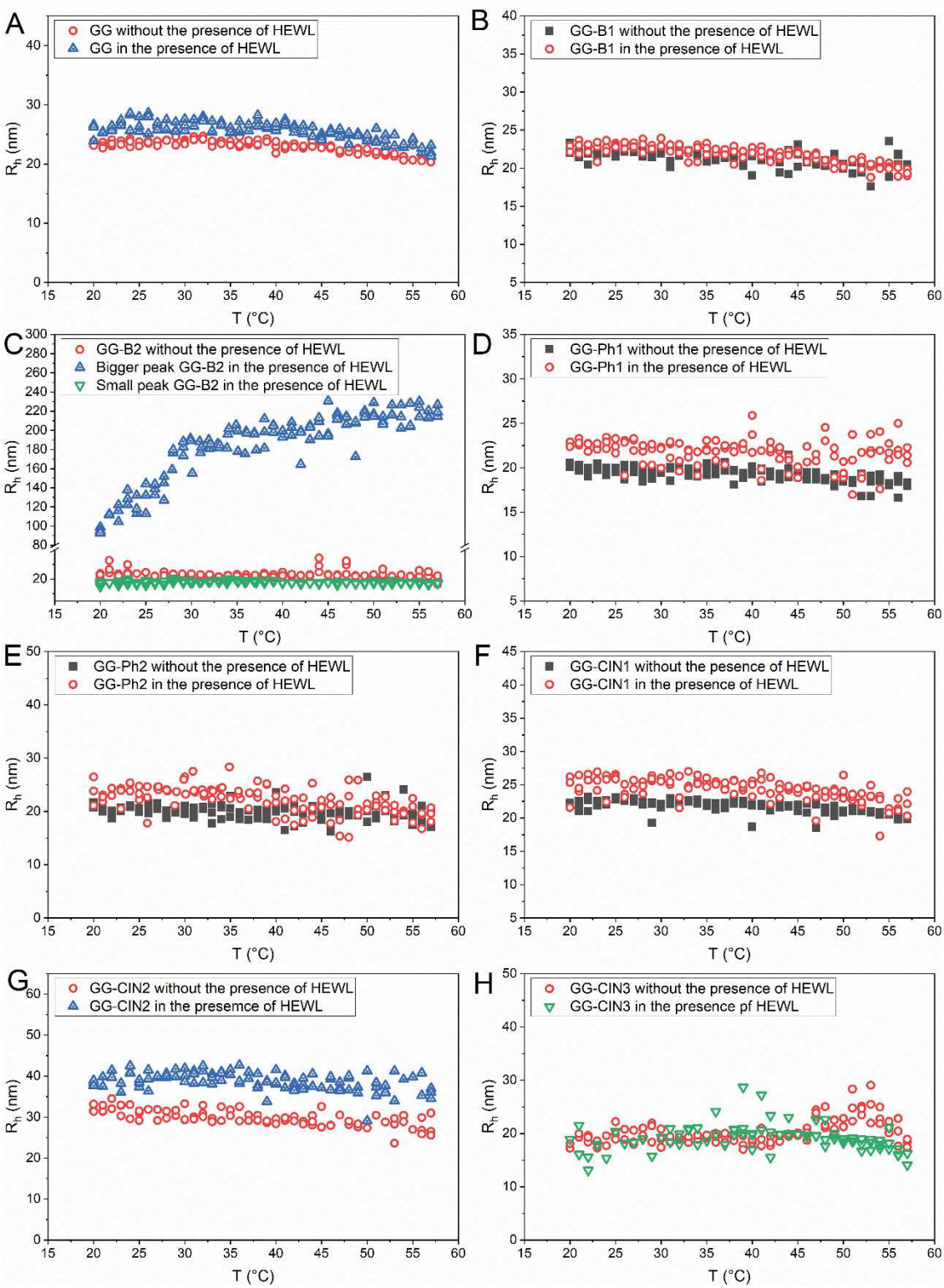

Fig. 7 Dependence of hydrodynamic radius R_h on temperature for the solutions of modifications without the presence of HEWL or in the presence of HEWL. (A) GG; (B) GG-B1; (C) GG-B2, (D) BB-Ph1; (E) GG-Ph2; (F) GG-CIN1; (G) GG-CIN2 and (H) GG-CIN3

than GG, indicating that how HEWL adsorbs onto the polysaccharide surface may be different for GG and GG-CIN2. On the other hand, highly cinnamoylated GG-CIN3 (2.6 mol. % cinnamoyl groups per D-glucose unit) had different effects (see Fig. 7H). There was an overlay of the data without HEWL and in the presence of HEWL in the case of GG-CIN3. Therefore, we assumed that there were no strong interactions but rather very weak or no interactions between HEWL and GG-CIN3. The data revealed a direct interaction of cinnamoylated GG (GG-CIN1 and GG-CIN2) with nonaggregated HEWL, which in turn can explain the effect on seeding (t_{lag}) observed in the fluorescence experiments.

For ITC experiments, we chose the native glycogen (GG) and three modifications with a similar number of functional groups: GG-B2 (1.5 mol. % benzoyl groups per D-glucose unit), GG-Ph1 (1.6 mol.% phenylacetyl groups per D-glucose unit) and GG-CIN2 (1.3 mol. % cinnamoyl groups per D-glucose unit). All modifications were chosen because of their different DLS results, and their influence on the process of amyloid fibril formation observed by fluorescence was also different. The titrations were performed at two temperatures, 25 C and 57 C. The thermodynamic parameters of the interaction of HEWL with GG and the modifications are summarized in Tab. 2. Upon titration of the HEWL solution with the native GG and the modifications, an exothermic heat flux was recorded for all samples and temperatures. The titration curves as well as integrated heats per injection, normalized to 1 mol HEWL, are shown in Figure S3-S6 in ESI. The native glycogen weakly binds to HEWL (K_a (25C) = 700 M^{-1}), and the binding strength decreases with temperature (K_a (57C) = 16 M^{-1}). A low affinity constant means that there is no detectable binding, but some exothermic effects upon mixing are due to rearrangement of the solvation shell. The modification of GG with 1.3% cinnamoyl residues (GG-CIN2), which resulted in moderate hydrophobicity of the surface of GG, drastically increased the affinity to HEWL. The modified GG-CIN2 showed two types of binding sites: first, the affinity constant (K_a) reached the range of 10^6 M^{-1}, but after fast saturation of the first type of binding site, the binding of HEWL proceeded similarly to native GG. At elevated temperature, the affinity of HEWL to the first binding site decreased (K_a = 2.1×10^3 M^{-1}), and the affinity to the second binding site become negligible (K_a = 16 M^{-1}). The binding of HEWL to GG-CIN2 could be observed with DLS in all temperature ranges. GG with 1.5% benzoyl residues (GG-B2), despite a clearly detectable increase in the R_h (Fig. 7C) in the whole temperature range, showed no binding at 25C and very weak binding at 57C (K_a = 227 M^{-1}). Finally, the modification of the GG surface with 1.6% phenylacetyl groups (GG-Ph1) showed similar trends as cinnamoyl-bearing GG-CIN2 - two types of binding sites at 25C (K_a in range 10^6 and 10^4 M^{-1}), which, however, at 57C, were reduced to one weak binding site (K_a = 609 M^{-1}). DLS, in turn, showed only a small increase in the R_h for GG-Ph1 in the presence of HEWL (Fig. 7D). Although GG-Ph1 prolonged the lag phase (it slowed down the nucleation of fibers), after 76 h incubation, it yielded shorter fibrils than native GG.

In case of the aryl-based substituents, the most pronounced impact on the binding of HEWL with modified GG was observed for cinnamoyl (GG-CIN2), the binding was weaker for phenylacetyl (GG-Ph1) and almost neglectable for benzoyl (GG-B2). The binding strength (in terms of K_a) and spontaneity of the process (in terms of ΔG) (Tab. 2) correlated with the length of spacer between aryl and the electron-accepting carbonyl.

A $_{1-42}$ fibrillation in the presence of chemically modified and native GG

When amyloid precursor protein is cleaved by the so-called amyloidogenic pathway, it forms an A peptide. Depending on the cleavage site, the size of A can range from 38 to 43 amino acids[28]. The most common isoform is A $_{1-40}$ (90%), followed by A $_{1-42}$ (10%). The disadvantage of the A $_{1-42}$ isoform is that it is the most fibrillogenic form[28]. However, A peptides have important functions at physiological concentrations related to normal memory function and synaptic plasticity[29]. A problem occurs at high concentrations of A peptides. High concentrations lead to the aggregation of A to form amyloid fibrils, which subsequently form senile plaques that cause neurotoxicity and cell death. These senile plaques are associated with Alzheimers disease [28 30]. We should mention that the A $_{1-42}$ peptide (our model system) has a pI of approximately 5.5[31]. The model system of A $_{1\ 42}$ is very often negatively charged in experiments[32,33], which was also the case in our experiments when we used pH 7.4. When experiments with A $_{1\ 42}$ are performed under different conditions, the results can be different. In the past, this difference has been mostly observed in the case of polymers with charge groups[34,35].

Tab. 2. Thermodynamic parameters of the interaction of GG, GG-B2; GG-Ph1 and GG-CIN2 with HEWL.

Sample	T, C	Conc., mg/mL	Conc., M	n[a]	K_a, M^{-1}	ΔG, kJ/mol	ΔH, kJ/mol	ΔS, J/K. mol
GG	25	50	8.8	515	0.7×10^3	-16.2	-9.3	23.0
	57				67[b]	-11.5	exoth.	-
GG-B2	25			515	16[b]	-6.9	exoth.	-
	57			510	227	-14.9	-103.3	-267.8
GG-Ph1	25			30	1.5×10^6	-35.2	-25.5	33.0
				744	2.2×10^4	-24.8	-0.7	80.8
	57			496	609	-17.6	-4.3	40.3
GG-CIN2	25	44	7.3	31	9.6×10^5	-34.1	-20.2	46.0
				1400	2.6×10^4	-25.2	-0.3	83.7
	57			31	2.1×10^3	-21.0	-1.9	57.8
				1400	16[b]	-7.6	exoth.	-

[a] Stoichiometry of the interaction: number of HEWL molecules binding one polysaccharide molecule

[b] Ka<100 M^{-1} reflects no detectable binding, the obtained values ΔH and ΔG are not used in the discussion.

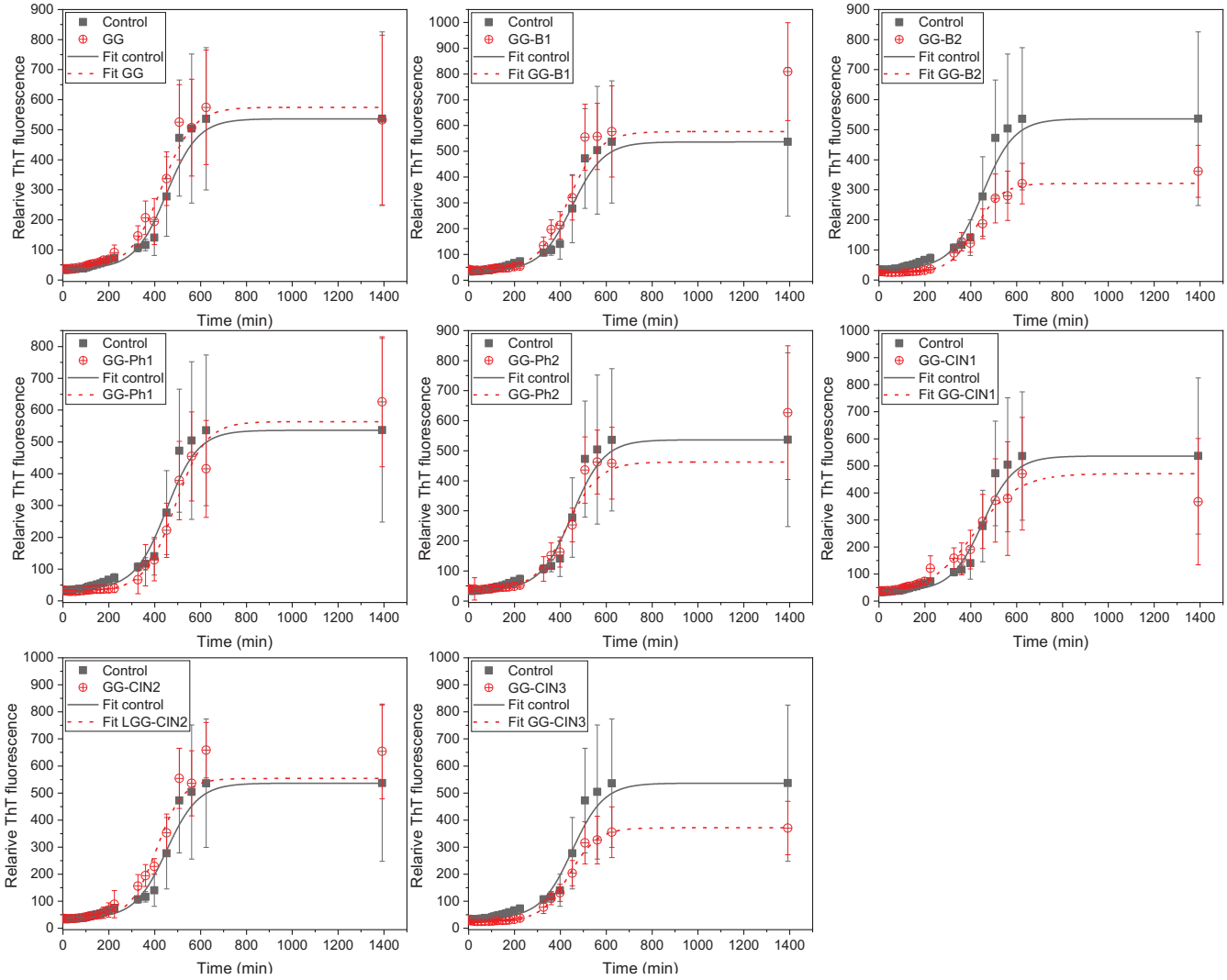

Fig. 8 Graphs of relative ThT fluorescence with black symbols representing the control data (A $_{1\text{-}42}$ without modifications or GG) and fits of the measured data.

The graphs of the relative ThT fluorescence with the data fits are shown in Fig. 8. The graph concerning $t_{lag\ time}$ and $t_{0.5}$ is shown in Fig. 9. Upon comparing these results with HEWL and $A\beta_{1\text{-}42}$, they are in good agreement. GG did not have a big an effect on the growth phase, that suggest that GG exerts a greater effect on the lag phase than on the growth phase. The first group, GG-B1 (0.5 mol. % benzoyl groups per D-glucose unit) and GG-B2 (0.5 mol. % benzoyl groups per D-glucose unit), had no effect on the lag phase of $A\beta_{1\text{-}42}$. In the case of the HEWL model, GG-B2 had a stronger accelerating effect than GG-B1. Both GG-B1 and GG-B2 had an accelerating effect on the growth phase because both $t_{0.5}$ were lower than in the control. The results of the second phenylacetylated group, GG-Ph1 (1.6 mol.% phenylacetyl groups per D-glucose unit) and GG-Ph2 (2.4 mol.% phenylacetyl groups per D-glucose unit), were in good agreement with the results obtained from the HEWL model. GG-Ph1 significantly prolonged the lag time, while GG-Ph2 significantly shortened the lag time. In the cinnamoylated group, GG-CIN1 (0.5 mol. % cinnamoyl groups per D-glucose unit), GG-CIN2 (1.3 mol. % cinnamoyl groups per D-glucose unit) and GG-CIN3 (2.6 mol. % cinnamoyl groups per D-glucose unit), the lag time was shortened for GG-CIN1 and GG-CIN2, while for GG-CIN3, there was no statistically significant change in the lag time. On the other hand, the time $t_{0.5}$ was shortened for all cinnamoylated modifications, which confirmed the fact that GG-CIN3 had a larger influence on the growth phase than the lag phase.

After approximately 28 h of incubation, we evaluated the morphology with TEM. Fig. 10 shows the TEM micrograph. Because $A\beta_{1\text{-}42}$ provided a lower contrast than HEWL, the amyloid fibers were less visible when the modification or unmodified GG were present. However, GG and the modifications could be visualized using uranyl acetate, and there was likely little overlap between the amyloid fibrils and the modifications. However, even so, there some fibrillar structures were observed in all samples.

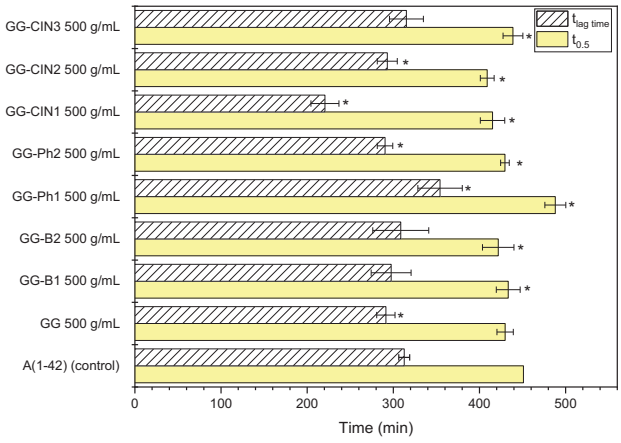

Fig. 9 A graph of $t_{lag\ time}$ and $t_{0.5}$ of the experiments with A_{1-42}, GG and GG modifications according to the data fitted by equation (1). The star (*) represents a statistically significant difference ($\alpha<0.05$) when compared to the control (only A_{1-42}).

Conclusion

Based on the obtained results, we showed that even a small change in the particle chemistry can change the process of amyloid fibril formation. The results with our proposed models (HEWL and $A\beta_{1-42}$) were in very good agreement.
We can conclude in the following main points:

- GG can play an important role in the promotion of amyloid fibril formation though direct interaction with protein
- It was confirmed that π-π interactions played an important role in the process of amyloid fibril formation, since there was a significant impact of amyloid fibril formation, even with a very small number of groups with an aromatic ring bound to polysaccharide.
- GG-CIN2 (1.3 mol. % cinnamoyl groups per D-glucose unit) and GG-Ph2 (2.4 mol. % phenylacetyl groups per D-glucose unit) had a rapid acceleration effect on the process of amyloid fibril formation.
- The effect of the modifications with benzoyl groups was less pronounced than that with phenylacetyl groups or cinnamoyl groups.
- Interestingly, GG-Ph1 (1.6 mol. % phenylacetyl groups per D-glucose unit) had a retarding effect compared to all other modifications.

The study also pointed out how relatively small changes in the structure could strongly influence the amyloidogenicity of biopolymer materials, which is important to consider in the design of drug delivery systems (due to possible amyloidogenic side effects) and polymer amyloid formation inhibitors in general to ensure their efficient biosafety.

Conflicts of interest

The authors have no conflicts of interest to declare.

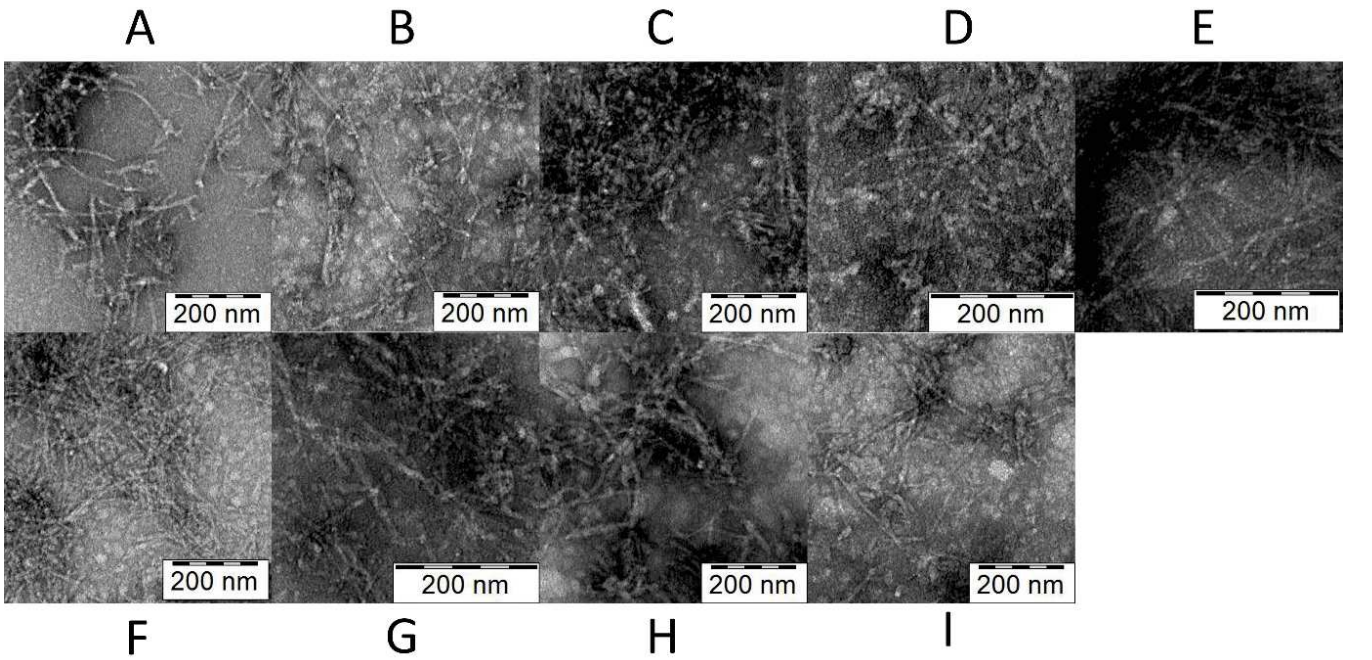

Fig. 10 TEM micrographs after 28 h incubation. (A) control (only $A\beta_{1-42}$); (B) GG 500 g/mL; (C) GG -B1 500 g/mL; (D) GG -B2 500 g/mL; (E) GG -Ph1 500 g/mL; (F) GG -Ph2 500 g/mL; (G) GG-CIN1 500 g/mL; (H) GG -CIN2 500 g/mL; and (I) GG-CIN3 500 g/mL

Acknowledgments

Monika Holubov acknowledges financial support from Charles University, project GA UK No. 386218. We would like to thank the Ministry of Education, Youth and Sports of the Czech Republic (grant # LM2015064 ERIC) and the Czech Science Foundation (M.H.: grant # 19-01602S and P.S.: grant # 18-07983S) for financial support.

References

1 K. Sideras and M. A. Gertz, in *Advances in clinical chemistry*, 2009, vol. 47, pp. 1 44.
2 J. D. Sipe, *WILEY-VCH Verlag GmbH Co. KGaA, Weinheim*.
3 M. D. Benson, in *Reference Module in Biomedical Sciences*, Elsevier, 2014, pp. 1 18.
4 J. D. Sipe, M. D. Benson, J. N. Buxbaum, S.-I. Ikeda, G. Merlini, M. J. M. Saraiva and P. Westermark, *Amyloid*, 2010, **17**, 101 104.
5 J.-C. Rochet and P. T. Lansbury, *Curr. Opin. Struct. Biol.*, 2000, **10**, 60 68.
6 S. Freire, M. H. De Araujo, W. Al-Soufi and M. Novo, *Dye. Pigment.*, 2014, **110**, 97 105.
7 L. Nielsen, R. Khurana, A. Coats, S. Frokjaer, J. Brange, S. Vyas, V. N. Uversky and A. L. Fink, *Biochemistry*, 2001, **40**, 6036 6046.
8 C. Wallin, M. Friedemann, S. B. Sholts, A. Noormägi, T. Svantesson, J. Jarvet, P. M. Roos, P. Palumaa, A. Gräslund and S. K. T. S. Wärmländer, *Biomolecules*, 2020, **10**, 44.
9 L. R. Engelking, in *Textbook of Veterinary Physiological Chemistry*, Elsevier, 2015, pp. 147 152.
10 L. Cole and P. R. Kramer, in *Human Physiology, Biochemistry and Basic Medicine*, Elsevier, 2016, pp. 17 30.
11 K. E. Marshall, K. L. Morris, D. Charlton, N. OReilly, L. Lewis, H. Walden and L. C. Serpell, *Biochemistry*, 2011, **50**, 2061 2071.
12 F. Chiti and C. M. Dobson, *Annu. Rev. Biochem.*, 2006, **75**, 333 366.
13 E. Gazit, *FEBS J.*, 2005, **272**, 5971 5978.
14 A. Paul, B. Sharma, T. Mondal, K. Thalluri, S. Paul and B. Mandal, *Medchemcomm*, 2016, **7**, 311 316.
15 P. Arosio, T. P. J. Knowles and S. Linse, *Phys. Chem. Chem. Phys.*, 2015, **17**, 7606 7618.
16 J. Jakeš, *Collect. Czechoslov. Chem. Commun.*, 1995, **60**, 1781 1797.
17 P. Štěpnek and R. M. Johnsen, *Collect. Czechoslov. Chem. Commun.*, 1995, **60**, 1941 1949.
18 P. Stepanek and T. P. Lodge, *Macromolecules*, 1996, **29**, 1244 1251.
19 S. P. Cadogan, C. J. Hahn, M. H. Rausch and A. P. Fröba, *J. Colloid Interface Sci.*, 2017, **499**, 202 208.
20 M. W. Ishaq, N. Hao, M. Zhu and L. Li, *Macromolecules*, 2020, **53**, 558 568.
21 G. Galinsky and W. Burchard, *Macromolecules*, 1997, **30**, 6966 6973.
22 S. Podzimek, *Light Scattering, Size Exclusion Chromatography and Asymmetric Flow Field Flow Fractionation: Powerful Tools for the Characterization of Polymers, Proteins and Nanoparticles*, John Wiley & Sons, Inc., Hoboken, NJ, USA, 2011.
23 A. Cao, D. Hu and L. Lai, *Protein Sci.*, 2004, **13**, 319 24.
24 R. Swaminathan, V. K. Ravi, S. Kumar, M. V. S. Kumar and N. Chandra, *Adv. Protein Chem. Struct. Biol.*, 2011, **84**, 63 111.
25 V. K. Ravi, T. Swain, N. Chandra and R. Swaminathan, *PLoS One*, 2014, **9**, e87256.
26 R. Vilcacundo, P. Méndez, W. Reyes, H. Romero, A. Pinto and W. Carrillo, *Sci. Pharm.*, 2018, **86**, 48.
27 M. Holubová, P. Štěpánek and M. Hrubý, *Colloid Polym. Sci.*, , DOI:10.1007/s00396-020-04710-8.
28 M. del C. Crdenas-Aguayo, M. del C. Silva-Lucero, M. Cortes-Ortiz, B. Jimnez-Ramos, L. Gmez-Virgilio, G. Ramrez-Rodrguez, E. Vera- Arroyo, R. Fiorentino-Prez, U. Garca, J. Luna-Muoz and M. A. Meraz Ros, in *Neurochemistry*, InTech, 2014.
29 Z. U. Khan, E. Martín-Montañez, I. Navarro-Lobato and E. C. Muly, in *Progress in Molecular Biology and Translational Science*, Academic Press, 2014, vol. 122, pp. 1 29.
30 G. Chen, T. Xu, Y. Yan, Y. Zhou, Y. Jiang, K. Melcher and H. E. Xu, *Acta Pharmacol. Sin.*, 2017, **38**, 1205 1235.
31 D. Jiang, I. Rauda, S. Han, S. Chen and F. Zhou, *Langmuir*, 2012, **28**, 12711 12721.
32 O. Klementieva, N. Benseny-Cases, A. Gella, D. Appelhans, B. Voit and J. Cladera, *Biomacromolecules*, 2011, **12**, 3903 3909.
33 A. G. Bobylev, M. D. Shpagina, L. G. Bobyleva, A. D. Okuneva, L. B. Piotrovsky and Z. A. Podlubnaya, *Biophysics (Oxf).*, 2012, **57**, 300 304.
34 Z. Jiang, X. Dong and Y. Sun, *Carbohydr. Res.*, 2018, **461**, 11 18.
35 H. Liu, B. Ojha, C. Morris, M. Jiang, E. P. Wojcikiewicz, P. P. N. Rao and D. Du, *Biomacromolecules*, 2015, **16**, 2363 2373.

Chemically modified glycogens: How they influence formation of amyloid fibrils?

Monika Holubová[a,b], Volodymyr Lobaz[a], Lenka Loukotová[a], Mariia Rabyk[a], Jiřina Hromádková[a], Olga Trhlková [a], Zdislava Pechrová[a], Ondřej Groborz[a,b], Petr těpánek [a], Martin Hrub [a1]

[a]*Institute of Macromolecular Chemistry, Academy of Sciences of the Czech Republic, Heyrovsk Sq. 2, 162 06 Prague 6, Czech Republic*

[b]*Charles University in Prague, Faculty of Science, Albertov 6, 128 43 Prague 2, Czech Republic*

Keywords: amyloid fibrils, glycogen, modification of glycogen, lysozyme, amyloid beta

Supporting information

[1]Corresponding author. Institute of Macromolecular Chemistry, Academy of Sciences of the Czech Republic, Heyrovsk Sq. 2, 162 06 Prague 6, Czech Republic
Email address: mhruby@centrum.cz

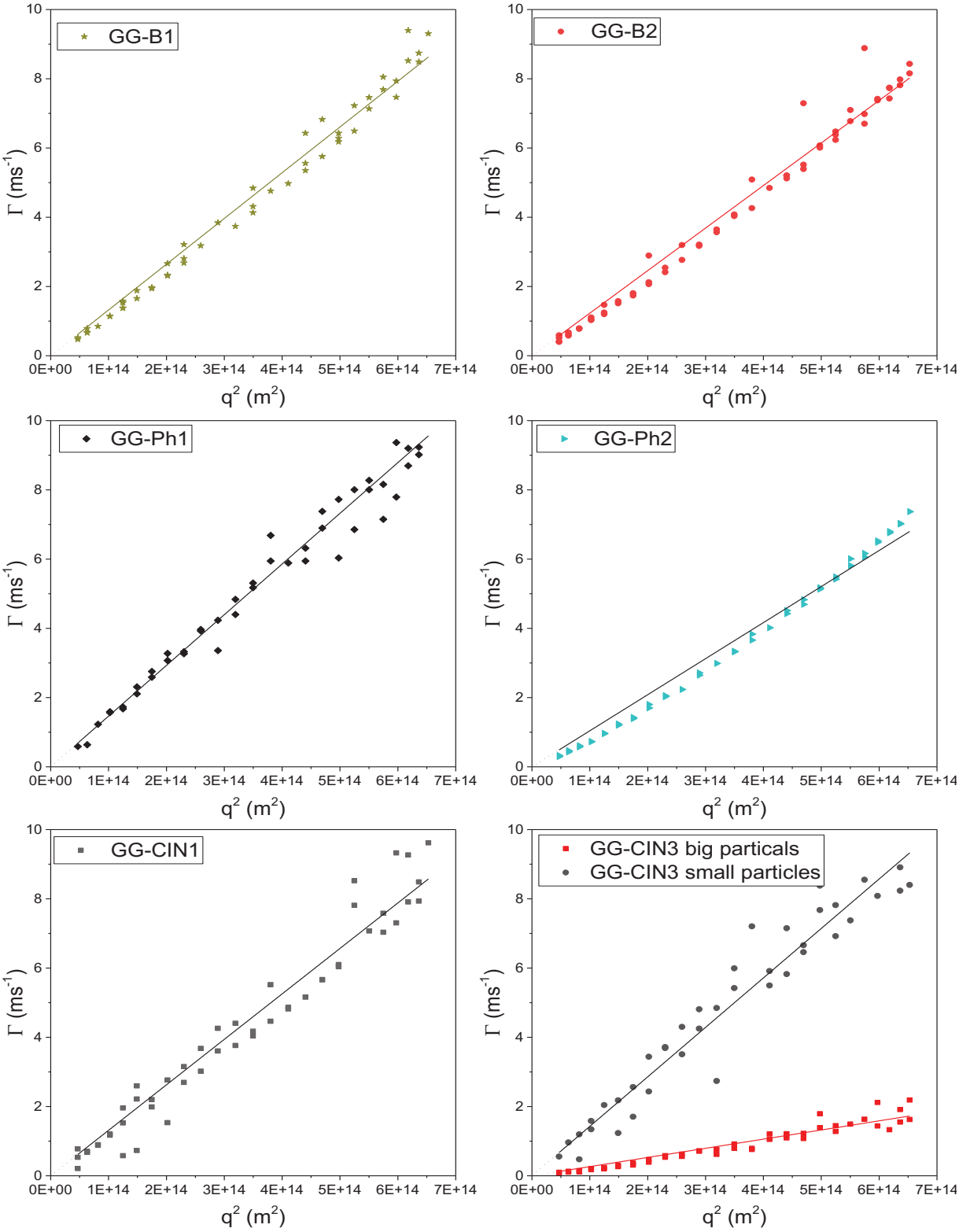

Figure S1 Dependence of on q ^{2} for modified glycogens.

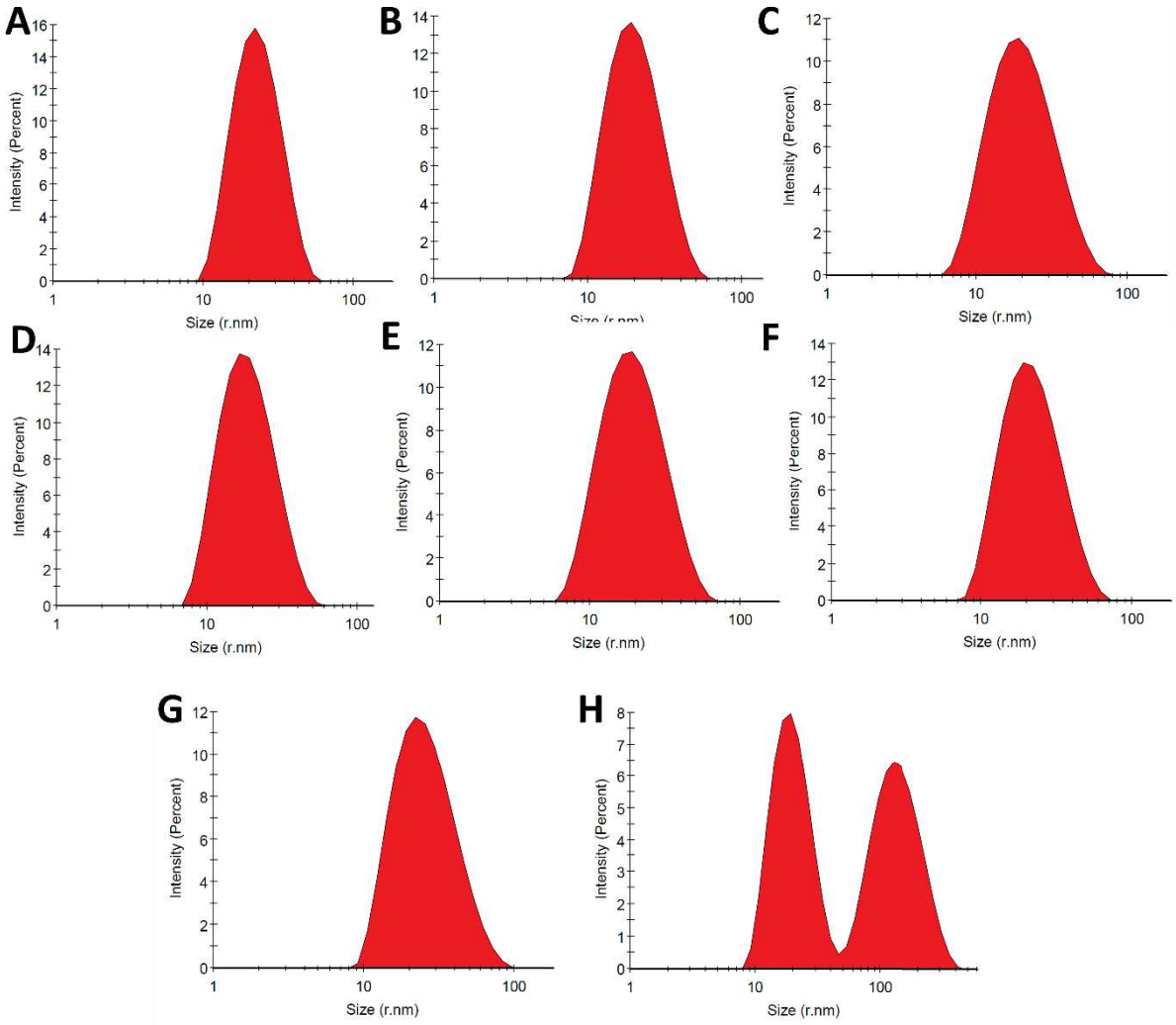

Figure S2 The size distribution of modified GG and GG by the intensity: (A) GG; (B) GG-B1; (C) GG-B2; (D) GG-Ph1; (E) GG-Ph2; (F) GG-CIN1; (G) GG-CIN2; (H) GG-CIN3

Isothermal titration calorimetry (ITC): heat flow per injection corrected to the heat of dilution (upper graph), integrated heat vs molar ratio (scatter) and fit to the model (line) (lower graph).

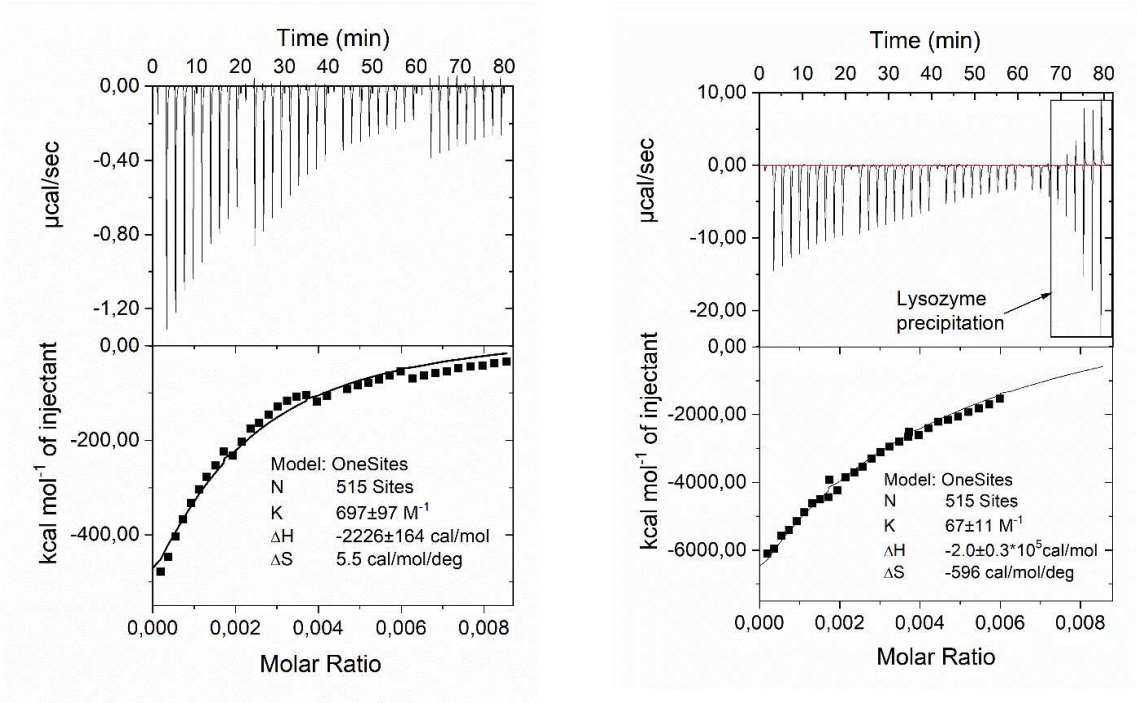

A B

Figure S3 Titration of 1mM HEWL with 8.8 M GG at 25C (A) and 57C (B).

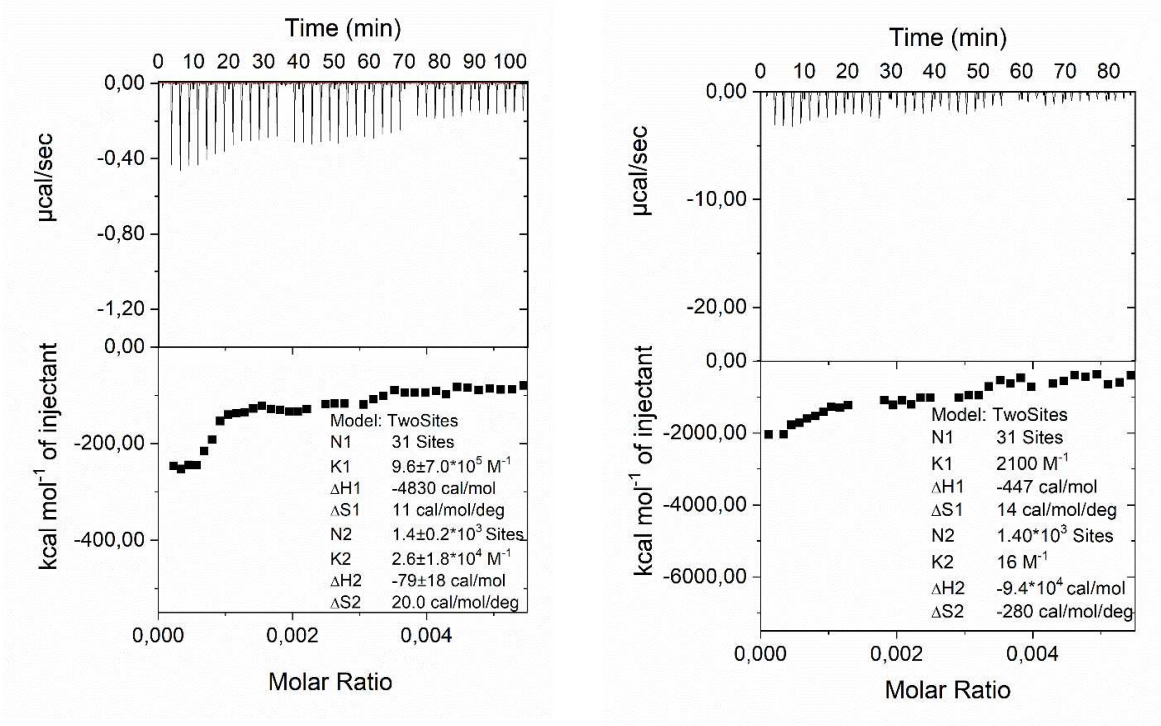

A B

Figure S4 Titration of 1mM HEWL with 7.2M GG -CIN2 at 25C (A) and 57C (B).

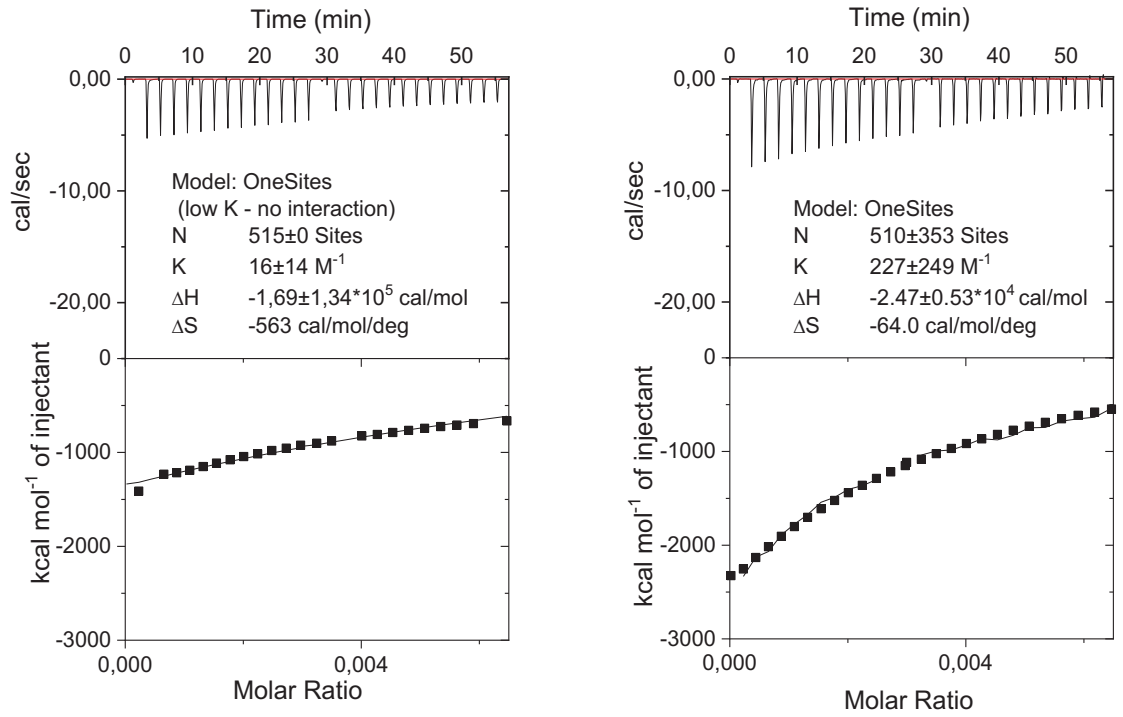

A *B*

Figure S5 Titration of 1mM HEWL with 14M GG-B2 at 25C (A) and 57C (B).

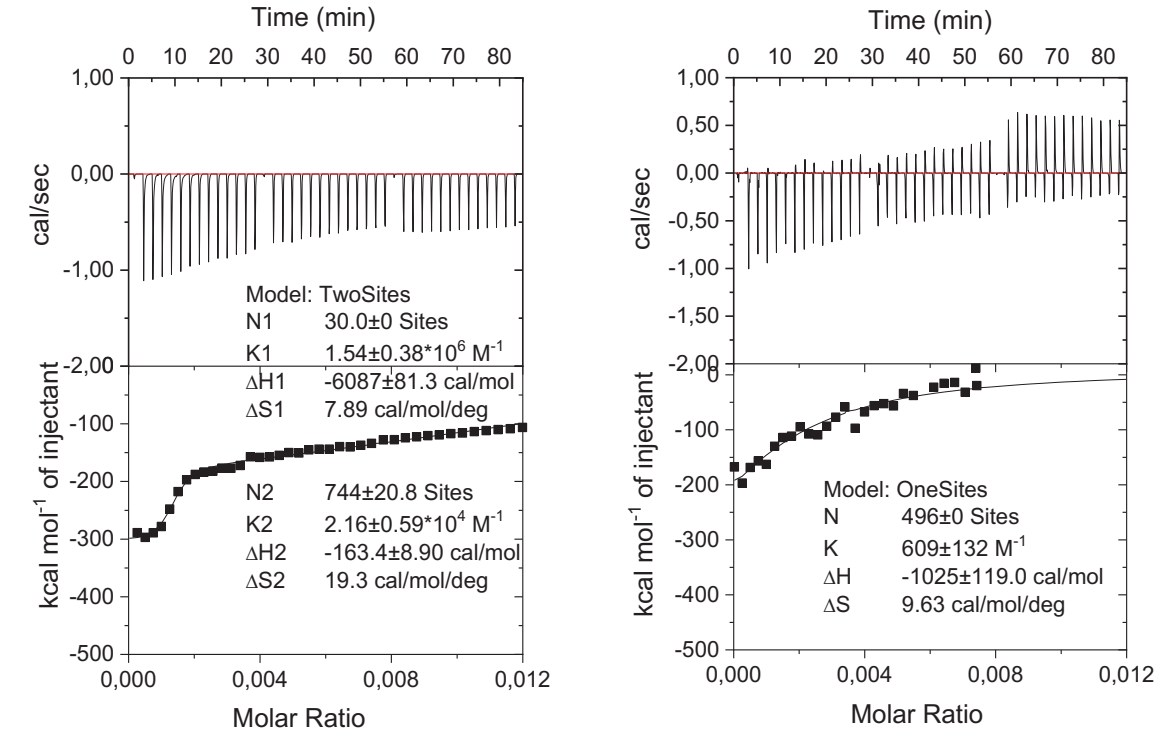

A *B*

Figure S6 Titration of 1mM HEWL with 16M GG-Ph1 at 25C (A) and 57C (B).